Department of Biotechnology, Chemistry and Pharmacy

Doctoral research school in Biochemistry and Molecular Biology

Cycle XXXIII

Antiviral drug development for treatment of acute and chronic viral infections

COORDINATOR OF THE DOCTORAL SCHOOL
Prof.ssa Lorenza Trabalzini

TUTOR
Prof. Alessandro Pini

SUPERVISOR
Prof. Maurizio Zazzi

CANDIDATE
Filippo Dragoni

Academic year 2019-2020

Index

My PhD activities

During the three years (2017-2020) of my attendance at the Doctoral School in Biochemistry and Molecular Biology, I joined the laboratory of Microbiology and Virology at the Department of Medical Biotechnologies of the University of Siena. The Department has been hosting the HIV Monitoring Laboratory (HML), started as a public health service and involved in a number of Human Immunodeficiency Virus (HIV) related research projects, since 1990. In the last few years, the HML has extended the research activity on emerging and re-emerging flaviviruses, including Dengue (DENV), West Nile (WNV) and Zika (ZIKV) Viruses. Moreover, due to the ongoing Coronavirus Disease 2019 (COVID-19) emergency, part of the research activity has been also directed to the newly discovered Severe Acute Respiratory Syndrome Coronavirus-2 (SARS-CoV-2).

Viruses are important agents able to cause many human diseases, ranging from mild to moderate and in some cases lethal infections. Generally, viral diseases can be distinguished into acute and chronic viral diseases. An acute viral infection is usually characterized by a rapid onset of disease, with mild to severe symptoms, followed by the resolution of the disease in a short time, with severe cases also leading to death rapidly. Conversely, in chronic viral infections, the virus persists in specific cells of the infected host in a variety of forms including true latency, continuous replication or alternating stages of silent and productive infection that can lead to severe consequences for the host (Deigendesch and Stenzel, 2018).

Currently, the main strategy for combating viral infections is a combination of large-scale vaccination and the use of antiviral drugs to treat disease cases. However, vaccines are available only for a minority of viral pathogens, thus the demand for new antiviral strategies has significantly increased. Factors contributing to this growing demand include the ever-increasing prevalence of chronic viral infections, the emergence of new and more infectious viruses and the re-emergence of old viruses. Indeed, due to the globalization and climate changes, viruses confined in specific and isolated areas are re-emerging and rapidly spreading to new geographic areas (Pierson and Diamond, 2020). While impressive advances in de novo drug design have significantly expedited drug discovery in the last decade, the process leading to the approval of new drugs takes a long time and remains economically challenging. As a workaround to this issue, drug repurposing has increasingly gained attention as a cost- and time-saving strategy to deliver safe and effective treatment. Anyway, the assessment of antiviral effects *in vitro* is a key approach for the screening of either de novo or repurposed candidate compounds. Among the variety of methods that have been developed, cell-based assays are the most valuable methods to define antiviral activity (Boldescu et al., 2017; Gong, 2013).

During my PhD, attending a lab with a strong focus in the area of antiviral drug discovery and a variety of running projects, gave me the opportunity to participate to multiple antiviral drug related activities.

We developed a robust, easy-to-perform and fast flavivirus immunodetection assay, which allows the quantification of ZIKV and DENV viral antigen in infected cells. The system uses a specific monoclonal antibody which binds to the fusion loop of domain II of the envelope protein, which is conserved among flaviviruses. The protocol was thoroughly assessed in terms of precision and accuracy and validated by determining the inhibitory effect of reference compounds (i.e. sofosbuvir and ribavirin). This assay can be applied as the read-out of a direct yield reduction assay and viral stocks generated during the first replication cycle can be transferred to a second cell culture in the absence of drug, to better characterize antiviral activity exerted at steps occurring later than envelope expression (Vicenti et al., 2020a).

Some studies reported that sofosbuvir, an RNA-dependent RNA polymerase (RdRp) inhibitor licensed for the treatment of Hepatitis C Virus (HCV) infection, exerts a measurable antiviral activity against the flaviviruses ZIKV and Yellow Fever Virus (YFV), both *in vitro* and in animal models, as well as against DENV *in vitro*. Since the flavivirus RdRp-coding non-structural protein 5 (NS5) is well conserved among flaviviruses, we investigated whether sofosbuvir may have an activity against WNV. Following exhaustive *in vitro*

experiments, we described for the first time sofosbuvir antiviral activity against WNV in the low micromolar range, as well as its genetic barrier through *in vitro* resistance selection experiments. Moreover, two collaborations, one with the Biophysics Institute of the National Research Council (Milano) and another with the Department of Biotechnology, Chemistry and Pharmacy of the University of Siena, allowed us to define the *in vitro* enzymatic activity of sofosbuvir using the purified WNV RdRp and to assess the role of the mutations observed during *in vitro* selection experiments through molecular docking experiments, respectively (Dragoni et al., 2020).

In the area of drug discovery, the HML is currently engaged in a project titled "ORIGINALE CHEMIAE in Antiviral Strategy" which was granted as a PRIN proposal (Progetti di Ricerca di Rilevante Interesse Nazionale). The project is aimed at exploiting Multi-Component Chemistry to synthesize promising broad-spectrum antivirals, which represent an attractive option to treat new emerging viral diseases. The project consists in a network of laboratories working in antiviral drug discovery and development from different Italian Universities (Tuscia, Parma, Roma Tor Vergata, Perugia, Siena and Roma Sapienza). The HML task in this project is to define the antiviral activity of candidate molecules in *in vitro* standardized virus-cell systems, against DENV, WNV, ZIKV, HIV-1 and the newly discovered SARS-CoV-2.

Italy has been one of the most and earliest affected countries by the SARS-CoV-2 pandemic. To trace SARS-COV-2 evolution, an Italian network named SCIRE (SARS-CoV-2 Italian Research Enterprise) was composed, consisting of 14 clinical centers, including the HML. The main objective of the SCIRE group was to characterize the COVID-19 Italian outbreak by full-length SARS-CoV-2 genome analysis during the first wave of the pandemic. Although the virus has been remarkably stable in its genetic make-up so far, molecular surveillance is warranted to follow the epidemic and deliver knowledge on the correlation between virus variants and clinically relevant properties, such as transmission rates, disease severity, response to treatment (Lai et al., 2020).

The introduction and continuous progress of antiretroviral therapy (ART) has brought a dramatic improvement of the quality and duration of life of HIV positive people, transforming HIV-1 infection from a fatal disease to a chronic manageable condition. However, ART is not able to clear the infection, since HIV-1 is able to persist in infected cells for several years. Therefore, strategies to eradicate or control HIV-1 without ART are a high priority. In recent years, most efforts have been focused on the so-called "Shock and kill" strategy. Few recent studies suggest that Maraviroc (MVC), the first approved anti-HIV-1 agent targeting a cellular factor, may exert a latency reversing activity in addition to its antiviral activity, hence representing a unique drug capable of combining the ability to awaken the latent provirus and block new infections. However, since the potential of MVC as a latency reversing agent was based on limited published data (López-Huertas et al., 2017; López-Huertas et al., 2020; Madrid-Elena et al., 2018), we investigated MVC ability to mediate HIV-1 induction in three cell line models, as well as in *ex vivo* CD4 T cells collected from six patients with suppressed viremia (Vicenti et al., 2020b).

1. Introduction – Flaviviruses

1.1 General overview and epidemiology

The *Flaviviridae* family includes four different genera of spherical and enveloped viruses with unsegmented positive-strand RNA. Among them, the *Flavivirus* genus includes more than 70 viruses, prevalently transmitted by insect vectors, mainly the *Aedes* and *Culex* mosquitoes; thus, they are included in the arbovirus (arthropod-borne) ecological group (Lindenbach et al., 2007; Payne, 2017). Flaviviruses include clinically relevant human pathogens such as Dengue (DENV), West Nile (WNV), Yellow Fever (YFV) and Zika (ZIKV) viruses. In the last years, these pathogens have dramatically increased in their incidence, disease severity and/or geographic range (www.who.int). This epidemic potential is related to many factors, such as adaptation of insect vectors, climatic change, deforestation and globalization. As a matter of fact, it is estimated that half of the global population may be at risk of infection with one or more of these viruses (Huang et al., 2014; Pierson and Diamond, 2020).

WNV was first isolated in 1937 (Smithburn et al., 1940) and since then, only few sporadic infections, characterized by a typically self-limited and minor illness, were reported in regions of Africa, the Middle East, Asia and Australia. However, in 1999 a WNV strain was responsible for a large and dramatic outbreak in New York City, that caused severe neurologic disease in seven humans in the New York area, as well as a large number of avian and equine deaths, spreading throughout the USA in the following years. Nowadays, WNV is endemic in Africa, Europe, Asia, north America, Australia, and the Middle East, with increasing number of human cases reporting severe diseases (Clark and Schaefer, 2020; Pierson and Diamond, 2020; www.who.int). Up to nine different WNV genetic lineages have been identified (Fall et al., 2017). The strains most often involved in human outbreaks, and thus clinically relevant, belong to lineages 1 and 2. Viruses from lineage 1 are divided in two clades, Clade 1a and Clade 1b, and they have been mostly isolated in Africa, Europe, Middle East, Asia, Oceania and north America (Fall et al., 2017), with Clade 1a more frequently associated to neurological outcome. Lineage 2 isolates appear to be less virulent to humans than lineage 1 and are found prevalently in Sub Saharan Africa, even though outbreaks both in animals and humans have been reported in central and eastern Europe (Donadieu et al., 2013; Magurano et al., 2012).

Since its discovery in 1947 (Dick et al., 1952), ZIKV remained confined to the equatorial zone across Africa and Asia, causing sporadic mild-febrile illness in a small number of humans. However, in 2007 a severe human outbreak was reported in Yap Island, followed by another large outbreak in French Polynesia and other Pacific Islands (Song et al., 2017). Later on, ZIKV rapidly spread to Brazil and other regions of the Americas, resulting in millions of infections. By March 2016, ZIKV transmission had been reported in 34 south and central American countries and territories (Faria et al., 2016; Fauci and Morens, 2016; Pierson and Diamond, 2020). Differently from previous outbreaks, ZIKV infection caused unique clinical features, including congenital malformations and other neurological disorders, leading the World Health Organization (WHO) to declare ZIKV "a public health emergency of international concern" (Hastings and Fikrig, 2017; WHO Report, 2016). Phylogenetic studies have revealed that ZIKV has evolved into African and Asian lineages (Liu et al., 2017). The African lineage strains circulated in central Africa, Senegal, Uganda and Nigeria and they were mainly detected from samples of enzootic vectors. The Asian lineage was mainly isolated throughout southeast Asia as Micronesia, Cambodia and French Polynesia. Following the introduction of ZIKV into the Americas, a new lineage within this cluster (lately defined as American strain) emerged, which has been responsible for the recent epidemics (Weaver et al., 2016). Interestingly, compared with the pre-epidemic strains from Asian lineage, the American epidemic strain has undergone the A188V substitution of NS1 protein, likely responsible for enhanced pathogenicity and increased disease severity (Liu et al., 2017; Pierson and Diamond, 2020; Xia et al., 2018). In 2019, all over the Americas about 35,000 ZIKV infections were reported (www.paho.org).

DENV is endemic in more than 100 countries of the southeast Asia, the Americas, the western Pacific, Africa and the eastern Mediterranean regions (www.who.int). Over the past 70 years, the number of people

infected has increased about 30-fold, making DENV the most prevalent arthropod-borne viral disease in the world. DENV causes an estimated 390 million total infections, 100 million clinically apparent cases and 500,000 presentations of severe dengue per year worldwide, and frequent DENV outbreaks have progressively increased in recent years (Bhatt et al., 2013; Maria G. Guzman and Harris, 2015; Pierson and Diamond, 2020). DENV is classified into four serotypes (DENV-1, DENV-2, DENV-3 and DENV-4) sharing limited homology (around 60–75%) at amino acid level. Within the same serotype, viruses differ about 3% at amino acid level, 6% at nucleotide level and are phylogenetically divided into genotypes and clades. Genetic variations between serotypes and clades are important determinants of differential viral fitness, virulence, and epidemic potential (M.G. Guzman and Harris, 2015; Weaver and Vasilakis, 2009). All four DENV serotypes circulate together in tropical and subtropical regions; however, the serotype 2 seems to be associated with increased disease severity (Chen et al., 2007; Vaughn et al., 2000).

1.2 Genome organization and structure

Flavivirus virions are around 50 nm in diameter, surrounded by a lipid envelope with surface proteins arranged in icosahedral-like symmetry and containing a single genomic RNA of positive-sense polarity of nearly 11 kb in length. The flavivirus genome (Fig 1) contains a single open reading frame, which is flanked by 5' and 3' untranslated regions (UTR), encoding a large polyprotein that is post-translationally cleaved by host and viral proteases (Lindenbach et al., 2007; Pierson and Diamond, 2020).
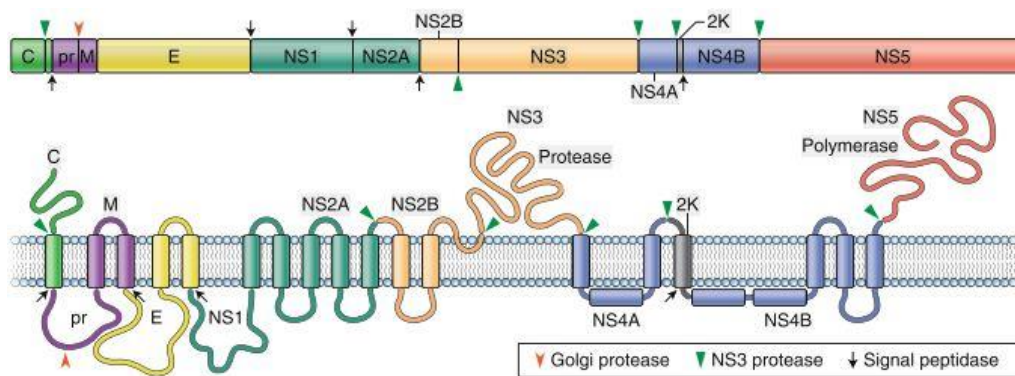

Fig 1. Flavivirus genome organization and structure. The genome is translated as a polyprotein, which is subsequently cleaved by viral and host cell proteases, which are indicated in the figure. (Adapted from Pierson and Diamond, 2020)

The non-coding 5'UTR of flaviviruses is around 100 nucleotides in length and is not well conserved among different flaviviruses. It contains a methyl-G-cap structure and two conserved stem-loop regions with secondary structures within this region, modulating viral RNA synthesis and translation. The non-coding 3'UTR ranges from 400 to 700 nucleotides in length, depending on the virus species, but sharing similar patterns of conserved sequence and structures among flaviviruses. 3'UTR can be divided into three domains and is important for the interaction with host and viral proteins (Lindenbach et al., 2007; Ng et al., 2017).

The N-terminal region of the polyprotein encodes for the three structural proteins, capsid (C), precursor membrane (prM) and envelope (E) which are present in the virion particle, while the C-terminal region includes the seven non-structural proteins (NS1, NS2A, NS2B, NS3, NS4A, NS4B and NS5) which accomplish essential steps during infection but are not present in the viral particle (Laureti et al., 2018; Lindenbach et al., 2007; Pierson and Diamond, 2020). The NS proteins are involved in the post-processing of structural proteins and are essential in viral replication, virion assembly, and defense against the host immune response (Lindenbach et al., 2007; Morrison et al., 2012).

The E protein is the major surface glycoprotein (≈53 kDa) and is involved in viral entry, pathogenesis and immune response. The mature virion is constituted by ninety dimers of the E glycoprotein arranged in a

herringbone pattern with icosahedral-like symmetry (Roby et al., 2015). The E protein is a three-domain structure, which is modified post-translationally by the addition of one or two asparagine-linked carbohydrates. Once glycosylated, it is involved in cell attachment. The folding of the E protein in the endoplasmic reticulum (ER) is facilitated by interactions with the structural prM protein shortly after synthesis (Mukhopadhyay et al., 2005; Pierson and Diamond, 2020; Rey et al., 2017; Zhang et al., 2004).

Flavivirus prM is a membrane glycoprotein of approximately 19–21 kDa mainly acting as a chaperone to promote folding and assembly of the E proteins (Konishi and Mason, 1993; Lorenz et al., 2003). Together with the E protein, prM forms an integral part of the flavivirus envelope that, in the mature form (M), is combined under a well-organized icosahedral architecture. Cleavage of prM to M is mediated by a host furin-like serine protease during the transit of immature virions through the trans-Golgi network. This step is required for the formation of infectious mature virions (Li et al., 2008). Since the Golgi compartment has a pH around 5.5, to avoid the premature fusion with the host membranes of the newly assembled virions, the prM peptide is not readily released from the virus surface, but it remains bound to the E protein, guaranteeing correct release of new virions (Yu et al., 2008; Zheng et al., 2014).

The nucleocapsid (N) viral core is formed by C protein subunits complexed with the single-stranded RNA viral genome. C protein is a small (14 kDa) cytosolic protein with structurally conserved α-helices, able to bind either viral nucleic acids or host lipids and it is necessary for the incorporation of the viral genome into the virion (Jones et al., 2003; Pierson and Diamond, 2020). C protein incorporation into the virion is regulated further by the coordinated cleavage of the polyprotein by the viral NS2B–NS3 serine protease.

Among non-structural proteins, NS1 is highly conserved with a molecular weight of 46-55 kDa, depending on the extent of glycosylation. The glycosylation of NS1 is fundamental for efficient secretion, virulence and viral replication (Somnuke et al., 2011). Indeed, *in vivo* experiments have shown that loss of N-linked glycans on NS1 results in attenuated DENV and WNV infection in mice (Pryor and Wright, 1994; Whiteman et al., 2010). NS1, in all its forms, is a multifaceted protein that hijacks the host replication system and interferes with the host immune response (Muller and Young, 2013). Indeed, soluble NS1 interacts both with the complement system and Toll-like receptor 4 (TLR4) to guarantee the survival of secreted virus progeny (Conde et al., 2016) and to initiate the inflammation process, respectively. This process further induces peripheral blood mononuclear cells (PBMCs) and macrophages to activate the inflammatory response (Muller and Young, 2013).

NS2 consists of two subunits, NS2A and NS2B. NS2A is a relatively small (≈22 kDa) protein containing several transmembrane domains and it is an activator of NS1. Besides its apparent roles in RNA replication and virus assembly, DENV-2 and WNV NS2A have also been shown to act as an interferon (IFN) antagonist by inhibiting IFN signaling during infection (Liu et al., 2006; Muñoz-Jordán et al., 2003). NS2B is a small membrane-associated protein (14 kDa) that forms a stable complex with NS3 and acts as a cofactor for the NS2B-NS3 serine protease (Clum et al., 1997; Lindenbach et al., 2007).

The NS4A and NS4B are small proteins (16 kDa and 27 kDa, respectively) participating to the virus replication complex formation on the ER membrane. NS4A consists of four transmembrane helices and an N-terminal cytosolic region. NS4A induces the rearrangements of ER membranes and interacts with NS1 (McLean et al., 2011; Miller et al., 2007), while NS4B colocalizes with NS3 and viral dsRNA in ER-derived membrane structures presumed to be sites of RNA replication (Lindenbach et al., 2007).

NS3 is a large (≈70 kDa) multifunctional protein which is well-conserved among the *Flavivirus* genus, with a sequence identity of approximately 65% among WNV, DENV and ZIKV (Lindenbach et al., 2007; Weber et al., 2015). NS3 has protease, helicase, nucleoside triphosphatase (NTPase) and RNA triphosphatase (RTPase) enzymatic activities. The N-terminal region of the NS3 protein constitutes the serine protease domain (NS3[pro]). Proper folding and catalytic activity of the NS3[pro] domain require NS2B as cofactor. NS3[hel] comprises three subdomains and harbours the enzymatic activities of NTPase and RTPase as well as dsRNA

unwinding activity (Wengler and Wengler, 1993, 1991). Some evidences suggest that one of these subdomains mediates the interaction between NS3 and NS5; disruption of this interaction could affect viral replication (Brooks et al., 2002; Tay et al., 2015). The RNA helicase is responsible for the unwinding of dsRNA intermediates in order to release the newly generated viral genome and to make the negative strand available as template for another round of viral genome synthesis. Moreover, NS3[hel] removes secondary structures from the viral RNA, especially in the 5' and 3' untranslated regions, facilitating the RTPase mediated capping. NTPase hydrolysis provides the chemical energy to power the translocation and unwinding processes, although the precise mechanism coupling these two activities remains elusive (Wang et al., 2009; Wengler and Wengler, 1991).

NS5 is the largest (103 kDa) and most conserved of the flavivirus proteins with a sequence identity of approximately 68% among WNV, DENV and ZIKV. It contains an N-terminal methyltransferase (MTase) and a C-terminal RNA-dependent RNA polymerase (RdRp), coupled via a short linker (Duan et al., 2019; Dubankova and Boura, 2019). The MTase domain (residues 1-≈265, 30 kDa) is responsible for capping the viral RNA through the guanylyl transferase and the N7 and 2'-O-ribose methylation activity, both of which are required to increase the stability and to prevent degradation by 5'–3' exoribonucleases of the newly synthesized RNAs (Devarkar et al., 2016; Züst et al., 2011). Additionally, the 2'-O-methylation protects viral RNA from being recognized by host cell sensors that stimulate the production of IFNs (Hyde and Diamond, 2015). The interaction of the MTase and the RdRp domains affects the replication activity, since full-length NS5 has higher polymerase activity than the RdRp alone for efficient viral replication (Duan et al., 2019; Potisopon et al., 2014; Saw et al., 2019).

Flavivirus RdRp carries out new RNA synthesis from the 3' end of the viral templates without any primer (*de novo* initiation). The structure of the RdRp is well conserved among flaviviruses (Dubankova and Boura, 2019; Godoy et al., 2017; Lu and Gong, 2017; Malet et al., 2007; Yap et al., 2007). RdRp (residues ≈272–900, 73 kDa) is divided in seven conserved motifs (from A to G) and it adopts a classic "right-hand" structure consisting of three subdomains with fingers, palm and thumb. Together, these regions are organized in a flat structure with three channels (the template entry, dsRNA, and the NTP entry channels) (Duan et al., 2019; Dubankova and Boura, 2019; Malet et al., 2007). Motifs A-B-C-D are located in the highly conserved palm domain and are important for dNTPs binding and catalysis; moreover, motif C, as well as motif E, interact with the backbone of the RNA product. Motif F, located in the finger domain, consists of 3-4 sub-motifs depending on the viral species and it is involved in the stabilizing of the nascent base pair. Motif G is proposed to regulate access of the ssRNA substrate to the template channel and/or RdRp translocation (Dubankova and Boura, 2019; Malet et al., 2007; Šebera et al., 2018; Yap et al., 2007; Zhao et al., 2017). In addition, a priming loop identified in the thumb subdomain is thought to play a major role in both ensuring correct de novo initiation and in controlling the conformational changes during the RdRp activity (Duan et al., 2019; Sahili and Lescar, 2017). RdRp appears to be responsible for the NS3-NS5 interaction in several flaviviruses, however the exact function of cooperation between these two enzymatic proteins is not completely understood (Duan et al., 2019; Lindenbach et al., 2007; Tay et al., 2015).

1.3 Flavivirus replication cycle

The flavivirus replication cycle (Fig 2) initiates with the stable attachment of the virion to the surface of the target cells, mainly keratinocytes, dermal fibroblast and Langerhans cells of the epidermis, through the interaction between viral surface E protein and host attachment/receptor molecules (Neufeldt et al., 2018). Host proteins defined as receptors are essential for the entry of viruses, since they catalyze conformational events. Although several host factors that increase the efficiency of flavivirus binding and infection of cells have been identified, they are not required to trigger the structural transitions that lead to membrane fusion. Therefore, these are defined as attachment factors (Pierson and Diamond, 2020). Indeed, a number of attachment factors/receptors have been identified for flaviviruses, including αvβ3 integrin, GRP78/BiP, CD14 or a closely related molecule (Mukhopadhyay et al., 2005). The most extensively studied attachment

factor is the C-type lectin dendritic cell-specific ICAM-grabbing non-integrin (DC-SIGN), mainly present at the surface of dermal dendritic cells and macrophages.
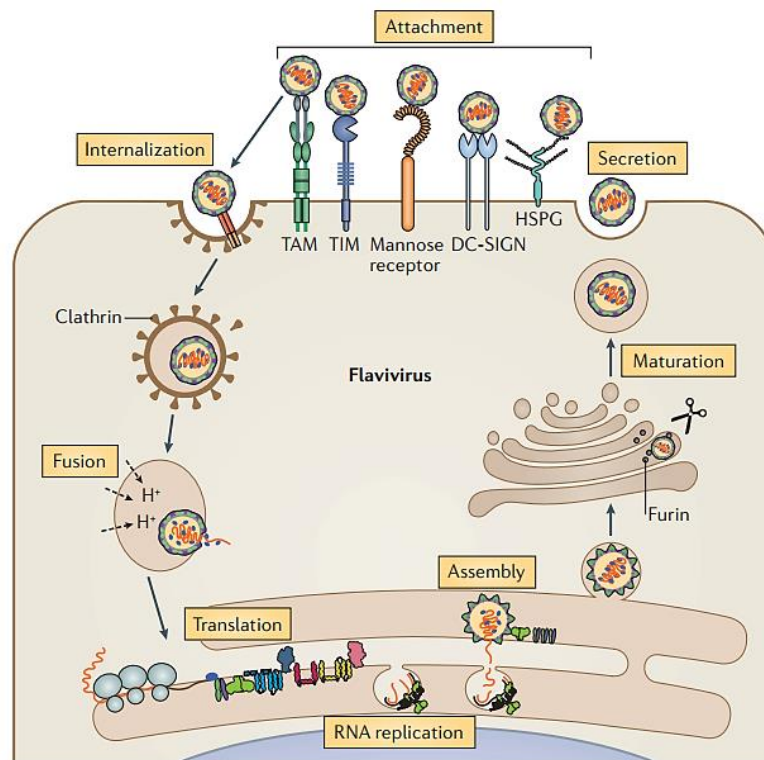

Fig 2. Flavivirus replication cycle. DC-SIGN: C-type lectin; TIM: T cell immunoglobulin mucin domain protein 1; TAM: tyrosine protein kinase receptor 3 (TYRO3)–AXL–MER; HSPG: heparan-sulfate proteoglycans. (Adapted from Neufeldt et al. 2018).

In addition, highly sulfated glycosaminoglycan, such as heparan-sulfate proteoglycans, act as attachment factors and have the function to concentrate viral particles at the target cell surface before their interaction with primary receptors. Recent studies show that several cellular receptors, as protein of TIM (T cell immunoglobulin and mucin domain) and TAM (TYRO3, AXL and MER) receptor families can mediate flavivirus entry through interactions occurring only between negatively charged lipids such as phosphatidylserine in the viral membrane (Diamond and Pierson, 2015; Hamel et al., 2015; Meertens et al., 2012; Mercer and Helenius, 2010; Pierson and Diamond, 2020).

After attachment, flaviviruses are internalized via clathrin-coated pits and transferred to a pre-lysosomal endocytic compartment. The low pH environment triggers viral E protein rearrangement, driving the fusion of the viral lipid envelope with cellular endosome membranes. After membrane fusion, the viral genomic RNA is released into the cytoplasm where the viral replication starts in vesicle packets, which contain the small hydrophobic NS proteins, dsRNA, nascent RNA and, presumably, some host factors (Payne, 2017). The penetration of the capped ssRNA(+) viral genome into the cytoplasm allows for the direct translation of the viral polyprotein on the rough ER. Replication occurs on virus-induced invaginations of the ER: NS1, prM and E are translated into the ER lumen, the transmembrane domains of NS2A, NS2B, NS4A and NS4B are translated into the ER membrane, whereas C, NS3 and NS5 remain in the cytoplasm. NS5 mediates the beginning of replication with the synthesis of a full genome-length ssRNA(-), followed by the formation of a dsRNA replication intermediate, which then serves as a template for the synthesis of additional ssRNA(+). Concomitantly, NS3 helicase interacts with NS5 to unwind the dsRNA. The progeny ssRNA (+) is subsequently capped at its 5' end and methylated to form the cap RNA structure. Following RNA synthesis, newly copied RNA molecules are either recycled for translation and replication or alternatively, extruded from the vesicle to bud out on ER membranes and packaged into nascent virions. The newly synthesized

immature flavivirus particles are produced by budding of the C protein and the associated genomic RNA, which forms the nucleocapsid into ER-derived membranes and is studded with prM and E proteins. These immature particles traffic along the secretory pathway across the Golgi complex, where undergo the cleavage of the pr portion from M protein by a trans-Golgi resident furin-like protease, that promotes particle maturation prior to their release from the infected cell (Arakawa and Morita, 2019; Payne, 2017; Pierson and Diamond, 2020).

1.4 Transmission

The evolution and the epidemiological characteristics of flaviviruses are associated to a combination of limitations imposed by the arthropod vector, the vertebrate hosts, the ecology and the influence of human commercial activities.

DENV and ZIKV transmission is mainly associated with the mosquito vector *Aedes aegypti* and *Aedes albopictus*; WNV is mostly transmitted by the members of the *Culex pipiens spp* (Ciota, 2017; Huang et al., 2014).

The African ZIKV lineage is thought to be maintained via the enzootic transmission cycle primarily between non-human primate and mosquitoes, with humans as incidental hosts. However, the Asian ZIKV lineage has gained the ability to sustain transmission in a human-endemic cycle (sub-urban transmission cycle), thus allowing humans to serve as the carrier, multiplier, and source of ZIKV for uninfected mosquitoes (Althouse et al., 2016). Differently, DENV is the only known arboviruses that has fully adapted to humans, having lost the need for an enzootic cycle for maintenance (Payne, 2017; www.who.int). WNV enzootic cycle is between mosquitoes and birds, the latter regarded as "amplifier hosts" and with mammals serving as "dead-end" hosts, since generally they do not develop high levels of virus in their bloodstream (Pierson and Diamond, 2020).

Despite vector-borne transmission is the favorite route for ZIKV, DENV and WNV infections, transmission through transplanted organs, transfused blood, contact with body fluids from a highly viremic patient, transplacental transmission and occupational transmission have been observed (Iwamoto et al., 2003; Julander et al., 2006; Musso et al., 2017; Swaminathan et al., 2016; Williamson et al., 2017; Wiwanitkit, 2009). ZIKV sexual transmission is possible from both asymptomatic and symptomatic infections and the duration of infectivity of genital fluids is unknown (Hastings and Fikrig, 2017; Musso et al., 2015). Recently, ZIKV vertical transmission has been extensively investigated and a high risk of fetal injury connected to ZIKV infection during the first trimester of pregnancy has been evidenced (Cauchemez et al., 2016; Honein et al., 2017).

1.5 Clinical manifestations and pathogenesis

Although flavivirus infections in humans are asymptomatic in the 80% cases, clinical manifestations range from influenza-like symptoms, frequently misdiagnosed, to severe conditions leading eventually to death. After the bite of an infected mosquito, the duration of the incubation period lasts a few days (average 4 to 7 days) (Gubler, 1998; Sejvar, 2016; Slavov et al., 2016).

It is estimate that 1 in 4 DENV infections are symptomatic, showing mild to moderate acute febrile illness. However, approximately 5% of symptomatic cases of DENV infection progress to a more severe disease, whose clinical progression can be differentiated into three phases: febrile phase, critical phase and recovery phase. The febrile phase, also named Dengue Fever, may cause, over the classical flu-like symptoms, transient maculopapular rash and mild-hemorrhagic illness. The critical phase occurs at the end of febrile phase before the appearance of specific antibodies, and could be associated to Dengue Hemorrhagic fever (DHF) which has four severity grades, with the more severe grades (III and IV) classified as dengue shock syndrome (DSS) (Rodriguez-Roche and Gould, 2013). Common manifestations include skin

hemorrhages such as petechiae, purpuric lesions and ecchymosis. Concomitantly, severe plasma leakage can lead to shock or fluid accumulation with respiratory distress, severe bleeding, which may further develop into multi-organ failure with fatal outcome (Kalayanarooj, 2011). Although the appearance of DHF/DSS might occur at any DENV exposure, it seems to be more frequent in secondary DENV infections, particularly in children or in newborns who are partially protected by maternal antibodies (Jain and Chaturvedi, 2010).

Symptomatic ZIKV clinical manifestations occur as acute onset of fever lasting for several days to a week, along with maculopapular rash in most of the patients. Other commonly reported symptoms include myalgia, arthralgia, headache and conjunctivitis. Although severe disease requiring hospitalization is uncommon, during the recent outbreak in the Americas, ZIKV infection has been associated to severe neurological complications, such as (i) the Guillain-Barré syndrome (GBS), a serious and life-threatening neurological disorder characterized by progressive muscular weakness, encephalitis and myelitis in adults and (ii) microcephaly and other severe fetal brain defects in fetuses and neonates caused by maternal ZIKV infection (Grossi-Soyster and Desiree La Beaud, 2017; Kazmi et al., 2020).

WNV infections cause disease in approximately 20% of infected humans; the vast majority of WNV symptomatic patients develops an acute, systemic febrile illness (West Nile fever, WNF) and less than 1% develops neuroinvasive disease including aseptic meningitis, encephalitis, or an acute poliomyelitis-like syndrome. The WNF is the predominant clinical syndrome and generally occurs with the abrupt onset of fever, headache, fatigue, myalgia and rash. The rash may be transient and appears to be more frequently seen in WNF than in more severe illness manifestations (Bai et al., 2019; Zannoli and Sambri, 2019).

Flavivirus virions released after a mosquito bite are able to infect a large variety of human target cells such as fibroblasts, keratinocytes, dendritic cells, monocytes, and endothelial cells.
DENV and ZIKV both initially infects cells in dermis and epidermis, such as immature Langerhans cells and keratinocytes. Infected cells migrate to the lymph nodes, triggering the recruitment of monocyte-macrophage lineage cells. As a result, the number and variety of infected cells increase and disseminate throughout the lymphatic system (Martina et al., 2009).

Concerning DENV infection, mononuclear cells are stimulated to produce cytokines and chemokines that provide an essential protective role during DENV infection. However, this "storm" of inflammatory cytokines and other inflammatory mediators acts on the endothelium and alters normal fluid barrier functions, leading to increased plasma leakage (Harapan et al., 2020; Martina et al., 2009). In addition, NS1 released from infected cells is proposed to modulate complement signaling cascade, that triggers cellular reactions further stimulating the production of inflammatory cytokines (Avirutnan et al., 2006; Diamond and Pierson, 2015). In addition to innate immunity, cellular and humoral immunity play an essential role too. During the infection, T cells and cross-reactive memory T cells are produced, as well as antibodies targeting the principle DENV epitopes (i.e. E, NS1 and pre-M proteins). However, whether these immune responses protect against or exacerbate subsequent infections is still controversial. Indeed, if the antibodies are not completely neutralizing against the new DENV strain, they can facilitate viral entry into Fc receptor-positive cells during a subsequent infection. Such phenomenon, defined as antibody-dependent enhancement (ADE), is associated with both increased DENV infectivity and the suppression of host immune responses. Indeed, is likely that severe dengue may occur in those experiencing a secondary infection with heterotypic strain of DENV and in infants who are born to dengue-immune mothers with primary anti-DENV antibody responses (Harapan et al., 2020; Valentine et al., 2020).

Following infection, ZIKV triggers innate immunity responses that exert antiviral and pro-inflammatory effects. The over activation of the immune and inflammatory pathways, such as T- and B-cells mediated immunity, leukocyte-mediated immunity and cytokine production, may attract T cells and other leukocytes to the site of infection, leading to tissue damage (Wang et al., 2017). The humoral response may drive the predisposition to severe illness too; indeed, it was observed in cell culture that the rates of ZIKV infection

can be enhanced by the cross-reactive anti-DENV antibodies (Priyamvada et al., 2016). In addition, cross-reactive human anti-ZIKV antibodies can enhance DENV infection (ADE activation) in cell culture and in mice (Stettler et al., 2016) and also in humans, as described recently (Katzelnick et al., 2020).

The overstimulation of the immune system and the consequent cascade of pro-inflammatory cytokines play a role in the pathogenesis of GBS; indeed, it was suggested that high levels of CXCL10 in ZIKV patients may contribute to neuronal damage, potentially targeting peripheral nerves (Maucourant et al., 2019; Naveca et al., 2018). The increase of microcephaly in infants caused by maternal ZIKV infection, suggests that ZIKV is capable of bypassing the placental barrier and infect human placental macrophages, resulting in the disruption of the placenta by strong activation of antiviral immune response (Wen et al., 2017). Moreover, ZIKV has the capacity to infect human neural progenitor cells and the microglia triggering their apoptosis (Ferraris et al., 2019; Zheng et al., 2015). Activation of microglia leads to the production of pro-inflammatory cytokines and cytotoxic molecules, such as nitric oxide, that contribute to neuronal damage during the fetal brain development (Maucourant et al., 2019).

Following an infectious mosquito bite, WNV replicates locally at the injection site in the keratinocytes and Langerhans cells of the epidermis. The local virus replication is enhanced due to the immune modulation of the host response by the mosquito saliva. It has been hypothesized that infected Langerhans cells migrate to the draining lymph nodes in which the virus replicates, further spreading the infection through the lymphatic system. Following WNV infection, a cascade of proinflammatory cytokines are upregulated as part of the innate immune response. However, overexpression and continuous upregulation of inflammatory cytokine genes may be detrimental by enhancing the severity of infection and/or inflammation. The exact mechanism of neuroinvasion by WNV is still unknown, despite several routes of entry have been proposed. Likely, free virus particles are able to across the disrupted blood-brain barrier (BBB) through a "transudative" mechanism, due to the increased vascular permeability caused by pro-inflammatory cytokines and chemokine (Suen et al., 2014). Alternatively, entry might occur via the "Trojan horse" mechanism, mediated by infected leukocytes trafficking into the central nervous system (CNS) through the leaking BBB (Lim et al., 2011), or by the "transneural" mechanism consisting in the virus migration following motor and sensory nerves from the point of entry (i.e. peripheral somatic nerves into the CNS and from the olfactory nerve into the CNS) (Habarugira et al., 2020). Following invasion of CNS, the virus directly infects neurons, and less frequently astrocytes, leading to neuronophagia and cell death. While nearly all brain regions may be affected, WNV appears to have a specific neurotropism for neurons in the basal ganglia, thalamus, and brainstem (Stonedahl et al., 2020).

1.6 Current status of antivirals and vaccines development

1.6.1 Antivirals development

Clinical availability of effective antivirals for the management of severe flavivirus diseases is an unmet medical need. Despite the increase of incidence of viral diseases, neither specific treatments nor immunoprophylaxis are currently available and the clinical management of symptomatic patients remains based on supportive care (i.e. intravenous infusion of fluids, respiratory support, and prevention of secondary infections, as suggested by WHO and CDC current guidelines) (www.who.int; www.cdc.gov).

Several promising drug candidate molecules have been reported via high-throughput compound library screening, by de novo design targeting viral or host proteins.

The most promising viral targets for de novo design are the NS5 RdRp and the NS3 protease, and, to a lesser degree, E-glycoprotein, C, NS4B, NS3 helicase and NS5 MTase (Boldescu et al., 2017). A different therapeutic approach is targeting cellular factors required for the viral life cycle. Targeting a cellular factor rather than a viral protein is an attractive solution, since host cellular proteins are less prone to mutations, as opposed to the high rate of mutations of viral proteins, hence overcoming the emergence of resistance mutations. On the other hand, targeting a cellular host factor has a higher potential for the development of side effects. Options for successful host targeting agents include blocking a function which is redundant for

the cell but essential for the virus or selectively impairing a cellular pathway only in virus-infected cells. Examples of molecules that target host factors exerting antiviral activity on flavivirus are mycophenolic acid (MPA) and cyclosporines, inhibiting the cellular enzyme inosine monophosphate dehydrogenase and cyclophilin A (CyPA), respectively (Barrows et al., 2016; Diamond et al., 2002; Morrey et al., 2002; Qing et al., 2009), and lovastatin a cholesterol synthesis inhibitor, thought to limit membrane mobilization required for the assembly of the viral replication complex (Españo et al., 2019; Mackenzie et al., 2007; Martínez-Gutierrez et al., 2011). A wide range of host factor involved in virus infection cycle are currently under investigation for de novo design of antiviral compounds (Brai et al., 2019, 2016; DeWald et al., 2020; Giovannoni et al., 2020; Yang et al., 2020)

Since the discovery and approval of new drugs takes a long time, an increasing trend is to take advantage of the cost- and time-saving benefits of drug repurposing. There are some relevant examples of drug repurposing in the flavivirus antivirals field. Ribavirin, a synthetic guanosine nucleoside analogue and one of the first broad-spectrum antivirals licensed by Food and Drug Administration (FDA) against several viruses (Fernandez et al., 1986; Khan et al., 1995; Lau et al., 2002), has been shown inhibitory activity *in vitro* against ZIKV (Kim et al., 2018; Vicenti et al., 2018), DENV (Koff et al., 1982) and WNV (Anderson and Rahal, 2002; Jordan et al., 2000). However, ribavirin was not effective for treating WNV disease (Chowers et al., 2001) and the possible use against ZIKV infection is contraindicated in pregnancy due to its teratogenic properties. With the same strategy, the anti-HCV nucleoside analogue targeting RdRp, sofosbuvir, has shown anti-ZIKV activity *in vitro* (Sacramento et al., 2017; Vicenti et al., 2018) and in animal models, preventing the vertical transmission of ZIKV in pregnant mice (Mesci et al., 2018), as well as anti-DENV activity *in vitro* (H. T. Xu et al., 2017), and anti-YFV activity both *in vitro* and *in vivo* (de Freitas et al., 2019). Exploiting a similar mechanism of action, BCX4430, an adenosine analogue originally designed as an anti-HCV agent, exerts antiviral activity against a wide range of RNA viruses including flaviviruses and filoviruses such as Ebola virus. The broad-spectrum potency of BCX4430 has been proved against ZIKV both *in vitro* and *in vivo* and against WNV *in vitro* (Eyer et al., 2017; Julander et al., 2017a).

1.6.2 Vaccines development

More than 80 years ago, the development of YFV 17D live-attenuated vaccine was considered a landmark in the history of flavivirus vaccines (Barrett, 2017). Effective anti-flavivirus vaccines are also available for active immunization against Japanese encephalitis and tick-borne encephalitis virus (Heinz and Stiasny, 2012), even if with some safety concerns (Chong et al., 2019).

To date, there are several open clinical trials testing a range of ZIKV vaccine candidates, including DNA vaccines, peptides, mRNA vaccines, purified inactivated vaccines and recombinant viral-vector vaccines (www.who.int; Chong et al., 2019). One of the most important goals of a ZIKV vaccine is to prevent the congenital ZIKV syndrome. Currently, some progress has been documented on nonhuman primates as preclinical pregnancy models to test vaccine efficacy (Nguyen et al., 2017; Waldorf et al., 2016).

Despite the lack of WNV vaccines for humans, several vaccines have been successfully developed and licensed for veterinary use. Among them, two are whole inactivated WNV equine vaccines (West Nile Innovator by Pfizer and Vetera by Boehringer Ingelheim). Another commercialized vaccine is the recombinant canarypox-vectored vaccine, expressing the prM and the E protein of the NY99 strain (Recombiteck Equine West Nile Virus Vaccine by Merial-Sanofi Aventis) (Brandler and Tangy, 2013). Among the WNV human vaccine candidates, progress has been made in the DNA-delivered subunit and chimeric vaccines (Chong et al., 2019; Habarugira et al., 2020). Two live chimeric/recombinant vaccines and one DNA-vectored vaccine entered phase I clinical trial, while one YFV-17D backbone expressing WNV prM/E recombinant vaccine entered phase II clinical trial (Amanna and Slifka, 2014; Habarugira et al., 2020).

Considering the severe clinical outcomes following DENV infections, huge efforts have been made in its vaccine field. On 1st May 2019, FDA has approved Dengvaxia® (CYD-TDV) produced by Sanofi Pasteur, as the first dengue vaccine, already licensed in several countries including European Union, Latin America and Asia. CYD-TDV was constructed using recombinant DNA technology by replacing the sequences encoding prM and E proteins of the YFV 17D vaccine with those encoding the homologous prM and E gene sequences of the four DENV serotypes. The indication of CYD-TDV is for individuals aged from 9 to 45, living in DENV endemic areas and it is not suggested for individuals not previously infected by any DENV serotype or for whom this information is unknown. As a matter of fact, its use has some significant controversies, since an increased risk of severe DENV infection was showed during primary infection of dengue-naive individuals following vaccination; such phenomenon may be explained by ADE mechanism. Indeed, serological studies demonstrated that individuals that were DENV-seropositive at the time of vaccine administration experienced benefit from CYD-TDV, whereas DENV-naive individuals were at increased risk for severe disease over this interval. For this reason, research to find other possible dengue vaccines is still underway and to date, two other live-attenuated tetravalent DENV vaccines are in advanced stages of clinical trials (Chong et al., 2019; Harapan et al., 2020; Pierson and Diamond, 2020).

1.7 Methods to define antiviral activity

Assessment of antiviral effects *in vitro* is a key approach for the screening of either de novo or repurposed candidate compounds. Among the variety of methods that have been developed (Gong, 2013), cell-based assays are the most predictive methods to define antiviral activity. Several cell-based assays have been developed and can be classified into: i) assays using live viruses, ii) assays that use sub-genomic viral replicons (VRPs), containing a subset of viral genes that are required for replication, and iii) assays using virus-like particles (VLPs), containing viral E protein and prM glycoproteins but no viral RNA (Boldescu et al., 2017).

Assays using live viruses are the reference standard for antiviral screening but with some drawbacks, as the need of high-level biosafety containment facilities, dedicated personnel training, high costs and times to execution. In contrast, VRP and VLP assays can overcome safety concerns and are prevalently based on convenient readouts, such as luminescence and fluorescence. However, since they do not simulate the complete virus life cycle, they are not amenable for the screening of compounds with unknown targets; moreover, VRP and VLP assay results must be validated carefully to avoid false-positive hits.

Assays using live viruses are based on several types of readouts, each characterized by a different degree of accuracy, complexity and cost. Indeed, following virus infection, measurement of virus replication can be performed in different ways, such as quantitative polymerase chain reaction (qPCR) (Gong et al., 2013; Vicenti et al., 2018), microscopy monitoring of cytopathic effect (H. T. Xu et al., 2017) and immunofluorescence-based assays, such as the fluorescence focus assay and the most advanced fluorescence-activated cell sorting assay (Kraus et al., 2007; Payne et al., 2006). Despite these advancements, the classical plaque reduction assay (PRA) is still considered as the gold standard for antiviral screening of compounds against viruses causing cytopathic effect and it is also commonly used for antibody titration in plaque reduction neutralization tests (Cordeiro, 2019). Nevertheless, it has several drawbacks including high labor, long-turnaround time and low throughput, making it not suitable for the analysis of large numbers of compounds or sera. Consequently, the development of accurate, easy-to-perform, and fast cell-based assays is highly valuable to test candidate inhibitors of flavivirus replication.

2. Introduction – SARS-CoV-2

2.1 General overview and epidemiology

Coronaviruses (CoVs) are positive sense, single stranded, enveloped RNA viruses with a propensity to cross species barriers and causing disease in humans and animals (Chan et al., 2013). Within the order of *Nidovirales* and the suborder of *Coronavirineae*, lies the family *Coronaviridae*. The latter is further specified into the subfamily of *Orthocoronavirinae*, which consists of four genera: the alpha, beta, gamma and delta CoV (Fehr and Perlman, 2015). Whereas alphacoronaviruses and betacoronaviruses exclusively infect mammalian species, gammacoronaviruses and deltacoronaviruses have a wider host range that includes avian species (V'kovski et al., 2020).

Prior to the recent outbreaks, CoVs were only though to cause mild, seasonal, self-limiting respiratory infection in humans associated with symptoms of the 'common cold'. Two of these human coronaviruses (HCoVs) are alphacoronaviruses, HCoV-229E and HCoV-NL63, while the other two are betacoronaviruses, HCoV-OC43 and HCoV-HKU1. HCoV-229E and HCoV-HKU1 were isolated nearly 50 years ago (Hamre and Procknow, 1966), while the last two were recently identified (Fehr and Perlman, 2015). In contrast to the mentioned CoVs, Severe Acute Respiratory Syndrome Coronavirus (SARS-CoV), Middle East Respiratory Syndrome Coronavirus (MERS-CoV) and the newly emerged SARS-CoV-2, all belonging to the betacoronavirus genera, subgenus Sarbecovirus, Merbecovirus and Sarbecovirus, respectively, are highly pathogenic and able to cause severe respiratory infection among humans (Gorbalenya et al., 2020; V'kovski et al., 2020).

During November 2002 an epidemic of pneumonia caused by SARS-CoV occurred in the Guangdong province of China and rapidly spread around the globe. Overall, SARS-CoV infected 8,098 people and caused 774 fatalities in 29 different countries by the end of the epidemic (Zumla et al., 2016).
Later, during April-June 2012, in Saudi Arabia several patients developed severe pneumonia and following analyses revealed that MERS-CoV caused the outbreak. The spread of MERS-CoV continued beyond the Middle East, causing further reports of infected individuals. Until 2020, 2,468 cases and 851 fatalities had been reported globally (Killerby et al., 2020).
During December 2019, several patients with atypical pneumonia were reported by local health facilities in Wuhan, China. The patients were found epidemiologically linked to the seafood market in Wuhan. Later, the infectious agent was confirmed and reported as a novel CoV, SARS-CoV-2, the causative agent of COVID-19 (Zhu et al., 2020). The incidence of COVID-19 grew dramatically in China and the virus rapidly spread to more than 200 countries since late February 2020. On March 11, 2020, the WHO declared the COVID-19 outbreak a global pandemic and as of 1 November 2020, nearly 46 million cases and 1.2 million deaths have been reported globally, with global death-to-cases ratio 2.6%, with these numbers still on the rise in most countries (www.who.int).

As SARS-CoV and MERS-CoV, SARS-COV-2 is a zoonotic pathogenic CoV derived from a spillover transmission from animal to human. While for SARS-CoV and MERS-CoV the primary host (bat) and the intermediate hosts have been identified (civets and camels respectively) (Krishnamoorthy et al., 2020), the source, reservoir, and cause of transmission of SARS-CoV-2 are still not well understood. However, given the similarity of SARS-CoV-2 to bat SARS-CoV-like CoVs, it is likely that bats served as reservoir hosts (Andersen et al., 2020; Krishnamoorthy et al., 2020), whereas pangolins as the probable intermediate hosts, since common features with CoVs of these animals have been identified (Lam et al., 2020; Zhang et al., 2020).

The SARS-CoV-2 whole genome share about 82% sequence identity with SARS-CoV and MERS-CoV and >90% sequence identity for essential enzymes and structural proteins (Naqvi et al., 2020).
Several nomenclatures have been introduced for SARS-CoV-2, including Nextstrain, Global Initiative on Sharing Avian Influenza Data (GISAID) and Phylogenetic Assignment of Named Global Outbreak LINeages

(PANGOLIN) (Alm et al., 2020; Rambaut et al., 2020). While Nextstrain and GISAID clade nomenclatures aim at providing a general categorization of globally circulating diversity, the lineages are meant to correspond to outbreaks.

To date, around 171,000 genome sequences have been submitted to GISAID. Sequences can be divided into 2 lineages (A and B, further specifications are given by a numerical value e.g. lineage A.1 or lineage B.2), 5 clades (19B, 19A, 20A, 20C and 20B) and 7 clades (S, L, O, V, G, GH and GR), according to the PANGOLIN, NextStrain and GISAID classification, respectively (Alm et al., 2020).

As other RNA viruses, even if with lower frequency, SARS-COV-2 introduces mutations in RNA sequence which can be positively selected because advantageous for the host pathogenesis. Among the variants detected, strains containing the spike D614G mutation became predominantly in the pandemic, dominating the large outbreaks in Europe and later in the Americas. Interestingly, the G614 variant seems to be associated with greater infectivity as well as higher viral loads. However, evidences of G614 variant on disease severity and on association with hospitalization status were not yet found (Eaaswarkhanth et al., 2020; Korber et al., 2020).

In the early summer 2020, a novel SARS-CoV-2 variant, characterized by the spike A222V mutation, has been rapidly spreading within Europe. Further data about this variant are still under research.

2.2 Genome organization and life cycle

SARS-CoV-2 virions are spherical, with a diameter of 70-100 nm conforming to the typical CoVs diameter (Kumar et al., 2017; Neerukonda and Katneni, 2020; Park et al., 2020). A prominent feature of the CoV virions is the club-shaped spike projections emanating from the surface of the virion, which prompt the name by resembling the appearance of a solar corona. CoVs have helically symmetrical nucleocapsids, which is uncommon among positive-sense RNA viruses, but far more common for negative-sense RNA viruses (Fehr and Perlman, 2015).

The genome of SARS-CoV-2 (Fig 3) is a single-stranded positive-sense RNA of about 29.9 kb and its structure follows the specific gene characteristics of known CoVs: (i) a highly conserved genomic organization with a large replicase gene, (ii) expression of many non-structural genes by ribosomal frameshifting, (iii) several enzymatic activities encoded within the large replicase-transcriptase polyprotein, (iv) expression of downstream genes by synthesis of 3' nested subgenomic mRNAs. The genome is flanked by two UTRs, similar to those of other betacoronaviruses, with nucleotide identities of $\geqslant$ 83.6% (Y. Chen et al., 2020; Changtai Wang et al., 2020).
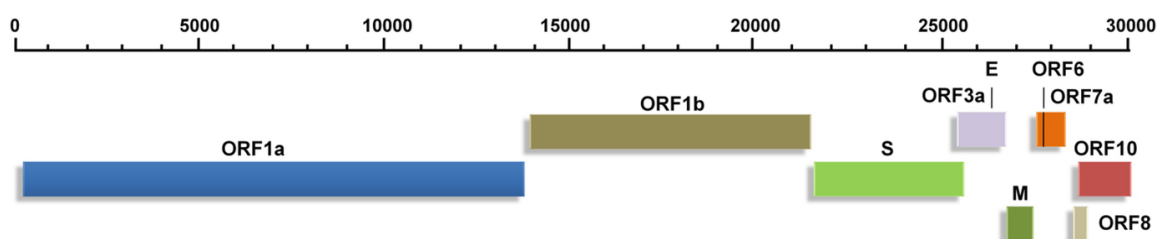

Fig 3. Genomic organization of SARS-CoV-2. (Adapted from Kumar et al., 2020)

The SARS-CoV-2 genomic RNA contains a 5'-cap structure and a 3'-poly-A tail, that allow immediate translation upon viral entry, to produce two coterminal replicase polyproteins from two large open reading frames (ORF1a and ORF1b), by utilizing a ribosomal frameshifting mechanism. Replicase polyproteins are subsequently cleaved by the action of two viral cysteine proteases, nsp3-PLpro and nsp5-Mpro, into the individual nsps, nsp1-11 and nsp1-16, respectively, which are necessary for the formation of the replication-transcription complex (RTC). Of note, nsp12 encodes for the RdRp, nsp13 for the viral helicase and nsp14 for the 3'-5' exonuclease with proofreading activity. The latter seems to have a peculiar role in the preservation of the CoV genome, which is larger in respect to other RNA viruses: the maintenance of

such genome may be related to the special features of the CoV RTC, in particular for the presence of the 3'-5' exoribonuclease (Y. Chen et al., 2020; Naqvi et al., 2020; Neerukonda and Katneni, 2020). The accessory and structural proteins constitute only the remaining 10kb of viral genome. Structural proteins include spike (S), E, M and N proteins.

The S glycoprotein plays a significant role in pathogenesis, by binding to the host cell through its receptor binding domain (RBD), which represents the most variable part of the CoV genome. It can be divided into S1 and S2 subunits, with the S1 domain containing the RBD that specifically engages the host cell receptor, thereby determining virus cell tropism and pathogenicity, while the transmembrane S2 domain containing the fusion peptide, which mediate the fusion of viral and cellular membranes upon extensive conformational rearrangements (Naqvi et al., 2020; Qing and Gallagher, 2020). A notable feature of SARS-CoV-2 is the polybasic cleavage site (RRAR) at the junction of S1 and S2, with the additional insertion of a leading proline, thus constituting the PRAAR site. This site seems to have a role in determining viral infectivity and host range and interestingly, such polybasic cleavage site has not been observed in related lineage B betacoronaviruses (Andersen et al., 2020; Coutard et al., 2020).

The E protein plays a significant role in the viral morphogenesis, pathogenesis, assembly and budding. This protein has a N-terminal ectodomain and a C-terminal endodomain and it is also act as ion-channelling viroporin, assembling into the host membrane to arrange protein-lipid pores involved in iontransport (Bianchi et al., 2020; Schoeman and Fielding, 2019).

The M protein has three transmembrane domains and it functions in concurrence with E, N, and S proteins, playing a major role in providing a distinct shape to the virus. M proteins are the most abundant viral proteins of CoVs (Naqvi et al., 2020).

The N protein constitutes the only protein present in the nucleocapsid. It plays an important role in the packaging of viral RNA into the ribonucleocapsid, by interacting with the viral genome, nsp3 and M protein during assembly. The heavy phosphorylation of N protein triggers structural changes enhancing the affinity for viral versus non-viral RNA. N protein of SARS-CoV-2 is highly conserved, sharing ~90% sequence identity with that of SARS-CoV (Cong et al., 2019; Naqvi et al., 2020).

SARS-CoV-2 has an RBD that binds with high affinity the angiotensin-converting enzyme 2 (ACE2) that can be found in humans, ferrets, cats and other species. ACE2 is a type I membrane glycoprotein which is mainly expressed in lungs, heart, intestines, and kidneys (Andersen et al., 2020; Hoffmann et al., 2020; Neerukonda and Katneni, 2020) and its binding is required as the initial step of CoV infection (Fig 4). Following receptor binding, the proteolytic cleavage of CoV S proteins by host cell-derived proteases is essential to permit fusion. The protease used by SARS-COV-2 to gain access to host cell cytosol, is the TMPRSS2, a cell-surface serine protease expressed mainly in the human respiratory tract; the S cleavage operated by TMPRSS2 represents a key event in SARS-CoV-2 replication cycle, because inhibition of TMPRSS2 is sufficient to prevent SARS-CoV-2 entry in lung cell lines and in primary lung cells (Hoffmann et al., 2020; V'kovski et al., 2020). As previously described, a peculiar feature of the SARS-CoV-2 S protein is the acquisition of a polybasic cleavage site (PRRAR) at the S1–S2 boundary, whose cleavage results in enhanced infection and it has been proposed to be a key event in SARS-CoV-2 evolution. Indeed, this pre-processing of the SARS-CoV-2 S protein may contribute to the expanded cell tropism and zoonotic potential and might increase transmissibility (Neerukonda and Katneni, 2020; V'kovski et al., 2020).

Following fusion and endocytosis, the SARS-CoV-2 genomic RNA is immediately translated. The newly formed nsps are assembled into the RTC, which begins to generate anti-sense genomic copies functioning as templates for genomic and sub-genomic RNAs. The nsps also promote membrane rearrangement of rough ER membranes, in which replication and transcription processes occur.
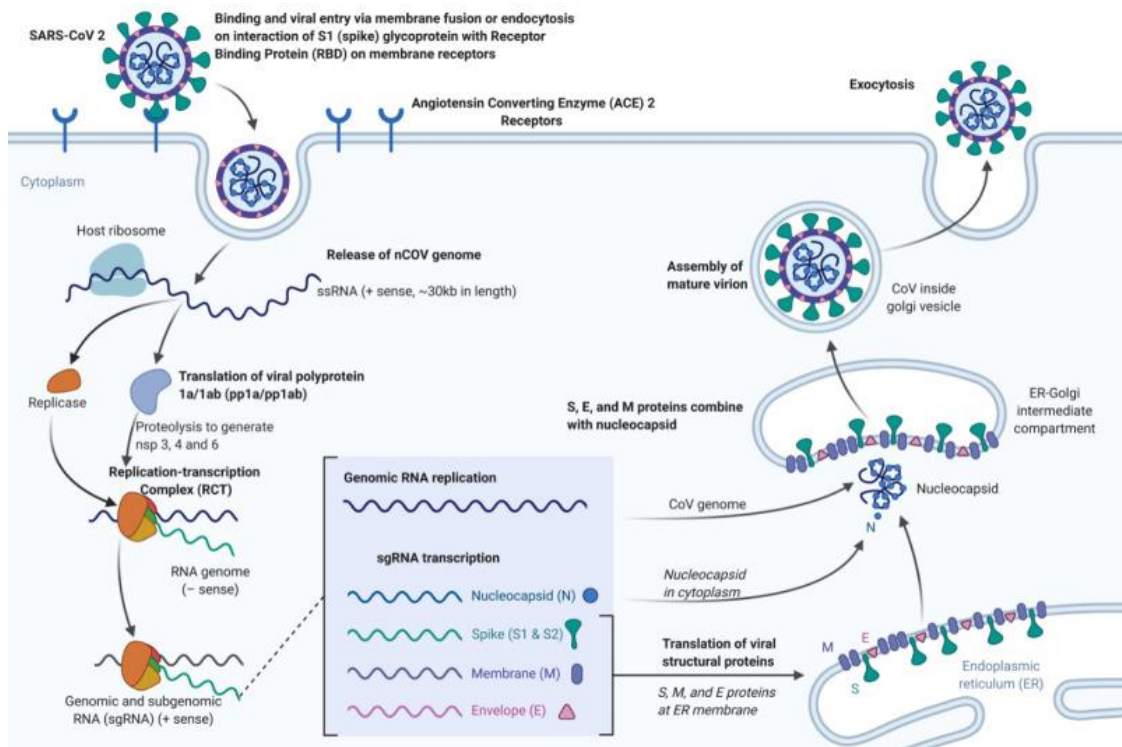
Fig 4. Binding, viral entry and replication cycle of SARS-CoV-2. (Adapted from Cascella et al., 2020)

Structural proteins translated from sub-genomic RNAs are inserted into the ER and pass along the secretory pathway to the ER-Golgi intermediate compartment. There, the newly synthesized genome forms a complex with the N protein to generate virions. Following assembly with the other structural proteins, virions are transported to the cell surface in vesicles and released outside the cell through exocytosis (Hoffmann et al., 2020; Neerukonda and Katneni, 2020; V'kovski et al., 2020).

2.3 Transmission

SARS-CoV-2 is mainly transmitted through symptomatic humans, while the role of asymptomatic people in the transmission is still debated (Gao et al., 2020; He et al., 2020; Oran and Topol, 2020), by respiratory droplets and aerosols and/or contact of mucosae with virus-contaminated fomites. Therefore, environmental factors, including temperature, humidity, stability on fomites, ventilation and filtering systems, could have a significant influence on the infection (Azuma et al., 2020; Y. Chen et al., 2020; Sungnak et al., 2020). Adequate control of these environmental factors and proper human behavior play a significant role in preventing the spread of COVID-19.

Interestingly, viral RNAs or live infectious viruses have been detected in feces and urine of patients with COVID-19. Binding of SARS-CoV-2 to the ACE2 is a vital pathway for the virus entry into human cells, whose presence is not limited to the respiratory mucosa, but is also extended to the esophageal epithelium as well as in the enterocytes from ileum and colon (Barbosa da Luz et al., 2020; Sun et al., 2020; Wang et al., 2020; Xiao et al., 2020). Therefore, a fecal-oral route of transmission for SARS-CoV-2 may be hypothesized; to date, however, there have been no published reports of transmission of SARS-CoV-2 through feces or urine. Some studies have also reported detection of SARS-CoV-2 RNA in either plasma or serum. However, the role of bloodborne transmission remains uncertain; anyway, low viral titers in plasma and serum suggest that the risk of transmission through this route may be low (Chang et al., 2020; Wang et al., 2020). There is no evidence for intrauterine transmission of SARS-CoV-2 from infected pregnant women to their fetuses, neither of breastfeeding transmission, even if viral RNA fragments have been found in a few breast milk samples, but no viable virus. As a matter of fact, WHO recommends that mothers with suspected or

confirmed COVID-19 should be encouraged to initiate or continue to breastfeed (www.who.int). Moreover, clinical course of COVID-19 in most women is not severe, and the infection does not significantly influence the pregnancy. Indeed, in most cases the disease does not threaten the mother, and vertical transmission has not been clearly demonstrated (Di Toro et al., 2020).

On this basis, to prevent SARS-CoV-2 diffusion, the WHO suggests physical distancing policy, the use of face masks in public places and frequent hand hygiene (www.who.int). Indeed, a drastic reduction of social contacts and total lockdown periods have been implemented in many countries with outbreaks of SARS-CoV-2, leading to rapid reductions in basic reproduction number (R0), defined as the average number of secondary infections produced by a typical case of an infection in a population where everyone is susceptible. In absence of measures preventing transmission, the estimate for the R0 is between 2 and 3, and the median incubation period is 6 days (range 2-14 days).

2.4 Clinical manifestations and pathogenesis

The clinical spectrum of COVID-19 can vary from asymptomatic (40-45% of infections) and mild symptomatic, to an adverse clinical condition characterized by severe respiratory failure, requiring mechanical ventilation and hospitalization (He et al., 2020; Oran and Topol, 2020). The most important risk factors for a severe disease are age, hypertension, diabetes, immunodeficiency and chronic cardiovascular and pulmonary diseases. Countries throughout the world have reported different mortality rate, ranging from 1 to 10%, with the incidence of mortality rising after the sixth decade of life (www.who.it; John Hopkins University https://coronavirus.jhu.edu/data/mortality).

Mild COVID-19 illness symptoms are those typical of an upper respiratory tract viral infection, including mild fever, dry cough sore throat, nasal congestion, malaise, headache and muscle pain. Moreover, nausea, vomiting, abdominal pain and diarrhea may occur. As the disease become more severe, patients display symptoms such as dyspnea, respiratory distress and hypoxia with oxygen saturation levels under 90%. Patients with sudden onset of respiratory failure or impaired lung function can experience SARS and require hospitalization and mechanical ventilation. Critically ill patients have systemic symptoms characterized by sepsis, septic shock, and multiple organ dysfunction syndromes (Neerukonda and Katneni, 2020).

As we currently know, severe COVID-19 symptoms are a consequence of dysregulated immune responses. Indeed, the rapid and uncontrolled viral replication of SARS-CoV-2 is able to evade the host innate immune response during its initial steps. Consequently, the quick activation of the cell-mediated response provokes an increased pro-inflammatory status with a massive release of cytokines, causing acute lung injury and contributing to the clinical manifestation of SARS (Khalaf et al., 2020). Indeed, in severe COVID-19 cases, as opposed to mild cases, an aberrant recruitment of inflammatory macrophages and the infiltration of T lymphocytes and neutrophils have been measured in the lungs.

The accumulating evidence of dysregulated pro-inflammatory responses during SARS-CoV-2 infections has led to the use of immune modulators to inhibit hyperactivated pathogenic immune responses, such as corticosteroids and tolicizumab (V'kovski et al., 2020). Corticosteroids are used to mitigate the host inflammatory response which contributes acute respiratory distress syndrome in severe pneumonia cases. However, these agents are responsible for some adverse effects, that include delayed viral clearance and enhanced risk of secondary infection (McCreary and Pogue, 2020; Neerukonda and Katneni, 2020). Tocilizumab is an approved humanized monoclonal antibody that inhibits IL-6 receptor, originally approved for the treatment of rheumatoid arthritis. IL-6 is a key driver of dysregulated inflammation that contributes to the pulmonary pathology and the organ damage observed in COVID-19 patients. Theoretically, antibodies targeting its receptor could reduce the IL-6 signal transduction and downstream inflammation, thus improving clinical outcomes (Neerukonda and Katneni, 2020; Xu et al., 2020).

2.5 Current status of antivirals and vaccines development

Considering the devastating economic and social impact of the SARS-CoV-2 pandemic, there is an unprecedently urgent need for effective therapeutics to reduce the clinical consequences of SARS-CoV-2 infection and to contain viral transmission. In addition to the use of anti-inflammatory drugs, it is necessary to develop drugs active against viral target to halt viral replication. For de-novo design of candidate compounds, therapeutic agents targeting nucleosides, nucleotides, viral nucleic acids, and enzymes/proteins involved in the replication and transcription (especially RdRp and viral proteases) of CoVs can be promising strategies (Artese et al., 2020; Khan et al., 2020). Drug repurposing has been used in response to emerging infectious diseases to rapidly identify potential therapeutics. The repurposing of drugs approved for treatment of other pathogens is a feasible and attractive strategy to deliver at least a partially effective agent(s) and mitigate SARS-CoV-2 pathology and spread. Indeed, recycling FDA approved compounds dramatically shortens the development time and cost allowing immediate drug testing in clinical trials. Viral enzymes are favourite targets for drug repurposing because specific domains are conserved within the *Coronaviridae* family and may show homology with other positive sense RNA viruses (Amin and Jha, 2020).

Among the variety of drugs that have been tested to determine whether they may have an activity against SARS-CoV-2, some of the most interesting attempts of drug repurposing are linked to the use of chloroquine, lopinavir/ritonavir and remdesivir.

Chloroquine is an anti-malarial drug approved by FDA in 1949 (www.fda.gov) with anti-inflammatory and immunomodulatory properties. It prevents endosomal acidification and interferes with glycosylation of viral entry receptors. Despite chloroquine and its derivative hydroxychloroquine demonstrated potent *in vitro* activity against SARS-CoV-2 (Wang et al., 2020; Yao et al., 2020), recent clinical trials (NCT04322123, NCT04381936) and preliminary results of others, showed evidences of little or no benefit compared to standard care for the treatment of COVID-19 (Cavalcanti et al., 2020); moreover, cardiotoxicity concerns limited the use of chloroquine in the USA (McCreary and Pogue, 2020). Hence, potential prevention and/or clinical benefits of chloroquine and hydroxychloroquine remain to be determined.

Lopinavir is a potent antiretroviral protease inhibitor used in combination with ritonavir to treat patients with HIV infection. Lopinavir/ritonavir has also been proposed as a possible treatment against SARS-CoV-2. Despite the promising *in vitro* activity (Choy et al., 2020; Jeon et al., 2020), the results of clinical trials (NCT02845843, NCT04252885) showed that the use of lopinavir/ritonavir had no significant benefit beyond standard-care, in either reduction of viral load or overall mortality (Cao et al., 2020; Li et al., 2020). Hence, the "COVID-19 Treatment Guidelines Panel" recommended the use of lopinavir/ritonavir with or without ribavirin for the treatment of SARS-CoV-2 infections only in the context of clinical trials, because of unfavorable pharmacodynamics and negative clinical trial data (https://www.covid19treatmentguidelines.nih.gov/).

Remdesivir is an adenosine analogue that function as a viral RNA chain terminator, initially developed for the management of the Ebola virus. Remdesivir has showed a high activity against SARS-CoV-2 *in vitro* (Sanders et al., 2020; Wang et al., 2020), as well as against SARS-CoV and MERS-CoV (Sheahan et al., 2017). Yet, results from clinical trials are conflicting. In a randomized trial involving more than 1000 patients (NCT04280705), remdesivir was superior to placebo in shortening the time of recovery in hospitalized adults (Beigel et al., 2020). Conversely, another clinical trial (NCT04292899) showed no significant difference in patients treated with remdesivir, whereas side effects such as nausea and respiratory problems were observed; however, such study were partially limited by the lack of a placebo control group (Goldman et al., 2020). An additional clinical trial (NCT04257656) reported no significant improvement in the clinical status, mortality, or time to clearance of virus in patients with serious COVID-19 compared with placebo (Wang et al., 2020). Therefore, clinical benefits of remdesvir remain to be further elucidated.

Recently, a large clinical trial involving 4 different treatments (remdesivir, hydroxychloroquine, lopinavir/ritonavir and IFN), the so-called Solidarity Trial (www.who.int, NCT04315948), found that all the 4 treatments had little or no effect on overall mortality, initiation of ventilation and duration of hospital stay in COVID-19 hospitalized patients.

Currently, no approved antivirals by FDA are available against SARS-CoV-2, with the exception of remdesivir, approved on October 2020 by FDA and also on July 2020 by the European Medicine Agency (EMA), despite the controversial results of clinical trials.

Apart from antiviral compounds, therapy research is also addressed to the use of neutralizing antibodies, using of convalescent plasma from recovered patients (Artese et al., 2020; Khalaf et al., 2020; Teimury and Khaledi, 2020) or use of human monoclonal antibodies, the latter showing promising results (Andreano et al., 2020; P. Chen et al., 2020; Chunyan Wang et al., 2020).

Simultaneously to antiviral development, vaccine research has been extensive too. Indeed, a vaccine is urgently needed to control the current exploding global pandemic of COVID-19 and to prevent recurrent epidemics. Currently, more than 180 vaccine candidates are in development against SARS-CoV-2. They are based on different methodologies including: (i) inactivated or live-virus vaccines, (ii) recombinant protein vaccines, (iii) vectored vaccines and (iv) RNA and DNA vaccines (Krammer, 2020). At the moment of this thesis, among all the candidate vaccines, more than 30 are under assessment in clinical trials, with 10 in phase 3 trial. Currently, phase 3 candidate vaccines can be grouped as follows: 3 are inactivated vaccines (the CoronaVac produced by Sinovac, the BBIBP-CorV of the Beijing Institute of Biological Products and one unnamed by Sinopharm in collaboration with the Wuhan institute of Biological Products), 4 are viral vectored vaccines (the ChAdOx1-S by University of Oxford/AstraZeneca; an AdV5-based vaccine by CanSino Biological; the Ad26COVS1 by Janssen; an AdV5/AdV26-based vaccine by the Gamaleya Research Institute), 1 is a recombinant spike-protein-based vaccine (NVX CoV2373 by Novavax) and 2 are RNA based vaccines (mRNA-1273 by Moderna; BNT162 produced by Pfizer in collaboration with BioNTech) (Dong et al., 2020; Jain et al., 2020; Krammer, 2020). Notably, preliminary data of phase 3 trials have been recently published for the RNA based vaccine BNT162, showing promising results with more than 90% of efficacy in preventing COVID-19 in participants.

3. Introduction – HIV-1

3.1 General Overview and Epidemiology

Human immunodeficiency Virus (HIV) was isolated for the first time in 1983 (Barré-Sinoussi et al., 1983) and later recognized as the causative agent of Acquired Immunodeficiency Syndrome (AIDS). HIV belongs to the Lentivirus group of the family Retroviridae (Chiu et al., 1985) and it is able to infect CD4 T cells causing a progressive depletion of CD4 T lymphocytes.

HIV continues to be a major global public health concern. Since the beginning of the epidemic, more than 76 million of people have been infected and almost 33 million people have died so far. At the end of 2019, there were an estimated 38 million people living with HIV (PLWH), and despite the pathogenicity of the virus is well known, in 2019 the numbers of new infections were about 1.7 million. Most of the PLWH live in low- and middle- income countries and, more precisely, 66% live in Sub-Saharan Africa.
Extensive efforts have been made to counteract the HIV epidemic. Indeed, in 2016 the Joint United Nations Programme on HIV/AIDS (UNAIDS), along with 11 united Nations Organizations, planned to end AIDS by reaching the 90–90–90 targets by 2020 (90% of people infected with HIV known about their conditions, 90% of all diagnosed people receiving antiretroviral therapy, 90% of all people receiving antiretroviral therapy having viral suppression). Even if remarkable progresses have been achieved (currently 81% of PLWH known their status, 67% are on treatment and 59% have their viral load suppressed), the global 90-90-90 target is unlikely to be met (www.unaids.org, update report 21.09.2020). According to WHO, at the end of 2019 25.4 million HIV-1 positive people were accessing ART, 19 million more in respect to 2009. However, basing on these results, the main and ambitious goal aimed to the ending of the HIV epidemic by 2030, may still be achieved.

According to the different genetic composition, two types of HIV, HIV-1 and HIV-2, originated from distinct cross-species transmission of nonhuman primate lentiviruses (Sharp and Beatrice H. Hahn, 2011), have been characterized so far and they are differently distributed worldwide. HIV-1 is responsible of the global pandemic, while HIV-2 is characterized by a reduced virulence and occurs mainly in west Africa region with sporadic cases in Europe, India and United States (Campbell-Yesufu and Gandhi, 2011).
One of the characteristic features of HIV is its exceptional genetic diversity. Genetic variability depends on three different factors: error-prone reverse transcriptase (RT), high replication rate and genetic recombination (E. Fenales-Belasio, M. Raimondo, B. Suligoi, 2010; Santoro and Perno, 2013).

Basing on genetic homology, HIV-1 is divided into four groups: M (main), N (non-M, non-O), O (outlier) and P, which have different geographic distributions, but all produce similar clinical symptoms (Santoro and Perno, 2013).
Group O correspond to less than 1% of global HIV-1 infection and it is mainly diffused in west and central African countries; group N is even less present then group O and group P, the last identified, is very infrequent; both of them are rarely identified in Cameroon (Alessandri-Gradt et al., 2018; Sharp and Beatrice H. Hahn, 2011).
Group M accounts for the most common circulating subtypes of HIV-1 and it is responsible for the global epidemic. According to accurate classification of HIV-1 sequences, 9 subtypes (A, B, C, D, F, G, H, J and K) belong to group M; in addition, some subtype can be additionally divided into distinct clusters (e.g. the subtypes A is subdivided into A1, A2, A3, A4, A5 and A6). However, the classification of such sequences is complicated by the HIV-1 high mutation rate and propensity to develop new recombinant forms. Indeed, in addition to pure subtypes, at least 102 circulating recombinant forms (CRFs) has been detected so far (http://www.hiv.lanl.gov/content/sequence/HIV/CRFs/CRFs.html, last accessed 30 September 2020) as well as multiple unique recombinant forms (URFs). CRFs indicate the case in which two unrelated subtypes of HIV-1, after sharing their genetic material, create a new hybrid mosaic virus and infect the same cell and they are identified in three or more epidemiologically unlinked individual. URFs are mosaic viruses which

have not spread from their original location (E. Fenales-Belasio, M. Raimondo, B. Suligoi, 2010; Rhee and Shafer, 2018; Santoro and Perno, 2013; Taylor et al., 2008; Tongo et al., 2016).

Despite the vast majority of data and research deal with subtype B, subtype C predominates worldwide with a prevalence of about 50%. It is mainly found in the southern African region, the Indian sub-continent, but also in east African countries, Brazil and the southern provinces of the People's Republic of China, whereas HIV-1 subtype B is most prevalent in north America, western Europe, Australia and Japan (Jacobs et al., 2014) and it is responsible for 12.1% of infections, followed by subtype A (10.3%), CRF02_AG (7.7%), CRF01_AE (5.3%), subtype G (4.6%), and subtype D (2.7%); Subtypes F, H, J, and K accounted for 0,9% of infections (Hemelaar et al., 2019) and the remaining are composed by other CRFs and URFs.

HIV-2 is divided into eight lineages (from A to H) and of these, only A and B had infected people in a relevant way (Sharp and Beatrice H. Hahn, 2011).

3.2 Genome organization and life cycle

By electron microscopy, the virion measures around 120 nm in diameter and is characterized by an icosahedral structure with a tapered inner electron-dense core, surrounded by an outermost structure that forms the envelope. The envelope is acquired during the virion budding and is made up of a phospholipid bilayer, on which are anchored the two major glycoprotein: gp120 (surface glycoprotein) and gp41 (transmembrane glycoprotein). The surface of the envelope exhibits 72 projections (spikes) formed by the heterodimers of the surface glycoproteins. The central core is composed of four viral proteins: the capsid protein (p24), the matrix protein (p17), the nucleocapsid (p7) and p6 (Hahn et al., 2014; Seitz, 2016).

The genome consists of two identical copies of single-stranded positive RNA of about 9,4 kb, which are capped at their 5' end and polyadenylated at their 3' end (Fig 5). At both 5' end and 3' end there is the presence of 150-200-nt repeated sequence (R); adjacent to them, unique regions called U5 (80-200 nt) and U3 (240-1200 nt), found at the 5' end and 3' end, respectively. The 5' LTR region codes for the promotor for transcription of the viral genes. The two identical long terminal repeats (LTR) regions are produced, during the translation process, at each terminus of the genome by juxtaposition with the U3-R-U5 orientation.

As for the other retroviruses, from 5' to 3' the viral genome contains the gene *gag*, encoding the proteins of the outer core membrane; the gene *pol* coding for the enzymes protease (PR), RT, RNase H and integrase (IN), and finally the gene *env* responsible for the production of the two envelope glycoproteins gp120 and gp41 (King, 1994). All the viral enzymes are produced by proteolytic cleavage from a large precursor molecule. The synthesis of a Gag-Pol precursor protein (p180) occurs during translation, by a ribosomal frameshift, between the open reading frame of the two genes. Subsequent cleavages of p180 yields the Gag proteins and PR (p10), RT/RNase H (p66/p51) and IN (p32).
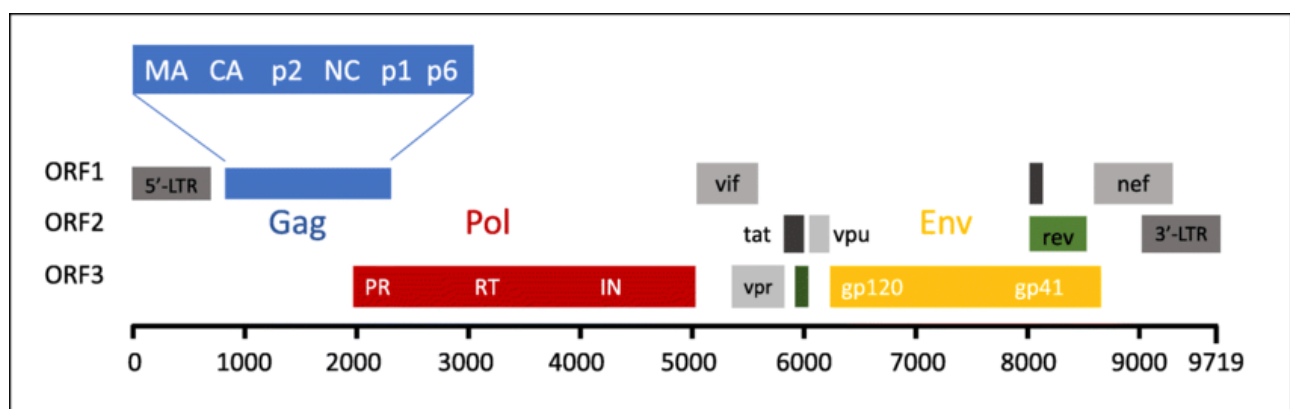

Fig 5. Schematic representation of the HIV-1 genome with its 9 coding genes. (Adapted from Cervera et al., 2019)

HIV PR is an aspartyl protease responsible for the post-translational processing of the viral Gag and Gag-Pol polyproteins and functions as a homodimer composed of two non-covalently associated monomers (Freed, 1998; Kaplan et al., 1994).

HIV RT is a heterodimer made up of p66 and p51 subunits. The p51 subunit is composed of the first 450 amino acids of the RT serving as a scaffold for p66 subunit. The latter is composed of all 560 amino acids of the entire RT-RNAseH protein, providing both to the RdRp and the specific degradation of RNA in RNA-DNA hybrid duplexes (Beard et al., 1994; Sluis-Cremer et al., 2004).

The 32-kDa IN protein is the C-terminal cleavage product of the pol region and catalyzes the insertion of viral cDNA into the host cell genome by cleaving the host DNA, then joining the linear double stranded form of the viral DNA creating covalent bonds between the ends of generated fragments. HIV IN comprises three structural domains: the N-terminal domain, the catalytic core domain and the C-terminal domain (Engelman and Cherepanov, 2012; Esposito and Craigie, 1999). Recently, it has been suggested that IN can also influence viral particle maturation, by interacting with the viral RNA genome during particle morphogenesis. Loss of IN–RNA binding leads to mislocalization of the viral genome in virions and prevents viral replication in target cells (Kessl et al., 2016).

The 55-kd Gag myristylated precursor is cleaved into the matrix (MA, p17), C (p24), N (p7), and p6 proteins during or after the release of progeny virions; as previously said, these proteins compose the central core.

Finally, the protein product of the env gene is synthesized in the endoplasmic reticulum (ER) as an 88-kDa polypeptide. This protein undergoes heavy glycosylation trough the ER and Golgi network. The resulting molecule, gp160, is cleaved by the cellular serine protease, furin, to generate the transmembrane (gp41) and surface (gp120) subunits; such cleavage is required for viral infectivity (Willey et al., 1991).

In addition to *gag*, *pol* and *env*, *tat* and *rev* genes products have been identified as regulatory proteins absolutely required for virus replication.
The 14-kDa trans-activating protein, Tat, is required for HIV-1 transcription and accumulates inside the nucleus. It enhances the rate of transcription through the binding of the transactivation response element found at the 5' end of beginning HIV transcript, and by recruiting cellular factors that improve the processivity of the cellular RNA polymerase II complex (Musinova et al., 2016; Wei et al., 1998).

The 18 kDa Rev protein mediates the transport to the cytoplasm of singly spliced and unspliced viral RNAs by the nuclear exportation system (Malim et al., 1989). Rev was also found to stimulate protein expression levels, to enhance encapsidation of the genomic RNA into virions (Blissenbach et al., 2010; Seitz, 2016) and interestingly, to inhibit the integration of the viral genome and thus playing a role in prevention of cellular superinfection (Grewe and Überla, 2010).

The other encoded four small proteins (nef, vpr, vif and vpu in HIV-1 or vpx in HIV-2) are referred to as "auxiliary" or "accessory" since, although they play a significant role *in vivo*, their expression is usually dispensable for virus growth in many *in vitro* systems.

Vif is a 193-amino acid protein presents in the cytoplasm and incorporated in the virion. It interferes with the activity of cellular protein APOBEC3G, inducing its ubiquitination and degradation by proteasomes. APOBEC3G is involved in the innate immune response and introduces mutations in the viral genome during transcription causing a reduction in the virus infectivity (Reddy et al., 2016).

Vpr is a 100-amino acid protein that is expressed late during the infection cycle and is packaged in significant quantities into virus particles through a specific interaction with the P6 domain of the viral Gag precursor. It has two main functions: (i) to prevent the proliferation of the host cells by arresting the cell cycle at the G2 phase, thus inducing cell death and progression of viral gene expression;

(ii) to allow the infection of non-dividing cells by helping the transport of the viral genome into the nucleus of the host cells (Fabryova and Strebel, 2019; Müller et al., 2000), as well as inducing proteasomal degradation of the DNA repair enzymes HLTF, UNG2 and MUS81 to prevent the restriction of viral cDNA RT products (Nodder and Gummuluru, 2019).

Vpu is an 81-amino acid single-pass trans-membrane protein that is only present during the late stages of HIV-1 infection. It prevents superinfection by inducing CD4 degradation and promotes virus release by antagonizing the restriction factor tetherin (González, 2015). Moreover, recently Vpu has been found to hijack DNA repair mechanisms to promote degradation of nuclear viral cDNA in cells that are already productively infected (Volcic et al., 2020). Vpu is absent in HIV-2, whereas its genome contains Vpx.

Nef is a 210-amino acid protein located at the inner face of the plasma membrane. It is responsible for several effects, as the downregulation of CD4 receptor by promoting its endocytosis and lysosomal degradation; the support in virus budding by removing the Env receptor from the cell surface; in reducing the expression of major histocompatibility complex class I on the cell's surface, thus limiting the ability of infected cells to be cleared by the immune system. It also activates T cells, inducing the translocation of transcription factors to the nucleus, leading to greater HIV transcription (Furler et al., 2019).

The entire replication cycle of HIV-1 is completed, *in vitro* and *in vivo*, in approximately 24 hours and can be divided into the following steps: binding and entry, uncoating, reverse transcription, provirus integration, viral protein synthesis and assembly, budding (Fig 6) (Kim et al., 1989).
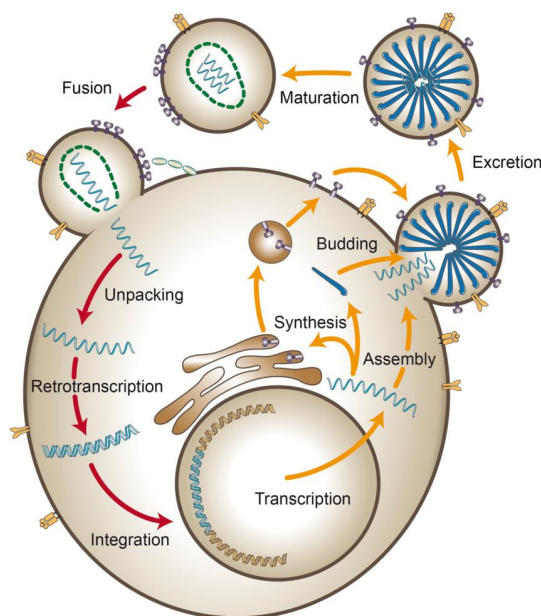

Fig 6. Schematic representation of the HIV life cycle inside a host cell. (Adapted from Cervera et al., 2019)

The binding and the entry pathways consist in a multi-step process that starts with the binding of the viral protein gp120 to the host cell CD4 receptor, which is expressed on the cell surface of macrophages, T-helper lymphocytes, hematopoietic/lymphoid lineage, dendritic cells and microglial cells. This action causes structural changes in the virus envelope, leading to the exhibition on the gp120 of a specific domain responsible of the binding with chemokine receptors and cell membrane of the virus. The interaction between the viral envelope glycoprotein, gp120, and the cellular receptor molecule, CD4, is the first step of the HIV-1 replication cycle. Although binding of virions to CD4 is essential for HIV infectivity, their subsequent interaction with a coreceptor, belonging to seven membrane-spanning CC or CXC families of chemokine receptors, is required for membrane fusion and entry (Choe et al., 1996). The most important chemokine coreceptors involved in the fusion of virion particles to the cell membrane are the CXCR4

(primarily localized in memory and naïve T cells, hematopoietic cells and thymocytes) and CCR5 (primarily used by macrophage and dendritic cells). Dual-tropic (R5X4) isolates can interact with either CCR5 or CXCR4 and can therefore infect both T cell lines and macrophages. Because primary lymphocytes express both CCR5 and CXCR4, they can be infected by X4, R5, and R5X4 isolates (E. Fenales-Belasio, M. Raimondo, B. Suligoi, 2010; Kuritzkes, 2009). In physiological conditions, the chemokines RANTES, MIP-1-α and MIP-1-β are the ligands for the CCR5 receptor, whereas the α-chemokine SDF-1 is the ligand for CXCR4.

Since the formation of a gp120/CD4/co-receptor complex, gp41 adopts a conformation that allows the interaction and the fusion between the viral and cellular membranes (Engelman and Cherepanov, 2012; Wu et al., 1996). Following entry, viral particles are partially uncoated in the cytoplasm and the viral RNA is reverse transcribed into a double strand of DNA (cDNA) by RT.

Conversion of RNA to DNA happens in the cytoplasm, starting at the primer-binding site of the viral RNA, involving involves two enzymatic activities of RT: polymerase and RNase H activities. The copying of the viral RNA into a minus-strand DNA is initiated at the 5' end of the primer binding sequence region using a tRNALys acting as a primer. The resulting RNA–DNA duplex is almost completely degraded by RNase H activity. Only the 3' polypurine tract, found to the left of U3 sequence, is resistant to RNase H degradation allowing its use as the primer for the plus-strand DNA synthesis during the reverse transcription process. The final result is the proviral DNA, a linear, double-stranded DNA longer than the RNA genome because of the presence of LTR regions at both ends generated during the retrotranscription process (Cimarelli and Darlix, 2014; Malet et al., 2019). Interestingly, it has been recently described that that nuclear import occurs relatively rapid, preceding the completion of reverse transcription in target cells, demonstrating that reverse transcription may be completed in the nucleus (Dharan et al., 2020). Following reverse transcription, IN, together with pre-integration complex with cellular and viral proteins made of both cellular and viral proteins, catalyses insertion of the viral DNA into the genome of the host cell through two sequential reactions: 3' processing and strand transfer (E. Fenales-Belasio, M. Raimondo, B. Suligoi, 2010; Malet et al., 2019).

Host enzymes complete the integration process by repairing the single-strand gaps abutting the unjoined viral DNA 5' ends, resulting in establishment of a stable provirus (Engelman and Cherepanov, 2012). As IN associates with the ends of the HIV DNA, the internal HIV sequence can be also defective or deleted, making the HIV proviral integration highly diverse in an individual. The exact sites of viral cDNA integration into the host genome is still to be defined; however, studies report that HIV integration site preferences include actively transcribed genes, gene rich regions of chromosomes, introns over exons, and generally exclude promoter regions (Anderson and Maldarelli, 2018).

Once inside, the proviral DNA is replicated together with DNA host. Activation of HIV transcription and gene expression is dependent on the activity of both cellular (Sp1, NFkB, and others) and viral (Tat) factors. The primary transcript is spliced by a finely regulated strategy to generate over 30 species of alternative viral mRNAs. The early proteins Tat, Rev and Nef increase the level of viral transcription, promoting transcription of other genes and exportation of viral mRNA from the nucleus into the cytoplasm.

The virion assembles at the plasma membrane when the genomic RNA is associated with the nucleocapsid proteins. The specificity of HIV-1 genome encapsidation results from an interaction between N and an approximately 120-nt sequence, known as the packaging signal or ψ-site, located between the 5' LTR and the Gag initiation codon (Berkowitz et al., 1996). The immature virion acquires its envelope by budding from the cell surface. In this step, in addition to the viral encoded proteins, virions incorporate several cellular proteins, including major histocompatibility antigens, intercellular cell adhesion molecules such as ICAM-1 and cyclophilin A. This strategy is believed to enhance the infectivity of the new viral particles.

HIV buds from specialized regions of the plasma membrane which are enriched in cholesterol and glycolipids. Presumably this envelope modified lipid composition facilitates virion morphogenesis and the

fusion with target cells (Nguyen and Hildreth, 2000). The final step of the viral life cycle is mediated by PR and occurs concomitant with or soon after budding, converting immature particles to infectious virions via the proteolysis of the precursor peptides Gag and Gag-Pol to yield the structural components MA, C and N, and the enzymes PR, RT and IN (Engelman and Cherepanov, 2012).

3.3 Route of transmission and natural history of infection

HIV-1 infection is the result of direct inoculation across a mucosal surface that may occur in case of sexual contact, parenteral or vertical transmission. Nowadays, the sexual transmission is the most common route, due to the exchange of semen, genital secretion or blood from an infected individual to the uninfected partner; however, the transmission from contaminated blood, blood products or transplantation of infected tissues account for the greatest risk (with as much as 95% persons becoming infected). Vertical transmission from mother to child occurs occasionally during pregnancy (intrauterine infection), during childbirth or during breast-feeding. The risk of mother-to-child transmission is 25 to 60% in untreated women, but it is dramatically reduced by prophylactic treatment of the mother with antiretroviral drugs and with bottle feeding (Abrams, 2004; Shaw and Hunter, 2012).

The natural history of HIV-1 infection can be divided into three phases: primary or acute infection, asymptomatic or paucisymptomatic period and symptomatic stage or opportunistic diseases stage. After the inoculation, HIV pass through mucosal, submucosal and lymphoreticular tissue while it is replicating. During the initial phase the virus directly infects and kills susceptible cells, eventually producing a high viremia that spreads the virus throughout the body (Melhuish and Lewthwaite, 2018). The time from exposure to the onset of signs and symptoms is approximately 10 to 30 days. A typical presentation may include acute onset of fever, lethargy, maculopapular rash, myalgia, headache, sore throat, cervical lymphadenopathy, arthralgia, oral ulcers, photophobia, oral candida, and rarely meningoencephalitis. The CD4 T cell count usually diminishes, reflecting both virus induced CD4 T cell depletion and sequestration of circulating CD4 T cells in lymphoid organ. After the acute illness resolves, CD4 T cell counts generally rise again but usually not to pre-infection levels. Typically, viremia decreases to a virus-host specific plateau level defined as the viral "set-point". Virus specific CD8 T lymphocytes appear early and help to reduce the level of circulating virus through the lysis of infected cells and also through the release of chemokines, which inhibit HIV-1 entry. At this point the CD8 T cells count is increased, and there is an inversion in the CD4/CD8 ratio, a hallmark of HIV-1 infection that will never be restored to normal levels even in the presence of successful therapy (McCune, 1995; Sabin and Lundgren, 2013).

Primary HIV-1 infection is followed by an asymptomatic period, characterized by a virologic quasi-steady state. The clinical latency is caused by a latent reservoir made up of proviruses integrated into the host cell genome and not transcriptionally active. The most important feature of this period is the gradual loss of CD4 T cells, caused by continuous viral replication. The arise in viral load is proportional to CD4 T cells loss, and the CD4 T cells count reflects the degree of impairment of immunological function and the consequent risk of opportunistic infections. The duration of this phase is highly variable, depending on still ununderstood virus and host genetic factors. A very small number of individuals called long-term non progressor, instead, can remain in the asymptomatic phase for decades even without taking antiretroviral therapy (ART) treatment. Due to some genetic mutations or immune system modifications, there are capable to maintain their CD4 T cells count stable and levels of viremia low, probably due to a natural control of HIV replication by the immune system (E. Fenales-Belasio, M. Raimondo, B. Suligoi, 2010).

The last phase is a clinically symptomatic stage, which is consequence of the progressive and profound deterioration of the immune system. When the CD4 T cell count drops to AIDS-defining levels (CD4 T cell count less than 200/µl) opportunistic infections, neoplastic diseases, and wasting syndrome can occur often being the cause of death in untreated individuals (Melhuish and Lewthwaite, 2018).

3.4 Antiretroviral therapy and current guidelines

The primary goals of ART are to improve the quality of survival and prolong the duration of life by restoring the immunological function, reducing the HIV-associated morbidity and maximally suppressing plasma HIV viral load.

Since ART introduction, the death of infected people decreased of 80% in industrialized countries. The drugs are divided in seven classes include the nucleoside/nucleotide RT inhibitors (NRTIs), non-nucleoside RT inhibitors (NNRTIs), protease inhibitors (PIs), integrase strand transfer inhibitors (INSTIs), a fusion inhibitor, a CCR5 antagonist and two attachment inhibitors. In addition, two drugs, ritonavir and cobicistat are used as pharmacokinetic enhancers (or boosters) to improve the pharmacokinetic profiles of PIs and the INSTI elvitegravir. All these drugs have a different target during the viral life cycle (Melhuish and Lewthwaite, 2018; Rathbun, 2018).

NRTIs: NRTIs inhibit the synthesis of viral DNA carried out by the RT. NRTIs are active against both HIV-1 and HIV-2. NRTIs mimic the structure of the DNA nucleoside bases, thus they are able to be incorporated into the proviral DNA chain with higher affinity than natural bases and to stop its elongation (Cihlar and Ray, 2010). Due to their low genetic barrier to the development of drug resistance, NRTIs are always administrated with other antiretrovirals (Geretti and Easterbrook, 2001; Luber, 2005).

NNRTIs: this class of drugs includes compounds active against only HIV-1 due to the specificity of the substrate. Differently to NRTIs, NNRTIs bind to the p66 subunit of the RT, inducing a conformational change in the enzyme that inhibit the enzymatic activity of reverse transcriptase (De Clercq and Li, 2016; Rathbun, 2018). A recently approved NNRTI, doravirine, seem to have a distinct resistance profile with respect to the other NNRTIs (Colombier and Molina, 2018).

PIs: this class of drug represents one of the most important elements in the combination therapy considering their potency in viral replication inhibition. They act against both HIV-1 and HIV-2 (De Clercq and Li, 2016). PIs imitate the substrate transition state, creating an interaction between its hydroxyl group and the carboxyl group of the active site of the protease, inhibiting the cleavage of polypeptides and resulting in the generation of not infectious viral particles. First-generation PIs were characterized by a modest antiviral activity but a low genetic barrier. However, second-generation PIs (e.g. darunavir) have overcome these limitations, showing a more favourable safety profile and a greater antiviral potency, as well as an increased genetic barrier (Fernández-Montero et al., 2009; Wensing et al., 2010).

INSTIs: molecules belonging to this class block the strand-transfer step of viral DNA integration into the host genome through competitive binding with cellular DNA to the active site of the enzyme. Despite first generation INSTIs were characterized by a moderate genetic barrier, second generation INSTIs (e.g. dolutegravir) have overcome this problem (Max, 2019). Second-generation INSTIs are recommended in ART-naive HIV-infected patients, based on their improved tolerability and once-daily dosing for many patients (De Clercq and Li, 2016; Malet et al., 2019; Rathbun, 2018).

Fusion inhibitor: enfuvirtide is the only approved fusion inhibitor and is able to prevent the fusion between cellular and viral membranes (Reeves et al., 2005). Enfuvirtide is no longer used, since it requires a twice-daily subcutaneous injections and the occurrence of side effects at the site of injection (Rathbun, 2018).

CCR5 antagonist: this drug class is represented by maraviroc (MVC), approved in the 2007 (Yost et al., 2009). This small molecule binds to the CCR5 coreceptor, avoiding the interaction between the V3 loop and therefore the fusion with the cellular membrane. MVC is effective only in patients harboring CCR5 tropic viral populations, while no efficacy was observed against CXCR4 tropic viruses (Rathbun, 2018), hence a tropism test is strictly recommended.

Attachment inhibitor: this class is represented by two compounds, ibalizumab and fostemsavir. Ibalizumab is a monoclonal antibody recently approved for the treatment of multidrug resistant HIV-1. Ibalizumab avoids the viral entry by halting the formation of CD4-HIV envelope complex through its binding to CD4 extracellular domain 2; ibalizumab is active against both CCR5 and CXCR4 tropic viruses (Emu et al., 2018; Kufel, 2020). Fostemsavir, a prodrug of the attachment inhibitor temsavir, binds directly to the gp 120 subunit within the HIV envelope and selectively inhibits the interaction between the virus and cellular CD4 receptors, preventing attachment. Fostemsavir has been approved for the treatment of HIV-1 patients on 2020 by FDA, but currently is not licensed by EMA (Markham, 2020).

Current guidelines recommend that ART should be start immediately or as soon as possible after diagnosis, regardless of CD4 count, in order to improve the rate of virologic suppression among persons with HIV and to reduce the risk of HIV transmission. Drug resistance test is recommended at diagnosis to guide treatment selection depending on the presence of transmitted drug resistance mutations (http://aidsinfo.nih.gov/guidelines; European AIDS Clinical Society, version 10.1, 2020).

The initial ART regimen generally consists of two NRTIs plus a second generation INSTI (dolutegravir or bictegravir), or an NNRTI (rilpivirine or doravirine), or a boosted PI (darunavir). As shown in many clinical trials, this strategy has resulted in suppression of HIV replication and in increased CD4 count in most people with HIV. Additional data now support the use of the two-drug regimen composed by the INSTI dolutegravir plus the NRTI lamivudine for initial treatment of people with HIV RNA <500,000 copies/mL (Cahn et al., 2020)(http://aidsinfo.nih.gov/guidelines 2019; European AIDS Clinical Society, version 10.1, 2020).
Drugs belonging to other classes are mainly recommended in second line regimen and/or in patients who lack sufficient treatment options to construct a fully suppressive regimen, mainly due to their adverse effects or costs.

In patients with suppressed viremia, meaning HIV-viral load < 50 copies/mL for at least 6 months, several clinical trials have explored switching or simplification strategies. The objectives of treatment modification should ideally eliminate or decrease adverse events, thus improving the quality of life. In particular, there is growing evidence that some two-drug simplification regimens are effective in maintaining virologic control in patients who initiated therapy and achieved virologic suppression with three-drug regimens, especially switching on dual regimens containing dolutegravir. Monotherapy for treatment simplification is not recommended by several guidelines. However, studies have assessed its efficacy and safety in patients with no baseline mutations or prior virologic failure (Pandit et al., 2019).

3.5 HIV-1 latency and eradication strategies

A hallmark of retroviruses, and a key step in the HIV-1 replication cycle, is the integration of the HIV-1 DNA into the host genome. Despite the success of ART to block viral replication and halt disease progression, ART is not a cure and cannot completely clear the infection, since HIV-1 is able to persists in blood and anatomic compartments for years (Anderson and Maldarelli, 2018; Ventura, 2020). Indeed, viral rebound from the latent reservoir following ART cessation is rapid, leading to detectable viremia within weeks of therapy interruption (Chun et al., 1999; Davey et al., 1999).

Despite the concept of reservoir is known from the introduction of the ART (Chun et al., 1997, 1995; Finzi et al., 1997), the molecular mechanisms leading to the establishment of reservoir and HIV persistence have still to be completely elucidated.
The latent reservoir is established when cells harboring proviral DNA are reverted to a resting phenotype with reduced gene expression, causing the cell to be non-permissive for HIV-1 production but providing a sanctuary to evade the immune response and ART (Thomas et al., 2020). The majority of the reservoir exists as defective provirus (about 90% are defective), unable to support HIV-1 infection due to deletions, insertions and hypermutation introduced into the genome during reverse transcription or by genes

activated by innate immunity such as APOBEC3G (Bruner et al., 2016a; Ho et al., 2013). However, defective HIV-1 proviruses have a role in the infection too: interestingly, the majority of them conserve intact promoter function, with the potential to express viral antigens upon stochastic reactivation, providing an important source for chronic immune activation.

Due to the extremely long half-life (~ 43–44 months) of some cellular population permissive for HIV infection, the natural decay of the latent reservoir in the absence of viral replication has been estimated in about 73 years. Therefore, all HIV-1-infected individuals need to take life-long ART (Anderson and Maldarelli, 2018; Liu et al., 2020). Indeed, if antiretroviral treatment is interrupted, viremia rebounds to near pre-therapy levels within weeks in most patients (Anderson and Maldarelli, 2018; Ventura, 2020).

Even if HIV-1 infects numerous host cell types of lymphocyte and myeloid lineage in diverse anatomic compartments (Anderson and Maldarelli, 2018; Wong and Yukl, 2016), the main cellular reservoir consists of resting memory CD4 T cells, since they contain 16-fold more integrated HIV DNA than naïve cells (Anderson and Maldarelli, 2018; Pinzone and O'Doherty, 2018). Memory T cells can be categorized into five general groups: central memory cells, transitional memory, effector memory cells, tissue-resident memory, and stem cell memory. Each group is defined phenotypically by the surface expression of specific chemokine and homing receptors (Vanhamel et al., 2019; Ventura, 2020) and studies have shown that the different CD4 memory T cell subsets are infected to a different extent and may support viral persistence through various mechanisms (Avettand-Fènoël et al., 2016).

Since its discovery, the stability of the latent reservoir was believed to be due to the natural longevity of different subsets of resting memory CD4 T cells. However, recent works suggest that HIV-1- infected cells undergo clonal expansion, with the proportion of clonally expanded HIV-1-infected cells increasing over time: this suggests that the persistence of HIV-1-infected cells is not due to the same infected cells that remain unchanged over the course of ART, but rather that even if the size of the HIV-1 latent reservoir does not change over time, the cells that maintain this reservoir expand over time (Liu et al., 2020; Thomas et al., 2020). Also other factors may contribute to the persistence of reservoirs, for instance residual viral replication during suppressive ART may indirectly maintain the latent reservoir (Anderson and Maldarelli, 2018; Ventura, 2020).

In this context, developing strategies to eradicate or control HIV-1 without ART are a high priority. Currently, only two people have been cured, the so-called Berlin and London patients, both tested negative for viral rebound for over 10 and 2 years, respectively, without ART (Gupta et al., 2019; Hütter et al., 2009). Both patients were affected by leukemia: during pretransplant therapy the infected cell pool was significantly depleted, followed by stem cell transplantation with homozygous CCR5Δ32 mutation donor cells (Liu et al., 1996). However, due to the relative paucity of these donor cells and the unique circumstances predetermining these cases, this type of cure is not feasible for widespread use (Thomas et al., 2020).

The majority of current efforts are concentrated on the so-called 'Shock and kill' strategy, a method proposed to eliminate latently infected cells, involving the use of small molecules, named latency reversal agents (LRAs), to induce viral transcription (shock), followed by the clearance of the reactivated cells (kill) (Walker-Sperling et al., 2016; W. Xu et al., 2017) (Fig 7). Reactivating HIV-1 latent cells exposes them to attack by the host immune system, but native responses may need to be enhanced in order to achieve full eradication of the reservoir. Different approaches involving the use of small molecules and broadly neutralizing antibody immunotherapies have been proposed as killing agents (Ventura, 2020). Currently, several compounds are being considered as LRAs in latently infected cells, and can be divided in six different groups basing on their mechanism of action: histone post-translational modification modulators, non-histone chromatin modulators, NF-κB stimulators, TLR agonists, extracellular stimulators, and a miscellaneous category of unique cellular mechanisms (Abner and Jordan, 2019). Unfortunately, many compounds able to exert a latency reversal activity *in vitro* are mitogenic compounds (e.g.

phytohaemagglutinin and phorbol myristate acetate, PMA) and cannot be used *in vivo* therapies (Spina et al., 2013).
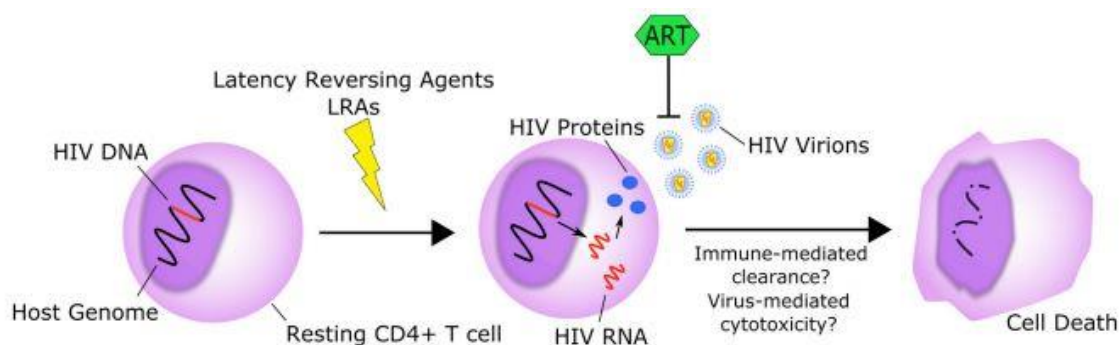

Fig 7. The schematic idea of the ''shock and kill'' strategy. (Adapted from Kim et al., 2018).

One effective single-compound in CD4 T cells was the protein kinase C (PKC) agonist bryostatin-1, which unfortunately resulted to be clinically toxic (Bullen et al., 2014). Additionally, clinical trials using the Histone deacetylase inhibitor valproic acid also failed to show significant reduction of the latent reservoir in treated patients (Archin et al., 2010; Siliciano et al., 2007). Alternative approaches for reservoir reactivation include targeting innate immune recognition pathways. Indeed, TLR-7 activation by the agonist GS-9620 has been demonstrated to promote profound reactivation of CD4 T cells via increased levels of type II IFN (Tsai et al., 2017).

Undoubtedly, a major challenge in this approach is the ability to achieve broad and efficient latency reversal without eliciting toxic side effects. Perhaps, combinations of LRAs could have improved effects by acting on different mechanisms; indeed, synergy between multiple combinations of LRAs has so far been identified *in vitro* (Thomas et al., 2020).

Recently, a novel cure strategy called "block and lock" has been proposed. Rather than inducing latency reversal, this strategy is aimed to reinforce latency to prevent viral rebound following ART interruption, utilizing small interfering RNAs to induce transcriptional gene silencing (Méndez et al., 2018; Mousseau et al., 2015). Even if this approach may offer an alternative cure mechanism to "shock and kill", its development is still in preliminary stages and is yet to be tested in human trials.

Another curative strategy is represented by promising gene editing tools, such as CRISPRCas9 and zinc-finger nucleases. Gene editing approaches have the advantage of highly specific gene targeting, so unlike LRAs, can produce the desired outcome without global physiological impact. Nevertheless, off-target effects have been observed in several studies and may affect the safety of these methods (Kimberland et al., 2018).

Finally, therapeutic vaccination aims to eliminate or significantly diminish rebound viremia by administering the vaccine regimen during sustained ART in patients with viral suppressed viremia, followed by a period of ART interruption. However, Davenport et al. suggest that, even with highly efficacious vaccines, rebound viremia would likely emerge within 5 weeks following ART interruption (Davenport et al., 2019).

However, to achieve clinically significant effects, all these mechanisms must affect the majority of the latent reservoirs, which is a major challenge considering the variety of anatomical compartments hosting a significant proportion of latently infected cells (Thomas et al., 2020).

3.6 Methods to assess viral latent reservoirs

Measuring the results of HIV-1 cure and vaccine strategies requires highly sensitive and accurate assays and there is currently no consensus of the most appropriate method to utilize. Several technical challenges limit the ability to measure accurately the size of the latent reservoirs.
Existing methods able to assess latent reservoirs can be divided in two different categories: cell culture-based assays and PCR-based assays.

Among the cell culture-based assays, the viral outgrowth assay (VOA) is regarded as the gold standard for the measure of the replication competent provirus. In this assay, dilutions of CD4 T cells are stimulated to reverse latency and drive HIV-1 expression from integrated provirus (Laird et al., 2013; Siliciano and Siliciano, 2005). Following activation, viral outgrowth is supported by incubation with CD4 T cells from HIV-1 negative donors for 2–3 weeks and measured via the detection of p24 capsid antigen. Cell positive are quantified and the frequency of cells latently infected with intact provirus is determined based on Poisson distribution and expressed as infectious units per million cells. The major drawback of VOA is the underestimation the size of the intact latent reservoirs by ~25 to 60-fold due to the presence of non-inducible replication competent viral proviruses (Bruner et al., 2016b; Ho et al., 2013). Furthermore, it is expensive, labor and resource intensive and it requires the presence of a biosafety level 3 facility. Recently, extensive analysis of VOA performance using the same samples across different labs has indicated significant variability of results (Rosenbloom et al., 2019).
Several improvements of the VOA have attempted to overcome these limitations, including the use of continuous cell lines to improve reproducibility (Badia et al., 2018; Buzon et al., 2014; Fun et al., 2017; Laird et al., 2013; Massanella et al., 2018), the use of qPCR to detect HIV-1 RNA (Laird et al., 2013) or utilizing improved p24 ELISA to increase sensitivity (Passaes et al., 2017).
Similar to VOA, another recently developed culture-based assay is the TZM-bl cell-based assay (TZA). This assay utilizes the TZM-bl cell line, which stably expresses CD4, CCR5, and CXCR4, and carries an integrated copy of the β-galactosidase and luciferase genes under control of the HIV-1 LTR promoter, allowing the detection of inducible replication-competent HIV-1. This assay is regarded as more sensitive (the inducible latent HIV-1 reservoir is approximately 70-fold larger than previous estimates), cost-efficient, and faster than the VOA (Gupta et al., 2017; Sanyal et al., 2019). However, this method is quite recent and lack of robust data necessary for comparative analyses.

Conversely, PCR-based assays offer a more practical, fast and relatively inexpensive approach to measure the size of the viral reservoir by the quantification of the total amount of HIV-1 DNA (Ho et al., 2013; Thomas et al., 2020). Total HIV-1 DNA quantification has been shown to predict viral rebound (Williams et al., 2014) and differential methods have been improved, offering the potential to identify different DNA forms, such as integrated HIV-1 DNA, non-integrated HIV-1 DNA (2-LTR and 1-LTR circular forms) (Avettand-Fènoël et al., 2009; Friedrich et al., 2010; Mexas et al., 2012; Vandergeeten et al., 2014). Anyway, several factors affect the specificity, accuracy and reproducibly of HIV-1 DNA assays and in absence of standardized methods the reproducibility of results between different laboratories must be investigated. Another key determinant of the accuracy and specificity of HIV-1 DNA quantification assays is the genomic location at which the primers and probes anneal; indeed, primer mismatches in target regions may result in false negative quantification. Moreover, amplification efficiency may be affected by the DNA input and the presence of inhibitory contaminants (Rutsaert et al., 2018b; Thomas et al., 2019). Digital droplet PCR (ddPCR) platform partially overcome these issues, since it provides absolute quantification of samples as well as showing a higher accuracy, precision and reproducibility; furthermore, factors that reduce PCR efficiency should not impair the accuracy of quantification. For these reasons ddPCR is becoming increasingly popular in HIV-1 research and clinical trials (Rutsaert et al., 2018a; Trypsteen et al., 2016).
In addition, PCR based assays rely on amplification of short genomic regions to quantify the amount of HIV-1 DNA. As a matter of fact, they are not able to distinguish between intact and defective provirus and therefore overestimate the size of the latent reservoir (Bruner et al., 2016b; Eriksson et al., 2013; Ho et al., 2013). Several assays have been developed to overcome this limitation. Quantification of cell associated

HIV-1 RNA (CAR) following CD4 T cell activation may be used as a surrogate for measuring the size of the inducible latent reservoir (Cillo et al., 2014; Pasternak et al., 2012; Shan et al., 2013); moreover, as well as CAR, by measuring cell-free HIV-1 RNA (CFR) from culture supernatant, indicative of virus release from cells, it is possible to more closely predict replication competence (Cillo et al., 2014; Massanella et al., 2018). However, these methods are prone to false positive results, since cells harboring defective provirus are still capable of producing HIV-1 mRNA following T cell activation, despite being unable to generate infectious virions.

A novel assay, the tat/rev induced limiting dilution assay (TILDA), has been developed to enhance accuracy and to reduce limitations of CAR and CFR quantification. TILDA relies on measurement of tat/rev transcripts from cells plated in limiting dilution, following activation with strong inductors; results obtained from TILDA quantification correlate well with HIV-1 DNA quantification, but not with those obtained from VOA, hence still susceptible to overestimating the size of the latent reservoirs due to the possibility that these transcripts arise from cells with defective HIV-1 genomes (Procopio et al., 2015).

More recently, a novel assay known as the intact proviral DNA assay (IPDA) has been developed. IPDA consists of a multiplexed ddPCR to measure the size of the intact latent reservoirs, relying on the presence of regions that are frequently mutated in defective genomes; the presence or absence of these regions is sufficient to distinguish 90% of defective genomes (Bruner et al., 2019) By determining replication competence based on DNA composition, this assay is not dependent on T cell stimulation and is therefore not impaired by the presence of non-inducible, intact proviruses that contribute to underestimation in the VOA. However, as for all PCR based HIV-1 assays, primer mismatches in target regions may result in false negative quantification.

4. Development of a Cell-Based Immunodetection Assay for Simultaneous Screening of Antiviral Compounds Inhibiting Zika and Dengue Virus Replication

Considering the potential impact on public health, the worldwide emergence of arboviral infections constitutes a global challenge to both high and low/middle-income countries. However, despite the urgent need for effective treatment, specific antiviral therapy for the management and the transmission control of flavivirus diseases is an unmet medical need (Silva et al., 2018).

High-throughput screening of libraries of small molecules is a powerful tool to identify novel flavivirus antivirals and several promising drug candidate molecules have been synthesized by de novo design targeting viral or host proteins. Parallelly, repurposing of "old" drugs to identify compounds with novel activity can be a useful tool to overcome the high cost and the time required for the antiviral drug-discovery pipeline (Balasubramanian et al., 2016; Boldescu et al., 2017).

In the area of drug discovery, the development of methods for the assessment of antiviral effects *in vitro* is a key approach for the screening of either de novo or repurposed candidate compounds. Indeed, following in silico analyses, *in vitro* screening is an essential step of every candidate compounds before the *in vivo* assessment. Among the variety of methods that have been developed (Gong, 2013), cell-based assays are the most predictive methods to define antiviral activity. Candidate antiflavivirus compounds are usually screened on monkey (VERO E6) or insect (C6/36) cell lines; however *in vitro* screening and analysis of candidate antiviral drugs is best performed by using human cell lines, which are more representative for *in vivo* drug therapy (Julander et al., 2017b; Sacramento et al., 2017).

In this context, the development of robust, easy-to-perform, and fast cell-based assays is highly valuable to test candidate inhibitors. Despite PRA is considered the gold standard method for titration of flavivirus and for the determination of antiviral activity of investigational compounds, this procedure is not amenable for high-throughput screening of candidate antivirals (Boldescu et al., 2017).

Consequently, in this study we developed a fast and accurate flavivirus immunodetection assay (IA) which allows the simultaneous quantification of ZIKV and DENV viral antigen in infected human hepatoma Huh7 cell line, using a specific monoclonal antibody which binds to the fusion loop of domain II of protein E, which is conserved among flaviviruses. This assay was applied as the read-out of a direct yield reduction assay (YRA), to determine the inhibitory effect of reference compounds. To validate the assay, sofosbuvir and ribavirin half-maximal inhibitory concentrations (IC_{50}) were determined in direct YRA using different viral inputs (100, 50 and 25 50% tissue culture infectious dose, $TCID_{50}$) and compared with values obtained by PRA and with values previously reported in the literature. In the direct YRA, at 100, 50, and 25 $TCID_{50}$, sofosbuvir IC_{50} values were 5.0 ± 1.5, 2.7 ± 0.5, 2.5 ± 1.1 µM against ZIKV and 16.6 ± 2.8, 4.6 ± 1.4, 2.6 ± 2.2 µM against DENV; ribavirin IC_{50} values were 6.8 ± 4.0, 3.8 ± 0.6, 4.5 ± 1.4 µM against ZIKV and 17.3 ± 4.6, 7.6 ± 1.2, 4.1 ± 2.3 µM against DENV. Based on reproducibility within replicates and correlation with PRA, the viral input corresponding to 50 $TCID_{50}$ was set as the optimal amount to perform the direct YRA.

In addition, viral stocks generated in the direct YRA can be transferred to a second cell culture in the absence of drug (secondary YRA), to better characterize antiviral activity exerted at steps occurring later than envelope expression. To evaluate the ability of the system to discriminate between early and late antiviral effects, the IC_{50} of celgosivir, an α-glucosidase inhibitor acting at late steps of DENV infection, was determined by both a direct and secondary YRA, as well as by the reference PRA against both viruses. In agreement with the proposed mechanism of late action, no antiviral activity was reported for the direct YRA, while celgosivir was able to inhibit DENV replication in the secondary YRA (IC50 11.0 ± 1.0 µM), really close to PRA IC_{50} (10.1 ± 1.1 µM) and to literature results.

In summary, the IA developed in this work combines several advantages with respect to the gold standard PRA and/or to other methods aimed to define antiflavivirus activity, including i) the use of the same protocol for two different viruses, (ii) the ability to distinguish between early and late antiviral effects, (iii) an automated readout directly proportional to virus production and consequently to virus inhibition,

opposed to manual and error-prone counting, (iv) the possibility to perform the entire assay within 6 days, compared to 8 and 13 days for ZIKV and DENV, respectively.

Thus, the system provides an opportunity to expand the potential for fast cell-based screening of multiple compounds for anti-flavivirus therapy.

All data can be found in the attached paper at the end of the thesis (Vicenti et al., 2020a).

5. Evaluation of sofosbuvir activity and resistance profile against West Nile virus *in vitro*

Parallelly to ZIKV and DENV, no therapy is available also for WNV, which can cause severe neurological disease in a small portion of infected patients. Hence, the identification of therapeutic options would achieve a strong reduction in WNV-associated morbidity and mortality (Kok, 2016).

Sofosbuvir is a nucleotide analog licensed for the treatment of HCV infections, which target the HCV RdRp and it is able to exert a potent inhibitory activity against this virus (Götte and Feld, 2016). Given the high degree of structural homology observed among RdRp enzymes within the Flaviviridae family (Lim et al., 2013), the antiviral activity of sofosbuvir has been recently evaluated as an anti-flavivirus lead candidate, showing inhibitory activity against ZIKV and YFV both *in vitro* and in animal models, as well as against DENV *in vitro* (de Freitas et al., 2019; Mesci et al., 2018; Sacramento et al., 2017); in addition an antiviral activity has been detected also against the alphavirus Chikungunya (CHIKV) both *in vitr*o and in animal models (Ferreira et al., 2019).

In this context, since the NS5 amino acid residues predicted to interact with sofosbuvir shares approximately 80% conservation among WNV, DENV and ZIKV, the aim of this work was to determine for the first time sofosbuvir activity against WNV *in vitro*, as well as its resistance profile through *in vitro* resistance selection experiments.

To set up the antiviral assay, the WNV strain was first propagated in different cell lines, including human hepatic (Huh-7), neuronal (LN-18 and U87) and pulmonary (A549) cell lines, as well as the reference monkey (VERO E6) cell line. Since all the cell lines were permissive to WNV infection, antiviral activity was tested only in the human cell lines, due to the better ability to mimic the virus human tropism.

Inhibitory activity was performed by the gold standard PRA, as well as an adapted version of the IA developed for the screening of anti-ZIKV and anti-DENV antiviral activity. Sofosbuvir was active in the low micromolar range in Huh-7 cell line (IC_{50} 1.2 ± 0.3 μM) and in both neuronal U87 (IC_{50} 5.3 ± 0.9 μM) and LN-18 (IC_{50} 7.8 ± 2.5 μM) cell lines, while a reduced activity was observed in A549 cell line (IC_{50} 63.4 ± 9.0 μM). The antiviral activity of sofosbuvir was also tested by IA, with IC_{50} results similar to those obtained by PRA, confirming the efficacy of sofosbuvir in inhibiting WNV replication in the human hepatic and neuronal cell lines in the low micromolar range.

The efficiency of sofosbuvir to inhibit WNV replication was also confirmed by an *in vitro* enzymatic assay using purified WNV RdRp, resulting in an IC_{50} of 11.1 ± 4.6 μM, consistent with data obtained by cell lines experiments.

During *in vitro* resistance selection experiments, sequence of viral stocks collected at the sofosbuvir concentration of 80 μM revealed several mutations in the NS5 gene. Among the variants appeared, the S604T mutation was detected, which corresponds to the well-known S282T sofosbuvir resistance mutation in HCV NS5B (Dutartre et al., 2006), providing the hypothesis that sofosbuvir interacts with the same conserved domain across flavivirus and hepacivirus RdRp. Notably, such mutation resulted in a modest increased fold resistance with respect to the WNV wild type virus. Molecular docking experiments confirmed that the S604T mutation within the catalytic site of RdRp is able to affect the binding mode of sofosbuvir.

In conclusion, this works strongly support the studies in animal models to confirm the relevance of these findings, speculating about sofosbuvir as a treatment option for WNV itself or as a lead structure for further development against multiple flaviviral infections.

All data can be found in the attached paper at the end of the thesis (Dragoni et al., 2020).

6. ORIGINALE CHEMIAE in Antiviral Strategy - Origin and Modernization of Multi-Component Chemistry as a Source of Innovative Broad Spectrum Antiviral Strategy

Background

General consensus exists on the fact that Multi-Component Chemistry (MCC) had been the pristine chemistry for the origin of nucleic acids and heterocyclic secondary metabolites on our Planet. This chemistry was characterized by the capability of generating high chemical diversity, setting the molecular evolution for the emergence of the Last Universal Common Ancestor (LUCA) (Shirt-Ediss et al., 2017). Even if viruses are representing simple organisms, they have evolved from the same prebiotic world leading to the emergence of LUCA. This makes reasonable and attractive the hypothesis that MCC can generate novel antivirals.

Viral pathogens, including old re-emerging viruses and new emerging viruses, still represent a serious threat for global health. Enhanced globalization and climate changes contribute to increase the worldwide spreading of different viruses, which are no longer confined to geographically limited risk areas. Despite a number of vaccines and antiviral drugs have been developed in the last century, several viruses belonging to different families are still untreatable (Clercq and E., 2016). The availability of broad-spectrum antivirals (BSAs) acting on a highly conserved target (viral or host) may offer the possibility to immediately initiate prophylactic as well as therapeutic treatments against viral pathogens for which no drugs have been developed so far. In addition, BSAs may offer better treatment options for multi-species co-infections. The original MCC has been recently reproduced in the lab (Rotelli et al., 2016) and nowadays the modernization of the MCC associated innovative chemical techniques can speed-up the production of complex heterocyclic derivatives (Radi et al., 2010). In this context, MCC may represent an innovative approach for the discovery of BSAs. To investigate this hypothesis, a network composed by a panel of experienced laboratories in antiviral drug discovery and development has been formed to fulfill the objectives of the "ORIGINALE CHEMIAE in Antiviral Strategy" project, aimed to explore the modern MCC approaches to generate innovative antiviral molecule.

Among the laboratories involved in the project, our task was to define the antiviral activity of molecules generated by the different research groups in standardized virus-cell systems.

Materials and Methods

Antiviral activity of the generated candidate antiviral molecules was firstly determined against: i) the flaviviruses DENV serotype 2 strain and WNV lineage 1 strain, ii) the lentivirus HIV-1 NL4-3 strain. Following the recent pandemic, the project was also extended to the newly discovered coronavirus SARS-CoV-2, which strain was kindly provided by the University of Milan.

To assess the antiviral activity of candidate molecules against DENV, WNV and HIV-1, cell-based assays were performed as previously published (Dragoni et al., 2020; Saladini et al., 2018; Vicenti et al., 2020a). The immunodetection assay was used as read-out in the infected Huh7 cells to quantify the flaviviruses E protein, while for HIV-1, the luciferase activity was determined in infected TZM- bl reporter cell line. For SARS-CoV-2, a new virus-cell line system has been optimized, employing the human colon adenocarcinoma Caco-2 cell line (ATCC HTB-37). Cytotoxicity was evaluated as described in Vicenti et al. (Vicenti et al., 2020a) with minor modification. Briefly, serial twofold dilutions of compounds were diluted in infection medium (EMEM supplemented with 1% FBS) and after 48 h of incubation, drug cytotoxicity was measured by using the CellTiter-Glo 2.0 Luminescent Cell Viability Assay. The luminescent signal generated by cells treated with the test compound was compared with that generated by cells treated with DMSO/water to determine the half-maximal cytotoxic concentration (CC_{50}). The IC_{50} was determined through an immunodetection assay. Briefly, Caco-2 cells were infected using 0.01 MOI of the viral stock; after 1h

30min, the viral stock was removed, and serial dilutions of the candidate molecules were added onto the cells. Following 48h of incubation, cells were fixed and treated as previously described in immunodetection assay (Vicenti et al., 2020a), but using a specific monoclonal antibody able to recognize the N protein of CoVs, including SARS-CoV-2. Absorbance values were used to determine IC_{50} by a nonlinear regression analysis of the dose–response curves generated with the GraphPad PRISM software version 6.01. The SARS-CoV-2 antiviral assay was validated using the nucleoside inhibitor remdesivir, which has shown potent anti-SARS-COV-2 activity *in vitro* (Sanders et al., 2020; Wang et al., 2020).

Molecules identified by the acronym MR were provided by the research group of Prof. Marco Radi from the University of Parma, whereas the remaining were provided by the research group of Prof. Lorenzo Botta from the University of Tuscia.

Results and discussion

Among a panel of 66 candidate molecules, 7 compounds were not soluble, thus their antiviral activity could not be assessed.

Anti-WNV and anti-DENV activity: a total of 59 candidate molecules were screened to determine a potential antiviral effect against WNV and/or DENV. One compound showed cytotoxicity in the Huh7 cell lines. Among the 58 compounds tested, 16 showed WNV antiviral activity with median IC_{50} value of 9.7 µM (IQR 5.6-21.1), while 17 showed DENV antiviral activity with median IC_{50} value of di 6.1 µM (IQR 4.4-12.3) (Tab 1).

Anti-HIV-1 activity: among the panel of candidate molecules, no relevant cytotoxicity was observed in the H9 cell line for the 59 compounds tested. Of these, 5 showed anti-HIV-1 activity with median IC_{50} value of 8.6 µM (IQR 5.2-14.8) (Tab 1).

Anti-SARS-CoV-2 activity: among 54 candidate molecules, of which 41 also tested against WNV/DENV/HIV-1, 2 compounds were cytotoxic in Caco-2 cells. Of the remaining 52, 23 are still under investigation, while 4 of 25 showed anti-SARS-CoV-2 activity with median IC_{50} value of 9.1 µM (IQR 5.9-12.1) (Tab 1).

Among the active candidate compounds, 8 were able to simultaneously inhibit WNV and DENV (namely MR326, MR380, MR47, SC97, ART41, ART21, MR423, MR429). Notably, the MR333 compound was able to inhibit in the micromolar range both WNV and DENV, as well as the newly discovered SARS-CoV-2, hence likely targeting a common feature shared by viruses belonging to different families. Moreover, MR333 showed a remarkable selectivity index (SI), defined as the ratio between the CC_{50} and the IC_{50}, against both WNV and DENV. The compound MR379 shares the same pattern of activity of MR333, but since the molecule used for SARS-CoV-2 experiments is derived from a different batch of compounds, experiments must be repeated for DENV and WNV using the same batch to ensure its broad antiviral effect. Interestingly, different compounds showed inhibitory activity against viruses belonging to different classes with remarkable differences in their replication cycle (Tab 1). This is the case of MR418 and MR421 which active against DENV and HIV-1 and, of MR422 and MR425 which showed antiviral activity against both the flaviviruses tested and HIV-1.

Tab 1. Antiviral activity of candidate molecules against WNV, DENV, HIV-1 and SARS-CoV-2, expressed as the mean of the IC_{50} ± the standard deviation (SD). Only molecules showing activity at least against one viral strain tested have been reported. Sofosbuvir, raltegravir and remdesivir were used as positive controls for WNV/DENV, HIV-1 and SARS-CoV-2 inhibitory activities, respectively.

CMP ID	WNV IC_{50} (µM) ± SD	SI	DENV IC_{50} (µM) ± SD	SI	HIV-1 IC_{50} (µM) ± SD	SI	SARS-CoV-2 IC_{50} (µM) ± SD	SI
MR326	22.7 ± 3.8	8.8	9.6 ± 2.5	20.9	-	-	NT	
MR333	3.9 ± 0.7	51	2.6 ± 0.3	77	-	-	5.9 ± 1.8	13.8
MR376	25.2 ± 8.1	9.9	-	-	-	-	NT	
MR377	16.7 ± 4.3	15.0	-	-	-	-	NT	
MR378	6.6 ± 0.6	37.9	-	-	-	-	NT	
MR379	13.9 ± 11.8	11.5	18.2 ± 6.9	8.8	-	-	**9.1 ± 5.0	3.6
MR380	7.9 ± 0.7	31.6	41.6 ± 16.4	6.0	-	-	NT	
MR381	22.5 ± 18.0	11.1	-	-	-	-	NT	
MR47	5.2 ± 1.4	28.8	33.9 ± 22.8	4.4	-	-	NT	
SC 97	1.1 ± 0.1	8.3	1.2 ± 0.4	7.3	-	-	NT	
SC 105	-	-	-	-	-	-	12.1 ± 1.1	33.0
ART 41	7.8 ± 3.1	3.2	4.3 ± 3.2	5.9	-	-	-	-
ART 48	-	-	15.0 ± 0.1	2.7	-	-	-	-
ART 21	4.2 ± 0.4	4.8	4.5 ± 1.3	4.5	-	-	-	-
AF 4,3	-	-	-	-	-	-	*0.02 ± 0.001	2.0
MR 418	-	-	1.1 ± 0.1	13.6	8.6 ± 7.1	4.7	UI	
MR 421	-	-	4.9 ± 2.6	51.5	4.0 ± 1.3	12.6	UI	
MR 422	28.3 ± 2.0	3.2	6.6 ± 0.7	13.6	13.9 ± 1.4	2.7	UI	
MR 423	10.9 ± 3.8	2.3	6.1 ± 3.9	4.1	-	-	UI	
MR 424	-	-	6.5 ± 0.1	10.1	-	-	UI	
MR 425	8.5 ± 6.6	3.1	4.8 ± 1.8	5.4	6.3 ± 0.6	6.3	UI	
MR 426	-	-	6.7 ± 1.1	8.9	-	-	UI	
MR 429	12.1 ± 9.6	2.5	5.0 ± 0.9	6.1	-	-	UI	
MR 430	-	-	-	-	15.6 ± 4.8	6.4	UI	
Sofosbuvir	1.7 ± 0.5	205.9	4.6 ± 1.4	76.1	NT		NT	
Raltegravir	NT		NT		0.006 ± 0.003	>1000	NT	
Remdesivir	NT		NT		NT		0.01±0.006	8000

-, no antiviral activity was observed; NT, Not Tested; UI, the compound is currently Under Investigation; SI, Selectivity Index, defined as the ratio between the CC_{50} (not shown) and the IC_{50}.

*results are expressed in mg/ml; **new batch of compound.

Conclusions

A first panel of candidate antiviral compounds was screened and antiviral activity was assessed against WNV, DENV, HIV- 1 and SARS-CoV-2 viruses. A total of 24 of the 66 molecules synthesized reported a measurable inhibitory activity against at least one of the viruses tested. However, one of the main objectives of the "ORIGINALE CHEMIAE in Antiviral Strategy" project was aimed at identifying BSAs. Indeed, the development of pan-viral drugs capable of inhibiting multiple viruses belonging to different families is an attractive option to immediately treat new emerging and re-emerging viral diseases, as well as widespread viral infections when effective antiviral therapy is not yet available.

Notably, among the 24 active compounds, 10 were able to inhibit simultaneously at least two different viruses, while 4 showed antiviral activity against 3 different viruses. In particular, the MR333 compound reported a promising broad-spectrum antiviral activity with IC_{50} in the low micromolar range for WNV, DENV and SARS-CoV-2, and a remarkable SI for WNV and DENV. Next steps of the project will be addressed at defining the antiviral activity of these leading compounds against flavivirus ZIKV too, as well as at the screening of a second panel of candidate antiviral molecules.

7. Molecular Tracing of SARS-CoV-2 in Italy in the First Three Months of the Epidemic

Following the rapid spread of the new coronavirus SARS-CoV-2 worldwide, Italy was one of the countries most and earliest affected by the COVID-19 pandemic. To improve the knowledge on SARS-COV-2 Italian spreading, 14 clinical centers and their associated laboratories created an Italian network named SCIRE. One of the main objectives of the SCIRE group was to conduct a longitudinal analysis to evaluate the COVID-19 epidemic in Italy by means of next-generation sequencing (NGS) whole genome sequencing of the circulating strains. Molecular characterization of the viral genome is useful not only to understand the ongoing SARS-CoV-2 epidemic and its evolution, but also to provide new basic knowledge which could be related to increased disease severity, different response to treatment and finally help to population control of SARS-CoV-2 infection.

In this context, the first study performed by SCIRE was aimed at the characterization and genomic tracing by phylogenetic analyses of 59 new SARS-CoV-2 Italian isolates, obtained from patients of north and central Italy during the first wave of the epidemic, specifically from the end of February until the end of April 2020. All but one of the newly characterized genomes belonged to a single clade, corresponding to the lineage B.1 (the old Nextstrain 2A clade, corresponding to the new Nextstrain clades 20A and 20B). At that moment, the clade was the most frequently reported in European countries, including Italy. This finding matched with the first autochthonous European cluster of SARS-CoV-2 transmission in Bavaria (Germany), originated by the introduction of a strain from Shanghai. The only strain excluded belonged to the lineage B, the same lineage of the first 2 cases imported into Italy from the Hubei region, China, at the end of January 2020. However, the transmission of this lineage remains unexplained, since the patient didn't report any recent trip outside Italy or contacts with subjects affected by COVID-19 and further investigations of its transmission are required.
Interestingly, the substitution D614G in the S protein was present in all the isolates belonging to the lineage B.1, as well as in the strain belonging to lineage B. This substitution has been already characterized and it emerged during the SARS-COV-2 spreading from Asia to Europe (Eaaswarkhanth et al., 2020; Korber et al., 2020).
The genetic distances among the Italian strains were relatively short, corresponding to an average of about 6.4 mutations per viral genome. After grouping the sequences according with the sampling months, a higher heterogeneity was observed among the strains isolated in February, in respect to those of March and April; however, the genetic distance between different months increased with time. This observation confirmed a continuous evolution of the viral genome (with the emergence of new divergent variants) mainly driven by genetic drift.

In conclusion, this study shows that the initial outbreak in Italy was mainly attributable to a single introduction of the virus and its uncontrolled circulation for a period of about four weeks. Such findings reaffirm the strategic importance of continuous surveillance and timely tracing to define effective containment measures.

All data can be found in the attached paper at the end of the thesis (Lai et al., 2020).

8. MVC as a potential HIV-1 latency-reversing agent in cell line models and *ex vivo* CD4 T cells

The main obstacle to an HIV cure is the formation of stable reservoirs following integration of the HIV DNA into the host genome. Despite the success of ART to block viral replication and halt disease progression, ART is not a cure and cannot completely clear the infection, since HIV-1 is able to persist in blood and anatomic compartments for years and consequently, treatment needs to be taken life-long (Anderson and Maldarelli, 2018). Therefore, developing strategies to eradicate or control HIV-1 without ART are a high priority. Most current efforts are concentrated on the so-called 'Shock and kill' strategy (W. Xu et al., 2017). MVC, the first approved anti-HIV-1 agent targeting a cellular factor, binds to the CCR5 chemokine receptor, preventing target cell recognition by CCR5-tropic viruses (Wood and Armour, 2005). Apart from its antiviral activity, the binding of MVC to CCR5 triggers a series of cellular events per se, independently from the virus coreceptor tropism or even from the HIV-1-positive status (Woollard and Kanmogne, 2015). Indeed, the interaction of CCR5 with its natural ligands plays an important role in priming the adaptive immune responses and in promoting the migration of CCR5-expressing cells to sites of infection and inflammation; therefore, blockade of this receptor by treatment with MVC has the potential to combine the antiviral and the immunomodulatory effect, as observed in pivotal studies, in which MVC treatment was associated to a decreased immune activation and to an increase in CD4 T cells (Asmuth et al., 2010; Funderburg et al., 2010). Following CCR5 binding, MVC seems to activate the PKC-mediated pathway, resulting in an increased expression of NF-kB. NF-kB is a key T cell transcription factor that is known to able to regulate HIV-1 transcription and replication and is a preferential target of other candidate LRAs targeting PKC pathways (Jiang and Dandekar, 2015). This activity, if confirmed, would make MVC a unique drug, combining the ability to awaken the latent provirus and block new infections. Interestingly, a latency reversal effect of MVC could explain the apparently unfavorable effect on viremia shown in MVC simplification studies, particularly when HIV-1 relapses occurred at low level and/or transiently (Pett et al., 2016; Rossetti et al., 2017). Indeed, such viremia blips could be attributed to release of virus from reservoir following MVC-mediated induction rather than true virologic failure.

However, the potential of MVC as an LRA is based on limited published data. A recent work showed that intensified MVC administration *in vivo* caused an increase in unspliced HIV-1 RNA levels in resting CD4 T cells, in association with enhanced expression of NF-kB-dependent genes. Unfortunately, no control group was included to rule out stochastic changes in HIV transcription independently of MVC treatment (Madrid-Elena et al., 2018). These findings are supported by *in vitro* data from two other studies, in which the effect of MVC in the reactivation of cell latent HIV-1 models treated with IL-7 or CCL19 was significant at different MVC concentrations (López-Huertas et al., 2017), and with no alterations in the viability of CD8 T cells (López-Huertas et al., 2020).

In this context, the aim of this study was to define MVC-mediated HIV-1 induction in three cell line models and in *ex vivo* CD4 T cells collected from six patients with suppressed viremia.

HIV-1 induction was evaluated after 24h in cell line models using scalar concentration of MVC; results were compared to a non-induced cell control and to cells treated with the combination of known strong-inducers (ionomycin and PMA, ION+PMA) as a positive control, for each cell line. As a readout of the induction, in TZM-bl cells the HIV-1 LTR-driven luciferase expression was measured, whereas in ACH-2 and U1 latently infected cell lines the CFR and CAR HIV-1 RNA was quantified by qPCR, along with the NF-κB p65 expression in all cell lines nuclear extracts. No LTR activation was observed in TZM-bl cells at any MVC concentration. Significant differences of HIV-1 expression were only detected at 80 µM MVC, specifically on HIV-1 CFR in U1 (3.1±0.9; P=0.034) and ACH-2 cells (3.9±1.4; P=0.037). NF-κB activation was only modestly upregulated (1.6±0.4) in TZM-bl cells with 5 µM MVC.

Ex-vivo induction experiments were performed on CD4 T cells, collected from six HIV-1-positive patients with suppressed viremia, that were induced for 24h using 5 µM MVC. For each sample a positive control (ION+PMA) and a non-treated cell control were added.

CAR, CFR and cell-associated DNA (CAD) were quantified by qPCR at baseline and 1–7–14 days post-induction (T1, T7, T14); moreover, at T7 and T14, the infectivity of the CD4 T cells co-cultured with MOLT-

4/CCR5 cells was evaluated in modified version of the TZA. Although no consistent pattern of MVC-mediated activation was observed in *ex vivo* experiments, substantial activation values were detected sparsely on individual samples with different parameters. In summary, in *ex vivo* CD4 T cells, MVC appeared to exert a weak stimulation but without a consistent pattern in specific indicators or at defined time points. Notably, in sample two, MVC stimulated all parameters at T7 (2.3±0.2 CAD, 6.8±3.7 CAR, 18.7±16.7 CFR, 7.3±0.2 TZA).

While progress with LRAs is certainly ongoing, there is still much to investigate. In this study, MVC was able to variably induce HIV-1 production in some cell line latency models, whereas in *ex vivo* CD4 T cells, MVC may exert patient-specific HIV-1 induction. However, a defined role for the MVC as a LRA with clinically relevant patterns remain to be defined.

All data can be found in the attached paper at the end of the thesis (Vicenti et al., 2020b).

9. Concluding remarks

Acute and chronic viral infections, both emerging and re-emerging, significantly affect human health. A significant number of viral pathogens remain without effective treatment or cure, with only a limited number of infections that can be prevented by vaccines. Thus, development of new antivirals is a high priority.

Flaviviruses infections caused by WNV, ZIKV and DENV have increasingly spread worldwide affecting a large number of human beings, causing considerable morbidity. Nowadays, DENV is considered the most prevalent flavivirus, infecting an estimated 400 million people each year, whereas WNV and ZIKV are endemic in different areas. Arboviral infections are indeed a serious threat affecting both high and low/middle-income countries. HIV-1 is a well-known pathogen and the most intensively studied virus ever, it has killed more than 33 million people so far and, despite major advances in treatment, still represents a major global public health concern. Indeed, at the end of 2019, there were an estimated 38 million of PLWH, and about 2 million of new infections are reported each year. The new SARS-COV-2 causing the COVID-19 disease, was isolated at the beginning of 2020 and in few months spread worldwide, leading the WHO to declare the new pandemic in March 2020. As of 1 November 2020, nearly 46 million cases and 1.2 million deaths have been reported globally, and these numbers are still rising every day.

Antiviral treatments, along with vaccination, are necessary to cure, prevent and mitigate the diseases caused by these pathogens. In the area of drug discovery, both de novo design and drug repurposing, the assessment of antiviral effects *in vitro* is a key approach for the screening of candidate compounds. Therefore, the setup of accurate, robust and convenient laboratory assays able to assess the antiviral activity of candidate molecules is highly relevant. In this context, we developed an easy-to-perform and fast flavivirus IA, which overcomes the relevant limitations of the gold standard PRA allowing a semi-automated readout through microplate reading. Other advantages of this homebrew method are the use of a pan-flaviviral monoclonal antibody, allowing the simultaneous application for different viruses, as well as the ability to distinguish between early and late antiviral effects. In synthesis, this IA can expand the potential for convenient cell-based screening of multiple compounds candidate for anti-flaviviral therapy.

Drug repurposing is an increasingly attractive trend, significantly saving cost and time with respect to the discovery and approval of new drugs. Genome characterization and protein structures of the *Flaviviridae* family have unveiled substantial homology in the RdRp enzyme. Recently, the activity of sofosbuvir, a nucleotide analog licensed for HCV infection, has been documented *in vitro* and in animal models against ZIKV and YFV and *in vitro* against DENV, as well as against the alphavirus CHIKV both *in vitro* and in animal models. Since the RdRp homology is shared also by WNV, we investigated whether sofosbuvir may exert an activity also against WNV. After the initial set-up of cell-based and enzymatic assays which were adapted to WNV features, we were able to describe for the first time the sofosbuvir antiviral activity against WNV in the low micromolar range. Since sofosbuvir high genetic barrier to resistance is a prominent hallmark of the anti-HCV treatment, we investigated the sofosbuvir genetic barrier against WNV. *In vitro* selection and molecular docking experiments indicated that HCV and WNV share a similar sofosbuvir resistance pattern.

Another promising direction to counteract viral diseases is the develop of BSAs, which may offer the possibility for the treatment of multi-species co-infections, as well as the treatments against novel viral agents or pathogens for which no drugs have been developed so far. In this scenario, the "ORIGINALE CHEMIAE in Antiviral Strategy" project aims to take advantage of the MCC strategy to identify promising BSAs. Even if the project is still ongoing, we were able to determine the activity of 2 compounds able to inhibit viral replication against two different families of viruses (DENV/WNV and SARS-CoV-2), as well as 2 compounds showing an antiviral activity against viruses with remarkable differences in their replication cycle (DENV/WNV and HIV-1).

Molecular characterization of the viral genome may provide useful information related to increase in disease severity and/or to a different response to therapy. Hence, during the first wave of SARS-CoV-2 in Italy, our laboratory has been included into the SCIRE Italian network, with the main objective to increase knowledge on the SARS-CoV-2 circulating strains, by means of NGS whole genome sequencing. We identified that the initial outbreak in Italy was mainly attributable to the SARS-CoV-2 lineage B.1 and to its uncontrolled circulation for an estimated period of 4 weeks.

Even if a therapy can improve the quality of survival and prolong the duration of life, it may not be sufficient to completely eradicate a chronic infection. This is the case of HIV-1, which is able to persist indefinitely in blood and other anatomic compartments and to rebound from the latent reservoir following ART cessation. Therefore, developing strategies to eradicate or control HIV-1 without ART are a high priority. In recent years, it has been hypothesized a double role for the CCR5 antagonist MVC, which may be able to combine the ability to awaken the latent provirus and to block new infections. Anyway, very few works have investigated such hypothesis. Thus, we defined MVC-mediated HIV-1 induction in three cell line models and in *ex vivo* CD4 T cells, since these models had not previously been used. Moreover, we explored a wider set of indicators compared to the previous works to better define any latency reversing activity of MVC. An increased expression of HIV-1 was detected in all the parameters observed at the highest MVC concentration in two of the three cell line models tested. In *ex vivo* CD4 T cells, no consistent pattern of MVC-mediated activation was observed, but MVC-mediated induction was detected sparsely on individual samples with different parameters. Such evidences suggest the role of MVC as a weak LRA of the HIV-1 provirus induction.

Control of viral infections is a continuous challenge for science and public health. New viruses can emerge or re-emerge under partly unpredictable circumstances. Technology in different biomedical areas has made impressive advancements, making it possible to characterize new pathogens and complex virus-host interactions at unprecedented speed and depth. Nevertheless, viruses will continue the explore the biosphere, occasionally attacking humans and any kind of living organisms. The inability to clear HIV infection despite >35 years of intensive work and the current disaster caused by SARS-CoV-2 are notable examples of the intrinsic limitations of our defense system. Drug design has also improved dramatically in the ability and speed to develop highly effective and selective antivirals. Virology remains at the core of the multidisciplinary effort required to cope with viral threatens, connecting drug design with final delivery of drugs protecting from clinically relevant infections.

10. Abbreviations

ACE2	Angiotensin-Converting Enzyme 2
ADE	Antibody-Dependent Enhancement
AIDS	Acquired Immunodeficiency Syndrome
ART	Antiretroviral Therapy
BBB	Blood-Brain Barrier
BSA	Broad-Spectrum Antiviral
C	Capsid (protein)
CAD	Cell-Associated DNA
CAR	Cell Associated HIV-1 RNA
CC_{50}	Half-Maximal Cytotoxic Concentration
CFR	Cell-Free HIV-1 RNA
CHIKV	Chikungunya Virus
CNS	Central Nervous System
CoV	Coronavirus
COVID-19	Coronavirus Disease 2019
CRF	Circulating Recombinant Form
DC-SIGN	Dendritic cell-specific ICAM-grabbing non-integrin
ddPCR	Digital Droplet PCR
DENV	Dengue Virus
DHF	Dengue Hemorrhagic Fever
DSS	Dengue Shock Syndrome
E	Envelope (protein)
EMA	European Medicine Agency
ER	Endoplasmic Reticulum
FDA	Food and Drug Administration
GBS	Guillain-Barré syndrome
GISAID	Global Initiative on Sharing Avian Influenza Data
HCoV	Human Coronavirus
HCV	Hepatitis C Virus
HIV	Human Immunodeficiency Virus
HML	HIV Monitoring Laboratory
IA	immunodetection assay
IC_{50}	Half-Maximal Inhibitory Concentration
IFN	Interferon
IN	Integrase
INSTI	Integrase Strand Transfer Inhibitor
ION	Ionomycin
IPDA	Intact Proviral DNA Assay
LRA	Latency Reversing Agent
LTR	Long Terminal Repeat
LUCA	Last Universal Common Ancestor
M	Membrane (protein)
MA	Matrix
MCC	Multi-Component Chemistry
MERS-CoV	Middle East respiratory syndrome coronavirus
MTase	Methyltransferase
MVC	Maraviroc
N	Nucleocapsid (protein)

NGS	Next Generation Sequencing
NNRTI	Non-Nucleoside RT Inhibitor
NRTI	Nucleoside/Nucleotide RT Inhibitor
NS-nsp	Non-structural (protein)
NT	Not Tested
NTPase	nucleoside triphosphatase
ORF	Open Reading frame
PANGOLIN	Phylogenetic Assignment of Named Global Outbreak LINeages
PBMC	Peripheral Blood Mononuclear Cell
PI	Protease Inhibitor
PKC	Protein Kinase C
PLWH	People Living With HIV
PMA	Phorbol Myristate Acetate
PR	Protease
PRA	Plaque Reduction Assay
prM	Precursor Membrane
qPCR	Quantitative Polymerase Chain Reaction
R	Repeated sequence
R0	basic Reproduction Number
RBD	Receptor Binding Domain
RdRp	RNA-dependent RNA polymerase
RT	Reverse Transcriptase
RTC	Replication-Transcription Complex
RTPase	RNA triphosphatase
S	Spike (protein)
SARS-CoV	Severe Acute Respiratory Syndrome Coronavirus
SARS-CoV-2	Severe Acute Respiratory Syndrome Coronavirus-2
SCIRE	SARS-CoV-2 Italian Research Enterprise
SI	Selectivity Index
TAM	Tyrosine protein kinase receptor 3 (TYRO3)–AXL–MER
$TCID_{50}$	50% Tissue Culture Infectious Dose
TILDA	Tat/Rev Induced Limiting Dilution Assay
TIM	T-cell immunoglobulin and mucin domain
TLR	Toll-like Receptor
TZA	TZM-bl Cell Based Assay
UI	Under Investigation
UNAIDS	United Nations Programme on HIV/AIDS
URF	Unique Recombinant Form
USA	United States of America
UTR	Untranslated Region
VLP	Virus-Like Particle
VOA	Viral Outgrowth Assay
VRP	Viral Replicon
WHO	World Health Organization
WNF	West Nile fever
WNV	West Nile Virus
YFV	Yellow Fever Virus
YRA	Yield Reduction Assay
ZIKV	Zika Virus

11. Bibliography

Abner, E., Jordan, A., 2019. HIV "shock and kill" therapy: In need of revision. Antiviral Res. https://doi.org/10.1016/j.antiviral.2019.03.008

Abrams, E.J., 2004. Prevention of mother-to-child transmission of HIV-successes, controversies and critical questions. AIDS Rev.

Alessandri-Gradt, E., De Oliveira, F., Leoz, M., Lemee, V., Robertson, D.L., Feyertag, F., Ngoupo, P.A., Mauclere, P., Simon, F., Plantier, J.C., 2018. HIV-1 group P infection: Towards a dead-end infection? AIDS. https://doi.org/10.1097/QAD.0000000000001791

Alm, E., Broberg, E.K., Connor, T., Hodcroft, E.B., Komissarov, A.B., Maurer-Stroh, S., Melidou, A., Neher, R.A., O'Toole, Á., Pereyaslov, D., 2020. Geographical and temporal distribution of SARS-CoV-2 clades in the WHO European Region, January to June 2020. Eurosurveillance. https://doi.org/10.2807/1560-7917.ES.2020.25.32.2001410

Althouse, B.M., Vasilakis, N., Sall, A.A., Diallo, M., Weaver, S.C., Hanley, K.A., 2016. Potential for Zika Virus to Establish a Sylvatic Transmission Cycle in the Americas. PLoS Negl. Trop. Dis. 10, 1–11. https://doi.org/10.1371/journal.pntd.0005055

Amanna, I.J., Slifka, M.K., 2014. Current trends in West Nile virus vaccine development. Expert Rev. Vaccines 13, 589–608. https://doi.org/10.1586/14760584.2014.906309

Amin, S.A., Jha, T., 2020. Fight against novel coronavirus: A perspective of medicinal chemists. Eur. J. Med. Chem. https://doi.org/10.1016/j.ejmech.2020.112559

Andersen, K.G., Rambaut, A., Lipkin, W.I., Holmes, E.C., Garry, R.F., 2020. The proximal origin of SARS-CoV-2. Nat. Med. https://doi.org/10.1038/s41591-020-0820-9

Anderson, E.M., Maldarelli, F., 2018. The role of integration and clonal expansion in HIV infection: live long and prosper. Retrovirology 15, 1–22. https://doi.org/10.1186/s12977-018-0448-8

Anderson, J.F., Rahal, J.J., 2002. Efficacy of interferon alpha-2b and ribavirin against West Nile virus in vitro [3]. Emerg. Infect. Dis. 8, 107–108. https://doi.org/10.3201/eid0801.010252

Andreano, E., Nicastri, E., Paciello, I., Pileri, P., Manganaro, N., Piccini, G., Manenti, A., Pantano, E., Kabanova, A., Troisi, M., Vacca, F., Cardamone, D., De Santi, C., Benincasa, L., Agrati, C., Capobianchi, M.R., Castilletti, C., Emiliozzi, A., Fabbiani, M., Montagnani, F., Depau, L., Brunetti, J., Bracci, L., Montomoli, E., Sala, C., Ippolito, G., Rappuoli, R., 2020. Extremely potent human monoclonal antibodies from convalescent Covid-19 patients. bioRxiv.

Arakawa, M., Morita, E., 2019. Flavivirus replication organelle biogenesis in the endoplasmic reticulum: Comparison with other single-stranded positive-sense RNA viruses. Int. J. Mol. Sci. 20. https://doi.org/10.3390/ijms20092336

Archin, N.M., Cheema, M., Parker, D., Wiegand, A., Bosch, R.J., Coffin, J.M., Eron, J., Cohen, M., Margolis, D.M., 2010. Antiretroviral intensification and valproic acid lack sustained effect on residual HIV-1 viremia or resting CD4+ cell infection. PLoS One. https://doi.org/10.1371/journal.pone.0009390

Artese, A., Svicher, V., Costa, G., Salpini, R., Di Maio, V.C., Alkhatib, M., Ambrosio, F.A., Santoro, M.M., Assaraf, Y.G., Alcaro, S., Ceccherini-Silberstein, F., 2020. Current status of antivirals and druggable targets of SARS CoV-2 and other human pathogenic coronaviruses. Drug Resist. Updat. https://doi.org/10.1016/j.drup.2020.100721

Asmuth, D.M., Goodrich, J., Cooper, D.A., Haubrich, R., Rajicic, N., Hirschel, B., Mayer, H., Valdez, H., 2010. CD4+ T-cell restoration after 48 weeks in the maraviroc treatment-experienced trials MOTIVATE 1 and 2. J. Acquir. Immune Defic. Syndr. 54, 394–397. https://doi.org/10.1097/QAI.0b013e3181c5c83b

Avettand-Fènoë, V., Chaix, M.L., Blanche, S., Burgard, M., Floch, C., Toure, K., Allemon, M.C., Warszawski, J., Rouzioux, C., 2009. LTR real-time PCR for HIV-1 DNA quantitation in blood cells for early diagnosis in infants born to seropositive mothers treated in HAART area (ANRS CO 01). J. Med. Virol. https://doi.org/10.1002/jmv.21390

Avettand-Fènoë, V., Hocqueloux, L., Ghosn, J., Cheret, A., Frange, P., Melard, A., Viard, J.P., Rouzioux, C., 2016. Total HIV-1 DNA, a marker of viral reservoir dynamics with clinical implications. Clin. Microbiol. Rev. https://doi.org/10.1128/CMR.00015-16

Avirutnan, P., Punyadee, N., Noisakran, S., Komoltri, C., Thiemmeca, S., Auethavornanan, K., Jairungsri, A., Kanlaya, R., Tangthawornchaikul, N., Puttikhunt, C., Pattanakitsakul, S., Yenchitsomanus, P., Mongkolsapaya, J., Kasinrerk, W., Sittisombut, N., Husmann, M., Blettner, M., Vasanawathana, S., Bhakdi, S., Malasit, P., 2006. Vascular Leakage in Severe Dengue Virus Infections: A Potential Role for the Nonstructural Viral Protein NS1 and Complement. J. Infect. Dis. 193, 1078–1088. https://doi.org/10.1086/500949

Azuma, K., Yanagi, U., Kagi, N., Kim, H., Ogata, M., Hayashi, M., 2020. Environmental factors involved in SARS-CoV-2 transmission: effect and role of indoor environmental quality in the strategy for COVID-19 infection control. Environ. Health Prev. Med. https://doi.org/10.1186/s12199-020-00904-2

Badia, R., Ballana, E., Castellví, M., García-Vidal, E., Pujantell, M., Clotet, B., Prado, J.G., Puig, J., Martínez, M.A., Riveira-Muñoz, E., Esté, J.A., 2018. CD32 expression is associated to T-cell activation and is not a marker of the HIV-1 reservoir. Nat. Commun. https://doi.org/10.1038/s41467-018-05157-w

Bai, F., Ashley Thompson, E., Vig, P.J.S., Arturo Leis, A., 2019. Current understanding of west nile virus clinical manifestations, immune responses, neuroinvasion, and immunotherapeutic implications. Pathogens 8. https://doi.org/10.3390/pathogens8040193

Balasubramanian, A., Manzano, M., Teramoto, T., Pilankatta, R., Padmanabhan, R., 2016. High-throughput screening for the identification of small-molecule inhibitors of the flaviviral protease. Antiviral Res. https://doi.org/10.1016/j.antiviral.2016.08.014

Barbosa da Luz, B., de Oliveira, N.M.T., França Dos Santos, I.W., Paza, L.Z., Braga, L.L.V. de M., Platner, F. da S., Werner, M.F. de P., Fernandes, E.S., Maria-Ferreira, D., 2020. An overview of the gut side of the SARS-CoV-2 infection. Intest. Res. https://doi.org/10.5217/ir.2020.00087

Barré-Sinoussi, F., Chermann, J.C., Rey, F., Nugeyre, M.T., Chamaret, S., Gruest, J., Dauguet, C., Axler-Blin, C., Vézinet-Brun, F., Rouzioux, C., Rozenbaum, W., Montagnier, L., 1983. Isolation of a T-lymphotropic retrovirus from a patient at risk for acquired immune deficiency syndrome (AIDS). Science (80-.). https://doi.org/10.1126/science.6189183

Barrett, A.D.T., 2017. Yellow fever live attenuated vaccine: A very successful live attenuated vaccine but still we have problems controlling the disease. Vaccine 35, 5951–5955. https://doi.org/10.1016/j.vaccine.2017.03.032

Barrows, N.J., Campos, R.K., Powell, S.T., Prasanth, K.R., Schott-Lerner, G., Soto-Acosta, R., Galarza-Muñoz, G., McGrath, E.L., Urrabaz-Garza, R., Gao, J., Wu, P., Menon, R., Saade, G., Fernandez-Salas, I., Rossi, S.L., Vasilakis, N., Routh, A., Bradrick, S.S., Garcia-Blanco, M.A., 2016. A Screen of FDA-Approved Drugs for Inhibitors of Zika Virus Infection. Cell Host Microbe 20, 259–270. https://doi.org/10.1016/j.chom.2016.07.004

Beard, W.A., Stahl, S.J., Kim, H.R., Bebenek, K., Kumar, A., Strub, M.P., Becerra, S.P., Kunkel, T.A., Wilson, S.H., 1994. Structure/function studies of human immunodeficiency virus type 1 reverse transcriptase. Alanine scanning mutagenesis of an α-helix in the thumb subdomain. J. Biol. Chem.

Beigel, J.H., Tomashek, K.M., Dodd, L.E., Mehta, A.K., Zingman, B.S., Kalil, A.C., Hohmann, E., Chu, H.Y., Luetkemeyer, A., Kline, S., Lopez de Castilla, D., Finberg, R.W., Dierberg, K., Tapson, V., Hsieh, L., Patterson, T.F., Paredes, R., Sweeney, D.A., Short, W.R., Touloumi, G., Lye, D.C., Ohmagari, N., Oh, M., Ruiz-Palacios, G.M., Benfield, T., Fätkenheuer, G., Kortepeter, M.G., Atmar, R.L., Creech, C.B., Lundgren, J., Babiker, A.G., Pett, S., Neaton, J.D., Burgess, T.H., Bonnett, T., Green, M., Makowski, M., Osinusi, A., Nayak, S., Lane, H.C., 2020. Remdesivir for the Treatment of Covid-19 — Final Report. N. Engl. J. Med. https://doi.org/10.1056/nejmoa2007764

Berkowitz, R., Fisher, J., Goff, S.P., 1996. RNA packaging. Curr. Top. Microbiol. Immunol. https://doi.org/10.1007/978-3-642-80145-7_6

Bhatt, S., Gething, P.W., Brady, O.J., Messina, J.P., Farlow, A.W., Moyes, C.L., Drake, J.M., Brownstein, J.S., Hoen, A.G., Sankoh, O., Myers, M.F., George, D.B., Jaenisch, T., William Wint, G.R., Simmons, C.P., Scott, T.W., Farrar, J.J., Hay, S.I., 2013. The global distribution and burden of dengue. Nature 496, 504–507. https://doi.org/10.1038/nature12060

Bianchi, M., Benvenuto, D., Giovanetti, M., Angeletti, S., Ciccozzi, M., Pascarella, S., 2020. Sars-CoV-2 Envelope and Membrane Proteins: Structural Differences Linked to Virus Characteristics? Biomed Res. Int. https://doi.org/10.1155/2020/4389089

Blissenbach, M., Grewe, B., Hoffmann, B., Brandt, S., Überla, K., 2010. Nuclear RNA Export and Packaging Functions of HIV-1 Rev Revisited. J. Virol. https://doi.org/10.1128/jvi.02264-09

Boldescu, V., Behnam, M.A.M., Vasilakis, N., Klein, C.D., 2017. Broad-spectrum agents for flaviviral infections: Dengue, Zika and beyond. Nat. Rev. Drug Discov. 16, 565–586. https://doi.org/10.1038/nrd.2017.33

Brai, A., Fazi, R., Tintori, C., Zamperini, C., Bugli, F., Sanguinetti, M., Stigliano, E., Esté, J., Badia, R., Franco, S., Martinez, M.A., Martinez, J.P., Meyerhans, A., Saladini, F., Zazzi, M., Garbelli, A., Maga, G., Botta, M., 2016. Human DDX3 protein is a valuable target to develop broad spectrum antiviral agents. Proc. Natl. Acad. Sci. U. S. A. https://doi.org/10.1073/pnas.1522987113

Brai, A., Martelli, F., Riva, V., Garbelli, A., Fazi, R., Zamperini, C., Pollutri, A., Falsitta, L., Ronzini, S., Maccari, L., Maga, G., Giannecchini, S., Botta, M., 2019. DDX3X Helicase Inhibitors as a New Strategy to Fight the West Nile Virus Infection. J. Med. Chem. 62, 2333–2347. https://doi.org/10.1021/acs.jmedchem.8b01403

Brandler, S., Tangy, F., 2013. Vaccines in development against West Nile virus. Viruses 5, 2384–2409. https://doi.org/10.3390/v5102384

Brooks, A.J., Johansson, M., John, A. V., Xu, Y., Jans, D.A., Vasudevan, S.G., 2002. The interdomain region of dengue NS5 protein that binds to the viral helicase NS3 contains independently functional importin β1 and importin α/β-recognized nuclear localization signals. J. Biol. Chem. 277, 36399–36407. https://doi.org/10.1074/jbc.M204977200

Bruner, K.M., Murray, A.J., Pollack, R.A., Soliman, M.G., Laskey, S.B., Capoferri, A.A., Lai, J., Strain, M.C., Lada, S.M., Hoh, R., Ho, Y.C., Richman, D.D., Deeks, S.G., Siliciano, J.D., Siliciano, R.F., 2016a. Defective proviruses rapidly accumulate during acute HIV-1 infection. Nat. Med. https://doi.org/10.1038/nm.4156

Bruner, K.M., Murray, A.J., Pollack, R.A., Soliman, M.G., Laskey, S.B., Capoferri, A.A., Lai, J., Strain, M.C., Lada, S.M., Hoh, R., Ho, Y.C., Richman, D.D., Deeks, S.G., Siliciano, J.D., Siliciano, R.F., 2016b. Defective proviruses rapidly accumulate during acute HIV-1 infection. Nat. Med. 22, 1043–1049. https://doi.org/10.1038/nm.4156

Bruner, K.M., Wang, Z., Simonetti, F.R., Bender, A.M., Kwon, K.J., Sengupta, S., Fray, E.J., Beg, S.A., Antar, A.A.R., Jenike, K.M., Bertagnolli, L.N., Capoferri, A.A., Kufera, J.T., Timmons, A., Nobles, C., Gregg, J., Wada, N., Ho, Y.C., Zhang, H., Margolick, J.B., Blankson, J.N., Deeks, S.G., Bushman, F.D., Siliciano, J.D., Laird, G.M., Siliciano, R.F., 2019. A quantitative approach for measuring the reservoir of latent HIV-1 proviruses. Nature 566, 120–125. https://doi.org/10.1038/s41586-019-0898-8

Bullen, C.K., Laird, G.M., Durand, C.M., Siliciano, J.D., Siliciano, R.F., 2014. New ex vivo approaches distinguish effective and ineffective single agents for reversing HIV-1 latency in vivo. Nat. Med. https://doi.org/10.1038/nm.3489

Buzon, M.J., Martin-Gayo, E., Pereyra, F., Ouyang, Z., Sun, H., Li, J.Z., Piovoso, M., Shaw, A., Dalmau, J., Zangger, N., Martinez-Picado, J., Zurakowski, R., Yu, X.G., Telenti, A., Walker, B.D., Rosenberg, E.S., Lichterfeld, M., 2014. Long-Term Antiretroviral Treatment Initiated at Primary HIV-1 Infection Affects the Size, Composition, and Decay Kinetics of the Reservoir of HIV-1-Infected CD4 T Cells. J. Virol. https://doi.org/10.1128/jvi.01046-14

Cahn, P., Madero, J.S., Arribas, J.R., Antinori, A., Ortiz, R., Clarke, A.E., Hung, C.C., Rockstroh, J.K., Girard, P.M., Sievers, J., Man, C.Y., Urbaityte, R., Brandon, D.J., Underwood, M., Tenorio, A.R., Pappa, K.A., Wynne, B., Gartland, M., Aboud, M., van Wyk, J., Smith, K.Y., 2020. Durable Efficacy of Dolutegravir Plus Lamivudine in Antiretroviral Treatment-Naive Adults With HIV-1 Infection: 96-Week Results From the GEMINI-1 and GEMINI-2 Randomized Clinical Trials. J. Acquir. Immune Defic. Syndr. https://doi.org/10.1097/QAI.0000000000002275

Campbell-Yesufu, O.T., Gandhi, R.T., 2011. Update on human immunodeficiency virus (HIV)-2 infection. Clin. Infect. Dis. 52, 780–787. https://doi.org/10.1093/cid/ciq248

Cao, B., Wang, Y., Wen, D., Liu, W., Wang, Jingli, Fan, G., Ruan, L., Song, B., Cai, Y., Wei, M., Li, X., Xia, J., Chen, N., Xiang, J., Yu, T.,

Bai, T., Xie, X., Zhang, L., Li, C., Yuan, Y., Chen, H., Li, Huadong, Huang, H., Tu, S., Gong, F., Liu, Y., Wei, Y., Dong, C., Zhou, F., Gu, X., Xu, J., Liu, Z., Zhang, Y., Li, Hui, Shang, L., Wang, K., Li, K., Zhou, X., Dong, X., Qu, Z., Lu, S., Hu, X., Ruan, S., Luo, S., Wu, J., Peng, L., Cheng, F., Pan, L., Zou, J., Jia, C., Wang, Juan, Liu, X., Wang, S., Wu, X., Ge, Q., He, J., Zhan, H., Qiu, F., Guo, L., Huang, C., Jaki, T., Hayden, F.G., Horby, P.W., Zhang, D., Wang, C., 2020. A Trial of Lopinavir–Ritonavir in Adults Hospitalized with Severe Covid-19. N. Engl. J. Med. https://doi.org/10.1056/nejmoa2001282

Cascella, M., Rajnik, M., Cuomo, A., Dulebohn, S.C., Di Napoli, R., 2020. Features, Evaluation and Treatment Coronavirus (COVID-19), StatPearls.

Cauchemez, S., Besnard, M., Bompard, P., Dub, T., Guillemette-Artur, P., Eyrolle-Guignot, D., Salje, H., Van Kerkhove, M., Abadie, V., Garel, C., Fontanet, A., Mallet, H.P., Mallet, H.-P., 2016. Association between Zika virus and microcephaly in French Polynesia, 2013–2015: a retrospective study. Lancet Infect. Dis. 387, 2125–2132. https://doi.org/10.1010.1016/S0140-6736(16)00651-6

Cavalcanti, A.B., Zampieri, F.G., Rosa, R.G., Azevedo, L.C.P., Veiga, V.C., Avezum, A., Damiani, L.P., Marcadenti, A., Kawano-Dourado, L., Lisboa, T., Junqueira, D.L.M., de Barros e Silva, P.G.M., Tramujas, L., Abreu-Silva, E.O., Laranjeira, L.N., Soares, A.T., Echenique, L.S., Pereira, A.J., Freitas, F.G.R., Gebara, O.C.E., Dantas, V.C.S., Furtado, R.H.M., Milan, E.P., Golin, N.A., Cardoso, F.F., Maia, I.S., Hoffmann Filho, C.R., Kormann, A.P.M., Amazonas, R.B., Bocchi de Oliveira, M.F., Serpa-Neto, A., Falavigna, M., Lopes, R.D., Machado, F.R., Berwanger, O., 2020. Hydroxychloroquine with or without Azithromycin in Mild-to-Moderate Covid-19. N. Engl. J. Med. https://doi.org/10.1056/nejmoa2019014

Cervera, L., Gòdia, F., Tarrés-Freixas, F., Aguilar-Gurrieri, C., Carrillo, J., Blanco, J., Gutiérrez-Granados, S., 2019. Production of HIV-1-based virus-like particles for vaccination: achievements and limits. Appl. Microbiol. Biotechnol. https://doi.org/10.1007/s00253-019-10038-3

Chang, L., Zhao, L., Gong, H., Gong, H., Gong, H., Wang, Lunan, Wang, Lunan, Wang, Lan, Yang, Z., Xu, B., 2020. Severe Acute Respiratory Syndrome Coronavirus 2 RNA Detected in Blood Donations. Emerg. Infect. Dis. https://doi.org/10.3201/eid2607.200839

Chen, P., Nirula, A., Heller, B., Gottlieb, R.L., Boscia, J., Morris, J., Huhn, G., Cardona, J., Mocherla, B., Stosor, V., Shawa, I., Adams, A.C., Van Naarden, J., Custer, K.L., Shen, L., Durante, M., Oakley, G., Schade, A.E., Sabo, J., Patel, D.R., Klekotka, P., Skovronsky, D.M., 2020. SARS-CoV-2 Neutralizing Antibody LY-CoV555 in Outpatients with Covid-19. N. Engl. J. Med. https://doi.org/10.1056/nejmoa2029849

Chen, R.F., Yang, K.D., Wang, L., Liu, J.W., Chiu, C.C., Cheng, J.T., 2007. Different clinical and laboratory manifestations between dengue haemorrhagic fever and dengue fever with bleeding tendency. Trans. R. Soc. Trop. Med. Hyg. 101, 1106–1113. https://doi.org/10.1016/j.trstmh.2007.06.019

Chen, Y., Liu, Q., Guo, D., 2020. Emerging coronaviruses: Genome structure, replication, and pathogenesis. J. Med. Virol. https://doi.org/10.1002/jmv.25681

Chiu, I.M., Yaniv, A., Dahlberg, J.E., Gazit, A., Skuntz, S.F., Tronick, S.R., Aaronson, S.A., 1985. Nucleotide sequence evidence for relationship of AIDS retrovirus to lentiviruses. Nature. https://doi.org/10.1038/317366a0

Choe, H., Farzan, M., Sun, Y., Sullivan, N., Rollins, B., Ponath, P.D., Wu, L., Mackay, C.R., LaRosa, G., Newman, W., Gerard, N., Gerard, C., Sodroski, J., 1996. The β-chemokine receptors CCR3 and CCR5 facilitate infection by primary HIV-1 isolates. Cell. https://doi.org/10.1016/S0092-8674(00)81313-6

Chong, H.Y., Leow, C.Y., Abdul Majeed, A.B., Leow, C.H., 2019. Flavivirus infection—A review of immunopathogenesis, immunological response, and immunodiagnosis. Virus Res. 274, 197770. https://doi.org/10.1016/j.virusres.2019.197770

Chowers, M.Y., Lang, R., Nassar, F., Ben-David, D., Giladi, M., Rubinshtein, E., Itzhaki, A., Mishal, J., Siegman-Igra, Y., Kitzes, R., Pick, N., Landau, Z., Wolf, D., Bin, H., Mendelson, E., Pitlik, S.D., Weinberger, M., 2001. Clinical characteristics of the West Nile fever outbreak, Israel, 2000. Emerg. Infect. Dis. 7, 675–678. https://doi.org/10.3201/eid0704.017414

Choy, K.T., Wong, A.Y.L., Kaewpreedee, P., Sia, S.F., Chen, D., Hui, K.P.Y., Chu, D.K.W., Chan, M.C.W., Cheung, P.P.H., Huang, X., Peiris, M., Yen, H.L., 2020. Remdesivir, lopinavir, emetine, and homoharringtonine inhibit SARS-CoV-2 replication in vitro. Antiviral Res. https://doi.org/10.1016/j.antiviral.2020.104786

Chun, T.W., Davey, R.T., Engel, D., Lane, H.C., Fauci, A.S., 1999. AIDS: Re-emergence of HIV after stopping therapy. Nature. https://doi.org/10.1038/44755

Chun, T.W., Finzi, D., Margolick, J., Chadwick, K., Schwartz, D., Siliciano, R.F., 1995. In vivo fate of HIV-1-infected T cells: Quantitative analysis of the transition to stable latency. Nat. Med. https://doi.org/10.1038/nm1295-1284

Chun, T.W., Stuyver, L., Mizell, S.B., Ehler, L.A., Mican, J.A.M., Baseler, M., Lloyd, A.L., Nowak, M.A., Fauci, A.S., 1997. Presence of an inducible HIV-1 latent reservoir during highly active antiretroviral therapy. Proc. Natl. Acad. Sci. U. S. A. https://doi.org/10.1073/pnas.94.24.13193

Cihlar, T., Ray, A.S., 2010. Nucleoside and nucleotide HIV reverse transcriptase inhibitors: 25 years after zidovudine. Antiviral Res. https://doi.org/10.1016/j.antiviral.2009.09.014

Cillo, A.R., Sobolewski, M.D., Bosch, R.J., Fyne, E., Piatak, M., Coffin, J.M., Mellors, J.W., 2014. Quantification of HIV-1 latency reversal in resting CD4+ T cells from patients on suppressive antiretroviral therapy. Proc. Natl. Acad. Sci. U. S. A. https://doi.org/10.1073/pnas.1402873111

Cimarelli, A., Darlix, J.L., 2014. HIV-1 reverse transcription. Methods Mol. Biol. 1087, 55–70. https://doi.org/10.1007/978-1-62703-670-2_6

Ciota, A.T., 2017. West Nile virus and its vectors. Curr. Opin. Insect Sci. 22, 28–36. https://doi.org/10.1016/j.cois.2017.05.002

Clark, M.B., Schaefer, T.J., 2020. West Nile Virus, StatPearls.

Clercq, E. de, E., D.C., 2016. Approved antiviral drugs over the past 50 years. . Clin. Microbiol. Rev. 29, 695–747. https://doi.org/10.1128/CMR.00102-15.Address

Clum, S., Ebner, K.E., Padmanabhan, R., 1997. Cotranslational membrane insertion of the serine proteinase precursor NS2B-

NS3(Pro) of dengue virus type 2 is required for efficient in vitro processing and is mediated through the hydrophobic regions of NS2B. J. Biol. Chem. 272, 30715–30723. https://doi.org/10.1074/jbc.272.49.30715

Colombier, M.A., Molina, J.M., 2018. Doravirine: A review. Curr. Opin. HIV AIDS. https://doi.org/10.1097/COH.0000000000000471

Conde, J.N., da Silva, E.M., Allonso, D., Coelho, D.R., Andrade, I. da S., de Medeiros, L.N., Menezes, J.L., Barbosa, A.S., Mohana-Borges, R., 2016. Inhibition of the Membrane Attack Complex by Dengue Virus NS1 through Interaction with Vitronectin and Terminal Complement Proteins. J. Virol. 90, 9570–9581. https://doi.org/10.1128/jvi.00912-16

Cong, Y., Ulasli, M., Schepers, H., Mauthe, M., V'kovski, P., Kriegenburg, F., Thiel, V., de Haan, C.A.M., Reggiori, F., 2019. Nucleocapsid Protein Recruitment to Replication-Transcription Complexes Plays a Crucial Role in Coronaviral Life Cycle. J. Virol. https://doi.org/10.1128/jvi.01925-19

Cordeiro, M.T., 2019. Laboratory diagnosis of Zika virus. Top. Magn. Reson. Imaging. https://doi.org/10.1097/RMR.0000000000000190

Coutard, B., Valle, C., de Lamballerie, X., Canard, B., Seidah, N.G., Decroly, E., 2020. The spike glycoprotein of the new coronavirus 2019-nCoV contains a furin-like cleavage site absent in CoV of the same clade. Antiviral Res. https://doi.org/10.1016/j.antiviral.2020.104742

Davenport, M.P., Khoury, D.S., Cromer, D., Lewin, S.R., Kelleher, A.D., Kent, S.J., 2019. Functional cure of HIV: the scale of the challenge. Nat. Rev. Immunol. https://doi.org/10.1038/s41577-018-0085-4

Davey, R.T., Bhat, N., Yoder, C., Chun, T.W., Metcalf, J.A., Dewar, R., Natarajan, V., Lempicki, R.A., Adelsberger, J.W., Miller, K.D., Kovacs, J.A., Polis, M.A., Walker, R.E., Falloon, J., Masur, H., Gee, D., Baseler, M., Dimitrov, D.S., Fauci, A.S., Lane, H.C., 1999. HIV-1 and T cell dynamics after interruption of highly active antiretroviral therapy (HAART) in patients with a history of sustained viral suppression. Proc. Natl. Acad. Sci. U. S. A. https://doi.org/10.1073/pnas.96.26.15109

De Clercq, E., Li, G., 2016. Approved antiviral drugs over the past 50 years. Clin. Microbiol. Rev. 29, 695–747. https://doi.org/10.1128/CMR.00102-15

de Freitas, C.S., Higa, L.M., Sacramento, C.Q., Ferreira, A.C., Reis, P.A., Delvecchio, R., Monteiro, F.L., Barbosa-Lima, G., James Westgarth, H., Vieira, Y.R., Mattos, M., Rocha, N., Hoelz, L.V.B., Leme, R.P.P., Bastos, M.M., Gisele, G.O., Carla, C.E., Queiroz-Junior, C.M., Lima, C.X., Costa, V. V., Teixeira, M.M., Bozza, F.A., Bozza, P.T., Boechat, N., Tanuri, A., Souza, T.M.L., 2019. Yellow fever virus is susceptible to sofosbuvir both in vitro and in vivo. PLoS Negl. Trop. Dis. https://doi.org/10.1371/journal.pntd.0007072

Deigendesch, N., Stenzel, W., 2018. Acute and chronic viral infections, 1st ed, Handbook of Clinical Neurology. Elsevier B.V. https://doi.org/10.1016/B978-0-12-802395-2.00017-1

Devarkar, S.C., Wang, C., Miller, M.T., Ramanathan, A., Jiang, F., Khan, A.G., Patel, S.S., Marcotrigiano, J., 2016. Structural basis for m7G recognition and 2'-O-methyl discrimination in capped RNAs by the innate immune receptor RIG-I. Proc. Natl. Acad. Sci. U. S. A. 113, 596–601. https://doi.org/10.1073/pnas.1515152113

DeWald, L.E., Starr, C., Butters, T., Treston, A., Warfield, K.L., 2020. Iminosugars: a host-targeted approach to combat Flaviviridae infections. Antiviral Res. https://doi.org/10.1016/j.antiviral.2020.104881

Dharan, A., Bachmann, N., Talley, S., Zwikelmaier, V., Campbell, E.M., 2020. Nuclear pore blockade reveals that HIV-1 completes reverse transcription and uncoating in the nucleus. Nat. Microbiol. https://doi.org/10.1038/s41564-020-0735-8

Di Toro, F., Gjoka, M., Di Lorenzo, G., De Seta, F., Maso, G., Risso, F.M., Romano, F., Wiesenfeld, U., Levi-D'Ancona, R., Ronfani, L., Ricci, G., 2020. Impact of COVID-19 on maternal and neonatal outcomes: a systematic review and meta-analysis. Clin. Microbiol. Infect.

Diamond, M.S., Pierson, T.C., 2015. Molecular Insight into Dengue Virus Pathogenesis and Its Implications for Disease Control. Cell 162, 488–492. https://doi.org/10.1016/j.cell.2015.07.005

Diamond, M.S., Zachariah, M., Harris, E., 2002. Mycophenolic acid inhibits dengue virus infection by preventing replication of viral RNA. Virology 304, 211–221. https://doi.org/10.1006/viro.2002.1685

Dick, G.W.A., Kitchen, S.F., Haddow, A.J., 1952. Zika virus isolation and serological specificity. Trans. R. Soc. Trop. Med. Hyg. 46, 509–520. https://doi.org/10.1016/0035-9203(52)90042-4

Donadieu, E., Bahuon, C., Lowenski, S., Zientara, S., Coulpier, M., Lecollinet, S., 2013. Differential virulence and pathogenesis of West Nile viruses. Viruses 5, 2856–2880. https://doi.org/10.3390/v5112856

Dong, Y., Dai, T., Wei, Y., Zhang, L., Zheng, M., Zhou, F., 2020. A systematic review of SARS-CoV-2 vaccine candidates. Signal Transduct. Target. Ther. https://doi.org/10.1038/s41392-020-00352-y

Dragoni, F., Boccuto, A., Picarazzi, F., Giannini, A., Giammarino, F., Saladini, F., Mori, M., Mastrangelo, E., Zazzi, M., Vicenti, I., 2020. Evaluation of sofosbuvir activity and resistance profile against West Nile virus in vitro. Antiviral Res. 175, 104708. https://doi.org/10.1016/j.antiviral.2020.104708

Duan, Y.P., Zeng, M., Jiang, B., Zhang, W., Wang, M., Jia, R., Zhu, D., Liu, M., Zhao, X., Yang, Q., Wu, Y., Zhang, S.Q., Liu, Y.Y., Zhang, L., Yu, Y.L., Pan, L., Chen, S., Cheng, A., 2019. Flavivirus RNA-dependent RNA polymerase interacts with genome UTRs and viral proteins to facilitate flavivirus RNA replication. Viruses 11. https://doi.org/10.3390/v11100929

Dubankova, A., Boura, E., 2019. Structure of the yellow fever NS5 protein reveals conserved drug targets shared among flaviviruses. Antiviral Res. 169, 104536. https://doi.org/10.1016/j.antiviral.2019.104536

Dutartre, H., Bussetta, C., Boretto, J., Canard, B., 2006. General catalytic deficiency of hepatitis C virus RNA polymerase with an S282T mutation and mutually exclusive resistance towards 2'-modified nucleotide analogues. Antimicrob. Agents Chemother. 50, 4161–4169. https://doi.org/10.1128/AAC.00433-06

E. Fenales-Belasio, M. Raimondo, B. Suligoi, S.B., 2010. HIV virology and pathogenetic mechanisms of infection: a brief overview. Ann Ist Super Sanità 7, 43–52. https://doi.org/10.4415/ANN

Eaaswarkhanth, M., Al Madhoun, A., Al-Mulla, F., 2020. Could the D614G substitution in the SARS-CoV-2 spike (S) protein be associated with higher COVID-19 mortality? Int. J. Infect. Dis. https://doi.org/10.1016/j.ijid.2020.05.071

Emu, B., Fessel, J., Schrader, S., Kumar, P., Richmond, G., Win, S., Weinheimer, S., Marsolais, C., Lewis, S., 2018. Phase 3 Study of Ibalizumab for Multidrug-Resistant HIV-1. N. Engl. J. Med. 379, 645–654. https://doi.org/10.1056/NEJMoa1711460

Engelman, A., Cherepanov, P., 2012. The structural biology of HIV-1: Mechanistic and therapeutic insights. Nat. Rev. Microbiol. 10, 279–290. https://doi.org/10.1038/nrmicro2747

Eriksson, S., Graf, E.H., Dahl, V., Strain, M.C., Yukl, S.A., Lysenko, E.S., Bosch, R.J., Lai, J., Chioma, S., Emad, F., Abdel-Mohsen, M., Hoh, R., Hecht, F., Hunt, P., Somsouk, M., Wong, J., Johnston, R., Siliciano, R.F., Richman, D.D., O'Doherty, U., Palmer, S., Deeks, S.G., Siliciano, J.D., 2013. Comparative Analysis of Measures of Viral Reservoirs in HIV-1 Eradication Studies. PLoS Pathog. https://doi.org/10.1371/journal.ppat.1003174

Españo, E., Nam, J.-H., Song, E.-J., Song, D., Lee, C.-K., Kim, J.-K., 2019. Lipophilic statins inhibit Zika virus production in Vero cells. Sci. Rep. 9, 1–11. https://doi.org/10.1038/s41598-019-47956-1

Esposito, D., Craigie, R., 1999. HIV integrase structure and function. Adv. Virus Res. https://doi.org/10.1016/s0065-3527(08)60304-8

Eyer, L., Zouharová, D., Širmarová, J., Fojtíková, M., Štefánik, M., Haviernik, J., Nencka, R., de Clercq, E., Růžek, D., 2017. Antiviral activity of the adenosine analogue BCX4430 against West Nile virus and tick-borne flaviviruses. Antiviral Res. 142, 63–67. https://doi.org/10.1016/j.antiviral.2017.03.012

Fabryova, H., Strebel, K., 2019. Vpr and Its Cellular Interaction Partners: R We There Yet? Cells. https://doi.org/10.3390/cells8111310

Fall, G., Di Paola, N., Faye, M., Dia, M., Freire, C.C. de M., Loucoubar, C., Zanotto, P.M. de A., Faye, O., Sall, A.A., 2017. Biological and phylogenetic characteristics of West African lineages of West Nile virus. PLoS Negl. Trop. Dis. 11. https://doi.org/10.1371/journal.pntd.0006078

Faria, N.R., Do Socorro Da Silva Azevedo, R., Kraemer, M.U.G., Souza, R., Cunha, M.S., Hill, S.C., Thézé, J., Bonsall, M.B., Bowden, T.A., Rissanen, I., Rocco, I.M., Nogueira, J.S., Maeda, A.Y., Da Silva Vasami, F.G., De Lima Macedo, F.L., Suzuki, A., Rodrigues, S.G., Cruz, A.C.R., Nunes, B.T., De Almeida Medeiros, D.B., Rodrigues, D.S.G., Queiroz, A.L.N., Da Silva, E.V.P., Henriques, D.F., Da Rosa, E.S.T., De Oliveira, C.S., Martins, L.C., Vasconcelos, H.B., Casseb, L.M.N., De Brito Simith, D., Messina, J.P., Abade, L., Lourenço, J., Alcantara, L.C., De Lima, M.M., Giovanetti, M., Hay, S.I., De Oliveira, R.S., Da Silva Lemos, P., De Oliveira, L.F., De Lima, C.P.S., Da Silva, S.P., De Vasconcelos, J.M., Franco, L., Cardoso, J.F., Da Silva Gonçalves Vianez-Júnior, J.L., Mir, D., Bello, G., Delatorre, E., Khan, K., Creatore, M., Coelho, G.E., De Oliveira, W.K., Tesh, R., Pybus, O.G., Nunes, M.R.T., Vasconcelos, P.F.C., 2016. Zika virus in the Americas: Early epidemiological and genetic findings. Science (80-.). 352, 345–349. https://doi.org/10.1126/science.aaf5036

Fauci, A.S., Morens, D.M., 2016. Zika virus in the americas-yet another arbovirus threat. N. Engl. J. Med. 374, 601–604. https://doi.org/10.1056/NEJMp1600297

Fehr, A.R., Perlman, S., 2015. Coronaviruses: An overview of their replication and pathogenesis, in: Coronaviruses: Methods and Protocols. https://doi.org/10.1007/978-1-4939-2438-7_1

Fernandez, H., Banks, G., Smith, R., 1986. Ribavirin: A clinical overview. Eur. J. Epidemiol. https://doi.org/10.1007/BF00152711

Fernández-Montero, J.V., Barreiro, P., Soriano, V., 2009. HIV protease inhibitors: Recent clinical trials and recommendations on use. Expert Opin. Pharmacother. https://doi.org/10.1517/14656560902980202

Ferraris, P., Cochet, M., Hamel, R., Gladwyn-Ng, I., Alfano, C., Diop, F., Garcia, D., Talignani, L., Montero-Menei, C.N., Nougairède, A., Yssel, H., Nguyen, L., Coulpier, M., Missé, D., 2019. Zika virus differentially infects human neural progenitor cells according to their state of differentiation and dysregulates neurogenesis through the Notch pathway. Emerg. Microbes Infect. 8, 1003–1016. https://doi.org/10.1080/22221751.2019.1637283

Ferreira, A.C., Reis, P.A., de Freitas, C.S., Sacramento, C.Q., Hoelz, L.V.B., Bastos, M.M., Mattos, M., Rocha, N., de Azevedo Quintanilha, I.G., da Silva Gouveia Pedrosa, C., Souza, L.R.Q., Loiola, E.C., Trindade, P., Vieira, Y.R., Barbosa-Lima, G., de Castro Faria Neto, H.C., Boechat, N., Rehen, S.K., Brüning, K., Bozza, F.A., Bozza, P.T., Souza, T.M.L., 2019. Beyond members of the Flaviviridae family, sofosbuvir also inhibits chikungunya virus replication. Antimicrob. Agents Chemother. 63. https://doi.org/10.1128/AAC.01389-18

Finzi, D., Hermankova, M., Pierson, T., Carruth, L.M., Buck, C., Chaisson, R.E., Quinn, T.C., Chadwick, K., Margolick, J., Brookmeyer, R., Gallant, J., Markowitz, M., Ho, D.D., Richman, D.D., Siliciano, R.F., 1997. Identification of a reservoir for HIV-1 in patients on highly active antiretroviral therapy. Science (80-.). https://doi.org/10.1126/science.278.5341.1295

Freed, E.O., 1998. HIV-1 Gag proteins: Diverse functions in the virus life cycle. Virology. https://doi.org/10.1006/viro.1998.9398

Friedrich, B., Li, G., Dziuba, N., Ferguson, M.R., 2010. Quantitative PCR used to assess HIV-1 integration and 2-LTR circle formation in human macrophages, peripheral blood lymphocytes and a CD4+ cell line. Virol. J. https://doi.org/10.1186/1743-422X-7-354

Fun, A., Mok, H.P., Wills, M.R., Lever, A.M., 2017. A highly reproducible quantitative viral outgrowth assay for the measurement of the replication-competent latent HIV-1 reservoir. Sci. Rep. https://doi.org/10.1038/srep43231

Funderburg, N., Kalinowska, M., Eason, J., Goodrich, J., Heera, J., Mayer, H., Rajicic, N., Valdez, H., Lederman, M.M., 2010. Effects of maraviroc and efavirenz on markers of immune activation and inflammation and associations with CD4+ cell rises in HIV-infected patients. PLoS One 5, 1–6. https://doi.org/10.1371/journal.pone.0013188

Furler, R.L., Ali, A., Yang, O.O., Nixon, D.F., 2019. Nef-induced differential gene expression in primary CD4+ T cells following infection with HIV-1 isolates. Virus Genes. https://doi.org/10.1007/s11262-019-01670-2

Gao, M., Yang, L., Chen, X., Deng, Y., Yang, S., Xu, H., Chen, Z., Gao, X., 2020. A study on infectivity of asymptomatic SARS-CoV-2 carriers. Respir. Med. https://doi.org/10.1016/j.rmed.2020.106026

Geretti, A.M., Easterbrook, P., 2001. Antiretroviral resistance in clinical practice. Int. J. STD AIDS. https://doi.org/10.1258/0956462011916938

Giovannoni, F., Bosch, I., Polonio, C.M., Torti, M.F., Wheeler, M.A., Li, Z., Romorini, L., Rodriguez Varela, M.S., Rothhammer, V.,

Barroso, A., Tjon, E.C., Sanmarco, L.M., Takenaka, M.C., Modaresi, S.M.S., Gutiérrez-Vázquez, C., Zanluqui, N.G., dos Santos, N.B., Munhoz, C.D., Wang, Z., Damonte, E.B., Sherr, D., Gehrke, L., Peron, J.P.S., Garcia, C.C., Quintana, F.J., 2020. AHR is a Zika virus host factor and a candidate target for antiviral therapy. Nat. Neurosci. https://doi.org/10.1038/s41593-020-0664-0

Godoy, A.S., Lima, G.M.A., Oliveira, K.I.Z., Torres, N.U., Maluf, F. V., Guido, R.V.C., Oliva, G., 2017. Crystal structure of Zika virus NS5 RNA-dependent RNA polymerase. Nat. Commun. 8, 1–6. https://doi.org/10.1038/ncomms14764

Goldman, J.D., Lye, D.C.B., Hui, D.S., Marks, K.M., Bruno, R., Montejano, R., Spinner, C.D., Galli, M., Ahn, M.-Y., Nahass, R.G., Chen, Y.-S., SenGupta, D., Hyland, R.H., Osinusi, A.O., Cao, H., Blair, C., Wei, X., Gaggar, A., Brainard, D.M., Towner, W.J., Muñoz, J., Mullane, K.M., Marty, F.M., Tashima, K.T., Diaz, G., Subramanian, A., 2020. Remdesivir for 5 or 10 Days in Patients with Severe Covid-19. N. Engl. J. Med. https://doi.org/10.1056/nejmoa2015301

Gong, E.Y., 2013. Antiviral Methods and Protocols, Methods in Molecular Biology. Humana Press, Totowa, NJ. https://doi.org/10.1007/978-1-62703-484-5

Gong, E.Y., Smets, A., Verheyen, N., Clynhens, M., Gustin, E., Lory, P., Kraus, G., 2013. A Duplex Real-Time RT-PCR Assay for Profiling Inhibitors of Four Dengue Serotypes. pp. 195–203. https://doi.org/10.1007/978-1-62703-484-5_16

González, M.E., 2015. Vpu protein: The viroporin encoded by HIV-1. Viruses. https://doi.org/10.3390/v7082824

Gorbalenya, A.E., Baker, S.C., Baric, R.S., de Groot, R.J., Drosten, C., Gulyaeva, A.A., Haagmans, B.L., Lauber, C., Leontovich, A.M., Neuman, B.W., Penzar, D., Perlman, S., Poon, L.L.M., Samborskiy, D. V., Sidorov, I.A., Sola, I., Ziebuhr, J., 2020. The species Severe acute respiratory syndrome-related coronavirus: classifying 2019-nCoV and naming it SARS-CoV-2. Nat. Microbiol. https://doi.org/10.1038/s41564-020-0695-z

Götte, M., Feld, J.J., 2016. Direct-acting antiviral agents for hepatitis C: Structural and mechanistic insights. Nat. Rev. Gastroenterol. Hepatol. 13, 338–351. https://doi.org/10.1038/nrgastro.2016.60

Grewe, B., Überla, K., 2010. The human immunodeficiency virus type 1 Rev protein: Ménage à trois during the early phase of the lentiviral replication cycle. J. Gen. Virol. https://doi.org/10.1099/vir.0.022509-0

Grossi-Soyster, E.N., Desiree La Beaud, A., 2017. Clinical aspects of Zika virus. Curr. Opin. Pediatr. 29, 102–106. https://doi.org/10.1097/MOP.0000000000000449

Gubler, D.J., 1998. Dengue and Dengue Hemorrhagic Fever. Clin. Microbiol. Rev. 11, 480–496. https://doi.org/10.1128/CMR.11.3.480

Gupta, P., Sanyal, A., Mailliard, R.B., 2017. TZA: a novel assay for measuring the latent HIV-1 reservoir. Expert Rev. Mol. Diagn. https://doi.org/10.1080/14737159.2017.1384315

Gupta, R.K., Abdul-Jawad, S., McCoy, L.E., Mok, H.P., Peppa, D., Salgado, M., Martinez-Picado, J., Nijhuis, M., Wensing, A.M.J., Lee, H., Grant, P., Nastouli, E., Lambert, J., Pace, M., Salasc, F., Monit, C., Innes, A.J., Muir, L., Waters, L., Frater, J., Lever, A.M.L., Edwards, S.G., Gabriel, I.H., Olavarria, E., 2019. HIV-1 remission following CCR5Δ32/Δ32 haematopoietic stem-cell transplantation. Nature. https://doi.org/10.1038/s41586-019-1027-4

Guzman, Maria G., Harris, E., 2015. Dengue. Lancet 385, 453–465. https://doi.org/10.1016/S0140-6736(14)60572-9

Guzman, M.G., Harris, E., 2015. Dengue. Lancet 385, 453–465. https://doi.org/http://dx.doi.org/10.1016/ S0140-6736(14)60572-9

Habarugira, G., Suen, W.W., Hobson-Peters, J., Hall, R.A., Bielefeldt-Ohmann, H., 2020. West Nile Virus: An Update on Pathobiology, Epidemiology, Diagnostics, Control and "One Health" Implications. Pathogens 9, 589. https://doi.org/10.3390/pathogens9070589

Hahn, F., Setz, C., Friedrich, M., Rauch, P., Solbak, S.M., Frøystein, N.Å., Henklein, P., Votteler, J., Fossen, T., Schubert, U., 2014. Mutation of the highly conserved ser-40 of the HIV-1 p6 gag protein to phe causes the formation of a hydrophobic patch, enhances membrane association, and polyubiquitination of gag. Viruses. https://doi.org/10.3390/v6103738

Hamel, R., Dejarnac, O., Wichit, S., Ekchariyawat, P., Neyret, A., Luplertlop, N., Perera-Lecoin, M., Surasombatpattana, P., Talignani, L., Thomas, F., Cao-Lormeau, V.-M., Choumet, V., Briant, L., Desprès, P., Amara, A., Yssel, H., Missé, D., 2015. Biology of Zika Virus Infection in Human Skin Cells. J. Virol. 89, 8880–8896. https://doi.org/10.1128/jvi.00354-15

Hamre, D., Procknow, J.J., 1966. A New Virus Isolated from the Human Respiratory Tract. Proc. Soc. Exp. Biol. Med. https://doi.org/10.3181/00379727-121-30734

Harapan, H., Michie, A., Sasmono, R.T., Imrie, A., 2020. Dengue : A Minireview 1, 1–35.

Hastings, A.K., Fikrig, E., 2017. Zika virus and sexual transmission: A new route of transmission for mosquito-borne flaviviruses. Yale J. Biol. Med. 90, 325–330.

He, J., Guo, Y., Mao, R., Zhang, J., 2020. Proportion of asymptomatic coronavirus disease 2019: A systematic review and meta-analysis. J. Med. Virol. https://doi.org/10.1002/jmv.26326

Heinz, F.X., Stiasny, K., 2012. Flaviviruses and flavivirus vaccines. Vaccine 30, 4301–4306. https://doi.org/10.1016/j.vaccine.2011.09.114

Hemelaar, J., Elangovan, R., Yun, J., Dickson-Tetteh, L., Fleminger, I., Kirtley, S., Williams, B., Gouws-Williams, E., Ghys, P.D., Abimiku, A.G., Agwale, S., Archibald, C., Avidor, B., Barbás, M.G., Barre-Sinoussi, F., Barugahare, B., Belabbes, E.H., Bertagnolio, S., Birx, D., Bobkov, A.F., Brandful, J., Bredell, H., Brennan, C.A., Brooks, J., Bruckova, M., Buonaguro, L., Buonaguro, F., Buttò, S., Buve, A., Campbell, M., Carr, J., Carrera, A., Carrillo, M.G., Celum, C., Chaplin, B., Charles, M., Chatzidimitriou, D., Chen, Z., Chijiwa, K., Cooper, D., Cunningham, P., Dagnra, A., de Gascun, C.F., Del Amo, J., Delgado, E., Dietrich, U., Dwyer, D., Ellenberger, D., Ensoli, B., Essex, M., Gao, F., Fleury, H., Fonjungo, P.N., Foulongne, V., Gadkari, D.A., García, F., Garsia, R., Gershy-Damet, G.M., Glynn, J.R., Goodall, R., Grossman, Z., Lindenmeyer-Guimarães, M., Hahn, B., Hamers, R.L., Hamouda, O., Handema, R., He, X., Herbeck, J., Ho, D.D., Holguin, A., Hosseinipour, M., Hunt, G., Ito, M., Bel Hadj Kacem, M.A., Kahle, E., Kaleebu, P.K., Kalish, M., Kamarulzaman, A., Kang, C., Kanki, P., Karamov, E., Karasi, J.C., Kayitenkore, K., Kelleher, T., Kitayaporn, D., Kostrikis, L.G., Kucherer, C., Lara, C., Leitner, T., Liitsola, K., Lingappa, J., Linka, M., Lorenzana de Rivera, I., Lukashov, V., Maayan, S., Mayr, L., McCutchan, F., Meda, N., Menu, E., Mhalu, F., Mloka, D., Mokili, J.L., Montes, B., Mor, O., Morgado, M., Mosha, F., Moussi, A., Mullins, J., Najera, R., Nasr, M., Ndembi, N., Neilson,

J.R., Nerurkar, V.R., Neuhann, F., Nolte, C., Novitsky, V., Nyambi, P., Ofner, M., Paladin, F.J., Papa, A., Pape, J., Parkin, N., Parry, C., Peeters, M., Pelletier, A., Pérez-Álvarez, L., Pillay, D., Pinto, A., Quang, T.D., Rademeyer, C., Raikanikoda, F., Rayfield, M.A., Reynes, J.M., Rinke de Wit, T., Robbins, K.E., Rolland, M., Rousseau, C., Salazar-Gonzales, J., Salem, H., Salminen, M., Salomon, H., Sandstrom, P., Santiago, M.L., Sarr, A.D., Schroeder, B., Segondy, M., Selhorst, P., Sempala, S., Servais, J., Shaik, A., Shao, Y., Slim, A., Soares, M.A., Songok, E., Stewart, D., Stokes, J., Subbarao, S., Sutthent, R., Takehisa, J., Tanuri, A., Tee, K.K., Thapa, K., Thomson, M., Tran, T., Urassa, W., Ushijima, H., van de Perre, P., van der Groen, G., van Laethem, K., van Oosterhout, J., van Sighem, A., van Wijngaerden, E., Vandamme, A.M., Vercauteren, J., Vidal, N., Wallace, L., Williamson, C., Wolday, D., Xu, J., Yang, C., Zhang, L., Zhang, R., 2019. Global and regional molecular epidemiology of HIV-1, 1990–2015: a systematic review, global survey, and trend analysis. Lancet Infect. Dis. https://doi.org/10.1016/S1473-3099(18)30647-9

Ho, Y.C., Shan, L., Hosmane, N.N., Wang, J., Laskey, S.B., Rosenbloom, D.I.S., Lai, J., Blankson, J.N., Siliciano, J.D., Siliciano, R.F., 2013. XReplication-competent noninduced proviruses in the latent reservoir increase barrier to HIV-1 cure. Cell. https://doi.org/10.1016/j.cell.2013.09.020

Hoffmann, M., Schroeder, S., Kleine-Weber, H., Müller, M.A., Drosten, C., Pöhlmann, S., 2020. Nafamostat mesylate blocks activation of SARS-CoV-2: New treatment option for COVID-19. Antimicrob. Agents Chemother. https://doi.org/10.1128/AAC.00754-20

Honein, M.A., Dawson, A.L., Petersen, E.E., Jones, A.M., Lee, E.H., Yazdy, M.M., Ahmad, N., Macdonald, J., Evert, N., Bingham, A., Ellington, S.R., Shapiro-Mendoza, C.K., Oduyebo, T., Fine, A.D., Brown, C.M., Sommer, J.N., Gupta, J., Cavicchia, P., Slavinski, S., White, J.L., Owen, S.M., Petersen, L.R., Boyle, C., Meaney-Delman, D., Jamieson, D.J., 2017. Birth defects among fetuses and infants of US women with evidence of possible zika virus infection during pregnancy. JAMA - J. Am. Med. Assoc. 317, 59–68. https://doi.org/10.1001/jama.2016.19006

Huang, Y.J.S., Higgs, S., Horne, K.M.E., Vanlandingham, D.L., 2014. Flavivirus-Mosquito interactions. Viruses 6, 4703–4730. https://doi.org/10.3390/v6114703

Hütter, G., Nowak, D., Mossner, M., Ganepola, S., Müßig, A., Allers, K., Schneider, T., Hofmann, J., Kücherer, C., Blau, O., Blau, I.W., Hofmann, W.K., Thiel, E., 2009. Long-Term Control of HIV by CCR5 Delta32/Delta32 Stem-Cell Transplantation . N. Engl. J. Med. https://doi.org/10.1056/nejmoa0802905

Hyde, J.L., Diamond, M.S., 2015. Innate immune restriction and antagonism of viral RNA lacking 2'-O methylation. Virology 479–480, 66–74. https://doi.org/10.1016/j.virol.2015.01.019

Iwamoto, M., Jernigan, D., Guasch, A., Trepka, M., Blackmore, C., Hellinger, W., Pham, S., Zaki, S., Lanciotti, RS Lance-Parker, S., M.D., M.P.H. for the West Nile Virus in Transplant Recipients Investigation Team DiazGranados CA, Winquist AG, Perlino CA, Wiersma S, Hillyer KL, Goodman JL, Marfin AA, Chamberland ME, P.L., 2003. Transmission of West Nile Virus from an Organ Donor to Four Transplant Recipients. N. Engl. J. Med. 348, 2196–2203. https://doi.org/10.1056/NEJMoa022987

Jacobs, G.B., Wilkinson, E., Isaacs, S., Spies, G., De Oliveira, T., Seedat, S., Engelbrecht, S., 2014. HIV-1 subtypes B and C unique recombinant forms (URFs) and transmitted drug resistance identified in the Western Cape Province, South Africa. PLoS One. https://doi.org/10.1371/journal.pone.0090845

Jain, A., Chaturvedi, U.C., 2010. Dengue in infants: An overview. FEMS Immunol. Med. Microbiol. 59, 119–130. https://doi.org/10.1111/j.1574-695X.2010.00670.x

Jain, S., Batra, H., Yadav, P., Chand, S., 2020. COVID-19 Vaccines Currently under Preclinical and Clinical Studies, and Associated Antiviral Immune Response. Vaccines 8, 1–16. https://doi.org/10.3390/vaccines8040649

Jeon, S., Ko, M., Lee, J., Choi, I., Byun, S.Y., Park, S., Shum, D., Kim, S., 2020. Identification of antiviral drug candidates against SARS-CoV-2 from FDA-approved drugs. Antimicrob. Agents Chemother. https://doi.org/10.1128/AAC.00819-20

Jiang, G., Dandekar, S., 2015. Targeting NF-κB signaling with protein Kinase C agonists as an emerging strategy for combating HIV latency. AIDS Res. Hum. Retroviruses. https://doi.org/10.1089/aid.2014.0199

Jones, C.T., Ma, L., Burgner, J.W., Groesch, T.D., Post, C.B., Kuhn, R.J., 2003. Flavivirus Capsid Is a Dimeric Alpha-Helical Protein. J. Virol. 77, 7143–7149. https://doi.org/10.1128/jvi.77.12.7143-7149.2003

Jordan, I., Briese, T., Fischer, N., Lau, J.Y., Lipkin, W.I., 2000. Ribavirin Inhibits West Nile Virus Replication and Cytopathic Effect in Neural Cells. J. Infect. Dis. 182, 1214–1217. https://doi.org/10.1086/315847

Julander, J.G., Siddharthan, V., Evans, J., Taylor, R., Tolbert, K., Apuli, C., Stewart, J., Collins, P., Gebre, M., Neilson, S., Van Wettere, A., Lee, Y.M., Sheridan, W.P., Morrey, J.D., Babu, Y.S., 2017a. Efficacy of the broad-spectrum antiviral compound BCX4430 against Zika virus in cell culture and in a mouse model. Antiviral Res. 137, 14–22. https://doi.org/10.1016/j.antiviral.2016.11.003

Julander, J.G., Siddharthan, V., Evans, J., Taylor, R., Tolbert, K., Apuli, C., Stewart, J., Collins, P., Gebre, M., Neilson, S., Van Wettere, A., Lee, Y.M., Sheridan, W.P., Morrey, J.D., Babu, Y.S., 2017b. Efficacy of the broad-spectrum antiviral compound BCX4430 against Zika virus in cell culture and in a mouse model. Antiviral Res. https://doi.org/10.1016/j.antiviral.2016.11.003

Julander, J.G., Winger, Q.A., Rickords, L.F., Shi, P.Y., Tilgner, M., Binduga-Gajewska, I., Sidwell, R.W., Morrey, J.D., 2006. West Nile virus infection of the placenta. Virology 347, 175–182. https://doi.org/10.1016/j.virol.2005.11.040

Kalayanarooj, S., 2011. Clinical manifestations and management of dengue/DHF/DSS. Trop. Med. Health 39, 83–87. https://doi.org/10.2149/tmh.2011-S10

Kaplan, A.H., Manchester, M., Swanstrom, R., 1994. The activity of the protease of human immunodeficiency virus type 1 is initiated at the membrane of infected cells before the release of viral proteins and is required for release to occur with maximum efficiency. J. Virol. https://doi.org/10.1128/jvi.68.10.6782-6786.1994

Katzelnick, L.C., Narvaez, C., Arguello, S., Lopez Mercado, B., Collado, D., Ampie, O., Elizondo, D., Miranda, T., Bustos Carillo, F., Mercado, J.C., Latta, K., Schiller, A., Segovia-Chumbez, B., Ojeda, S., Sanchez, N., Plazaola, M., Coloma, J., Halloran, M.E., Premkumar, L., Gordon, A., Narvaez, F., de Silva, A.M., Kuan, G., Balmaseda, A., Harris, E., 2020. Zika virus infection enhances

future risk of severe dengue disease. Science In press, 1123–1128.

Kazmi, S.S., Ali, W., Bibi, N., Nouroz, F., 2020. A review on Zika virus outbreak, epidemiology, transmission and infection dynamics. J. Biol. Res. 27, 1–11. https://doi.org/10.1186/s40709-020-00115-4

Kessl, J.J., Kutluay, S.B., Townsend, D., Rebensburg, S., Slaughter, A., Larue, R.C., Shkriabai, N., Bakouche, N., Fuchs, J.R., Bieniasz, P.D., Kvaratskhelia, M., 2016. HIV-1 Integrase Binds the Viral RNA Genome and Is Essential during Virion Morphogenesis. Cell. https://doi.org/10.1016/j.cell.2016.07.044

Khalaf, K., Papp, N., Chou, J.T.T., Hana, D., Mackiewicz, A., Kaczmarek, M., 2020. SARS-CoV-2: Pathogenesis, and Advancements in Diagnostics and Treatment. Front. Immunol. https://doi.org/10.3389/fimmu.2020.570927

Khan, J.A., Rehman, S., Fisher-Hoch, S.P., Mirza, S., Khurshid, M., McCormick, J.B., 1995. Crimean Congo-Haemorrhagic Fever treated with oral ribavirin. Lancet. https://doi.org/10.1016/S0140-6736(95)91323-8

Khan, S., Siddique, R., Shereen, M.A., Ali, A., Liu, J., Bai, Q., Bashir, N., Xue, M., 2020. Emergence of a novel coronavirus, severe acute respiratory syndrome coronavirus 2: Biology and therapeutic options. J. Clin. Microbiol. https://doi.org/10.1128/JCM.00187-20

Killerby, M.E., Biggs, H.M., Midgley, C.M., Gerber, S.I., Watson, J.T., 2020. Middle east respiratory syndrome coronavirus transmission. Emerg. Infect. Dis. https://doi.org/10.3201/eid2602.190697

Kim, J.A., Seong, R.K., Kumar, M., Shin, O.S., 2018. Favipiravir and ribavirin inhibit replication of Asian and African strains of zika virus in different cell models. Viruses 10. https://doi.org/10.3390/v10020072

Kim, S.Y., Byrn, R., Groopman, J., Baltimore, D., 1989. Temporal aspects of DNA and RNA synthesis during human immunodeficiency virus infection: evidence for differential gene expression. J. Virol. https://doi.org/10.1128/jvi.63.9.3708-3713.1989

Kim, Y., Anderson, J.L., Lewin, S.R., 2018. Getting the "Kill" into "Shock and Kill": Strategies to Eliminate Latent HIV. Cell Host Microbe. https://doi.org/10.1016/j.chom.2017.12.004

Kimberland, M.L., Hou, W., Alfonso-Pecchio, A., Wilson, S., Rao, Y., Zhang, S., Lu, Q., 2018. Strategies for controlling CRISPR/Cas9 off-target effects and biological variations in mammalian genome editing experiments. J. Biotechnol. https://doi.org/10.1016/j.jbiotec.2018.08.007

King, S.R., 1994. HIV: Virology and mechanisms of disease. Ann. Emerg. Med. 24, 443–449. https://doi.org/10.1016/S0196-0644(94)70181-4

Koff, W.C., Elm, J.L., Halstead, S.B., 1982. Antiviral effects of ribavirin and 6-mercapto-9-tetrahydro-2-furylpurine against dengue viruses in vitro. Antiviral Res. 2, 69–79. https://doi.org/10.1016/0166-3542(82)90027-4

Kok, W.M., 2016. New developments in flavivirus drug discovery. Expert Opin. Drug Discov. 11, 433–445. https://doi.org/10.1517/17460441.2016.1160887

Konishi, E., Mason, P.W., 1993. Proper maturation of the Japanese encephalitis virus envelope glycoprotein requires cosynthesis with the premembrane protein. J. Virol. 67, 1672–5.

Korber, B., Fischer, W.M., Gnanakaran, S., Yoon, H., Theiler, J., Abfalterer, W., Hengartner, N., Giorgi, E.E., Bhattacharya, T., Foley, B., Hastie, K.M., Parker, M.D., Partridge, D.G., Evans, C.M., Freeman, T.M., de Silva, T.I., Angyal, A., Brown, R.L., Carrilero, L., Green, L.R., Groves, D.C., Johnson, K.J., Keeley, A.J., Lindsey, B.B., Parsons, P.J., Raza, M., Rowland-Jones, S., Smith, N., Tucker, R.M., Wang, D., Wyles, M.D., McDanal, C., Perez, L.G., Tang, H., Moon-Walker, A., Whelan, S.P., LaBranche, C.C., Saphire, E.O., Montefiori, D.C., 2020. Tracking Changes in SARS-CoV-2 Spike: Evidence that D614G Increases Infectivity of the COVID-19 Virus. Cell. https://doi.org/10.1016/j.cell.2020.06.043

Krammer, F., 2020. SARS-CoV-2 vaccines in development. Nature. https://doi.org/10.1038/s41586-020-2798-3

Kraus, A.A., Messer, W., Haymore, L.B., De Silva, A.M., 2007. Comparison of plaque- and flow cytometry-based methods for measuring dengue virus neutralization. J. Clin. Microbiol. https://doi.org/10.1128/JCM.00827-07

Krishnamoorthy, S., Swain, B., Verma, R.S., Gunthe, S.S., 2020. SARS-CoV, MERS-CoV, and 2019-nCoV viruses: an overview of origin, evolution, and genetic variations. VirusDisease. https://doi.org/10.1007/s13337-020-00632-9

Kufel, W.D., 2020. Antibody-based strategies in HIV therapy. Int. J. Antimicrob. Agents 106186. https://doi.org/10.1016/j.ijantimicag.2020.106186

Kumar, S., Nyodu, R., Maurya, V.K., Saxena, S.K., 2020. Morphology, Genome Organization, Replication, and Pathogenesis of Severe Acute Respiratory Syndrome Coronavirus 2 (SARS-CoV-2). https://doi.org/10.1007/978-981-15-4814-7_3

Kumar, V., Shin, J.S., Shie, J.J., Ku, K.B., Kim, C., Go, Y.Y., Huang, K.F., Kim, M., Liang, P.H., 2017. Identification and evaluation of potent Middle East respiratory syndrome coronavirus (MERS-CoV) 3CLPro inhibitors. Antiviral Res. https://doi.org/10.1016/j.antiviral.2017.02.007

Kuritzkes, D.R., 2009. HIV-1 entry inhibitors: An overview. Curr. Opin. HIV AIDS 4, 82–87. https://doi.org/10.1097/COH.0b013e328322402e

Lai, A., Bergna, A., Caucci, S., Clementi, N., Vicenti, I., Dragoni, F., Cattelan, A.M., Menzo, S., Pan, A., Callegaro, A., Tagliabracci, A., Caruso, A., Caccuri, F., Ronchiadin, S., Balotta, C., Zazzi, M., Vaccher, E., Clementi, M., Galli, M., Zehender, G., 2020. Molecular tracing of SARS-CoV-2 in Italy in the first three months of the epidemic. Viruses 12, 1–12. https://doi.org/10.3390/v12080798

Laird, G.M., Eisele, E.E., Rabi, S.A., Lai, J., Chioma, S., Blankson, J.N., Siliciano, J.D., Siliciano, R.F., 2013. Rapid Quantification of the Latent Reservoir for HIV-1 Using a Viral Outgrowth Assay. PLoS Pathog. https://doi.org/10.1371/journal.ppat.1003398

Lam, T.T.Y., Jia, N., Zhang, Y.W., Shum, M.H.H., Jiang, J.F., Zhu, H.C., Tong, Y.G., Shi, Y.X., Ni, X.B., Liao, Y.S., Li, W.J., Jiang, B.G., Wei, W., Yuan, T.T., Zheng, K., Cui, X.M., Li, J., Pei, G.Q., Qiang, X., Cheung, W.Y.M., Li, L.F., Sun, F.F., Qin, S., Huang, J.C., Leung, G.M., Holmes, E.C., Hu, Y.L., Guan, Y., Cao, W.C., 2020. Identifying SARS-CoV-2-related coronaviruses in Malayan pangolins. Nature. https://doi.org/10.1038/s41586-020-2169-0

Lau, J.Y.N., Tam, R.C., Liang, T.J., Hong, Z., 2002. Mechanism of action of ribavirin in the combination treatment of chronic HCV infection. Hepatology. https://doi.org/10.1053/jhep.2002.32672

Laureti, M., Narayanan, D., Rodriguez-Andres, J., Fazakerley, J.K., Kedzierski, L., 2018. Flavivirus Receptors: Diversity, Identity, and Cell Entry. Front. Immunol. 9, 2180. https://doi.org/10.3389/fimmu.2018.02180

Li, L., Lok, S.M., Yu, I.M., Zhang, Y., Kuhn, R.J., Chen, J., Rossmann, M.G., 2008. The flavivirus precursor membrane-envelope protein complex: Structure and maturation. Science (80-.). 319, 1830–1834. https://doi.org/10.1126/science.1153263

Li, Y., Xie, Z., Lin, W., Cai, W., Wen, C., Guan, Y., Mo, X., Wang, J., Wang, Y., Peng, P., Chen, X., Hong, W., Xiao, G., Liu, J., Zhang, L., Hu, F., Li, F., Zhang, F., Deng, X., Li, L., 2020. Efficacy and Safety of Lopinavir/Ritonavir or Arbidol in Adult Patients with Mild/Moderate COVID-19: An Exploratory Randomized Controlled Trial. Med. https://doi.org/10.1016/j.medj.2020.04.001

Lim, S.M., Koraka, P., Osterhaus, A.D.M.E., Martina, B.E.E., 2011. West Nile virus: Immunity and pathogenesis. Viruses 3, 811–828. https://doi.org/10.3390/v3060811

Lim, S.P., Koh, J.H.K., Seh, C.C., Liew, C.W., Davidson, A.D., Chua, L.S., Chandrasekaran, R., Cornvik, T.C., Shi, P.Y., Lescar, J., 2013. A crystal structure of the dengue virus non-structural protein 5 (NS5) polymerase delineates interdomain amino acid residues that enhance its thermostability and de novo initiation activities. J. Biol. Chem. 288, 31105–31114. https://doi.org/10.1074/jbc.M113.508606

Lindenbach, B.D., Rice, C.M., 1999. Genetic interaction of flavivirus nonstructural proteins NS1 and NS4A as a determinant of replicase function. J. Virol. 73, 4611–21.

Lindenbach, B.D., Thiel, H., Rice, C.M., 2007. Flaviviridae:The Viruses and Their Replication. Fields Virol. 5th Ed. 1101–1113.

Liu, R., Paxton, W.A., Choe, S., Ceradini, D., Martin, S.R., Horuk, R., MacDonald, M.E., Stuhlmann, H., Koup, R.A., Landau, N.R., 1996. Homozygous defect in HIV-1 coreceptor accounts for resistance of some multiply-exposed individuals to HIV-1 infection. Cell. https://doi.org/10.1016/S0092-8674(00)80110-5

Liu, R., Simonetti, F.R., Ho, Y.C., 2020. The forces driving clonal expansion of the HIV-1 latent reservoir. Virol. J. 17, 1–13. https://doi.org/10.1186/s12985-019-1276-8

Liu, W.J., Wang, X.J., Clark, D.C., Lobigs, M., Hall, R.A., Khromykh, A.A., 2006. A Single Amino Acid Substitution in the West Nile Virus Nonstructural Protein NS2A Disables Its Ability To Inhibit Alpha/Beta Interferon Induction and Attenuates Virus Virulence in Mice. J. Virol. 80, 2396–2404. https://doi.org/10.1128/jvi.80.5.2396-2404.2006

Liu, Y., Liu, J., Du, S., Shan, C., Nie, K., Zhang, Rudian, Li, X.F., Zhang, Renli, Wang, T., Qin, C.F., Wang, P., Shi, P.Y., Cheng, G., 2017. Evolutionary enhancement of Zika virus infectivity in Aedes aegypti mosquitoes. Nature 545, 482–486. https://doi.org/10.1038/nature22365

López-Huertas, M.R., Jiménez-Tormo, L., Madrid-Elena, N., Gutiérrez, C., Rodríguez-Mora, S., Coiras, M., Alcamí, J., Moreno, S., 2017. The CCR5-Antagonist Maraviroc reverses HIV-1 latency in vitro alone or in combination with the PKC-Agonist Bryostatin-1. Sci. Rep. 7, 1–13. https://doi.org/10.1038/s41598-017-02634-y

López-Huertas, M.R., Jiménez-Tormo, L., Madrid-Elena, N., Gutiérrez, C., Vivancos, M.J., Luna, L., Moreno, S., 2020. Maraviroc reactivates HIV with potency similar to that of other latency reversing drugs without inducing toxicity in CD8 T cells. Biochem. Pharmacol. 182. https://doi.org/10.1016/j.bcp.2020.114231

Lorenz, I.C., Kartenbeck, J., Mezzacasa, A., Allison, S.L., Heinz, F.X., Helenius, A., 2003. Intracellular Assembly and Secretion of Recombinant Subviral Particles from Tick-Borne Encephalitis Virus 77, 4370–4382. https://doi.org/10.1128/JVI.77.7.4370–4382.2003

Lu, G., Gong, P., 2017. A structural view of the RNA-dependent RNA polymerases from the Flavivirus genus. Virus Res. 234, 34–43. https://doi.org/10.1016/j.virusres.2017.01.020

Luber, A.D., 2005. Genetic barriers of resistance and impact on clinical response. MedGenMed Medscape Gen. Med. https://doi.org/10.1186/1758-2652-7-3-69

Mackenzie, J.M., Khromykh, A.A., Parton, R.G., 2007. Cholesterol Manipulation by West Nile Virus Perturbs the Cellular Immune Response. Cell Host Microbe 2, 229–239. https://doi.org/10.1016/j.chom.2007.09.003

Madrid-Elena, N., García-Bermejo, M.L., Serrano-Villar, S., Díaz-de Santiago, A., Sastre, B., Gutiérrez, C., Dronda, F., Coronel Díaz, M., Domínguez, E., López-Huertas, M.R., Hernández-Novoa, B., Moreno, S., 2018. Maraviroc Is Associated with Latent HIV-1 Reactivation through NF-κB Activation in Resting CD4 + T Cells from HIV-Infected Individuals on Suppressive Antiretroviral Therapy . J. Virol. 92, 1–13. https://doi.org/10.1128/jvi.01931-17

Magurano, F., Remoli, M.E., Baggieri, M., Fortuna, C., Marchi, A., Fiorentini, C., Bucci, P., Benedetti, E., Ciufolini, M.G., Rizzo, C., Piga, S., Salcuni, P., Rezza, G., Nicoletti, L., 2012. Circulation of West Nile virus lineage 1 and 2 during an outbreak in Italy. Clin. Microbiol. Infect. 18, E545–E547. https://doi.org/10.1111/1469-0691.12018

Malet, H., Egloff, M.P., Selisko, B., Butcher, R.E., Wright, P.J., Roberts, M., Gruez, A., Sulzenbacher, G., Vonrhein, C., Bricogne, G., Mackenzie, J.M., Khromykh, A.A., Davidson, A.D., Canard, B., 2007. Crystal structure of the RNA polymerase domain of the West Nile virus non-structural protein 5. J. Biol. Chem. 282, 10678–10689. https://doi.org/10.1074/jbc.M607273200

Malet, I., Delelis, O., Nguyen, T., Leducq, V., Abdi, B., Morand-Joubert, L., Calvez, V., Marcelin, A.G., 2019. Variability of the HIV-1 3' polypurine tract (3'PPT) region and implication in integrase inhibitor resistance. J. Antimicrob. Chemother. https://doi.org/10.1093/jac/dkz377

Malim, M.H., Hauber, J., Le, S.Y., Maizel, J. V., Cullen, B.R., 1989. The HIV-1 rev trans-activator acts through a structured target sequence to activate nuclear export of unspliced viral mRNA. Nature. https://doi.org/10.1038/338254a0

Markham, A., 2020. Correction to: Fostemsavir: First Approval (Drugs, (2020), 80, 14, (1485-1490), 10.1007/s40265-020-01386-w). Drugs 80, 1615. https://doi.org/10.1007/s40265-020-01403-y

Martina, B.E.E., Koraka, P., Osterhaus, A.D.M.E., 2009. Dengue virus pathogenesis: An integrated view. Clin. Microbiol. Rev. 22, 564–581. https://doi.org/10.1128/CMR.00035-09

Martínez-Gutierrez, M., Castellanos, J.E., Gallego-Gómez, J.C., 2011. Statins reduce dengue virus production via decreased virion assembly. Intervirology 54, 202–216. https://doi.org/10.1159/000321892

Massanella, M., Yek, C., Lada, S.M., Nakazawa, M., Shefa, N., Huang, K., Richman, D.D., 2018. Improved assays to measure and

characterize the inducible HIV reservoir. EBioMedicine. https://doi.org/10.1016/j.ebiom.2018.09.036

Maucourant, C., Queiroz, G.A.N., Samri, A., Grassi, M.F.R., Yssel, H., Vieillard, V., 2019. Zika virus in the eye of the cytokine storm. Eur. Cytokine Netw. 30, 74–81. https://doi.org/10.1684/ecn.2019.0433

Max, B., 2019. Update on HIV integrase inhibitors for the treatment of HIV-1 infection. Future Virol. https://doi.org/10.2217/fvl-2019-0077

McCreary, E.K., Pogue, J.M., 2020. Coronavirus disease 2019 treatment: A review of early and emerging options. Open Forum Infect. Dis. https://doi.org/10.1093/ofid/ofaa105

McCune, J.M., 1995. Viral latency in HIV disease. Cell. https://doi.org/10.1016/0092-8674(95)90305-4

McLean, J.E., Wudzinska, A., Datan, E., Quaglino, D., Zakeri, Z., 2011. Flavivirus NS4A-induced autophagy protects cells against death and enhances virus replication. J. Biol. Chem. 286, 22147–22159. https://doi.org/10.1074/jbc.M110.192500

Meertens, L., Carnec, X., Lecoin, M.P., Guivel-benhassine, F., Lew, E., Lemke, G., Schwartz, O., Amara, A., 2012. The TIM and TAM Families of Phosphatidylserine Receptors. Cell Host Microbe 12, 544–557. https://doi.org/10.1016/j.chom.2012.08.009.The

Melhuish, A., Lewthwaite, P., 2018. Natural history of HIV and AIDS. Med. (United Kingdom) 46, 356–361. https://doi.org/10.1016/j.mpmed.2018.03.010

Méndez, C., Ledger, S., Petoumenos, K., Ahlenstiel, C., Kelleher, A.D., 2018. RNA-induced epigenetic silencing inhibits HIV-1 reactivation from latency. Retrovirology. https://doi.org/10.1186/s12977-018-0451-0

Mercer, J., Helenius, A., 2010. Apoptotic mimicry: Phosphatidylserine-mediated macropinocytosis of vaccinia virus. Ann. N. Y. Acad. Sci. 1209, 49–55. https://doi.org/10.1111/j.1749-6632.2010.05772.x

Mesci, P., Macia, A., Moore, S.M., Shiryaev, S.A., Pinto, A., Huang, C.T., Tejwani, L., Fernandes, I.R., Suarez, N.A., Kolar, M.J., Montefusco, S., Rosenberg, S.C., Herai, R.H., Cugola, F.R., Russo, F.B., Sheets, N., Saghatelian, A., Shresta, S., Momper, J.D., Siqueira-Neto, J.L., Corbett, K.D., Beltrão-Braga, P.C.B., Terskikh, A. V., Muotri, A.R., 2018. Blocking Zika virus vertical transmission. Sci. Rep. 8, 1–13. https://doi.org/10.1038/s41598-018-19526-4

Mexas, A.M., Graf, E.H., Pace, M.J., Yu, J.J., Papasavvas, E., Azzoni, L., Busch, M.P., Di Mascio, M., Foulkes, A.S., Migueles, S.A., Montaner, L.J., O'Doherty, U., 2012. Concurrent measures of total and integrated HIV DNA monitor reservoirs and ongoing replication in eradication trials. AIDS. https://doi.org/10.1097/QAD.0b013e32835a5c2f

Miller, S., Kastner, S., Krijnse-Locker, J., Bühler, S., Bartenschlager, R., 2007. The non-structural protein 4A of dengue virus is an integral membrane protein inducing membrane alterations in a 2K-regulated manner. J. Biol. Chem. 282, 8873–8882. https://doi.org/10.1074/jbc.M609919200

Morrey, J.D., Smee, D.F., Sidwell, R.W., Tseng, C., 2002. Identification of active antiviral compounds against a New York isolate of West Nile virus. Antiviral Res. 55, 107–116. https://doi.org/10.1016/S0166-3542(02)00013-X

Morrison, J., Aguirre, S., Fernandez-Sesma, A., 2012. Innate immunity evasion by dengue virus. Viruses 4, 397–413. https://doi.org/10.3390/v4030397

Mousseau, G., Kessing, C.F., Fromentin, R., Trautmann, L., Chomont, N., Valente, S.T., 2015. The tat inhibitor didehydro-cortistatin a prevents HIV-1 reactivation from latency. MBio. https://doi.org/10.1128/mBio.00465-15

Mukhopadhyay, S., Kuhn, R.J., Rossmann, M.G., 2005. A structural perspective of the Flavivirus life cycle. Nat. Rev. Microbiol. 3, 13–22. https://doi.org/10.1038/nrmicro1067

Müller, B., Tessmer, U., Schubert, U., Kräusslich, H.-G., 2000. Human Immunodeficiency Virus Type 1 Vpr Protein Is Incorporated into the Virion in Significantly Smaller Amounts than Gag and Is Phosphorylated in Infected Cells. J. Virol. https://doi.org/10.1128/jvi.74.20.9727-9731.2000

Muller, D.A., Young, P.R., 2013. The flavivirus NS1 protein: Molecular and structural biology, immunology, role in pathogenesis and application as a diagnostic biomarker. Antiviral Res. 98, 192–208. https://doi.org/10.1016/j.antiviral.2013.03.008

Muñoz-Jordán, J.L., Sánchez-Burgos, G.G., Laurent-Rolle, M., García-Sastre, A., 2003. Inhibition of interferon signaling by dengue virus. Proc. Natl. Acad. Sci. U. S. A. 100, 14333–14338. https://doi.org/10.1073/pnas.2335168100

Musinova, Y.R., Sheval, E. V., Dib, C., Germini, D., Vassetzky, Y.S., 2016. Functional roles of HIV-1 Tat protein in the nucleus. Cell. Mol. Life Sci. https://doi.org/10.1007/s00018-015-2077-x

Musso, D., Broult, J., Bierlaire, D., Lanteri, M.C., Aubry, M., 2017. Prevention of transfusion-transmitted Zika virus in French Polynesia, nucleic acid testing versus pathogen inactivation. ISBT Sci. Ser. 12, 254–259. https://doi.org/10.1111/voxs.12335

Musso, D., Roche, C., Robin, E., Nhan, T., Teissier, A., Cao-Lormeau, V.M., 2015. Potential sexual transmission of zika virus. Emerg. Infect. Dis. 21, 359–361. https://doi.org/10.3201/eid2102.141363

Naqvi, A.A.T., Fatima, K., Mohammad, T., Fatima, U., Singh, I.K., Singh, A., Atif, S.M., Hariprasad, G., Hasan, G.M., Hassan, M.I., 2020. Insights into SARS-CoV-2 genome, structure, evolution, pathogenesis and therapies: Structural genomics approach. Biochim. Biophys. Acta - Mol. Basis Dis. https://doi.org/10.1016/j.bbadis.2020.165878

Naveca, F.G., Pontes, G.S., Chang, A.Y.H., da Silva, G.A.V., do Nascimento, V.A., Monteiro, D.C. da S., da Silva, M.S., Abdalla, L.F., Santos, J.H.A., de Almeida, T.A.P., Mejía, M. del C.C., de Mesquita, T.G.R., Encarnação, H.V. de S., Gomes, M. de S., Amaral, L.R., Campi-Azevedo, A.C., Coelho-Dos-Reis, J.G., Antonelli, L.R. do V., Teixeira-Carvalho, A., Martins-Filho, O.A., Ramasawmy, R., 2018. Analysis of the immunological biomarker profile during acute zika virus infection reveals the overexpression of CXCL10, a chemokine linked to neuronal damage. Mem. Inst. Oswaldo Cruz 113, 1–13. https://doi.org/10.1590/0074-02760170542

Neerukonda, S.N., Katneni, U., 2020. A review on sars-cov-2 virology, pathophysiology, animal models, and anti-viral interventions. Pathogens. https://doi.org/10.3390/pathogens9060426

Neufeldt, C.J., Cortese, M., Acosta, E.G., Bartenschlager, R., 2018. Rewiring cellular networks by members of the Flaviviridae family. Nat. Rev. Microbiol. 16, 125–142. https://doi.org/10.1038/nrmicro.2017.170

Ng, W.C., Soto-Acosta, R., Bradrick, S.S., Garcia-Blanco, M.A., Ooi, E.E., 2017. The 5' and 3' untranslated regions of the flaviviral genome. Viruses 9, 1–14. https://doi.org/10.3390/v9060137

Nguyen, D.H., Hildreth, J.E.K., 2000. Evidence for Budding of Human Immunodeficiency Virus Type 1 Selectively from Glycolipid-Enriched Membrane Lipid Rafts. J. Virol. https://doi.org/10.1128/jvi.74.7.3264-3272.2000

Nguyen, S.M., Antony, K.M., Dudley, D.M., Kohn, S., Simmons, H.A., Wolfe, B., Shahriar Salamat, M., Teixeira, L.B.C., Wiepz, G.J., Thoong, T.H., Aliota, M.T., Weiler, A.M., Barry, G.L., Weisgrau, K.L., Vosler, L.J., Mohns, M.S., Breitbach, M.E., Stewart, L.M., Rasheed, M.N., Newman, C.M., Graham, M.E., Wieben, O.E., Turski, P.A., Johnson, K.M., Post, J., Hayes, J.M., Schultz-Darken, N., Schotzko, M.L., Eudailey, J.A., Permar, S.R., Rakasz, E.G., Mohr, E.L., Capuano, S., Tarantal, A.F., Osorio, J.E., O'connor, S.L., Friedrich, T.C., O'connor, D.H., Golos, T.G., 2017. Highly efficient maternal-fetal Zika virus transmission in pregnant rhesus macaques Author summary. PLoS Pathog. 13. https://doi.org/10.1371/journal.ppat.1006378

Nodder, S.B., Gummuluru, S., 2019. Illuminating the Role of Vpr in HIV Infection of Myeloid Cells. Front. Immunol. https://doi.org/10.3389/fimmu.2019.01606

Oran, D.P., Topol, E.J., 2020. Prevalence of Asymptomatic SARS-CoV-2 Infection : A Narrative Review. Ann. Intern. Med. https://doi.org/10.7326/M20-3012

Pandit, N.S., Chastain, D.B., Pallotta, A.M., Badowski, M.E., Huesgen, E.C., Michienzi, S.M., 2019. Simplifying ARV Therapy in the Setting of Resistance. Curr. Infect. Dis. Rep. https://doi.org/10.1007/s11908-019-0691-8

Park, W.B., Kwon, N.J., Choi, S.J., Kang, C.K., Choe, P.G., Kim, J.Y., Yun, J., Lee, G.W., Seong, M.W., Kim, N.J., Seo, J.S., Oh, M.D., 2020. Virus isolation from the first patient with SARS-CoV-2 in Korea. J. Korean Med. Sci. https://doi.org/10.3346/jkms.2020.35.e84

Passaes, C.P.B., Bruel, T., Decalf, J., David, A., Angin, M., Monceaux, V., Muller-Trutwin, M., Noel, N., Bourdic, K., Lambotte, O., Albert, M.L., Duffy, D., Schwartz, O., Sáez-Cirión, A., 2017. Ultrasensitive HIV-1 p24 Assay Detects Single Infected Cells and Differences in Reservoir Induction by Latency Reversal Agents. J. Virol. https://doi.org/10.1128/jvi.02296-16

Pasternak, A.O., De Bruin, M., Jurriaans, S., Bakker, M., Berkhout, B., Prins, J.M., Lukashov, V. V., 2012. Modest nonadherence to antiretroviral therapy promotes residual HIV-1 replication in the absence of virological rebound in plasma. J. Infect. Dis. https://doi.org/10.1093/infdis/jis502

Payne, A.F., Binduga-Gajewska, I., Kauffman, E.B., Kramer, L.D., 2006. Quantitation of flaviviruses by fluorescent focus assay. J. Virol. Methods. https://doi.org/10.1016/j.jviromet.2006.01.003

Payne, S., 2017. Family Flaviviridae. Viruses 129–139. https://doi.org/10.1016/b978-0-12-803109-4.00015-5

Pett, S.L., Amin, J., Horban, A., Andrade-Villanueva, J., Losso, M., Porteiro, N., Madero, J.S., Belloso, W., Tu, E., Silk, D., Kelleher, A., Harrigan, R., Clark, A., Sugiura, W., Wolff, M., Gill, J., Gatell, J., Fisher, M., Clarke, A., Ruxrungtham, K., Prazuck, T., Kaiser, R., Woolley, I., Arnaiz, J.A., Cooper, D., Rockstroh, J.K., Mallon, P., Emery, S., 2016. Maraviroc, as a switch option, in HIV-1-infected individuals with stable, well-controlled HIV replication and R5-tropic virus on their first Nucleoside/Nucleotide reverse transcriptase inhibitor plus ritonavir-boosted protease inhibitor regimen: Week 48 R. Clin. Infect. Dis. https://doi.org/10.1093/cid/ciw207

Pierson, T.C., Diamond, M.S., 2020. The continued threat of emerging flaviviruses. Nat. Microbiol. https://doi.org/10.1038/s41564-020-0714-0

Pinzone, M.R., O'Doherty, U., 2018. Measuring integrated HIV DNA ex vivo and in vitro provides insights about how reservoirs are formed and maintained. Retrovirology. https://doi.org/10.1186/s12977-018-0396-3

Potisopon, S., Priet, S., Collet, A., Decroly, E., Canard, B., Selisko, B., 2014. The methyltransferase domain of dengue virus protein NS5 ensures efficient RNA synthesis initiation and elongation by the polymerase domain. Nucleic Acids Res. 42, 11642–11656. https://doi.org/10.1093/nar/gku666

Priyamvada, L., Quicke, K.M., Hudson, W.H., Onlamoon, N., Sewatanon, J., Edupuganti, S., Pattanapanyasat, K., Chokephaibulkit, K., Mulligan, M.J., Wilson, P.C., Ahmed, R., Suthar, M.S., Wrammert, J., 2016. Human antibody responses after dengue virus infection are highly cross-reactive to Zika virus. Proc. Natl. Acad. Sci. U. S. A. 113, 7852–7857. https://doi.org/10.1073/pnas.1607931113

Procopio, F.A., Fromentin, R., Kulpa, D.A., Brehm, J.H., Bebin, A.G., Strain, M.C., Richman, D.D., O'Doherty, U., Palmer, S., Hecht, F.M., Hoh, R., Barnard, R.J.O., Miller, M.D., Hazuda, D.J., Deeks, S.G., Sékaly, R.P., Chomont, N., 2015. A Novel Assay to Measure the Magnitude of the Inducible Viral Reservoir in HIV-infected Individuals. EBioMedicine. https://doi.org/10.1016/j.ebiom.2015.06.019

Pryor, M.J., Wright, P.J., 1994. Glycosylation mutants of dengue virus NS1 protein. J. Gen. Virol. 75, 1183–1187. https://doi.org/10.1099/0022-1317-75-5-1183

Qing, E., Gallagher, T., 2020. SARS Coronavirus Redux. Trends Immunol. https://doi.org/10.1016/j.it.2020.02.007

Qing, M., Yang, F., Zhang, B., Zou, G., Robida, J.M., Yuan, Z., Tang, H., Shi, P.Y., 2009. Cyclosporine inhibits flavivirus replication through blocking the interaction between host cyclophilins and viral NS5 protein. Antimicrob. Agents Chemother. 53, 3226–3235. https://doi.org/10.1128/AAC.00189-09

Radi, M., Botta, L., Casaluce, G., Bernardini, M., Botta, M., 2010. Practical one-pot two-step protocol for the microwave-assisted synthesis of highly functionalized rhodanine derivatives. J. Comb. Chem. https://doi.org/10.1021/cc9001789

Rambaut, A., Holmes, E.C., O'Toole, Á., Hill, V., McCrone, J.T., Ruis, C., du Plessis, L., Pybus, O.G., 2020. A dynamic nomenclature proposal for SARS-CoV-2 lineages to assist genomic epidemiology. Nat. Microbiol. https://doi.org/10.1038/s41564-020-0770-5

Rathbun, 2018. Antiretroviral Therapy for HIV Infection. Medscape 57, 2789–2798.

Reddy, K., Ooms, M., Letko, M., Garrett, N., Simon, V., Ndung'U, T., 2016. Functional characterization of Vif proteins from HIV-1 infected patients with different APOBEC3G haplotypes. AIDS. https://doi.org/10.1097/QAD.0000000000001113

Reeves, J.D., Lee, F.H., Miamidian, J.L., Jabara, C.B., Juntilla, M.M., Doms, R.W., 2005. Enfuvirtide resistance mutations: impact on human immunodeficiency virus envelope function, entry inhibitor sensitivity, and virus neutralization. J. Virol. 79, 4991–4999. https://doi.org/79/8/4991 [pii]\r10.1128/JVI.79.8.4991-4999.2005

Rey, F.A., Stiasny, K., Heinz, F.X., 2017. Flavivirus structural heterogeneity: implications for cell entry. Curr. Opin. Virol. https://doi.org/10.1016/j.coviro.2017.06.009

Rhee, S.Y., Shafer, R.W., 2018. Data descriptor: Geographically-stratified HIV-1 group M pol subtype and circulating recombinant form sequences. Sci. Data. https://doi.org/10.1038/sdata.2018.148

Roby, J.A., Setoh, Y.X., Hall, R.A., Khromykh, A.A., 2015. Post-translational regulation and modifications of flavivirus structural proteins. J. Gen. Virol. 96, 1551–1569. https://doi.org/10.1099/vir.0.000097

Rodriguez-Roche, R., Gould, E.A., 2013. Understanding the dengue viruses and progress towards their control. Biomed Res. Int. 2013, 1–20. https://doi.org/10.1155/2013/690835

Rosenbloom, D.I.S., Bacchetti, P., Stone, M., Deng, X., Bosch, R.J., Richman, D.D., Siliciano, J.D., Mellors, J.W., Deeks, S.G., Ptak, R.G., Hoh, R., Keating, S.M., Dimapasoc, M., Massanella, M., Lai, J., Sobolewski, M.D., Kulpa, D.A., Busch, M.P., Staprans, S., Mellors, J., Richman, D., Deeks, S., Fitzgibbon, J., Keating, S., Bakkour, S., Bosch, R., Ho, R., Siliciano, R., Siliciano, J., Chomont, N., Rosenbloom, D., Ptak, R., Lee, S., 2019. Assessing intra-lab precision and inter-lab repeatability of outgrowth assays of hiv-1 latent reservoir size. PLoS Comput. Biol. https://doi.org/10.1371/journal.pcbi.1006849

Rossetti, B., Gagliardini, R., Meini, G., Sterrantino, G., Colangeli, V., Re, M.C., Latini, A., Colafigli, M., Vignale, F., Rusconi, S., Micheli, V., Biagio, A. Di, Orofino, G., Ghisetti, V., Fantauzzi, A., Vullo, V., Grima, P., Francisci, D., Mastroianni, C., Antinori, A., Trezzi, M., Lisi, L., Navarra, P., Canovari, B., D'Arminio Monforte, A., Lamonica, S., D'Avino, A., Zazzi, M., Giambenedetto, S. Di, De Luca, A., 2017. Switch to maraviroc with darunavir/r, both QD, in patients with suppressed HIV-1 was well tolerated but virologically inferior to standard antiretroviral therapy: 48-Week results of a randomized trial. PLoS One. https://doi.org/10.1371/journal.pone.0187393

Rotelli, L., Trigo-Rodríguez, J.M., Moyano-Cambero, C.E., Carota, E., Botta, L., Di Mauro, E., Saladino, R., 2016. The key role of meteorites in the formation of relevant prebiotic molecules in a formamide/water environment. Sci. Rep. https://doi.org/10.1038/srep38888

Rutsaert, S., Bosman, K., Trypsteen, W., Nijhuis, M., Vandekerckhove, L., 2018a. Digital PCR as a tool to measure HIV persistence. Retrovirology 15, 1–8. https://doi.org/10.1186/s12977-018-0399-0

Rutsaert, S., De Spiegelaere, W., Van Hecke, C., De Scheerder, M.A., Kiselinova, M., Vervisch, K., Trypsteen, W., Vandekerckhove, L., 2018b. In-depth validation of total HIV-1 DNA assays for quantification of various HIV-1 subtypes. Sci. Rep. https://doi.org/10.1038/s41598-018-35403-6

Sabin, C.A., Lundgren, J.D., 2013. The natural history of HIV infection. Curr. Opin. HIV AIDS. https://doi.org/10.1097/COH.0b013e328361fa66

Sacramento, C.Q., Melo, G.R. De, Rocha, N., Villas, L., Hoelz, B., Mesquita, M., Freitas, C.S. De, Fintelman-rodrigues, N., Marttorelli, A., Ferreira, A.C., Barbosa-lima, G., Bastos, M.M., Volotao, E.D.M., Tschoeke, D.A., Leomil, L., Bozza, F.A., Bozza, P.T., Boechat, N., Thompson, F.L., Filippis, A.M.B. De, Bruning, K., 2017. Next ○ The clinically approved antiviral drug sofosbuvir impairs Brazilian zika virus replication Neurochecklists Cérebro Reverso Ibrahim Imam. Nat. Publ. Gr. 7, 2016–2018. https://doi.org/10.1038/srep40920

Sahili, A. El, Lescar, J., 2017. Dengue virus non-structural protein 5. Viruses 9, 1–20. https://doi.org/10.3390/v9040091

Saladini, F., Giannini, A., Boccuto, A., Vicenti, I., Zazzi, M., 2018. Agreement between an in-house replication competent and a reference replication defective recombinant virus assay for measuring phenotypic resistance to HIV-1 protease, reverse transcriptase, and integrase inhibitors. J. Clin. Lab. Anal. 32, 1–10. https://doi.org/10.1002/jcla.22206

Sanders, J.M., Monogue, M.L., Jodlowski, T.Z., Cutrell, J.B., 2020. Pharmacologic Treatments for Coronavirus Disease 2019 (COVID-19): A Review. JAMA - J. Am. Med. Assoc. https://doi.org/10.1001/jama.2020.6019

Santoro, M.M., Perno, C.F., 2013. HIV-1 Genetic Variability and Clinical Implications. ISRN Microbiol. 2013, 1–20. https://doi.org/10.1155/2013/481314

Sanyal, A., Rangachar, V., Gupta, P., 2019. TZA, a sensitive reporter cell-based assay to accurately and rapidly quantify inducible, replication-competent latent HIV-1 from resting CD4 T cells. BIO-PROTOCOL. https://doi.org/10.21769/bioprotoc.3232

Saw, W.G., Chan, K.W.K., Vasudevan, S.G., Grüber, G., 2019. Zika virus nonstructural protein 5 residue R681 is critical for dimer formation and enzymatic activity. FEBS Lett. https://doi.org/10.1002/1873-3468.13437

Schoeman, D., Fielding, B.C., 2019. Coronavirus envelope protein: Current knowledge. Virol. J. https://doi.org/10.1186/s12985-019-1182-0

Šebera, J., Dubankova, A., Sychrovský, V., Ruzek, D., Boura, E., Nencka, R., 2018. The structural model of Zika virus RNA-dependent RNA polymerase in complex with RNA for rational design of novel nucleotide inhibitors. Sci. Rep. 8, 1–13. https://doi.org/10.1038/s41598-018-29459-7

Seitz, R., 2016. Human Immunodeficiency Virus (HIV). Transfus. Med. Hemotherapy 43, 203–222. https://doi.org/10.1159/000445852

Sejvar, J.J., 2016. West Nile Virus Infection. Microbiol. Spectr. 4, 1–19. https://doi.org/doi:10.1128/microbiolspec.EI10- 0021-2016

Shan, L., Rabi, S.A., Laird, G.M., Eisele, E.E., Zhang, H., Margolick, J.B., Siliciano, R.F., 2013. A Novel PCR Assay for Quantification of HIV-1 RNA. J. Virol. https://doi.org/10.1128/jvi.00006-13

Sharp, P.M., Beatrice H. Hahn, 2011. Origins of HIV and the AIDS epidemic. Cold Spring Harb. Perspect. Med. https://doi.org/10.1101/cshperspect.a006841 a006841 [pii]

Shaw, G.M., Hunter, E., 2012. HIV Transmission. Cold Spring Harb. Lab. Press 1–24.

Sheahan, T.P., Sims, A.C., Graham, R.L., Menachery, V.D., Gralinski, L.E., Case, J.B., Leist, S.R., Pyrc, K., Feng, J.Y., Trantcheva, I., Bannister, R., Park, Y., Babusis, D., Clarke, M.O., MacKman, R.L., Spahn, J.E., Palmiotti, C.A., Siegel, D., Ray, A.S., Cihlar, T., Jordan, R., Denison, M.R., Baric, R.S., 2017. Broad-spectrum antiviral GS-5734 inhibits both epidemic and zoonotic coronaviruses. Sci. Transl. Med. https://doi.org/10.1126/scitranslmed.aal3653

Shirt-Ediss, B., Murillo-Sànchez, S., Ruiz-Mirazo, K., 2017. Framing major prebiotic transitions as stages of protocell development:

Three challenges for origins-of-life research. Beilstein J. Org. Chem. https://doi.org/10.3762/bjoc.13.135

Siliciano, J.D., Lai, J., Callender, M., Pitt, E., Zhang, H., Margolick, J.B., Gallant, J.E., Cofrancesco, J., Moore, R.D., Gange, S.J., Siliciano, R.F., 2007. Stability of the latent reservoir for HIV-1 in patients receiving valproic acid. J. Infect. Dis. https://doi.org/10.1086/511823

Siliciano, J.D., Siliciano, R.F., 2005. Enhanced culture assay for detection and quantitation of latently infected, resting CD4+ T-cells carrying replication-competent virus in HIV-1-infected individuals. Methods Mol. Biol. https://doi.org/10.1385/1-59259-907-9:003

Silva, J.V.J., Lopes, T.R.R., Oliveira-Filho, E.F. d., Oliveira, R.A.S., Durães-Carvalho, R., Gil, L.H.V.G., 2018. Current status, challenges and perspectives in the development of vaccines against yellow fever, dengue, Zika and chikungunya viruses. Acta Trop. https://doi.org/10.1016/j.actatropica.2018.03.009

Slavov, S.N., Otaguiri, K.K., Kashima, S., Covas, D.T., 2016. Overview of Zika virus (ZIKV) infection in regards to the Brazilian epidemic. Brazilian J. Med. Biol. Res. 49, 1–11. https://doi.org/10.1590/1414-431X20165420

Sluis-Cremer, N., Arion, D., Abram, M.E., Parniak, M.A., 2004. Proteolytic processing of an HIV-1 pol polyprotein precursor: Insights into the mechanism of reverse transcriptase p66/p51 heterodimer formation. Int. J. Biochem. Cell Biol. https://doi.org/10.1016/j.biocel.2004.02.020

Smithburn, K.C., Hughes, T.P., Burke, A.W., Paul, J.H., 1940. A Neurotropic Virus Isolated from the Blood of a Native of Uganda 1. Am. J. Trop. Med. Hyg. https://doi.org/10.4269/ajtmh.1940.s1-20.471

Somnuke, P., Hauhart, R.E., Atkinson, J.P., Diamond, M.S., Avirutnan, P., 2011. N-linked glycosylation of dengue virus NS1 protein modulates secretion, cell-surface expression, hexamer stability, and interactions with human complement. Virology 413, 253–264. https://doi.org/10.1016/j.virol.2011.02.022

Song, B.H., Yun, S.I., Woolley, M., Lee, Y.M., 2017. Zika virus: History, epidemiology, transmission, and clinical presentation. J. Neuroimmunol. 308, 50–64. https://doi.org/10.1016/j.jneuroim.2017.03.001

Spina, C.A., Anderson, J., Archin, N.M., Bosque, A., Chan, J., Famiglietti, M., Greene, W.C., Kashuba, A., Lewin, S.R., Margolis, D.M., Mau, M., Ruelas, D., Saleh, S., Shirakawa, K., Siliciano, R.F., Singhania, A., Soto, P.C., Terry, V.H., Verdin, E., Woelk, C., Wooden, S., Xing, S., Planelles, V., 2013. An In-Depth Comparison of Latent HIV-1 Reactivation in Multiple Cell Model Systems and Resting CD4+ T Cells from Aviremic Patients. PLoS Pathog. https://doi.org/10.1371/journal.ppat.1003834

Stettler, K., Beltramello, M., Espinosa, D.A., Graham, V., Cassotta, A., Bianchi, S., Vanzetta, F., Minola, A., Jaconi, S., Mele, F., Foglierini, M., Pedotti, M., Simonelli, L., Dowall, S., Atkinson, B., Percivalle, E., Simmons, C.P., Varani, L., Blum, J., Baldanti, F., Cameroni, E., Hewson, R., Harris, E., Lanzavecchia, A., Sallusto, F., Corti, D., 2016. Specificity, cross-reactivity, and function of antibodies elicited by Zika virus infection. Science (80-.). 353, 823–826. https://doi.org/10.1126/science.aaf8505

Stonedahl, S., Clarke, P., Tyler, K.L., 2020. The Role of Microglia during West Nile Virus Infection of the Central Nervous System 1–14.

Suen, W.W., Prow, N.A., Hall, R.A., Bielefeldt-Ohmann, H., 2014. Mechanism of west nile virus neuroinvasion: A critical appraisal. Viruses 6, 2796–2825. https://doi.org/10.3390/v6072796

Sun, J., Zhu, A., Li, H., Zheng, K., Zhuang, Z., Chen, Z., Shi, Y., Zhang, Z., Chen, S. bei, Liu, X., Dai, J., Li, X., Huang, S., Huang, X., Luo, L., Wen, L., Zhuo, J., Li, Yuming, Wang, Y., Zhang, L., Zhang, Y., Li, F., Feng, L., Chen, X., Zhong, N., Yang, Z., Huang, J., Zhao, J., Li, Yi min, 2020. Isolation of infectious SARS-CoV-2 from urine of a COVID-19 patient. Emerg. Microbes Infect. https://doi.org/10.1080/22221751.2020.1760144

Sungnak, W., Huang, N., Bécavin, C., Berg, M., Queen, R., Litvinukova, M., Talavera-López, C., Maatz, H., Reichart, D., Sampaziotis, F., Worlock, K.B., Yoshida, M., Barnes, J.L., Banovich, N.E., Barbry, P., Brazma, A., Collin, J., Desai, T.J., Duong, T.E., Eickelberg, O., Falk, C., Farzan, M., Glass, I., Gupta, R.K., Haniffa, M., Horvath, P., Hubner, N., Hung, D., Kaminski, N., Krasnow, M., Kropski, J.A., Kuhnemund, M., Lako, M., Lee, H., Leroy, S., Linnarson, S., Lundeberg, J., Meyer, K.B., Miao, Z., Misharin, A. V., Nawijn, M.C., Nikolic, M.Z., Noseda, M., Ordovas-Montanes, J., Oudit, G.Y., Pe'er, D., Powell, J., Quake, S., Rajagopal, J., Tata, P.R., Rawlins, E.L., Regev, A., Reyfman, P.A., Rozenblatt-Rosen, O., Saeb-Parsy, K., Samakovlis, C., Schiller, H.B., Schultze, J.L., Seibold, M.A., Seidman, C.E., Seidman, J.G., Shalek, A.K., Shepherd, D., Spence, J., Spira, A., Sun, X., Teichmann, S.A., Theis, F.J., Tsankov, A.M., Vallier, L., van den Berge, M., Whitsett, J., Xavier, R., Xu, Y., Zaragosi, L.E., Zerti, D., Zhang, H., Zhang, K., Rojas, M., Figueiredo, F., 2020. SARS-CoV-2 entry factors are highly expressed in nasal epithelial cells together with innate immune genes. Nat. Med. https://doi.org/10.1038/s41591-020-0868-6

Swaminathan, S., Schlaberg, R., Lewis, J., Hanson, K.E., Couturier, M.R., 2016. Fatal Zika Virus Infection with Secondary Nonsexual Transmission. N. Engl. J. Med. 375, 1907–1909. https://doi.org/10.1056/NEJMc1610613

Tay, M.Y.F., Saw, W.G., Zhao, Y., Chan, K.W.K., Singh, D., Chong, Y., Forwood, J.K., Ooi, E.E., Grüber, G., Lescar, J., Luo, D., Vasudevan, S.G., 2015. The C-terminal 50 amino acid residues of dengue NS3 protein are important for NS3-NS5 interaction and viral replication. J. Biol. Chem. 290, 2379–2394. https://doi.org/10.1074/jbc.M114.607341

Taylor, B.S., Sobieszczyk, M.E., McCutchan, F.E., Hammer, S.M., 2008. The challenge of HIV-1 subtype diversity. N. Engl. J. Med. https://doi.org/10.1056/NEJMra0706737

Teimury, A., Khaledi, E.M., 2020. Current options in the treatment of covid-19: A review. Risk Manag. Healthc. Policy. https://doi.org/10.2147/RMHP.S265030

Thomas, J., Ruggiero, A., Paxton, W.A., Pollakis, G., 2020. Measuring the Success of HIV-1 Cure Strategies. Front. Cell. Infect. Microbiol. https://doi.org/10.3389/fcimb.2020.00134

Thomas, J., Ruggiero, A., Procopio, F.A., Pantaleo, G., Paxton, W.A., Pollakis, G., 2019. Comparative analysis and generation of a robust HIV-1 DNA quantification assay. J. Virol. Methods. https://doi.org/10.1016/j.jviromet.2018.10.010

Tongo, M., Dorfman, J.R., Martin, D.P., 2016. High Degree of HIV-1 Group M (HIV-1M) Genetic Diversity within Circulating Recombinant Forms: Insight into the Early Events of HIV-1M Evolution. J. Virol. https://doi.org/10.1128/jvi.02302-15

Trypsteen, W., Kiselinova, M., Vandekerckhove, L., De Spiegelaere, W., 2016. Diagnostic utility of droplet digital PCR for HIV

reservoir quantification. J. virus Erad. 2, 162–9.

Tsai, A., Irrinki, A., Kaur, J., Cihlar, T., Kukolj, G., Sloan, D.D., Murry, J.P., 2017. Toll-Like Receptor 7 Agonist GS-9620 Induces HIV Expression and HIV-Specific Immunity in Cells from HIV-Infected Individuals on Suppressive Antiretroviral Therapy. J. Virol. https://doi.org/10.1128/jvi.02166-16

V'kovski, P., Kratzel, A., Steiner, S., Stalder, H., Thiel, V., 2020. Coronavirus biology and replication: implications for SARS-CoV-2. Nat. Rev. Microbiol. https://doi.org/10.1038/s41579-020-00468-6

Valentine, K.M., Croft, M., Shresta, S., 2020. Protection against dengue virus requires a sustained balance of antibody and T cell responses. Curr. Opin. Virol. 43, 22–27. https://doi.org/10.1016/j.coviro.2020.07.018

Vandergeeten, C., Fromentin, R., Merlini, E., Lawani, M.B., DaFonseca, S., Bakeman, W., McNulty, A., Ramgopal, M., Michael, N., Kim, J.H., Ananworanich, J., Chomont, N., 2014. Cross-Clade Ultrasensitive PCR-Based Assays To Measure HIV Persistence in Large-Cohort Studies. J. Virol. https://doi.org/10.1128/jvi.00609-14

Vanhamel, J., Bruggemans, A., Debyser, Z., 2019. Establishment of latent HIV-1 reservoirs: What do we really know? J. Virus Erad. https://doi.org/10.1016/s2055-6640(20)30275-2

Vaughn, D.W., Green, S., Kalayanarooj, S., Innis, B.L., Nimmannitya, S., Suntayakorn, S., Endy, T.P., Raengsakulrach, B., Rothman, A.L., Ennis, F.A., Nisalak, A., 2000. Dengue Viremia Titer, Antibody Response Pattern, and Virus Serotype Correlate with Disease Severity. J. Infect. Dis. 181, 2–9. https://doi.org/10.1086/315215

Ventura, J.D., 2020. Human immunodeficiency virus 1 (Hiv-1): Viral latency, the reservoir, and the cure. Yale J. Biol. Med. 93, 549–560.

Vicenti, I., Boccuto, A., Giannini, A., Dragoni, F., Saladini, F., Zazzi, M., 2018. Comparative analysis of different cell systems for Zika virus (ZIKV) propagation and evaluation of anti-ZIKV compounds in vitro. Virus Res. 244, 64–70. https://doi.org/10.1016/j.virusres.2017.11.003

Vicenti, I., Dragoni, F., Giannini, A., Giammarino, F., Spinicci, M., Saladini, F., Boccuto, A., Zazzi, M., 2020a. Development of a Cell-Based Immunodetection Assay for Simultaneous Screening of Antiviral Compounds Inhibiting Zika and Dengue Virus Replication. SLAS Discov. 25, 506–514. https://doi.org/10.1177/2472555220911456

Vicenti, I., Dragoni, F., Monti, M., Trombetta, C.M., Giannini, A., Boccuto, A., Saladini, F., Rossetti, B., De Luca, A., Ciabattini, A., Pastore, G., Medaglini, D., Orofino, G., Montomoli, E., Zazzi, M., 2020b. Maraviroc as a potential HIV-1 latency-reversing agent in cell line models and ex vivo CD4 T cells. J. Gen. Virol. 0–9. https://doi.org/10.1099/jgv.0.001499

Volcic, M., Sparrer, K.M.J., Koepke, L., Hotter, D., Sauter, D., Stürzel, C.M., Scherer, M., Stamminger, T., Hofmann, T.G., Arhel, N.J., Wiesmüller, L., Kirchhoff, F., 2020. Vpu modulates DNA repair to suppress innate sensing and hyper-integration of HIV-1. Nat. Microbiol. https://doi.org/10.1038/s41564-020-0753-6

Waldorf, K.M.A., Stencel-Baerenwald, J.E., Kapur, R.P., Studholme, C., Boldenow, E., Vornhagen, J., Baldessari, A., Dighe, M.K., Thiel, J., Merillat, S., Armistead, B., Tisoncik-Go, J., Davis, M.A., Dewey, E.C., Fairgrieve, M.R., Gatenby, C., Richards, T., Garden, G.A., Fernandez, E., Diamond, M.S., Juul, S.E., Gale, M., Rajagopal, L., 2016. Fetal brain lesions after subcutaneous inoculation of Zika virus in pregnant non human primates. Nat. Med. 15, 1256–1259. https://doi.org/10.1038/nm.4193

Walker-Sperling, V.E., Pohlmeyer, C.W., Tarwater, P.M., Blankson, J.N., 2016. The Effect of Latency Reversal Agents on Primary CD8+ T Cells: Implications for Shock and Kill Strategies for Human Immunodeficiency Virus Eradication. EBioMedicine 8, 217–229. https://doi.org/10.1016/j.ebiom.2016.04.019

Wang, A., Thurmond, S., Islas, L., Hui, K., Hai, R., 2017. Zika virus genome biology and molecular pathogenesis. Emerg. Microbes Infect. 6, 1–6. https://doi.org/10.1038/emi.2016.141

Wang, Chunyan, Li, W., Drabek, D., Okba, N.M.A., van Haperen, R., Osterhaus, A.D.M.E., van Kuppeveld, F.J.M., Haagmans, B.L., Grosveld, F., Bosch, B.J., 2020. A human monoclonal antibody blocking SARS-CoV-2 infection. Nat. Commun. https://doi.org/10.1038/s41467-020-16256-y

Wang, Changtai, Liu, Z., Chen, Z., Huang, X., Xu, M., He, T., Zhang, Z., 2020. The establishment of reference sequence for SARS-CoV-2 and variation analysis. J. Med. Virol. https://doi.org/10.1002/jmv.25762

Wang, C.C., Huang, Z.S., Chiang, P.L., Chen, C.T., Wu, H.N., 2009. Analysis of the nucleoside triphosphatase, RNA triphosphatase, and unwinding activities of the helicase domain of dengue virus NS3 protein. FEBS Lett. 583, 691–696. https://doi.org/10.1016/j.febslet.2009.01.008

Wang, M., Cao, R., Zhang, L., Yang, X., Liu, J., Xu, M., Shi, Z., Hu, Z., Zhong, W., Xiao, G., 2020. Remdesivir and chloroquine effectively inhibit the recently emerged novel coronavirus (2019-nCoV) in vitro. Cell Res. https://doi.org/10.1038/s41422-020-0282-0

Wang, W., Xu, Y., Gao, R., Lu, R., Han, K., Wu, G., Tan, W., 2020. Detection of SARS-CoV-2 in Different Types of Clinical Specimens. JAMA - J. Am. Med. Assoc. https://doi.org/10.1001/jama.2020.3786

Wang, Yeming, Zhang, D., Du, G., Du, R., Zhao, J., Jin, Y., Fu, S., Gao, L., Cheng, Z., Lu, Q., Hu, Y., Luo, G., Wang, K., Lu, Y., Li, H., Wang, S., Ruan, S., Yang, C., Mei, C., Wang, Yi, Ding, D., Wu, F., Tang, X., Ye, X., Ye, Y., Liu, B., Yang, J., Yin, W., Wang, A., Fan, G., Zhou, F., Liu, Z., Gu, X., Xu, J., Shang, L., Zhang, Y., Cao, L., Guo, T., Wan, Y., Qin, H., Jiang, Y., Jaki, T., Hayden, F.G., Horby, P.W., Cao, B., Wang, C., 2020. Remdesivir in adults with severe COVID-19: a randomised, double-blind, placebo-controlled, multicentre trial. Lancet. https://doi.org/10.1016/S0140-6736(20)31022-9

Weaver, S.C., Costa, F., Garcia-Blanco, M.A., Ko, A.I., Ribeiro, G.S., Saade, G., Shi, P.-Y., Vasilakis, N., 2016. Zika Virus: History, Emergence, Biology, and Prospects for Control HHS Public Access. Antivir. Res 130, 69–80. https://doi.org/10.1016/j.antiviral.2016.03.010

Weaver, S.C., Vasilakis, N., 2009. Molecular Evolution of Dengue Viruses: Contributions of Phylogenetics to Understanding the History and Epidemiology of the Preeminent Arboviral Disease. Infect Genet Evol 9, 523–540. https://doi.org/10.1016/j.meegid.2009.02.003

Weber, G., Marceau, K., Ruttle, P.L., Shirtcliff, E.A., Essex, M.J., Susman, E.J., Studies, A., Hospital, R.I., Studies, F., Orleans, N., 2015. Interleukin-3 amplifies acute inflammation and is a potential therapeutic target in sepsis. Science. 57, 742–768.

https://doi.org/10.1002/dev.21214.Developmental

Wei, P., Garber, M.E., Fang, S.M., Fischer, W.H., Jones, K.A., 1998. A novel CDK9-associated C-type cyclin interacts directly with HIV-1 Tat and mediates its high-affinity, loop-specific binding to TAR RNA. Cell. https://doi.org/10.1016/S0092-8674(00)80939-3

Wen, Z., Song, H., Ming, G.L., 2017. How does Zika virus cause microcephaly? Genes Dev. 31, 849–861. https://doi.org/10.1101/gad.298216.117

Wengler, Gerd, Wengler, Gisela, 1993. The NS 3 nonstructural protein of flaviviruses contains an RNA triphosphatase activity. Virology 197, 265–273. https://doi.org/10.1006/viro.1993.1587

Wengler, Gerd, Wengler, Gisela, 1991. The carboxy-terminal part of the NS 3 protein of the West Nile Flavivirus can be isolated as a soluble protein after proteolytic cleavage and represents an RNA-stimulated NTPase. Virology 184, 707–715. https://doi.org/10.1016/0042-6822(91)90440-M

Wensing, A.M.J., van Maarseveen, N.M., Nijhuis, M., 2010. Fifteen years of HIV Protease Inhibitors: raising the barrier to resistance. Antiviral Res. https://doi.org/10.1016/j.antiviral.2009.10.003

Whiteman, M.C., Li, L., Wicker, J.A., Kinney, R.M., Huang, C., Beasley, D.W.C., Chung, K.M., Diamond, M.S., Solomon, T., Barrett, A.D.T., 2010. Development and characterization of non-glycosylated E and NS1 mutant viruses as a potential candidate vaccine for West Nile virus. Vaccine 28, 1075–1083. https://doi.org/10.1016/j.vaccine.2009.10.112

Willey, R.L., Klimkait, T., Frucht, D.M., Bonifacinot, J.S., Martin, M.A., 1991. Mutations within the human immunodeficiency virus type 1 gp160 envelope glycoprotein alter its intracellular transport and processing. Virology. https://doi.org/10.1016/0042-6822(91)90848-6

Williams, J.P., Hurst, J., Stöhr, W., Robinson, N., Brown, H., Fisher, M., Kinloch, S., Cooper, D., Schechter, M., Tambussi, G., Fidler, S., Carrington, M., Babiker, A., Weber, J., Koelsch, K.K., Kelleher, A.D., Phillips, R.E., Frater, J., 2014. HIV-1 DNA predicts disease progression and post-treatment virological control. Elife. https://doi.org/10.7554/eLife.03821

Williamson, P.C., Linnen, J.M., Kessler, D.A., Shaz, B.H., Kamel, H., Vassallo, R.R., Winkelman, V., Gao, K., Ziermann, R., Menezes, J., Thomas, S., Holmberg, J.A., Bakkour, S., Stone, M., Lu, K., Simmons, G., Busch, M.P., 2017. First cases of Zika virus–infected US blood donors outside states with areas of active transmission. Transfusion 57, 770–778. https://doi.org/10.1111/trf.14041

Wiwanitkit, V., 2009. Unusual mode of transmission of dengue. J. Infect. Dev. Ctries. 4, 51–54. https://doi.org/10.3855/jidc.145

Wong, J.K., Yukl, S.A., 2016. Tissue reservoirs of HIV. Curr. Opin. HIV AIDS. https://doi.org/10.1097/COH.0000000000000293

Wood, A., Armour, D., 2005. The Discovery of the CCR5 Receptor Antagonist, UK-427,857, A New Agent for the Treatment of HIV Infection and AIDS. Prog. Med. Chem. https://doi.org/10.1016/S0079-6468(05)43007-6

Woollard, S.M., Kanmogne, G.D., 2015. Maraviroc: A review of its use in hivinfection and beyond. Drug Des. Devel. Ther. 9, 5447–5468. https://doi.org/10.2147/DDDT.S90580

Wu, L., Gerard, N.P., Wyatt, R., Choe, H., Parolin, C., Ruffing, N., Borsetti, A., Cardoso, A.A., Desjardin, E., Newman, W., Gerard, C., Sodroski, J., 1996. CD4-induced interaction of primary HIV-1 gp120 glycoproteins with the chemokine receptor CCR-5. Nature. https://doi.org/10.1038/384179a0

Xia, H., Luo, H., Shan, C., Muruato, A.E., Nunes, B.T.D., Medeiros, D.B.A., Zou, J., Xie, X., Giraldo, M.I., Vasconcelos, P.F.C., Weaver, S.C., Wang, T., Rajsbaum, R., Shi, P.-Y., 2018. An evolutionary NS1 mutation enhances Zika virus evasion of host interferon induction. Nat. Commun. 9. https://doi.org/10.1038/s41467-017-02816-2

Xiao, F., Sun, J., Xu, Y., Li, F., Huang, X., Li, H., Zhao, Jingxian, Huang, J., Zhao, Jincun, 2020. Infectious SARS-CoV-2 in feces of patient with severe COVID-19. Emerg. Infect. Dis. https://doi.org/10.3201/eid2608.200681

Xu, H.T., Colby-Germinario, S.P., Hassounah, S.A., Fogarty, C., Osman, N., Palanisamy, N., Han, Y., Oliveira, M., Quan, Y., Wainberg, M.A., 2017. Evaluation of Sofosbuvir (β-D-2′-deoxy-2′-α-fluoro-2′-β-C-methyluridine) as an inhibitor of Dengue virus replication. Sci. Rep. 7, 1–11. https://doi.org/10.1038/s41598-017-06612-2

Xu, W., Li, H., Wang, Q., Hua, C., Zhang, H., Li, W., Jiang, S., Lu, L., 2017. Advancements in Developing Strategies for Sterilizing and Functional HIV Cures. Biomed Res. Int. https://doi.org/10.1155/2017/6096134

Xu, X., Han, M., Li, T., Sun, W., Wang, D., Fu, B., Zhou, Y., Zheng, X., Yang, Y., Li, X., Zhang, X., Pan, A., Wei, H., 2020. Effective treatment of severe COVID-19 patients with tocilizumab. Proc. Natl. Acad. Sci. U. S. A. https://doi.org/10.1073/pnas.2005615117

Yang, J., Xu, Y., Yan, Y., Li, W., Zhao, L., Dai, Q., Li, Y., Li, S., Zhong, J., Cao, R., Zhong, W., 2020. Small Molecule Inhibitor of ATPase Activity of HSP70 as a Broad-Spectrum Inhibitor against Flavivirus Infections. ACS Infect. Dis. https://doi.org/10.1021/acsinfecdis.9b00376

Yao, X., Ye, F., Zhang, M., Cui, C., Huang, B., Niu, P., Liu, X., Zhao, L., Dong, E., Song, C., Zhan, S., Lu, R., Li, H., Tan, W., Liu, D., 2020. In vitro antiviral activity and projection of optimized dosing design of hydroxychloroquine for the treatment of severe acute respiratory syndrome coronavirus 2 (SARS-CoV-2). Clin. Infect. Dis. https://doi.org/10.1093/cid/ciaa237

Yap, T.L., Xu, T., Chen, Y.-L., Malet, H., Egloff, M.-P., Canard, B., Vasudevan, S.G., Lescar, J., 2007. Crystal Structure of the Dengue Virus RNA-Dependent RNA Polymerase Catalytic Domain at 1.85-Angstrom Resolution. J. Virol. 81, 4753–4765. https://doi.org/10.1128/jvi.02283-06

Yost, R., Pasquale, T.R., Sahloff, E.G., 2009. Maraviroc: A coreceptor CCR5 antagonist for management of HIV infection. Am. J. Heal. Pharm. https://doi.org/10.2146/ajhp080206

Yu, I.M., Zhang, W., Holdaway, H.A., Li, L., Kostyuchenko, V.A., Chipman, P.R., Kuhn, R.J., Rossmann, M.G., Chen, J., 2008. Structure of the immature dengue virus at low pH primes proteolytic maturation. Science (80-.). 319, 1834–1837. https://doi.org/10.1126/science.1153264

Zannoli, S., Sambri, V., 2019. West nile virus and usutu virus co-circulation in europe: Epidemiology and implications. Microorganisms 7, 1–13. https://doi.org/10.3390/microorganisms7070184

Zhang, T., Wu, Q., Zhang, Z., 2020. Probable Pangolin Origin of SARS-CoV-2 Associated with the COVID-19 Outbreak. Curr. Biol.

https://doi.org/10.1016/j.cub.2020.03.022

Zhang, Y., Zhang, W., Ogata, S., Clements, D., Strauss, J.H., Baker, T.S., Kuhn, R.J., Rossmann, M.G., 2004. Conformational changes of the flavivirus E glycoprotein. Structure 12, 1607–1618. https://doi.org/10.1016/j.str.2004.06.019

Zhao, B., Yi, G., Du, F., Chuang, Y.C., Vaughan, R.C., Sankaran, B., Kao, C.C., Li, P., 2017. Structure and function of the Zika virus full-length NS5 protein. Nat. Commun. 8. https://doi.org/10.1038/ncomms14762

Zheng, A., Yuan, F., Kleinfelter, L.M., Kielian, M., 2014. A toggle switch controls the low pH-triggered rearrangement and maturation of the dengue virus envelope proteins. Nat. Commun. 5, 1–9. https://doi.org/10.1038/ncomms4877

Zheng, W., Thorne, N., Mckew, J.C., 2015. Zika Virus Infects Human Cortical Neural Precursors and Attenuates Their Growth 18, 1067–1073. https://doi.org/10.1016/j.drudis.2013.07.001.Phenotypic

Zhu, N., Zhang, D., Wang, W., Li, X., Yang, B., Song, J., Zhao, X., Huang, B., Shi, W., Lu, R., Niu, P., Zhan, F., Ma, X., Wang, D., Xu, W., Wu, G., Gao, G.F., Tan, W., 2020. A Novel Coronavirus from Patients with Pneumonia in China, 2019. N. Engl. J. Med. https://doi.org/10.1056/nejmoa2001017

Zumla, A., Chan, J.F.W., Azhar, E.I., Hui, D.S.C., Yuen, K.Y., 2016. Coronaviruses-drug discovery and therapeutic options. Nat. Rev. Drug Discov. https://doi.org/10.1038/nrd.2015.37

Züst, R., Cervantes-barragan, L., Habjan, M., Maier, R., Diamond, M.S., Siddell, S.G., Ludewig, B., Thiel, V., 2011. Ribose 2'-O-methylation provides a molecular signature for the distinction of self and non-self mRNA dependent on the RNA sensor Mda5 12, 137–143. https://doi.org/10.1038/ni.1979.Ribose

Original Research

Development of a Cell-Based Immunodetection Assay for Simultaneous Screening of Antiviral Compounds Inhibiting Zika and Dengue Virus Replication

Ilaria Vicenti[1] (iD), Filippo Dragoni[1], Alessia Giannini[1], Federica Giammarino[1], Michele Spinicci[2], Francesco Saladini[1], Adele Boccuto[1], and Maurizio Zazzi[1]

Abstract

Practical cell-based assays can accelerate anti-Zika (ZIKV) and anti-dengue (DENV) virus drug discovery. We developed an immunodetection assay (IA), using a pan-flaviviral monoclonal antibody recognizing a conserved envelope domain. The final protocol includes a direct virus yield reduction assay (YRA) carried out in the human Huh7 cell line, followed by transfer of the supernatant to a secondary Huh7 culture to characterize late antiviral effects. Sofosbuvir and ribavirin were used to validate the assay, while celgosivir was used to evaluate the ability to discriminate between early and late antiviral activity. In the direct YRA, at 100, 50, and 25 $TCID_{50}$, sofosbuvir IC_{50} values were 5.0 ± 1.5, 2.7 ± 0.5, 2.5 ± 1.1 µM against ZIKV and 16.6 ± 2.8, 4.6 ± 1.4, 2.6 ± 2.2 µM against DENV; ribavirin IC_{50} values were 6.8 ± 4.0, 3.8 ± 0.6, 4.5 ± 1.4 µM against ZIKV and 17.3 ± 4.6, 7.6 ± 1.2, 4.1 ± 2.3 µM against DENV. Sofosbuvir and ribavirin IC_{50} values determined in the secondary YRA were reproducible and comparable with those obtained by direct YRA and plaque reduction assay (PRA). In agreement with the proposed mechanism of late action, celgosivir was active against DENV only in the secondary YRA (IC_{50} 11.0 ± 1.0 µM) and in PRA (IC_{50} 10.1 ± 1.1 µM). The assay format overcomes relevant limitations of the gold standard PRA, allowing concurrent analysis of candidate antiviral compounds against different viruses and providing preliminary information about early versus late antiviral activity.

Introduction

Dengue (DENV) and Zika (ZIKV) viruses are related members of the Flaviviridae family, transmitted by mosquitoes of the *Aedes* genus.[1–3] Multiple factors, such as globalization,[4] environmental changes favoring reproduction of the vector,[5] and viral adaptation to the urban setting,[6] have recently spread these viruses to novel areas. DENV is the most prevalent arboviral infection in humans, as indicated by the World Health Organization (WHO) (https://www.who.int/dengue-control/disease/en/), causing severe flu-like illness and occasionally lethal dengue hemorrhagic fever or dengue shock syndrome. Over the last 50 years, the incidence of DENV has increased dramatically with an estimated 400 million new infections per year occurring mainly in tropical and subtropical areas.[1] Since the first recognized large outbreak of ZIKV in Micronesia in 2007, ZIKV has also spread rapidly to many countries in the Americas affecting millions of individuals. The association of ZIKV infection with Guillain-Barré syndrome in adults and congenital brain abnormalities in newborn infants,[7] established during the last Brazilian

outbreak, has renewed the interest in ZIKV. Consequently, the WHO has ranked DENV as the most critical mosquito-borne viral disease and ZIKV as an international public health emergency.

Despite the urgent need for effective treatment, no specific antiviral therapy is available to control ZIKV or DENV infection and transmission.[8,9] In addition, increasing rates of co-infections with different flaviviruses co-circulating within the same vector complicate the clinical outcome and

[1]Department of Medical Biotechnologies, University of Siena, Siena, Italy
[2]Unit of Infectious Diseases, Careggi University Hospital, Florence, Toscana, Italy

Corresponding Author:
Ilaria Vicenti, Department of Medical Biotechnologies, University of Siena, Viale Bracci 16, Siena, 53100, Italy.
Email: ilariavicenti@gmail.com

treatment options.[10] Potential targets for antiflavivirus compounds include viral proteins, such as protease or polymerase, and host cell functions essential for virus replication, such as α-glucosidase and proteins involved in nucleoside biosynthesis.[11,12]

High-throughput screening (HTS) of libraries of small molecules is a powerful tool to identify novel flavivirus inhibitors;[13–15] however, measurement of virus replication can be cumbersome, expensive, and prone to inaccuracy. To date, a variety of methods have been developed, including the classical plaque reduction assay (PRA),[16–18] microscopy monitoring of cytopathic effect (CPE),[19] and immunofluorescence-based assays such as the fluorescence focus assay and the most advanced fluorescence-activated cell sorting assay.[20,21] Cell-based assays using live viruses, such as PRA or CPE, are indicated as the reference standard for antiviral screening, despite poor reproducibility, the requirement of experienced technicians, and high-turnaround times.[8] Consequently, the development of accurate, easy-to-perform, and fast cell-based assays is highly valuable to test candidate inhibitors of ZIKV and DENV replication.

In this study, we describe a fast and accurate cell-based flavivirus immunodetection assay (IA) allowing quantification of ZIKV and/or DENV antigen by a specific monoclonal antibody to the fusion loop of the E protein domain II, which is shared among different flaviviruses. The assay is applied as a readout of a direct yield reduction assay (YRA) measuring inhibition of virus replication in the initially infected cell culture. In addition, viral stocks generated in the direct YRA can be transferred to a second cell culture in the absence of drug, to better characterize antiviral activity exerted at steps occurring later than envelope expression. To validate the assay, sofosbuvir and ribavirin half-maximal inhibitory concentrations (IC_{50}) were determined and compared with values obtained by a standardized PRA[22] and with values previously reported in the literature.[23–26] To evaluate the ability of the system to discriminate between early and late antiviral effects, the IC_{50} of celgosivir, an α-glucosidase inhibitor acting at late steps of DENV infection and recently evaluated in a phase Ib/IIa randomized clinical trial (NCT01619969),[27,28] was determined by both a direct and a secondary YRA, as well as by the reference PRA against both viruses. In the literature, celgosivir anti-DENV effects were also determined in vitro[29,30] and in animal models.[31] Even though a possible activity of celgosivir against ZIKV has been hypothesized based on the high similarity between ZIKV and DENV,[28] in a recently published work[32] celgosivir was not active in vitro against ZIKV when a monkey cell line (VERO) was used.

Materials and Methods

Cells

Vero E6 (African green monkey kidney cell line; ATCC, Manassas, VA, USA, CRL-1586), A549 (human lung carcinoma cell line; ATCC CCL-185), Huh7 (human hepatoma cell line; kindly provided by Istituto Toscano Tumori, Core Research Laboratory, Siena, Italy), and LN-18 (glioblastoma cell line; ATCC CRL-2610) cells were used to titrate ZIKV and DENV viral stocks by IA. The C6/36 (*Aedes albopictus* mosquito; ATCC CRL-1660) cell line was used to expand DENV, and the VERO E6 cell line was used to expand ZIKV. The cell propagation medium was Dulbecco's modified Eagle's medium (DMEM), high glucose with sodium pyruvate, and L-glutamine (Euroclone, Milan, Italy) supplemented with 10% fetal bovine serum (FBS; Euroclone) and 1% penicillin/streptomycin (pen/strep; Euroclone). Additional L-glutamine (2 mM) and HEPES (25 mM) were used only in C6/36 medium. The cell infection medium was the same as the propagation medium but with 1% FBS. The mammalian cells were incubated at 37 °C in a humidified incubator supplemented with 5% CO_2, whereas the mosquito cell line was maintained at 28 °C.

Viruses

The H/PF/2013 ZIKV strain, belonging to the Asian lineage, and the New Guinea C DENV serotype 2 strain were kindly provided by the Istituto Superiore di Sanità, Rome, Italy. Once expanded in VERO E6 (ZIKV) and C6/36 (DENV) cells, viral stocks were titrated by plaque assay[22] in A549 and VERO E6 cells, yielding viral titers of 400,000 and 20,000 plaque-forming units (PFU) per milliliter, respectively. Briefly, confluent cells in six-well plate format were infected with three 10-fold dilutions of viral stock, and after 1 h viral adsorption at 37 °C with 5% CO_2, cells were washed with PBS and infection medium with 0.75% Sea Plaque Agarose (Lonza, Rockland, ME, USA) was added to each well. After 5 days' incubation at 37 °C, the monolayers were fixed with 10% formaldehyde (Carlo Erba Chemicals, Milan, Italy) and stained with 0.1% crystal violet (Carlo Erba Chemicals). After at least 3 h of incubation, the agar overlay was removed by water washing and PFU were counted.

Antivirals

The FDA-approved anti-hepatitis C virus compounds sofosbuvir (β-D-2′-deoxy-2′-α-fluoro-2′-β-C-methyluridine; MedChemExpress, Monmouth Junction, NJ, USA, cat. HY-15005) and ribavirin (1-β-D-ribofuranosyl-1,2,4-triazole-3-carboxamide; Sigma Aldrich, St. Louis, MO, USA, cat. R9644) were used to validate the system. The inhibitor of viral protein glycosylation celgosivir (6-O-butanoyl castanospermine; Sigma Aldrich cat. SML2314), acting at the late stage of DENV replication, was used to evaluate the ability of the assay to discriminate between early and late antiviral effects. All reference compounds were supplied as powder; ribavirin and sofosbuvir were dissolved in 100% DMSO, while celgosivir was dissolved in bi-distilled sterile water.

Cytotoxicity Assay

Serial twofold dilutions of antivirals in infection medium (propagation medium supplemented with 1% FBS) were added to Huh7 cells seeded at 7000 cells/well in a 96-well plate. After 72 h of incubation, drug cytotoxicity was measured by using the CellTiter-Glo 2.0 Luminescent Cell Viability Assay (Promega, Madison, WI, USA) according to the manufacturer's protocol. The luminescent signal generated by cells treated with the test compound was compared with that generated by cells treated with DMSO/water to determine the half-maximal cytotoxic concentration (CC_{50}).

Setup of the Immunodetection Assay

Optimal experimental conditions for the detection of viral antigen by IA were defined by growing viral stocks in human cell lines (A549, Huh7, and LN-18) and in the reference monkey line (VERO E6) that were titrated at 48, 72, and 96 h. The day before infection, each cell line was seeded in a 96-well plate format at the appropriate concentration to obtain 90% confluence at the time of antigen detection. Serial twofold dilutions of viral stocks were adsorbed to target cells in quadruplicate for 1 h at 37 °C in a humidified incubator with 5% CO_2. After removal of the virus inoculum, DMEM infection medium with 1% or 3% FBS was added to cultures to be maintained for 48/72 h or 96 h, respectively.

For the immunodetection of virus antigen, the supernatant was removed and cells were fixed for 30 min with 10% formaldehyde (Carlo Erba Chemicals), rinsed with 1% PBS, and permeabilized for 10 min with 1% Triton X-100 (Carlo Erba). Following washing with PBS containing 0.05% Tween 20 (Carlo Erba Chemicals), cells were incubated for 1 h with monoclonal antiflavivirus mouse antibody (clone D1-4G2-4-15; Novus Biologicals, Centennial, CO, USA, NBP2-52709) diluted 1:400 in blocking buffer (PBS containing 1% BSA and 0.1% Tween 20). After washing four times, cells were incubated for 1 h with a polyclonal horseradish peroxidase (HRP)-coupled anti-mouse IgG secondary antibody (Novus Biologicals NB7570) diluted 1:10,000 in blocking buffer. Next, cells were washed five times and the 3,3′,5,5′-tetramethylbenzidine substrate (Sigma Aldrich) was added to each well. After 15 min of incubation in the dark, the reaction was stopped with one volume of 0.5 M sulfuric acid. All incubation steps were performed at room temperature. Absorbance was measured at 450 nm optical density (OD_{450}) using the Absorbance Module of the GloMax Discover Multimode Microplate Reader (Promega) and adjusted by subtracting the background value, established as twofold the mean OD_{450} value of quadruplicate uninfected cells. The 50% tissue culture infectious dose ($TCID_{50}$) of each virus was calculated according to Reed and Muench.[33]

Direct Yield Reduction Assay

The direct YRA is based on the infection of cells in the presence of serial drug dilutions followed by absorbance measurement by IA. Since the readout is based on the detection of the E protein, the system allows us to measure interference with the virus life cycle up to protein production but not at later steps. To define the optimal virus inoculum, 7000 Huh7 cells/well were infected with ZIKV or DENV at 100, 50, and 25 $TCID_{50}$, as determined by the IA described above. Viral adsorption was performed in 96-well plates for 1 h at 37 °C with 5% CO_2. After virus removal, serial dilutions of sofosbuvir or ribavirin were added to the cell media at final concentrations ranging from 0.03 to 100 µM and the plates were incubated at 37 °C with 5% CO_2. All drug concentrations were tested in triplicate and three independent experiments at each $TCID_{50}$ used were performed to determine the assay reproducibility. Infected and uninfected cells without antivirals were used to calculate 100% and 0% of viral replication, respectively. After 72 h, supernatants were harvested and stored at –80 °C for subsequent analysis, and IA was performed on cell monolayers as described above. Based on initial experiments, each IA run was validated when the OD_{450} value in the virus control culture was above 1. This value was taken as 100% replication and IC_{50} values were calculated based on this reference by a nonlinear regression analysis of the dose–response curves generated with the GraphPad PRISM software version 6.01 (La Jolla, CA, USA). The activity of celgosivir against ZIKV and DENV was determined by YRA with 50 $TCID_{50}$ as described above.

Secondary Yield Reduction Assay

The secondary YRA is designed to measure viral protein production driven by the virus generated in the first round in the presence of drug. Thus, antiviral effects exerted at late steps of the virus life cycle, for example, virus glycosylation and assembly, not detected by the direct YRA, can be measured. The secondary YRA was carried out by infecting 7000 Huh7 cells/well in a 96-well plate with ZIKV and DENV viral supernatants generated by direct YRA with reference compounds. Triplicate viral stocks derived from the direct YRA were used and two independent runs of the secondary YRA were performed to assess the reproducibility of results. After 72 h of incubation at 37 °C with 5% CO_2, cells were fixed, and IA was performed to determine the IC_{50} value for each drug as described in the "Direct Yield Reduction Assay" section (**Suppl. Fig. S1**). The DENV glycosylation inhibitor celgosivir was chosen as a reference compound to assess the ability of assay to discriminate between early and late antiviral effects.
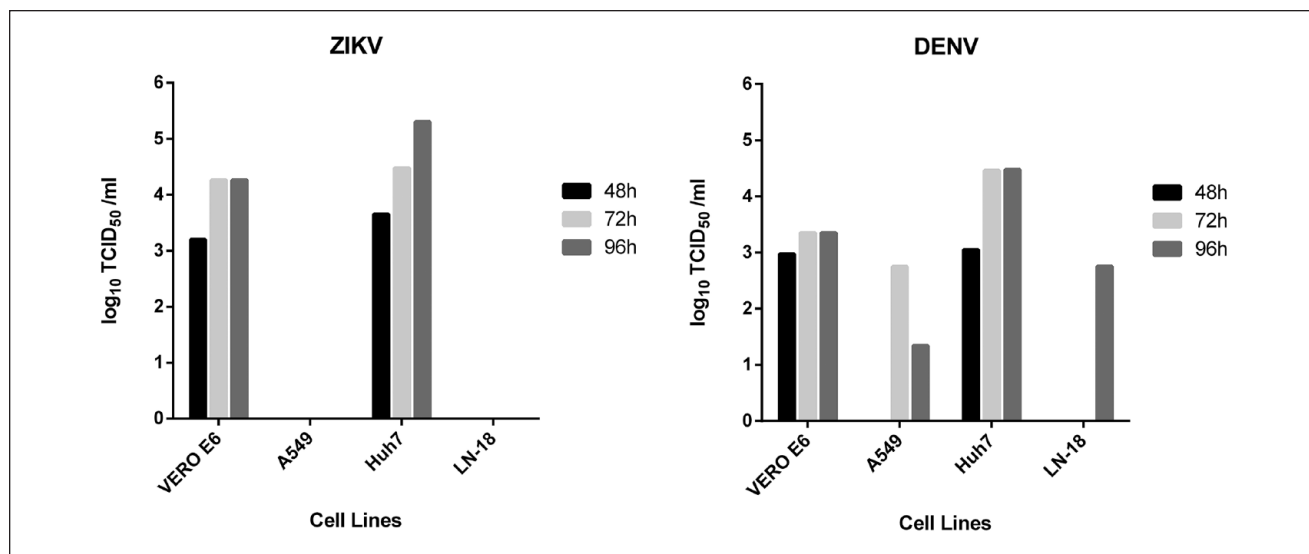
Figure 1. Titration of ZIKV and DENV viral stocks in Huh7, A549, LN-18, and VERO E6 cells at 48, 72, and 96 h by IA.

Plaque Reduction Assay of ZIKV and DENV on Reference Compounds

The PRA on reference compounds was performed as previously described.[22] Briefly, Huh7 cells were infected with ZIKV or DENV at 0.1 multiplicity of infection (MOI), as determined by plaque assay quantification, in the presence of serial fivefold drug dilutions, with a final drug concentration ranging from 0.03 to 100 μM for sofosbuvir and ribavirin and from 0.02 to 50 μM for celgosivir. After 72 h of incubation, three 10-fold dilutions of cell supernatant were used to infect in duplicate A549 (ZIKV) and VERO E6 (DENV) cells. Each experiment included a positive control (original viral stock) and a mock-infected well with infection medium only (**Suppl. Fig. S2**). Viral plaques were visualized 5 and 10 days following infection for ZIKV and DENV, respectively, and the viral titers were calculated by PFU counting. IC_{50} values were calculated by nonlinear regression analysis of the dose–response curves generated with the GraphPad PRISM software version 6.01.

Results

Choice of Cell System and Incubation Time for IA

Titration of ZIKV and DENV viral stocks by IA was possible at 48, 72, and 96 h in VERO E6 and Huh7 cell lines (**Fig. 1**). Despite a visible CPE at 48 h in A549 cells and the ability of both viruses to produce plaques in LN-18 cells (data not shown), ZIKV infection in these cell lines gave negative results by IA, while a weak signal of DENV infection was detected at 72 and 96 h in A549 cells (viral stock titrated as 564 and 22 $TCID_{50}$/mL, respectively) and at 96 h in LN-18

cells (566 $TCID_{50}$/mL). The increasing amount of FBS in infection medium (3% instead of 1%), required to keep cells healthy after 96 h of incubation, probably decreased viral infectivity, as also suggested by the lack of increase of ZIKV viral titers in VERO E6 cells and DENV viral titers in A549, Huh7, and VERO E6 cells. Although the ZIKV viral titer increased up to 96 h in Huh7 (6.6-fold increase with respect to 72 h), the virus yield assay was finally set at 72 h of incubation to maintain the infection medium at 1% FBS concentration and standardize the procedure with both viruses. Huh7 cells, rather than VERO E6 cells, were chosen since human-derived cell lines are more appropriate for the screening of antiviral compounds expected to be used for the treatment of human viral infections, particularly when cellular factors are targeted. The linear dynamic range in such experimental conditions covered 4 logs for both ZIKV and DENV. ZIKV and DENV stocks, titrated in Huh7 at 72 h and subsequently used by direct YRA, were 30,000 and 29,000 $TCID_{50}$/mL, respectively.

Performance of the Direct and Secondary YRA in Determining the Antiviral Activity of Reference Compounds

Reference compounds showed no cytotoxicity in the tested concentration range (0.78–200 μM) (**Suppl. Fig. S3**). The activity of the reference compounds against ZIKV and DENV was first assessed by PRA. Sofosbuvir IC_{50} values were 2.0 ± 1.1 μM against ZIKV and 3.8 ± 1.1 μM against DENV; ribavirin IC_{50} values were 2.2 ± 1.2 against ZIKV and 4.1 ± 1.1 μM against DENV. In PRA, the celgosivir IC_{50} value was 10.1 ± 1.1 μM against DENV, while the compound was not active against ZIKV (**Fig. 2**). The
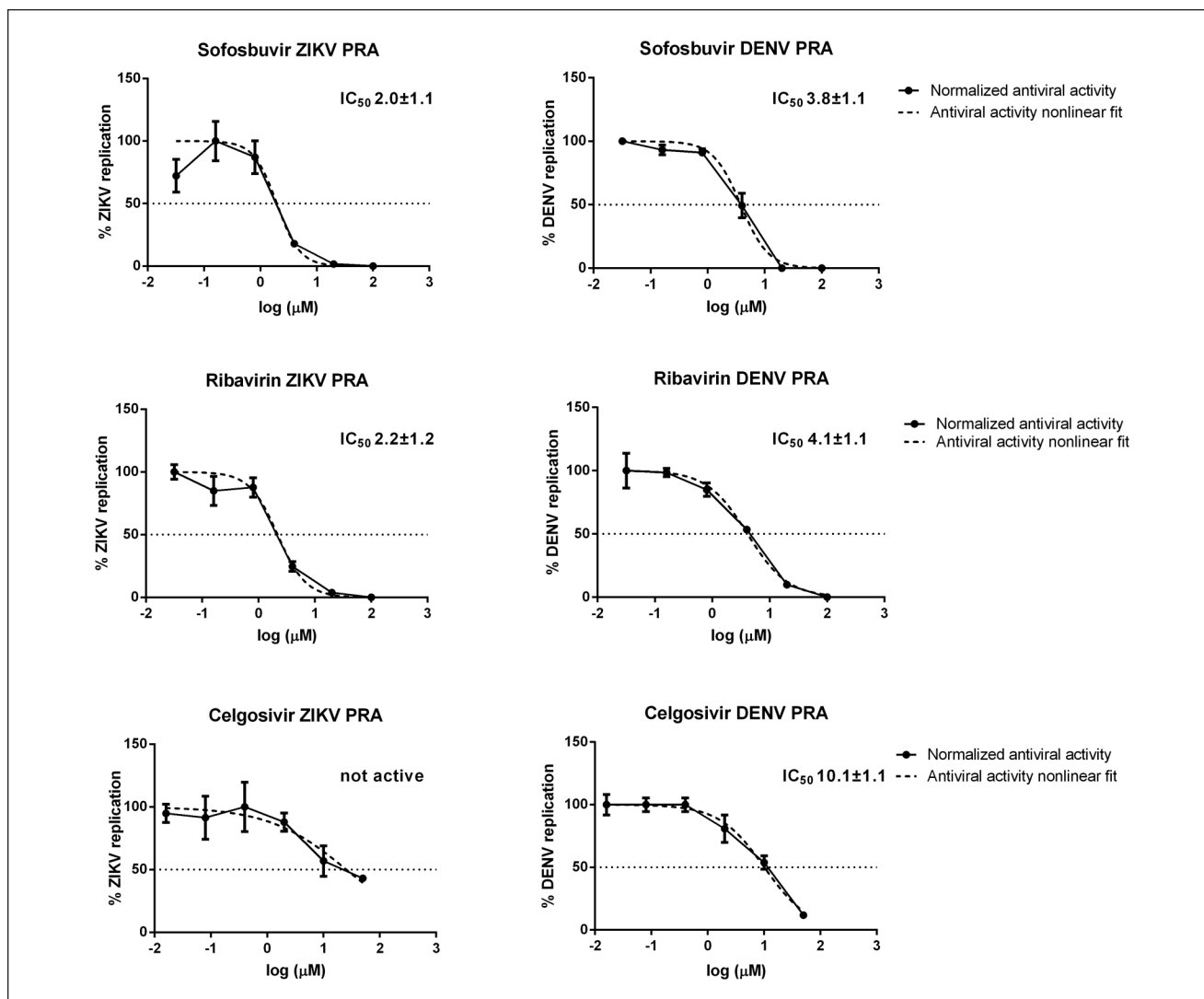
Figure 2. Activity of sofosbuvir and ribavirin against ZIKV and DENV as determined by PRA at 0.1 MOI.

Table 1. IC_{50} of Sofosbuvir and Ribavirin against ZIKV and DENV.

	Sofosbuvir						Ribavirin					
	ZIKV			DENV			ZIKV			DENV		
$TCID_{50}$ viral input	100	50	25	100	50	25	100	50	25	100	50	25
IC_{50}, mean ± SD (μM)[a]	5.0 ± 1.5	2.7 ± 0.5	2.5 ± 1.1	16.6 ± 2.8	4.6 ± 1.4	2.6 ± 2.2	6.8 ± 4.0	3.8 ± 0.6	4.5 ± 1.4	17.3 ± 4.6	7.6 ± 1.2	4.1 ± 2.3
IC_{50} direct YRA/PRA	2.6	1.4	1.3	4.4	1.2	0.7	3.1	1.7	2.1	4.2	1.9	1.0

[a]Values are derived from three independent experiments.

antiviral activities of sofosbuvir and ribavirin for each virus as determined by the direct YRA are shown in **Table 1**. Based on reproducibility within replicates (i.e., lowest coefficient of variation) and correlation with PRA (i.e., ratio of direct YRA IC_{50} to PRA IC_{50} closest to 1), 50

$TCID_{50}$ was set as the optimal amount of viral input to perform the YRA. In the direct YRA, celgosivir was inactive not only against ZIKV but also against DENV, since the step expected to be targeted in the virus life cycle occurs after synthesis of the viral E protein that is detected by IA.
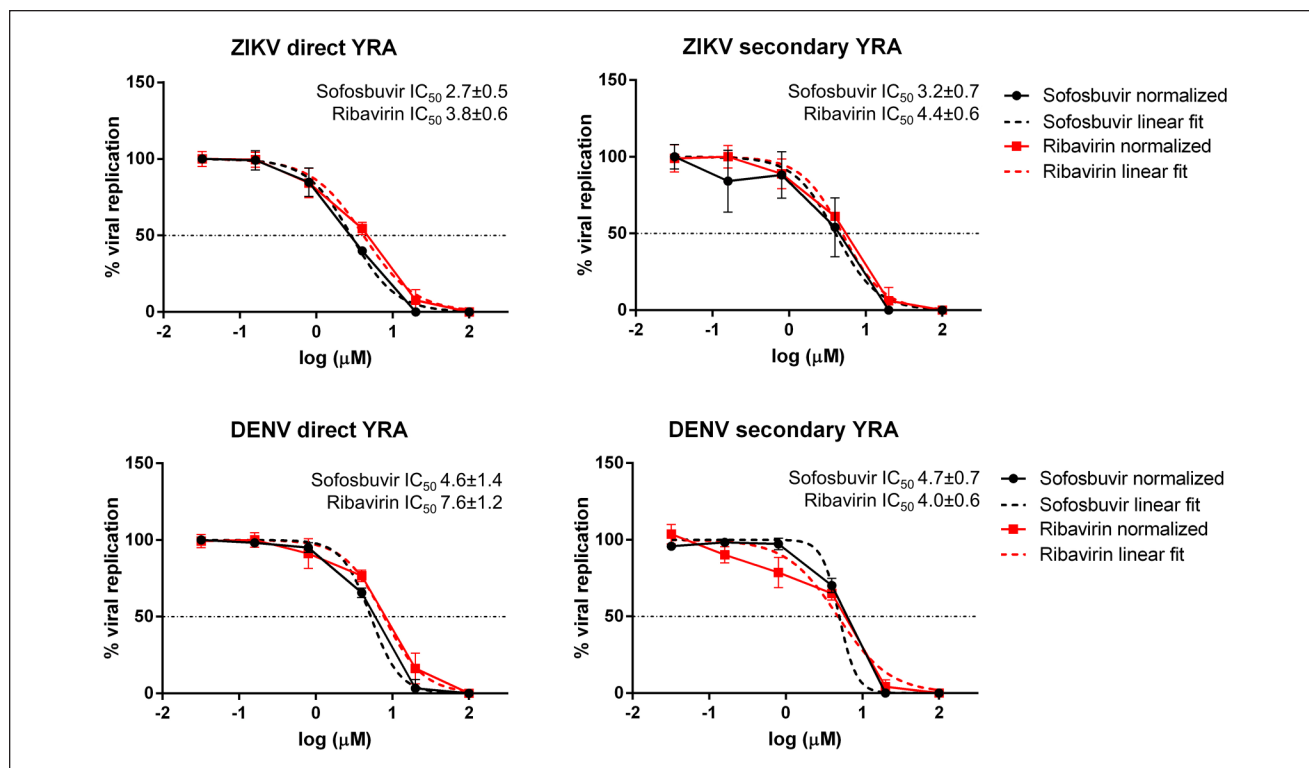
Figure 3. Activity of sofosbuvir and ribavirin against ZIKV and DENV in the direct and secondary YRA.

Table 2. IC$_{50}$ Values of Sofosbuvir, Ribavirin, and Celgosivir against ZIKV and DENV.

	Sofosbuvir		Ribavirin		Celgosivir	
	ZIKV	DENV	ZIKV	DENV	DENV	ZIKV
IC$_{50}$, mean $\pm$ SD (μM)[a]	3.2 $\pm$ 0.7	4.7 $\pm$ 0.7	4.4 $\pm$ 0.6	4.0 $\pm$ 0.6	11.0 $\pm$ 1	Not active
Secondary YRA IC$_{50}$/PRA IC$_{50}$ ratio[b]	1.6	1.2	2.0	1.0	1.1	NA
IC$_{50}$ secondary YRA/IC$_{50}$ direct YRA ratio[b]	1.2	0.8	1.2	0.5	NA	NA

NA, not applicable.
[a]Values are derived from three independent experiments.
[b]The ratio is expressed in fold of differences.

In the secondary YRA, using viral stocks generated in the direct YRA to reinfect Huh7 cell lines, sofosbuvir and ribavirin IC$_{50}$ values against ZIKV and DENV were reproducible and comparable to those obtained by direct YRA and PRA (**Fig. 3**). In addition, celgosivir was active against DENV with a mean IC$_{50}$ value comparable to those obtained in PRA (11.0 $\pm$ 1.0 μM and 10.1 $\pm$ 1.1 μM, respectively), confirming the value of the secondary YRA to preliminarily identify candidate compounds acting at late steps of viral replication (**Table 2 and Fig. 4**).

Discussion

In the absence of effective vaccines and therapeutic options, supportive care is the only available option for the treatment of flavivirus infections.[34] Assessment of antiviral effects in cultured cells is a key approach for screening candidate compounds. Several cell-based phenotypic assays have been developed, including assays using live virus, subgenomic viral replicons, or virus-like particles.[35] The main disadvantage of the live-virus assays is the obvious necessity for high-level biosafety containment. Subgenomic viral replicons and virus-like particles can overcome safety concerns and are prevalently based on convenient readouts, such as luminescence and fluorescence; however, they do not recapitulate the complete virus life cycle and thus are not amenable for the screening of compounds with unknown targets. Moreover, these assays must be validated carefully to avoid false-positive hits resulting from cytotoxicity or interaction with the luciferase readout.[8] Among live-virus
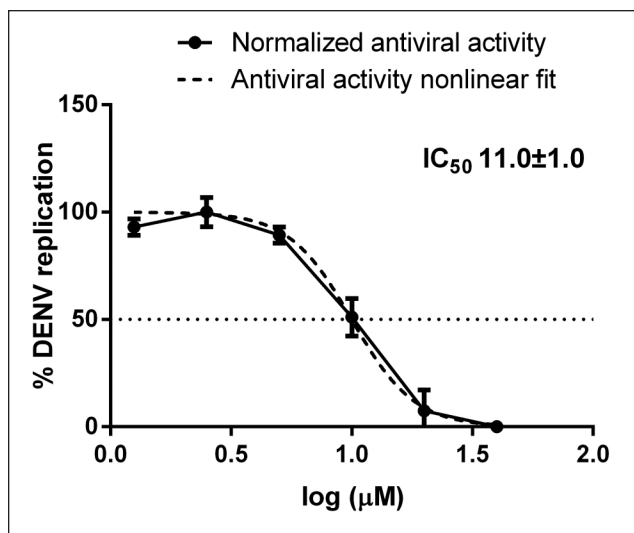
Figure 4. Activity of celgosivir against DENV as determined by the secondary YRA.

assays, PRA has long been considered the gold standard for antiviral screening and is commonly used for anti-DENV and anti-ZIKV antibody titration in plaque reduction neutralization tests.[36] However, PRA has several drawbacks, including high labor, long-turnaround time, and low throughput, making it not suitable for the analysis of large numbers of compounds or sera.

This study describes the development and validation of an IA-based yield reduction test to simultaneously determine the antiviral activity of candidate compounds against ZIKV and DENV in vitro. To define the best experimental conditions, both viruses were propagated in four different cell lines (Huh7, A549, LN-18, and VERO E6) and the viral titer was determined by IA at different time points. The most effective combination of shorter propagation time and better maintenance of cell health was obtained with Huh7 cells, a widely used human hepatoma cell line, and with VERO E6, the monkey cell line mostly used for the propagation and titration of flaviviruses. However, differences in drug metabolism in monkey cells with respect to human cells[37] impact the activity of sofosbuvir and ribavirin against ZIKV and DENV,[25,38] as well as West Nile virus (WNV).[39] Thus, Huh7 was chosen as the model cell line for assay validation. In addition, human cell lines are clearly preferred when assaying candidate host targeting agents for a possible antiviral effect.

The antiviral activity of sofosbuvir and ribavirin was determined by a direct YRA in which the immunodetection of the E protein is directly performed on cells infected with viral stocks and subjected to drug pressure. In the secondary YRA, the antiviral activity is determined by measuring the infectivity of viral stocks generated in the direct YRA. Both drugs were shown to be active against ZIKV and DENV in

the low-micromolar range with IC_{50} values that were comparable in both the direct and secondary YRA performed in this work and in previously reported studies.[11,23,24,26] The secondary YRA can additionally screen compounds exerting antiviral activity at the late stage of the viral cycle (i.e., assembly and maturation of viral particles) that would go undetected or only partially detected by direct YRA. For example, a similar two-step system is adopted to measure the anti-HIV activity of drugs acting at different steps of virus replication.[40,41] Thus, the combined use of the direct and secondary YRA can not only measure antiviral activity but also help characterize the mechanism of action. As proof of concept, we tested celgosivir, an inhibitor of endoplasmic reticulum (ER) α-glycosidases, found to be active against DENV both in vitro, with IC_{50} values ranging from the sub- (0.2 μM) to low- (5.7 μM) micromolar range,[30,42] and in vivo in a mouse model, demonstrating the reduction of viremia and inducement of protection against virus-induced mortality.[30,31] Celgosivir impairs viral protein glycosylation affecting virus assembly and egress, inducing ER stress and the unfolded protein response.[43] We observed that celgosivir did not interfere with the expression of viral E protein at each drug concentration tested in the direct YRA, while a dose-dependent effect of celgosivir on the expression of the E protein was detected in the secondary YRA (**Fig. 4**). The mean celgosivir IC_{50} values against DENV, calculated in the secondary YRA (11.0 μM) or PRA (10.1 μM), were comparable to the values obtained in primary human macrophages (5.2 μM) but significantly higher with respect to the IC_{50} values obtained in BHK-21 cells,[30] reinforcing the importance of antiviral testing in human cell lines for proper assessment of antiviral activity. Globally, these data support the ability of the direct and secondary YRA in the determination of antiviral activity according to the mechanism of action, suggesting that the secondary YRA can be successfully adopted when the mechanism of action of investigational compounds is expected to involve the late phase of viral replication or is unknown.

Importantly, the IA format overcomes relevant limitations of the gold standard PRA. The direct YRA and the secondary YRA are completed in 72 and 144 h, respectively, compared with 192 h for ZIKV and 312 h for DENV required by PRA. In addition, the readout is automated through microplate reading as opposed to manual and error-prone counting in PRA. The use of a pan-flaviviral monoclonal antibody allows use of the same system for different viruses, and indeed similar systems have been described for screening antiviral candidates against DENV.[26,44] However, several of these procedures rely on high-content fluorescence imaging, which may be not easily available, and none are designed to simultaneously screen multiple viruses or to distinguish between early and late antiviral effects.[44–46] Some published protocols were adapted to HTS of large libraries of compounds.[32,47] However, these systems are

based on CPE readout, an indirect measurement of viral infectivity possibly confounded by cell death caused by candidate compounds, as opposed to direct estimates of virus activity like PRA and IA. In terms of turnaround time (about 4 h for 12 compounds analyzed simultaneously for ZIKV and DENV), our system can be defined as a medium-throughput screening assay suitable for testing small to medium libraries of candidate compounds. In summary, the system described here combines several advantages with respect to previously published work, including (1) the use of the same protocol for two different viruses, (2) the ability to distinguish between early and late antiviral effects, (3) a readout directly proportional to virus production and consequently to virus inhibition, and (4) the completion of the assay within 6 days. Thus, the system provides an opportunity to expand the potential for fast cell-based screening of multiple compounds for antiflavivirus therapy.

References

1. Bhatt, S.; Gething, P.; Brady, O.; et al. The Global Distribution and Burden of Dengue. *Nature* **2013**, *496*, 504–507.
2. Marchette, N. J.; Garcia, R.; Rudnick, A. Isolation of Zika Virus from *Aedes aegypti* Mosquitoes in Malaysia. *Am. J. Trop. Med. Hyg.* **1969**, *18*, 411–415.
3. Suwanmanee, S.; Luplertlop, N. Dengue and Zika Viruses: Lessons Learned from the Similarities between These *Aedes* Mosquito-Vectored Arboviruses; *J. Microbiol.* **2017**, *55*, 81–89.
4. Imperato, P. J. The Convergence of a Virus, Mosquitoes, and Human Travel in Globalizing the Zika Epidemic. *J. Commun. Health* **2016**, *41*, 674–679.
5. Liang, G.; Gao, X.; Gould, E. A. Factors Responsible for the Emergence of Arboviruses, Strategies, Challenges and Limitations for Their Control. *Emerg. Microbes Infect.* **2015**, *4*, e18.
6. Vorou, R. Zika Virus, Vectors, Reservoirs, Amplifying Hosts, and Their Potential to Spread Worldwide: What We Know and What We Should Investigate Urgently. *Int. J. Infect. Dis.* **2016**, *48*, 85–90.
7. Krauer, F.; Riesen, M.; Reveiz, L.; et al. Zika Virus Infection as a Cause of Congenital Brain Abnormalities and Guillain–Barré Syndrome: Systematic Review. *PLoS Med.* **2017**, *14*, e1002203.
8. Boldescu, V.; Behnam, M. A. M.; Vasilakis, N.; et al. Broad-Spectrum Agents for Flaviviral Infections: Dengue, Zika and Beyond. *Nat. Rev. Drug Discov.* **2017**, *16*, 565–586.
9. Silva, J. V. J.; Lopes, T. R. R.; Oliveira-Filho, E. F.; et al. Current Status, Challenges and Perspectives in the Development of Vaccines against Yellow Fever, Dengue, Zika and Chikungunya Viruses. *Acta Trop.* **2018**, *182*, 257–263.
10. Estofolete, C. F.; Terzian, A. C. B.; Colombo, T. E.; et al. Co-Infection between Zika and Different Dengue Serotypes during DENV Outbreak in Brazil. *J. Infect. Public Health.* **2018**, *12*, 178–181.
11. Chang, J.; Schul, W.; Butters, T. D.; et al. Combination of α-Glucosidase Inhibitor and Ribavirin for the Treatment of Dengue Virus Infection In Vitro and In Vivo. *Antiviral Res.* **2011**, *89*, 26–34.
12. Munjal, A.; Khandia, R.; Dhama, K.; et al. Advances in Developing Therapies to Combat Zika Virus: Current Knowledge and Future Perspectives. *Front. Microbiol.* **2017**, *8*, 1469.
13. Lo, M. K.; Tilgner, M.; Shi, P. Y. Potential High-Throughput Assay for Screening Inhibitors of West Nile Virus Replication. *J. Virol.* **2003**, *77*, 12901–12906.
14. Puig-Basagoiti, F.; Deas, T. S.; Ren, P.; et al. High-Throughput Assays Using a Luciferase-Expressing Replicon, Virus-Like Particles, and Full-Length Virus for West Nile Virus Drug Discovery. *Antimicrob. Agents Chemother.* **2005**, *49*, 4980–4988.
15. Xie, X.; Zou, J.; Wang, Q. Y.; et al. Targeting Dengue Virus NS4B Protein for Drug Discovery. *Antiviral Res.* **2015**, *118*, 39–45.
16. Balasubramanian, A.; Manzano, M.; Teramoto, T.; et al. High-Throughput Screening for the Identification of Small-Molecule Inhibitors of the Flaviviral Protease. *Antiviral Res.* **2016**, *134*, 6–16.
17. Dulbecco, R. Production of Plaques in Monolayer Tissue Cultures by Single Particles of an Animal Virus. *Proc. Natl. Acad. Sci. U.S.A.* **1952**, *38*, 747–752.
18. Roehrig, J. T.; Hombach, J.; Barrett, A. D. T. Guidelines for Plaque-Reduction Neutralization Testing of Human Antibodies to Dengue Viruses. *Viral Immunol.* **2008**, *21*, 123–132.
19. Bernatchez, J. A.; Yang, Z.; Coste, M.; et al. Development and Validation of a Phenotypic High-Content Imaging Assay for Assessing the Antiviral Activity of Small-Molecule Inhibitors Targeting Zika Virus. *Antimicrob. Agents Chemother.* **2018**, *62*, e00725-18.
20. Kraus, A. A.; Messer, W.; Haymore, L. B.; et al. Comparison of Plaque- and Flow Cytometry-Based Methods for Measuring Dengue Virus Neutralization. *J. Clin. Microbiol.* **2007**, *45*, 3777–3780.

21. Payne, A. F.; Binduga-Gajewska, I.; Kauffman, E. B.; et al. Quantitation of Flaviviruses by Fluorescent Focus Assay. *J. Virol. Methods* **2006**, *134*, 183–189.

22. Vicenti, I.; Boccuto, A.; Giannini, A.; et al. Comparative Analysis of Different Cell Systems for Zika Virus (ZIKV) Propagation and Evaluation of Anti-ZIKV Compounds In Vitro. *Virus Res*. **2018**, *244*, 64–70.

23. Bullard-Feibelman, K. M.; Govero, J.; Zhu, Z.; et al. The FDA-Approved Drug Sofosbuvir Inhibits Zika Virus Infection. *Antiviral Res*. **2017**, *137*, 134–140.

24. Julander, J. G.; Siddharthan, V.; Evans, J.; et al. Efficacy of the Broad-Spectrum Antiviral Compound BCX4430 against Zika Virus in Cell Culture and in a Mouse Model. *Antiviral Res*. **2017**, *137*, 14–22.

25. Sacramento, C. Q.; de Melo, G. R.; de Freitas, C. S.; et al. The Clinically Approved Antiviral Drug Sofosbuvir Inhibits Zika Virus Replication. *Sci. Rep*. **2017**, *7*, 40920.

26. Xu, H. T.; Colby-Germinario, S. P.; Hassounah, S. A.; et al. Evaluation of Sofosbuvir (β-D-2′-Deoxy-2′-α-Fluoro-2′-β-C-Methyluridine) as an Inhibitor of Dengue Virus Replication. *Sci. Rep*. **2017**, *7*, 6345.

27. Low, J. G.; Sung, C.; Wijaya, L.; et al. Efficacy and Safety of Celgosivir in Patients with Dengue Fever (CELADEN): A Phase 1b, Randomised, Double-Blind, Placebo-Controlled, Proof-of-Concept Trial. *Lancet Infect. Dis*. **2014**, *14*, 706–715.

28. Sung, C.; Wei, Y.; Watanabe, S.; et al. Extended Evaluation of Virological, Immunological and Pharmacokinetic Endpoints of CELADEN: A Randomized, Placebo-Controlled Trial of Celgosivir in Dengue Fever Patients. *PLoS Negl. Trop. Dis*. **2016**, *10*, e0004851.

29. Courageot, M.-P.; Frenkiel, M.-P.; Duarte Dos Santos, C; et al. Alpha-Glucosidase Inhibitors Reduce Dengue Virus Production by Affecting the Initial Steps of Virion Morphogenesis in the Endoplasmic Reticulum. *J. Virol*. **2000**, *74*, 564–572.

30. Rathore, A. P. S.; Paradkar, P. N.; Watanabe, S.; et al. Celgosivir Treatment Misfolds Dengue Virus NS1 Protein, Induces Cellular Pro-Survival Genes and Protects against Lethal Challenge Mouse Model. *Antiviral Res*. **2011**, *92*, 453–460.

31. Watanabe, S.; Chan, K. W. K.; Dow, G.; et al. Optimizing Celgosivir Therapy in Mouse Models of Dengue Virus Infection of Serotypes 1 and 2: The Search for a Window for Potential Therapeutic Efficacy. *Antiviral Res*. **2016**, *127*, 10–19.

32. Adcock, R. S.; Chu, Y. K.; Golden, J. E.; et al. Evaluation of Anti-Zika Virus Activities of Broad-Spectrum Antivirals and NIH Clinical Collection Compounds Using a Cell-Based, High-Throughput Screen Assay. *Antiviral Res*. **2017**, *138*, 47–56.

33. Reed, L. J.; Muench, H. A Simple Method of Estimating Fifty Per Cent Endpoints. *Am. J. Epidemiol*. **1938**, *27*, 493–497.

34. Kok, W. M. New Developments in Flavivirus Drug Discovery. *Expert Opin. Drug Discov*. **2016**, *11*, 433–445.

35. Green, N.; Ott, R. D.; Isaacs, J.; et al. Cell-Based Assays to Identify Inhibitors of Viral Disease. *Expert Opin. Drug Discov*. **2008**, *3*, 671–676.

36. Cordeiro, M. T. Laboratory Diagnosis of Zika Virus. *Top. Magn. Reson. Imaging*. **2019**, *28*, 15–17.

37. Guo, D.; Zhu, Q.; Zhang, H.; et al. Proteomic Analysis of Membrane Proteins of Vero Cells: Exploration of Potential Proteins Responsible for Virus Entry. *DNA Cell Biol*. **2014**, *33*, 20–28.

38. Gan, C. S.; Lim, S. K.; Chee, C. F.; et al. Sofosbuvir as Treatment against Dengue? *Chem. Biol. Drug Des*. **2018**, *91*, 448–455.

39. Day, C. W.; Smee, D. F.; Julander, J. G.; et al. Error-Prone Replication of West Nile Virus Caused by Ribavirin. *Antiviral Res*. **2005**, *67*, 38–45.

40. Puertas, M. C.; Buzón, M. J.; Ballestero, M.; et al. Novel Two-Round Phenotypic Assay for Protease Inhibitor Susceptibility Testing of Recombinant and Primary HIV-1 Isolates. *J. Clin. Microbiol*. **2012**, *50*, 3909–3916.

41. Saladini, F.; Giannini, A.; Boccuto, A.; et al. Agreement between an In-House Replication Competent and a Reference Replication Defective Recombinant Virus Assay for Measuring Phenotypic Resistance to HIV-1 Protease, Reverse Transcriptase, and Integrase Inhibitors. *J. Clin. Lab. Anal*. **2017**, *32*, e22206.

42. Sayce, A. C.; Alonzi, D. S.; Killingbeck, S. S.; et al. Iminosugars Inhibit Dengue Virus Production via Inhibition of ER Alpha-Glucosidases—Not Glycolipid Processing Enzymes. *PLoS Negl. Trop. Dis*. **2016**, *10*, e0004524.

43. Zakaria, M. K.; Carletti, T.; Marcello, A. Cellular Targets for the Treatment of Flavivirus Infections. *Front. Cell. Infect. Microbiol*. **2018**, *8*, 398.

44. Tan, K. H.; Wing Ki, K. C.; Watanabe, S.; et al. Cell-Based Flavivirus Infection (CFI) Assay for the Evaluation of Dengue Antiviral Candidates Using High-Content Imaging. *Methods Mol. Biol*. **2014**, *1138*, 99–109.

45. Lee, E. M.; Titus, S. A.; Xu, M.; et al. High-Throughput Zika Viral Titer Assay for Rapid Screening of Antiviral Drugs. *Assay Drug Dev*. **2019**, *17*, 128–139.

46. Wang, Q. Y.; Patel, S. J.; Vangrevelinghe, E.; et al. A Small-Molecule Dengue Virus Entry Inhibitor. *Antimicrob. Agents Chemother*. **2009**, *53*, 1823–1831.

47. Han, Y.; Mesplède, T.; Xu, H.; et al. The Antimalarial Drug Amodiaquine Possesses Anti-ZIKA Virus Activities. *J Med Virol*. **2018**, *90*, 796–802.

Research paper

Evaluation of sofosbuvir activity and resistance profile against West Nile virus in vitro

Filippo Dragoni[a], Adele Boccuto[a], Francesca Picarazzi[b], Alessia Giannini[a], Federica Giammarino[a], Francesco Saladini[a], Mattia Mori[b], Eloise Mastrangelo[c], Maurizio Zazzi[a], Ilaria Vicenti[a,*]

[a] Department of Medical Biotechnologies, University of Siena, Italy
[b] Department of Biotechnology, Chemistry and Pharmacy, University of Siena, Italy
[c] National Research Council, Biophysics Institute of Milano, Italy

A B S T R A C T

Sofosbuvir, a licensed nucleotide analog targeting hepatitis C virus (HCV) RNA-dependent RNA polymerase (RdRp), has been recently evaluated as a broad anti-Flavivirus lead candidate revealing activity against Zika and Dengue viruses both in vitro and in animal models. In this study, the in vitro antiviral activity of sofosbuvir against West Nile virus (WNV) was determined by plaque assay (PA) and Immunodetection Assay (IA) in human cell lines and by enzymatic RdRp assay. By PA, the sofosbuvir half-maximal inhibitory concentration (IC_{50}) was 1.2 ± 0.3 μM in Huh-7, 5.3 ± 0.9 μM in U87, 7.8 ± 2.5 μM in LN-18 and 63.4 ± 14.1 μM in A549 cells. By IA, anti-WNV activity was confirmed in both hepatic (Huh-7, 1.7 ± 0.5 μM) and neuronal (U87, 7.3 ± 2.0 μM) cell types. Sofosbuvir was confirmed to inhibit the purified WNV RdRp (IC_{50} 11.1 ± 4.6 μM). In vitro resistance selection experiments were performed by propagating WNV in the Huh-7 cell line with two-fold increasing concentrations of sofosbuvir. At 80 μM, a significantly longer time for viral breakthrough was observed compared with lower concentrations (18 vs. 7–9 days post infection; $p = 0.029$), along with the detection of the S604T mutation, corresponding to the well-known S282T substitution in the motif B of HCV NS5B, which confers resistance to sofosbuvir. Molecular docking experiments confirmed that the S604T mutation within the catalytic site of RdRp affected the binding mode of sofosbuvir. To our knowledge, this is the first report of the antiviral activity of sofosbuvir against WNV as well as of selection of mutants in vitro.

1. Introduction

West Nile virus (WNV) is a neurotropic Flavivirus preferentially transmitted by the Culex spp. Mosquitoes (Chancey et al., 2015). While most WNV infections are asymptomatic or paucisymptomatic, occasional patients experience severe neurological disease, including meningitis, encephalitis and flaccid paralysis (Sejvar, 2014). Due to lack of vaccine and specific antiviral drugs, only symptomatic treatment or supportive care is available for WNV disease (Kok, 2016).

Viral enzymes are attractive targets for the development of antiviral therapeutics against WNV and other flaviviruses (Acharya and Bai, 2016; Boldescu et al., 2017). The nonstructural protein 5 (NS5) is the key Flavivirus replication enzyme, about 900 amino acids in length, composed of two different domains: the N-terminal methyltransferase (MTase) and the C-terminal RNA dependent RNA-dependent RNA polymerase (RdRp). The MTase domain mediates both guanine-N7 and nucleoside-2′-O methylation of the cap structure, increasing the stability of newly synthesized RNA, facilitating the translation of the viral polyprotein and influencing the RdRp domain, which is essential for viral RNA replication. The structure of the WNV RdRp resembles the classical viral RdRp architecture with thumb, palm and fingers sub-domains and consists of six catalytic motifs (A-F), plus a G-loop (Malet et al., 2008, 2007; Zhang et al., 2008).

Given the high degree of structural homology observed among RdRp enzymes within the Flaviviridae family (Lim et al., 2013), sofosbuvir, a nucleotide analog licensed for hepatitis C virus (HCV) infection (Götte and Feld, 2016), has been recently evaluated as an anti-Flavivirus lead candidate. Indeed, the inhibitory activity of sofosbuvir has been documented in vitro against Zika virus (ZIKV) and Dengue virus (DENV) and in animal models against ZIKV (Mesci et al., 2018; Sacramento et al., 2017; H. T. Xu et al., 2017a). In addition, sofosbuvir has shown activity against the Alphavirus chikungunya (CHIKV), both in vitro and in an animal model (Ferreira et al., 2019). Since the NS5 amino acid residues predicted to interact with sofosbuvir show approximately 80% conservation among WNV, DENV and ZIKV (Appleby et al., 2015), sofosbuvir could also be active against WNV, providing a treatment option by itself or a lead structure for further development. The aim of this work was to determine for the first time sofosbuvir activity against the purified WNV RdRp and against WNV replication in a yield reduction system as measured by plaque assay (PA) and by Immunodetection Assay (IA) using different cell lines, as well as its resistance profile through in vitro resistance selection experiments.

---

2. Materials and methods

2.1. Cells and virus

VERO E6 (African green monkey kidney cell line; ATCC® CRL-1586™), A549 (human lung carcinoma cell line; ATCC® CCL-185™), Huh-7 (human hepatoma cell line; kindly provided from Istituto Toscano Tumori, Core Research Laboratory, Siena, Italy), LN-18 (glio-blastoma cell line; ATCC® CRL-2610™) and U87 (astroglioma cell line; NIBSC 044) were maintained in Dulbecco's Modified Eagle's Medium High Glucose with sodium pyruvate and L-Glutamine (DMEM; Euroclone) supplemented with 10% Fetal Bovine Serum (FBS; Euroclone) and 1% Penicillin/Streptomycin (Pen/Strep, Euroclone) at 37 °C with 5% CO_2. The same medium was used but with a lower FBS concentration for viral propagation and drug susceptibility testing (1%) and for in vitro selection experiments (3%). The WNV lineage 1 strain Italy/2009 (Magurano et al., 2012) was kindly provided by the Istituto Superiore di Sanità, Rome, Italy. Once expanded, WNV viral stock was titrated in VERO E6 cells by PA, as described below, yielding 4.2×10^7 PFU/ml.

2.2. Drugs and cytotoxicity assay

The FDA-approved anti-HCV compounds sofosbuvir (β-d-2′-deoxy-2′-α-fluoro-2′-β-C-methyluridine; MCE® cat. HY-15005), its active 5′-triphosphate metabolite (SOF-TP; MCE® cat. HY-15745), and ribavirin (1-β-D-Ribofuranosyl-1,2,4-Triazole-3-Carboxamide; Sigma Aldrich cat. R9644), used as reference compound, were supplied as powder and dissolved in 100% dimethyl sulfoxide (DMSO). Drug cytotoxicity was measured by the CellTiter-Glo 2.0 Luminescent Cell Viability Assay (Promega), according to the manufacturer's protocol. After 48 h incubation, the luminescent signal generated by the cells treated with the test compound was compared to that generated by the cells treated with DMSO to determine the 50% cytotoxic concentration (CC_{50}).

2.3. WNV propagation in different cell lines

Propagation of the titrated viral stock was tested in different cell lines and at different time points (24, 48 and 72 h).

For the PA readout, the day before infection each cell line (VERO E6, A549, Huh-7, LN-18 and U87) was seeded in 6-well plate to obtain 90% confluence at the time of collection of supernatants. Viral stock was diluted in infection medium and used to infect cells in duplicate for each time point at 0.1 multiplicity of infection (MOI). After 1 h adsorption at 37 °C, the viral stock was removed and replaced by infection medium, then the cells were incubated for 24, 48 and 72 h. For each time point, the PA was performed on harvested supernatants as previously described with minor modifications (Vicenti et al., 2018). Briefly, confluent cells in 6-well format were infected with three tenfold dilutions of viral stock and after 1 h adsorption at 37 °C, the cells were washed with PBS and 0.75% Sea Plaque Agarose (Lonza) was added to each well. After 3 days incubation at 37 °C, the monolayers were fixed with 10% formaldehyde (Carlo Erba Chemicals) and stained with 0.1% crystal violet (Carlo Erba Chemicals). After 3 h incubation, the agar overlay was removed by water washing and PFU were counted.

For the IA readout, the day before infection each cell line (Huh-7 and U87) was seeded in 96-well plate to obtain 90% confluence at the time of antigen detection. Serial two-fold dilutions of viral stocks were adsorbed to the target cells in quadruplicate for 1 h at 37 °C. After removal of the virus inoculum, DMEM infection medium was added to the cultures and the cells were incubated for 24, 48 and 72 h.

For the immunodetection of virus antigen, the supernatant was removed and the cells were fixed for 30 min with 10% formaldehyde (Carlo Erba), rinsed with 1% PBS and permeabilized for 10 min with 1% Triton X-100 (Carlo Erba). After washing with PBS containing 0.05% Tween 20 (Carlo Erba), the cells were incubated for 1 h with a

monoclonal anti-flavivirus mouse antibody (clone D1-4G2-4-15; Novus Bio NBP2-52709) diluted 1:400 in blocking buffer (PBS containing 1% BSA and 0.1% Tween 20). After washing, the cells were incubated for 1 h with a polyclonal HRP-coupled anti-mouse IgG secondary antibody (Novus Bio NB7570) diluted 1:10,000 in blocking buffer. Next, the cells were washed and the 3,3′,5,5′-Tetramethylbenzidine substrate (Sigma Aldrich) was added to each well. After 15 min incubation in the dark, the reaction was stopped with one volume of 0.5 M sulfuric acid. All the incubation steps were performed at room temperature. Absorbance was measured at 450 nm optical density (OD450) using the Absorbance Module of the GloMax® Discover Multimode Microplate Reader (Promega) and adjusted by subtracting the background value established as 2-fold the mean OD450 value of quadruplicate uninfected cells. The 50% tissue culture infectious dose ($TCID_{50}$) of each virus was calculated according to Reed and Munch (Reed and Muench, 1938).

2.4. Determination of sofosbuvir and ribavirin antiviral activity in cell line models

The antiviral activity of sofosbuvir and ribavirin against WNV was determined by PA in A549, Huh-7, U87 and LN-18 cells using 0.1 MOI based on published work (Escribano-Romero et al., 2017) and confirmed by IA in U87 and Huh-7 cells using 100, 50 and 25 $TCID_{50}$ to assess the reproducibility of the IC_{50} values using different virus inputs. For PA, the cells were pre-seeded in 96-well plate to obtain 90% confluence at the time of supernatant collection; for IA, the cells were pre-seeded in 96-well plate to obtain 10,000 cells for each well at the time of infection. The cells were then incubated in propagation medium at 37 °C. After 24 h, each cell line was infected with the specified input of viral stock and after 1 h adsorption the virus inoculum was removed and 5-fold dilutions of each drug (from 100 to 0.032 μM) were added to the cell monolayer. For PA, the viral supernatants were collected at 24 h for A549, at 48 h for Huh-7 and U87 and at 72 h for LN-18 cells according to the propagation experiments and PA was performed as previously indicated (paragraph 2.3). For the IA, the Huh-7 and U87 cell lines were incubated at 37 °C for 48 h, then the plates where fixed and stained as described in paragraph 2.3. Each drug concentration was tested in triplicate and infected and uninfected cells were tested as reference; three independent experiments were performed. IC_{50} values were calculated by a non-linear regression analysis of the dose-response curves generated with the Graphpad PRISM software version 6.01 (La Jolla, California, USA).

2.5. In vitro enzymatic inhibition assay with WNV RdRp

The WNV RdRp protein was expressed and purified as already described (Tarantino et al., 2016). RdRp activity was assessed following the synthesis of dsRNA from a single-stranded poly(C) template (10 μg) and 100 μM GTP in a reaction mixture containing 20 mM Tris/HCl (pH 7.5), 1 mM DTT, 25 mM NaCl, 5 mM $MgCl_2$, 0.3 mM $MnCl_2$, 2U RiboLock Ribonuclease inhibitor (Life technologies), 1 μl PicoGreen Quantitation Reagent (Life technologies) as already described (Gong et al., 2013; Tarantino et al., 2016; Van Dycke et al., 2018). WNV RdRp, at the concentration of 1 μM, was added to the reaction mixture together with SOF-TP (ranging from 0 to 250 μM). The PicoGreen fluorescence (excitation/emission = 485/530 nm) was measured at 30 °C for 30 min (Varian, Cary Eclipse Fluorescence Spectrophotometer). RdRp activity (i.e. linear slope of fluorescence increasing over time, Y) vs. inhibitor concentration (X) was used to estimate the IC_{50} of the SOF-TP using the equation $Y = (Range/(1 + (X/IC_{50}))$ where Range is the difference between the values observed for the uninhibited and completely inhibited RdRp.

2.6. In vitro selection experiments

In vitro selection experiments were performed in Huh-7 cells at 70%

confluence in T25 flasks with 0.05 and 0.01 MOI, each in duplicate. After 1 h adsorption at 37 °C, the virus inoculum was removed and the cells were incubated with 5 μM sofosbuvir, corresponding to about 4-fold IC50. The cell cultures were monitored every 24 h, and when 80% of viral cytopathic effect (CPE) was observed, the cells and supernatants were freeze-thawed, cleared by centrifugation and used to re-infect fresh pre-seeded Huh-7 in the presence of 2-fold higher sofosbuvir concentration. At each step, negative (cells with drug) and positive (cells with virus for each MOI) controls were included. Sanger sequencing of the WNV NS5 region was performed to detect emergent mutations at each drug increment. Mutant viruses were titrated by IA and sofosbuvir IC50 was measured as described above using 25 TCID50, in triplicate experiments. Fold changes (FC) values were calculated as the ratio between the IC50 of the mutant virus stock and the IC50 of the paired wild type control grown without drug pressure under the same experimental conditions (no-drug control).

2.7. Viral RNA amplification and sequencing

All the viral stocks collected during in vitro selection experiments were analyzed by population sequencing to detect emergent mutations in the NS5 region. Briefly, 150 μl of viral stocks were extracted using the ZR Viral RNA Kit (Zymo Research) according to the manufacturer's protocol. cDNA was generated by random hexamer-driven reverse transcription using 10 μl of RNA extract, 664 μM dNTPs, 6 μl of 5X ImProm-II TM Reaction Buffer, 50 ng Hexanucleotides, 1.5 mM MgCl$_2$, 20U RNasin® Plus RNase Inhibitor and 1U of ImProm-II™ Reverse Transcriptase (Promega) in a final volume of 30 μl. The reactions included an initial 5-min step at 25 °C, followed by 30 min at 37 °C and a 5-min final step at 80 °C. cDNA was used as the template for PCR amplification of the whole NS5 gene, using the Q5 Hot Start High-Fidelity DNA Polymerase (NEB) protocol. To design primers with a high degree of conservation, the WNV alignment available at the NCBI web site was used (https://www.ncbi.nlm.nih.gov/genomes/VirusVariation); the primer sequences and coordinates, as referred to the WNV strain NY99 (GenBank accession no. DQ211652) are indicated in Table 1. Bidirectional DNA sequencing was performed using the BrilliantDye TM Terminator Kit v1.1 (Nimagen) with 8 different primers spanning the whole NS5 region (Table 1). The sequencing reactions were treated with the X-Terminator® Purification kit (Applied Biosystems) in a 96-well plate as suggested by the manufacturer, resolved by capillary electrophoresis on the 3130 XL Genetic Analyzer (Applied Biosystems) and analyzed with the DNAStar Lasergene 7.1.0 SeqMan Pro module.

2.8. Statistical analysis

Results of the replicate antiviral activity measurements were reported as mean and standard deviation (SD). The difference in time for viral growth under different experimental conditions was analyzed by Mann Whitney *U* test. Statistical analysis was performed using GraphPad PRISM software version 6.01.

2.9. Molecular docking experiments

Since the crystal structure of the whole WNV NS5 is not available, the crystallographic structures of RNA-free WNV RdRp (PDB-ID: 2HCN) (Malet et al., 2007) and RNA-bound HCV RdRp (PDB-ID: 4WTD) (Appleby et al., 2015) were used as structural templates to build a homology model of WNV RdRp according to Šebera (Šebera et al., 2018). WNV RdRp sequence was retrieved from UniProtKB (P06935). Chimeric homology models were generated by PrimeX software (Bell et al., 2012). The 793VPTGRTTWSIHAKGEWMTT810 loop was removed from the WNV RdRp template as it was overlapping with the RNA. Each model was solvated in TIP3P type water molecules and the total charge was neutralized by counter ions. The solvent was first energy minimized for 500 steps by the steepest descent algorithm (SDA) and 1500 steps by the conjugated gradient algorithm (CGA). Subsequently, the whole system was energy minimized for 1500 steps SDA and 8500 steps CGA. Amber18 software was used in energy minimization (Case et al., 2018), with the following force fields: i) ff14SB for the protein; ii) OL3 for RNA; iii) GAFF for ADP (partial charges and bond parameters were retrieved from the AMBER parameter database (Meagher et al., 2003).

Docking simulations were carried out with GOLD program (Jones et al., 1997), using the CHEMPLP as a scoring function. The binding site was centered on Tyr610 with a radius of 13 Å. The protonation state of sofosbuvir was assigned by FixpKa (OpenEye Scientific Software Santa Fe, NM) QUACPAC version 2.0.0.3 using default parameters and the molecule was energy minimized by Szybki (OpenEye Scientific Software Santa Fe, NM) version 1.10.0.3 using the MMFF94S force field (http://www.eyesopen.com).

3. Results

3.1. Viral propagation and determination of sofosbuvir and ribavirin antiviral activity

All the cell lines tested were permissive to WNV infection, as shown in Fig. 1a. By PA, the peak virus production was observed at 24 h in A549 cells ($1.7 \times 10^7 \pm 2.0 \times 10^6$ PFU/ml), at 48 h in Huh-7 ($4.4 \times 10^8 \pm 3.2 \times 10^7$ PFU/ml), VERO E6 ($2.7 \times 10^7 \pm 1.6 \times 10^6$ PFU/ml) and U87 ($1.7 \times 10^7 \pm 4.9 \times 10^5$ PFU/ml) cells, and at 72 h in LN-18 cells ($9.4 \times 10^6 \pm 8.8 \times 10^5$ PFU/ml). When WNV was quantified in Huh-7 and U87 cells by IA, a similar trend in viral growth was observed in both cell lines (Fig. 1b). Based on these results, the yield reduction assays to determine antiviral activity were specifically set at the peak of virus production of each cell line. Antiviral activity was tested only in the human cell lines, based on better ability to mimic the virus human tropism in different tissues.

In the range tested (0.78–400 μM), sofosbuvir and ribavirin showed no cytotoxicity in all the cell lines evaluated (Supplementary Fig. 1). The antiviral activity of sofosbuvir and ribavirin, measured by PA at 0.1 MOI, is shown in Fig. 2 and Table 2. Sofosbuvir was active in the low micromolar range in Huh-7 (1.2 ± 0.3 μM) cells and in both neuronal

Table 1
Primer used to sequence the whole NS5 region.

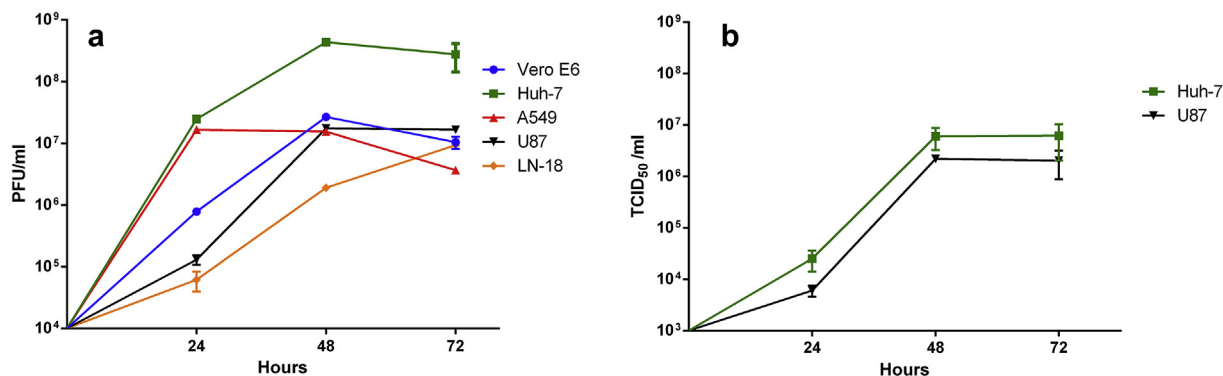| PRIMER	SEQUENCE	SENSE	GENE	From	To
P882	GACTYTGYCACATCATGCGTG	Forward	NS4B	7589	7609
P883	GCAGCACCGTCTACTCAACTTC	Reverse	3'UTR	10532	10553
P884	CAGCTGGTGAGRATGATGGAAGG	Forward	NS5	9541	9563
P885	GAGATGGTGGATGAGGAGCG	Forward	NS5	8983	9002
P886	TTGGTGAARGTGTTYAGGGCGTA	Reverse	NS5	9508	9530
P887	GAAGATGTMAACTTGGGAAGTGGAA	Forward	NS5	8446	8470
P888	CTRCCGTGRTAGTTCCAGGTTCT	Reverse	NS5	8587	8609
P890	CTCCRCTCTTCATGGTGACAATGTT	Reverse	NS5	8044	8068

Fig. 1. (a) WNV propagation as measured by Plaque Assay in four different human cell lines Huh-7, A549, U87 and LN-18 and in the monkey VERO E6 cell line; results were expressed as Plaque Forming Units per ml (PFU/ml). (b) WNV propagation as measured by Immunodetection Assay in Huh-7 and U87 cells; results were expressed as Tissue Culture Infectious Doses per milliliter (TCID50/ml).

cell lines U87 (5.3 ± 0.9 μM) and LN-18 (7.8 ± 2.5 μM), while a reduced activity was observed in A549 cells (63.4 ± 9.0 μM). Ribavirin was less active than sofosbuvir in Huh-7 (6.7 ± 0.6 μM), LN-18 (10.7 ± 0.5 μM) and U87 (60.5 ± 11.8 μM) cells, with 1.4- to 11.4-fold difference. Conversely, ribavirin was more active than sofosbuvir in A549 cells (6.2 vs. 63.4 μM, respectively). The antiviral activity of both compounds was also determined by IA in Huh-7 and U87 cells using three different viral inputs (Table 3). The IA IC_{50} was closest to the PA IC_{50} at the lowest viral input used, i.e. 25 $TCID_{50}$. Globally, IA confirmed the results obtained with PA showing the efficacy of sofosbuvir in inhibiting WNV replication in the human hepatic and neuronal cell lines in the low micromolar range.

The inhibitory effect of SOF-TP on WNV was determined also in vitro using the purified recombinant WNV RdRp in a *de novo* RdRp assay synthesizing dsRNA from the single-stranded poly(C) template. Sofosbuvir inhibited the WNV RdRp activity in a dose-dependent manner, with an IC_{50} of 11.1 ± 4.6 μM.

Table 2

Antiviral activity of sofosbuvir and ribavirin against WNV as measured by PA using the MOI of 0.1 in different human cell lines. Three independent experiments for each cell line were performed.

Cell line	Sofosbuvir	Ribavirin
	Mean IC_{50} (μM) ± SD	Mean IC_{50} (μM) ± SD
Huh-7	1.2 ± 0.3	6.7 ± 0.6
U87	5.3 ± 0.9	60.5 ± 11.8
A549	63.4 ± 9.0	6.2 ± 1.3
LN-18	7.8 ± 2.5	10.7 ± 0.5

IC_{50}: Half maximal inhibitory concentration; SD: Standard Deviation.

3.2. WNV In vitro selection experiments under sofosbuvir drug pressure

Two WNV inputs (0.01 and 0.05 MOI), each in duplicate, were used to infect Huh-7 cells in the presence of increasing concentration of
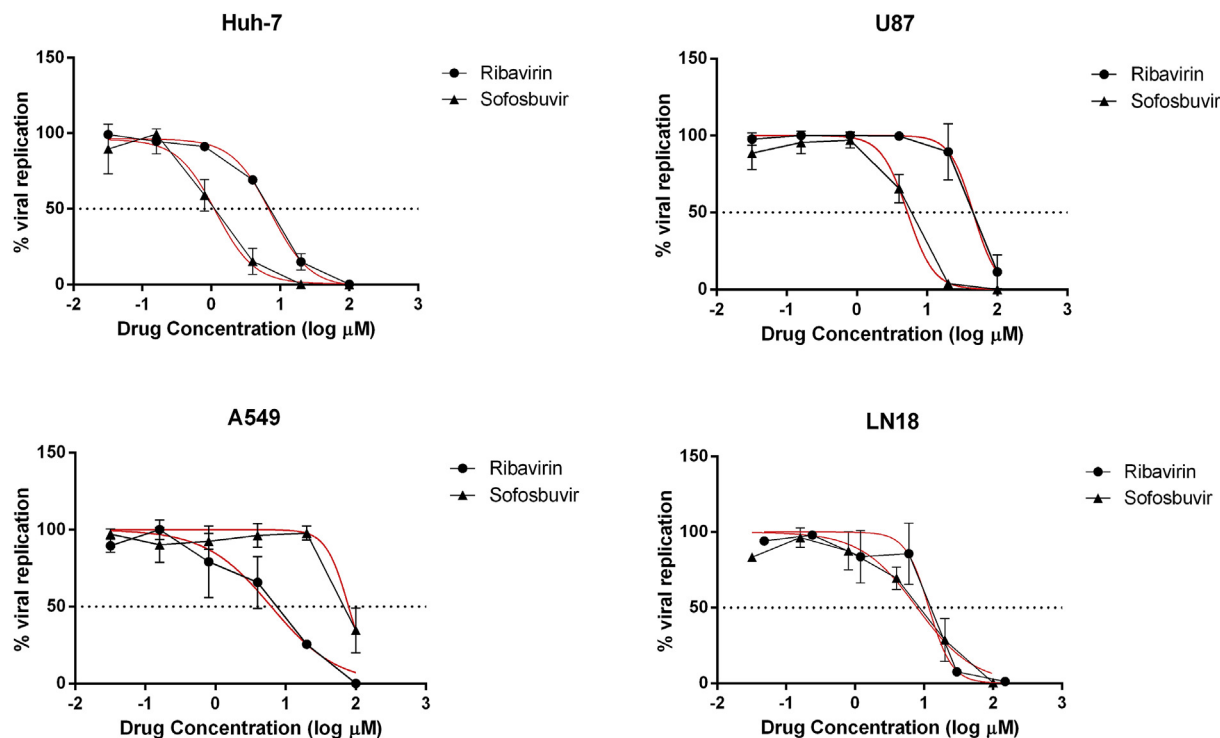
Fig. 2. Normalized antiviral activity of sofosbuvir and ribavirin as determined by Plaque Assay at 0.1 MOI in four different human cell lines (Huh-7, A549, U87 and LN-18). The non linear fitting curve as calculated by GraphPad Prism is depicted in red.

Table 3

Antiviral activity of sofosbuvir and ribavirin against WNV as measured by IA in Huh-7 and U87 cells using three different viral inputs in three independent experiments for each cell line.

Cell line	Sofosbuvir		Ribavirin	
	$TCID_{50}$	Mean IC_{50} (μM) $\pm$ SD	$TCID_{50}$	Mean IC_{50} (μM) $\pm$ SD
Huh-7	100	3.1 $\pm$ 0.6	100	14.4 $\pm$ 3.6
	50	2.0 $\pm$ 0.1	50	13.5 $\pm$ 3.1
	25	1.7 $\pm$ 0.5	25	9.5 $\pm$ 4.0
U87	100	15.1 $\pm$ 2.0	100	92.0 $\pm$ 13.8
	50	10.6 $\pm$ 2.1	50	73.0 $\pm$ 32.6
	25	7.3 $\pm$ 2.0	25	61.6 $\pm$ 13.7

$TCID_{50}$: Tissue Culture Infectious Dose; IC_{50}: Half maximal inhibitory concentration; SD: Standard Deviation.

sofosbuvir, starting from 5 μM, corresponding to about 4-fold the sofosbuvir IC_{50} as measured by PA in the same cells. Drug pressure significantly delayed viral growth with respect to the no-drug control. Indeed, around 80% of CPE was reached at 7–9 days post infection (dpi) with 5–40 μM sofosbuvir while the no-drug control virus was consistently collected at 3 dpi (p = 0.029). With 80 μM sofosbuvir, a significantly longer time for viral breakthrough was required (18 dpi for all experiments), with respect to lower concentrations, (p = 0.029) and several NS5 mutations emerged (Table 4). Notably, the S604T mutation, corresponding to the well-known S282T sofosbuvir resistance mutation in HCV NS5B (Wu et al., 2015; H. T. Xu et al., 2017b), was detected in three of four experiments, alone or in association with other mutations. Mutations detected in the MTase domain (Malet et al., 2008) included G2E, K76R and T216M, all occurring only once. The RdRp mutation A483G, detected in 2 experiments, is located in the finger domain, highly conserved among flaviviruses (Dubankova and Boura, 2019). In the experiment 4, the only without S604T, the A483G mutation was accompanied by M479K and L721M, located in a conserved domain of the motif F in the RdRp finger domain (Dubankova and Boura, 2019; Malet et al., 2007) and in the motif E of the RdRp thumb close to residues involved in the binding site of Zn_{2+} ion, respectively (Malet et al., 2008).

To assess whether emergent NS5 mutations were associated with drug resistance, sofosbuvir IC_{50} was measured against the mutant viruses collected at 80 μM as well as the wild type viruses collected at 40 μM sofosbuvir, to exclude FC variation independent by the NS5 substitutions. As indicated in Table 4, no changes in FC were observed in the absence of the NS5 mutations. In the presence of the NS5 mutations, IC_{50} values consistently increased with respect to the paired no-drug control virus (median FC 7.7, IQR 5.5–9.7). The maximum increase in FC was observed in experiment 1, where S604T was associated with the K76R and T216M MTase mutations.
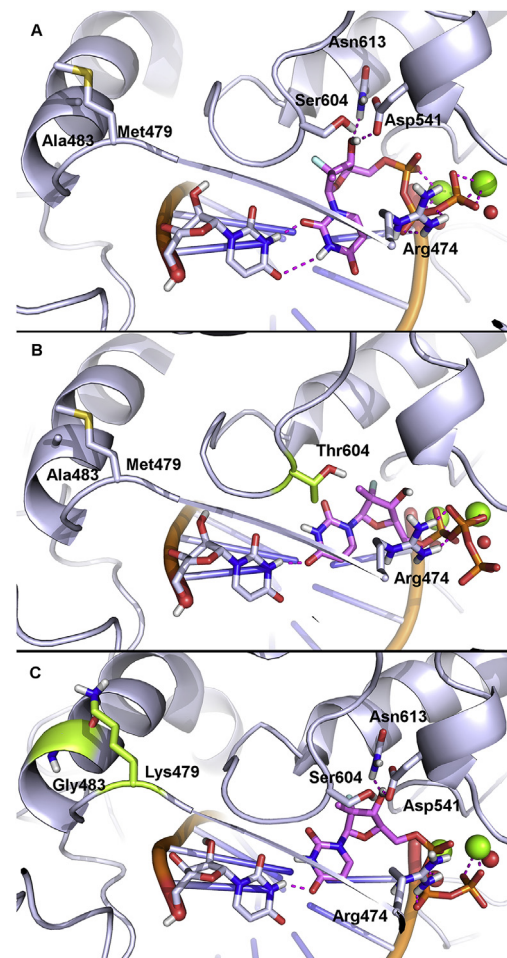
Fig. 3. Docking-based binding mode of sofosbuvir in the catalytic site of (a) wild type WNV RdRp, (b) S604T WNV RdRp, and (c) M479K/A483G/L721M WNV RdRp. Polar contacts are highlighted by magenta dashed lines. Residues involved in polar and non-polar interactions with sofosbuvir are shown as sticks and are labelled. Mg2+ ions and water molecules bound to Mg2+ ions are shown as green and red spheres, respectively. For the sake of clarity, in panel (c) only the M479K and A483G mutations, which are located near the catalytic site, are visible.

3.3. Molecular docking of sofosbuvir in wild type and mutant viruses

Available structures of RNA-free WNV RdRp and RNA-bound HCV RdRp were used as structural templates to generate the homology model of wild type, as well as S604T and M479K/A483G/L721M

Table 4

Changes in NS5 amino acid sequence detected at virus breakthrough with increasing sofosbuvir concentration in duplicate sample at MOI of 0.01 and of 0.05. The sofosbuvir half maximal inhibitory concentration (IC_{50}) of viral strains growth at the selective pressure of 40 and 80 μM was determined by IA in three independent assays for each experiment.

Experiment	MOI	Increasing sofosbuvir concentration						
		[5,10,20 μM]	[40 μM]			[80 μM]		
		Mutations	Mutations	Mean IC_{50} (μM) $\pm$ SD	FC	Mutations	Mean IC_{50} (μM) $\pm$ SD	FC
1	0.01	None	None	3.3 $\pm$ 0.7	1.4	K76RK, T216MT, S604T	20.1 $\pm$ 2.9	10.3
2	0.01	None	None	2.3 $\pm$ 0.2	1.0	G2EG, A483GA, S604T	10.4 $\pm$ 2.7	5.3
3[a]WT	0.01	None	None	2.3 $\pm$ 1.1	1.0	None	2.0 $\pm$ 0.4	1.0
4	0.05	None	None	2.2 $\pm$ 0.4	1.0	M479KM, A483G, L721M	14.4 $\pm$ 1.8	6.5
5	0.05	None	None	1.6 $\pm$ 0.9	0.7	S604T	19.5 $\pm$ 6.2	8.8
6[a]WT	0.05	None	None	2.2 $\pm$ 1.5	1.0	None	2.2 $\pm$ 0.4	1.0

FC: Fold-change with respect to the wild type control virus (WT); NM: None.

[a] WT were not subjected to sofosbuvir drug pressure.

variants of WNV RdRp. Docking results showed that the bioactive triphosphate form of sofosbuvir (Murakami et al., 2010) binds the catalytic site of WNV RdRp wild type by pairing the uracil from RNA template in a wobble-like conformation. The hydroxyl group of the drug establishes two H-bonds with Asp541 and Asn613, while phosphate groups are H-bonded to Arg474 and coordinated to catalytic Mg^{2+} ions (Fig. 3a). Probably, because of the steric hindrance of Thr604, which partially occludes the catalytic pocket, in WNV RdRp S604T sofosbuvir establishes only one H-bond with the uracil from the RNA template, while phosphate groups are H-bonded to Arg474. Moreover, only α and β phosphate groups coordinate to Mg^{2+} ions (Fig. 3b). Similarly, docking to the WNV M479K/A483G/L721M triple RdRp mutant showed that sofosbuvir binds within the catalytic site by establishing only one H-bond with the uracil from RNA template and losing the wobble base pairing. The hydroxyl group is H-bonded to Asp541 and Asn613, while phosphate groups are H-bonded to Arg474, although only α and γ phosphate groups coordinate to Mg^{2+} ions (Fig. 3c). Overall, docking results suggest that mutations within the catalytic site affect its overall shape and pharmacophoric features, and impair the binding mode of sofosbuvir particularly with respect to the base pairing with uracil from RNA template. This latter interaction seems to play a crucial role in the inhibition of WNV RdRp catalytic activity by sofosbuvir.

4. Discussion

WNV spreading, together with expanded transmission (Chancey et al., 2015) and increased virulence (Patel et al., 2015), prompts for intensive antiviral drug discovery efforts. Repurposing of licensed drugs can dramatically reduce the developing time for drug testing and validation. Sofosbuvir, a key agent in HCV treatment, has already been considered for the treatment of ZIKV and DENV infection, showing efficacy in vitro and in mouse models (Mesci et al., 2018; Sacramento et al., 2017; H. T. Xu et al., 2017a). We investigated the anti-WNV sofosbuvir activity in vitro in multiple human cell lines. Considering WNV tropism and pathogenesis, we included astroglioma (U87) and glioblastoma (LN-18) cell lines, in addition to epithelial and hepatic cells commonly used for WNV propagation (Ma et al., 2009; Urbanowski and Hobman, 2013). Sofosbuvir was active in the low micromolar range in all human cell lines tested except for the A549 cell line (around one log lower activity). These data, measured by the gold standard PA, were confirmed by the more convenient IA performed in the representative Huh-7 and U87 cells. On the other hand, the lack of sofosbuvir and ribavirin activity in A549 and U87 cells, respectively, underlines the need to choose a suitable cell substrate when testing candidate antiviral agents. The inhibitory activity of sofosbuvir against the purified WNV RdRp measured in a *de novo* enzymatic assay (Tarantino et al., 2016) was in the low micromolar range, comparable to the results previously reported with ZIKV (Xu et al., 2017b).

In vitro sofosbuvir resistance selection experiments have been performed with HCV (Lam et al., 2012; Xu et al., 2017), but not with any flavivirus. Based on homology with the HCV NS5B S282T selected by sofosbuvir, Xu et al. (H. T. Xu et al., 2017b) introduced the S604T mutation in ZIKV NS5 and documented 4.9-fold resistance to sofosbuvir in a biochemical assay. Our work definitely demonstrates that S604T is a major pathway of WNV escape to sofosbuvir pressure in vitro. Indeed, the S604T mutation emerged in three of four resistance selection experiments, resulting in 5.3- to 10.3-fold resistance which is comparable to the extent of sofosbuvir resistance described for the HCV replicons harboring S282T (Han et al., 2019). Both Ser604 and Gly605 are highly conserved residues among flaviviruses, located in the motif B of the RdRp palm (Dubankova and Boura, 2019). Despite limited sequence identity between Flavivirus and HCV RdRp (Malet et al., 2008), these residues are also conserved in HCV, corresponding to S282 and G283 (Appleby et al., 2015; Wu et al., 2015). In addition, a homolog S600T substitution in DENV RdRp has been reported to be involved in

resistance to nucleotide inhibitors in vitro (Latour et al., 2010).

Few other mutations were detected in association with the S604T (Table 4) mutation, all as mixtures with the wild type codon, possibly reflecting adaptation of the enzyme to compensate for loss of fitness consequent to selection of the key S604T resistance mutation, with minimal impact on resistance level. Of note, one experiment generated a 6.5-fold resistant mutant without S604T but harboring three mutations (M479K, A483G, L721M) which have no known counterpart in HCV. This highlights that alternative sofosbuvir escape pathways may occasionally occur.

An atomistic picture of the interaction between sofosbuvir and WNV RdRp was described by molecular modeling. Given the lack of experimental structural information, the 3D structures of catalytically competent wild type and mutant WNV RdRp forms in complex with RNA, metals and ADP were generated by homology modeling, and used as receptors in molecular docking simulations. Compared to the wild type WNV RdRp, in both mutant forms sofosbuvir loses the wobble-like base pairing with the uracil from the RNA template, as well as additional interactions with the catalytic Mg^{2+} ions. These binding modes might account for the different efficacy of sofosbuvir against the three variants of WNV RdRp and highlight the key pharmacophores in WNV RdRp inhibition by small molecules.

To our knowledge, these data show for the first time that sofosbuvir is active against WNV in vitro in human hepatic and neuronal cell lines in the low micromolar range, at levels comparable to those reported for ZIKV and DENV. Based on selection of the S604T mutation, sofosbuvir appears to interact with the same conserved domain across Flavivirus and Hepacivirus RdRp. Studies in animal models are required to confirm the relevance of these findings and better define opportunities for sofosbuvir use or further development against multiple flaviviral infections.

Declaration of competing interest

M. Z. reports consultancy for ViiV Healthcare, Gilead Sciences and Janssen-Cilag, and grants for his institution from ViiV Healthcare and Gilead outside the submitted work. All other authors: none to declare.

Appendix A. Supplementary data

Supplementary data to this article can be found online at https://doi.org/10.1016/j.antiviral.2020.104708.

References

Acharya, D., Bai, F., 2016. An overview of current approaches toward the treatment and prevention of west Nile virus infection. Methods Mol. Biol. 1435, 249–291. https://doi.org/10.1007/978-1-4939-3670-0_19.

Appleby, T.C., Perry, J.K., Murakami, E., Barauskas, O., Feng, J., Cho, A., Fox, D., Wetmore, D.R., McGrath, M.E., Ray, A.S., Sofia, M.J., Swaminathan, S., Edwards, T.E., 2015. Structural basis for RNA replication by the hepatitis C virus polymerase. Science 347, 771–775. https://doi.org/10.1126/science.1259210.

Bell, J.A., Cao, Y., Gunn, J.R., Day, T., Gallicchio, E., Zhou, Z., Levy, R., Farid, R., 2012. PrimeX and the Schrödinger Computational Chemistry Suite of Programs 534–538. https://doi.org/10.1107/97809553602060000864.

Boldescu, V., Behnam, M.A.M., Vasilakis, N., Klein, C.D., 2017. Broad-spectrum agents for flaviviral infections: dengue, Zika and beyond. Nat. Rev. Drug Discov. 16, 565–586. https://doi.org/10.1038/nrd.2017.33.

Case, D.A., Ben-Shalom, I.Y., Brozell, S.R., Cerutti, D.S., Cheatham III, T.E., Cruzeiro, V.W.D., Darden, T.A., Duke, R.E., Ghoreishi, D., Gilson, M.K., Gohlke, H., Goetz, A.W., Greene, D., Harris, R., Homeyer, N., Izadi, S., Kovalenko, A., Kurtzman, T., Lee, T.S., LeGrand, S., Li, P., Lin, C., Liu, J., Luchko, T., Luo, R., Mermelstein, D.J., Merz, K.M., Miao, Y., Monard, G., Nguyen, C., Nguyen, H., Omelyan, I., Onufriev, A., Pan, F., Qi, R., Roe, D.R., Roitberg, A., Sagui, C., Schott-Verdugo, S., Shen, J., Simmerling, C.L., Smith, J., Salomon-Ferrer, R., Swails, J., Walker, R.C., Wang, J., Wei, H., Wolf, R.M., Wu, X., Xiao, L., York, D.M., Kollman, P.A., 2018. AMBER 2018. University of California, San Francisco.

Chancey, C., Grinev, A., Volkova, E., Rios, M., 2015. The global ecology and epidemiology of west nile virus. BioMed Res. Int. 2015, 376230. https://doi.org/10.1155/2015/376230.

Dubankova, A., Boura, E., 2019. Structure of the yellow fever NS5 protein reveals conserved drug targets shared among flaviviruses. Antivir. Res. 169, 104536. https://doi.org/10.1016/j.antiviral.2019.104536.

Escribano-Romero, E., De Oya, N.J., Domingo, E., Saiza, J.C., 2017. Extinction of west nile virus by favipiravir through lethal mutagenesis. Antimicrob. Agents Chemother. 61, 1–9. https://doi.org/10.1128/AAC.01400-17.

Ferreira, A.C., Reis, P.A., de Freitas, C.S., Sacramento, C.Q., Hoelz, L.V.B., Bastos, M.M., Mattos, M., Rocha, N., de Azevedo Quintanilha, I.G., da Silva Gouveia Pedrosa, C., Souza, L.R.Q., Loiola, E.C., Trindade, P., Vieira, Y.R., Barbosa-Lima, G., de Castro Faria Neto, H.C., Boechat, N., Rehen, S.K., Brüning, K., Bozza, F.A., Bozza, P.T., Souza, T.M.L., 2019. Beyond members of the Flaviviridae family, sofosbuvir also inhibits chikungunya virus replication. Antimicrob. Agents Chemother. 63, 18. https://doi.org/10.1128/AAC.01389-18. e01389.

Gong, E.Y., Kenens, H., Ivens, T., Dockx, K., Vermeiren, K., Vandercruyssen, G., Devogelaere, B., Lory, P., Kraus, G., 2013. Expression and purification of dengue virus NS5 polymerase and development of a high-throughput enzymatic assay for screening inhibitors of dengue polymerase. Methods Mol. Biol. 1030, 237–247. https://doi.org/10.1007/978-1-62703-484-5_19. PubMed PMID: 23821273.

Götte, M., Feld, J.J., 2016. Direct-acting antiviral agents for hepatitis C: structural and mechanistic insights. Nat. Rev. Gastroenterol. Hepatol. 13, 338–351. https://doi.org/10.1038/nrgastro.2016.60.

Han, B., Martin, R., Xu, S., Parvangada, A., Svarovskaia, E.S., Mo, H., Dvory-Sobol, H., 2019. Sofosbuvir susceptibility of genotype 1 to 6 HCV from DAA-naïve subjects. Antivir. Res. 170, 104574. https://doi.org/10.1016/j.antiviral.2019.104574.

Jones, G., Willett, P., Glen, R.C., Leach, A.R., Taylor, R., 1997. Development and validation of a genetic algorithm for flexible docking. J. Mol. Biol. https://doi.org/10.1006/jmbi.1996.0897.

Kok, W.M., 2016. New developments in flavivirus drug discovery. Expert Opin. Drug Discov. 11, 433–445. https://doi.org/10.1517/17460441.2016.1160887.

Lam, A.M., Espiritu, C., Bansal, S., Micolochick Steuer, H.M., Niu, C., Zennou, V., Keilman, M., Zhu, Y., Lan, S., Otto, M.J., Furman, P.A., 2012. Genotype and subtype profiling of PSI-7977 as a nucleotide inhibitor of hepatitis C virus. Antimicrob. Agents Chemother. 56, 3359–3368. https://doi.org/10.1128/AAC.00054-12.

Latour, D.R., Jekle, A., Javanbakht, H., Henningsen, R., Gee, P., Lee, I., Tran, P., Ren, S., Kutach, A.K., Harris, S.F., Wang, S.M., Lok, S.J., Shaw, D., Li, J., Heilek, G., Klumpp, K., Swinney, D.C., Deval, J., 2010. Biochemical characterization of the inhibition of the dengue virus RNA polymerase by beta-d-2'-ethynyl-7-deaza-adenosine triphosphate. Antivir. Res. 87, 213–222. https://doi.org/10.1016/j.antiviral.2010.05.003.

Lim, S.P., Koh, J.H.K., Seh, C.C., Liew, C.W., Davidson, A.D., Chua, L.S., Chandrasekaran, R., Cornvik, T.C., Shi, P.Y., Lescar, J., 2013. A crystal structure of the dengue virus non-structural protein 5 (NS5) polymerase delineates interdomain amino acid residues that enhance its thermostability and de novo initiation activities. J. Biol. Chem. 288, 31105–31114. https://doi.org/10.1074/jbc.M113.508606.

Ma, D., Jiang, D., Qing, M., Weidner, J.M., Qu, X., Guo, H., Chang, J., Gu, B., Shi, P.Y., Block, T.M., Guo, J.T., 2009. Antiviral effect of interferon lambda against West Nile virus. Antivir. Res. 83, 53–60. https://doi.org/10.1016/j.antiviral.2009.03.006.

Magurano, F., Remoli, M.E., Baggieri, M., Fortuna, C., Marchi, A., Fiorentini, C., Bucci, P., Benedetti, E., Ciufolini, M.G., Rizzo, C., Piga, S., Salcuni, P., Rezza, G., Nicoletti, L., 2012. Circulation of West Nile virus lineage 1 and 2 during an outbreak in Italy. Clin. Microbiol. Infect. 18, E545–E547. https://doi.org/10.1111/1469-0691.12018.

Malet, H., Egloff, M.P., Selisko, B., Butcher, R.E., Wright, P.J., Roberts, M., Gruez, A., Sulzenbacher, G., Vonrhein, C., Bricogne, G., Mackenzie, J.M., Khromykh, A.A., Davidson, A.D., Canard, B., 2007. Crystal structure of the RNA polymerase domain of the West Nile virus non-structural protein 5. J. Biol. Chem. 282, 10678–10689. https://doi.org/10.1074/jbc.M607273200.

Malet, H., Massé, N., Selisko, B., Romette, J.L., Alvarez, K., Guillemot, J.C., Tolou, H., Yap, T.L., Vasudevan, S.G., Lescar, J., Canard, B., 2008. The flavivirus polymerase as a target for drug discovery. Antivir. Res. 80, 23–35. https://doi.org/10.1016/j.antiviral.2008.06.007.

Meagher, K.L., Redman, L.T., Carlson, H.A., 2003. Development of polyphosphate parameters for use with the AMBER force field. J. Comput. Chem. 24, 1016–1025. https://doi.org/10.1002/jcc.10262.

Mesci, P., Macia, A., Moore, S.M., Shiryaev, S.A., Pinto, A., Huang, C.T., Tejwani, L., Fernandes, I.R., Suarez, N.A., Kolar, M.J., Montefusco, S., Rosenberg, S.C., Herai, R.H., Cugola, F.R., Russo, F.B., Sheets, N., Saghatelian, A., Shresta, S., Momper, J.D., Siqueira-Neto, J.L., Corbett, K.D., Beltrão-Braga, P.C.B., Terskikh, A.V., Muotri, A.R., 2018. Blocking Zika virus vertical transmission. Sci. Rep. 8, 1218. https://doi.org/10.1038/s41598-018-19526-4.

Murakami, E., Tolstykh, T., Bao, H., Niu, C., Micolochick Steuer, H.M., Bao, D., Chang, W., Espiritu, C., Bansal, S., Lam, A.M., Otto, M.J., Sofia, M.J., Furman, P.A., 2010. Mechanism of activation of PSI-7851 and its diastereoisomer PSI-7977. J. Biol. Chem. 285, 34337–34347. https://doi.org/10.1074/jbc.M110.161802.

Patel, H., Sander, B., Nelder, M.P., 2015. Long-term sequelae of West Nile virus-related illness: a systematic review. Lancet Infect. Dis. 15, 951–959. https://doi.org/10.1016/S1473-3099(15)00134-6.

Reed, L.J., Muench, H., 1938. A simple method of estimating fifty per cent endpoints. Am. J. Epidemiol. 27, 493–497. https://doi.org/10.1093/oxfordjournals.aje.a118408.

Sacramento, C.Q., de Melo, G.R., de Freitas, C.S., Rocha, N., Hoelz, L.V.B., Miranda, M., Fintelman-Rodrigues, N., Marttorelli, A., Ferreira, A.C., Barbosa-Lima, G., Abrantes, J.L., Vieira, Y.R., Bastos, M.M., de Mello Volotão, E., Nunes, E.P., Tschoeke, D.A., Leomil, L., Loiola, E.C., Trindade, P., Rehen, S.K., Bozza, F.A., Bozza, P.T., Boechat, N., Thompson, F.L., de Filippis, A.M.B., Brüning, K., Souza, T.M.L., 2017. The clinically approved antiviral drug sofosbuvir inhibits Zika virus replication. Sci. Rep. 7, 40920. https://doi.org/10.1038/srep40920.

Šebera, J., Dubankova, A., Sychrovský, V., Ruzek, D., Boura, E., Nencka, R., 2018. The structural model of Zika virus RNA-dependent RNA polymerase in complex with RNA for rational design of novel nucleotide inhibitors. Sci. Rep. 8, 1–13. https://doi.org/10.1038/s41598-018-29459-7.

Sejvar, J.J., 2014. Clinical manifestations and outcomes of West Nile virus infection. Viruses 6, 606–623. https://doi.org/10.3390/v6020606.

Tarantino, D., Cannalire, R., Mastrangelo, E., Croci, R., Querat, G., Barreca, M.L., Bolognesi, M., Manfroni, G., Cecchetti, V., Milani, M., 2016. Targeting flavivirus RNA dependent RNA polymerase through a pyridobenzothiazole inhibitor. Antivir. Res. 134, 226–235. https://doi.org/10.1016/j.antiviral.2016.09.007.

Urbanowski, M.D., Hobman, T.C., 2013. The West Nile virus capsid protein blocks apoptosis through a phosphatidylinositol 3-kinase-dependent mechanism. J. Virol. 87, 872–881. https://doi.org/10.1128/jvi.02030-12.

Van Dycke, J., Arnoldi, F., Papa, G., Vandepoele, J., Burrone, O.R., Mastrangelo, E., Tarantino, D., Heylen, E., Neyts, J., Rocha-Pereira, J., 2018. A single nucleoside viral polymerase inhibitor against norovirus, rotavirus, and sapovirus-induced diarrhea. J. Infect. Dis. 218, 1753–1758. https://doi.org/10.1093/infdis/jiy398.

Vicenti, I., Boccuto, A., Giannini, A., Dragoni, F., Saladini, F., Zazzi, M., 2018. Comparative analysis of different cell systems for Zika virus (ZIKV) propagation and evaluation of anti-ZIKV compounds in vitro. Virus Res. 244, 64–70. https://doi.org/10.1016/j.virusres.2017.11.003.

Wu, J., Liu, W., Gong, P., Gong, P., 2015. A structural overview of RNA-dependent RNA polymerases from the Flaviviridae family. Int. J. Mol. Sci. 16, 12943–12957. https://doi.org/10.3390/ijms160612943.

Xu, H.T., Colby-Germinario, S.P., Hassounah, S.A., Fogarty, C., Osman, N., Palanisamy, N., Han, Y., Oliveira, M., Quan, Y., Wainberg, M.A., 2017a. Evaluation of Sofosbuvir (β-D-2'-deoxy-2'-α-fluoro-2'-β-C-methyluridine) as an inhibitor of Dengue virus replication. Sci. Rep. 7, 6345. https://doi.org/10.1038/s41598-017-06612-2.

Xu, H.T., Hassounah, S.A., Colby-Germinario, S.P., Oliveira, M., Fogarty, C., Quan, Y., Han, Y., Golubkov, O., Ibanescu, I., Brenner, B., Stranix, B.R., Wainberg, M.A., 2017b. Purification of Zika virus RNA-dependent RNA polymerase and its use to identify small-molecule Zika inhibitors. J. Antimicrob. Chemother. 72, 727–734. https://doi.org/10.1093/jac/dkw514.

Xu, S., Doehle, B., Rajyaguru, S., Han, B., Barauskas, O., Feng, J., Perry, J., Dvory-Sobol, H., Svarovskaia, E.S., Miller, M.D., Mo, H., 2017. In vitro selection of resistance to sofosbuvir in HCV replicons of genotype-1 to -6. Antivir. Ther. 22, 587–597. https://doi.org/10.3851/IMP3149.

Zhang, B., Dong, H., Zhou, Y., Shi, P.-Y., 2008. Genetic interactions among the West Nile virus methyltransferase, the RNA-dependent RNA polymerase, and the 5' stem-loop of genomic RNA. J. Virol. 82, 7047–7058. https://doi.org/10.1128/jvi.00654-08.

Molecular Tracing of SARS-CoV-2 in Italy in the First Three Months of the Epidemic

Alessia Lai [1,*]**, Annalisa Bergna** [1]**, Sara Caucci** [2]**, Nicola Clementi** [3]**, Ilaria Vicenti** [4]**,
Filippo Dragoni** [4]**, Anna Maria Cattelan** [5]**, Stefano Menzo** [2]**, Angelo Pan** [6]**, Annapaola Callegaro** [7]**,
Adriano Tagliabracci** [8]**, Arnaldo Caruso** [9]**, Francesca Caccuri** [9]**, Silvia Ronchiadin** [10]**,
Claudia Balotta** [1]**, Maurizio Zazzi** [4]**, Emanuela Vaccher** [11]**, Massimo Clementi** [3]**,
Massimo Galli** [1] **and Gianguglielmo Zehender** [1]

1 Department of Biomedical and Clinical Sciences Luigi Sacco, University of Milan, 20157 Milan, Italy;
bergna.anna@gmail.com (A.B.); claudia.balotta@unimi.it (C.B.); massimo.galli@unimi.it (M.G.);
gianguglielmo.zehender@unimi.it (G.Z.)

2 Department of Biomedical Sciences and Public Health, Virology Unit, Polytechnic University of Marche,
60131 Ancona, Italy; s.caucci@univpm.it (S.C.); menzo@univpm.it (S.M.)

3 Microbiology and Virology Unit, "Vita-Salute" San Raffaele University, 20132 Milan, Italy;
clementi.nicola@hsr.it (N.C.); clementi.massimo@hsr.it (M.C.)

4 Department of Medical Biotechnologies, University of Siena, 53100 Siena, Italy;
ilariavicenti@gmail.com (I.V.); dragonifilippo@gmail.com (F.D.); maurizio.zazzi@gmail.com (M.Z.)

5 Infectious Diseases Unit, Department of Internal Medicine, Azienda Ospedaliera-Universitaria di Padova,
35128 Padua, Italy; annamaria.cattelan@aopd.veneto.it

6 Infectious Diseases, ASST Cremona, 26100 Cremona, Italy; a.pan@asst-cremona.it

7 Microbiology and Virology Laboratory, ASST Papa Giovanni XXIII, 24127 Bergamo, Italy;
acallegaro@hpg23.it

8 Section of Legal Medicine, Universita Politecnica delle Marche, 60126 Ancona, Italy;
a.tagliabracci@staff.univpm.it

9 Microbiology Unit, Department of Molecular and Translational Medicine, University of Brescia and ASST
Spedali Civili Hospital, 25123 Brescia, Italy; arnaldo.caruso@unibs.it (A.C.); francesca.caccuri@unibs.it (F.C.)

10 Intesa Sanpaolo Innovation Center—AI LAB, 10138 Turin, Italy; silvia.ronchiadin@intesasanpaolo.com

11 Medical Oncology and Immune-related Tumors, Centro di Riferimento Oncologico di Aviano (CRO), IRCCS,
33081 Aviano, Italy; evaccher@cro.it

* Correspondence: alessia.lai@unimi.it; Tel.: +39-0250319775

Abstract: The aim of this study is the characterization and genomic tracing by phylogenetic analyses of 59 new SARS-CoV-2 Italian isolates obtained from patients attending clinical centres in North and Central Italy until the end of April 2020. All but one of the newly-characterized genomes belonged to the lineage B.1, the most frequently identified in European countries, including Italy. Only a single sequence was found to belong to lineage B. A mean of 6 nucleotide substitutions per viral genome was observed, without significant differences between synonymous and non-synonymous mutations, indicating genetic drift as a major source for virus evolution. tMRCA estimation confirmed the probable origin of the epidemic between the end of January and the beginning of February with a rapid increase in the number of infections between the end of February and mid-March. Since early February, an effective reproduction number (R_e) greater than 1 was estimated, which then increased reaching the peak of 2.3 in early March, confirming the circulation of the virus before the first COVID-19 cases were documented. Continuous use of state-of-the-art methods for molecular surveillance is warranted to trace virus circulation and evolution and inform effective prevention and containment of future SARS-CoV-2 outbreaks.

1. Introduction

Italy is one of the countries most- and earliest-affected in Europe by the COVID-19 pandemic (https://gisanddata.maps.arcgis.com/apps/opsdashboard/index.html#/bda7594740fd40299423467b48e9ecf6). The first autochthonous cases of Coronavirus 2019 Disease (COVID-19) were observed starting from 21 February 2020 in Codogno (Lodi province), determining on 22 February 2020 the establishment of a "red zone" to contain the epidemic, encompassing 11 municipalities. Thereafter, in a short time, it became evident that the epidemic had already involved a large part of Lombardy region and then spread to neighboring regions and, substantially less, to the rest of the country. On 9 March lockdown was declared for the entire country. The rapidly increasing number of patients who required hospitalization in the intensive care unit suggested that the virus may have circulated for a long period and caused thousands of contagions before the epidemic became manifest [1].

SARS-CoV-2 was first detected in Italy in a couple of Chinese tourists coming from Wuhan on 31 January [2]. Subsequent evaluations have not shown a relationship between the sequence of these strains and those implicated in the epidemic in Lombardy [3].

On the contrary, the Codogno strains resulted strictly related with a strain of SARS-CoV-2 coming from Shanghai which caused a small outbreak in Munich around 20 January [1] and was probably spread later to other European countries and beyond the Atlantic [4]. These sequences are part of a clade initially defined as a European clade, the old Nexstrain A2a subclade, which is currently the most widespread outside China and probably responsible for most of the world pandemic [5].

In the face of more than 240,000 notified cases in Italy, the entire genomes available in public databases are still scarce (77 at the time of this study). The availability of large numbers of sequences collected over time is necessary for molecular surveillance of the epidemic and for evaluation and planning of effective control strategies. To perform this study, a network of Italian Clinical centres and Laboratories across Italy generated additional 59 full-length SARS-CoV-2 sequences from COVID-19 patients ranging from the end of February to the end of April. This contribution helps to trace the temporal origin, the rate of viral evolution and the population dynamics of SARS-CoV-2 in Italy by phylogeny.

2. Materials and Methods

2.1. Patients and Methods

A total of 59 SARS-CoV-2 whole genomes were newly-characterized from an equal number of patients affected by COVID-19, attending different clinical centres in Northern and Central Italy, from the beginning of the epidemic (22 February 2020) until 27 April 2020 (Table S1).

All of the data used in this study were previously anonymized as required by the Italian Data Protection Code (Legislative Decree 196/2003) and the general authorizations issued by the Data Protection Authority. Ethics Committee approval was deemed unnecessary because, under Italian law, all sensitive data were deleted and we collected only age, gender and sampling date (Art. 6 and Art. 9 of Legislative Decree 211/2003).

Eighteen sequences were obtained after isolating the virus in Vero E6 cells while the remaining 41 were obtained directly from biological samples such as nasopharyngeal swabs or broncho-alveolar lavages (39 and 2, respectively).

SARS-CoV-2 RNA was extracted using the Kit QIAsymphony DSP Virus/Pathogen Midi kit on the QIAsymphony automated platform (QIAGEN, Hilden, Germany) ($n = 9$) and manually with QIAamp Viral RNA Mini Kit (QIAGEN, Hilden, Germany) ($n = 50$).

Full genome sequences were obtained with different protocols by amplifying 26 fragments as previously described (*n* = 42) [1] or using random hexamer primers (*n* = 8) or Ion AmpliSeq SARS-CoV-2 Research Panel (Thermo Fisher Scientific, Waltham, Massachusetts, USA) (*n* = 9). The PCR products were used to prepare a library for Illumina deep sequencing using a Nextera XT DNA Sample Preparation and Index kit (Illumina, San Diego, California, USA) in accordance with the manufacturer's manual, and sequencing was carried out on a Illumina MiSeq platform for 50 samples, while the remaining nine were sequenced on Ion GeneStudio™ S5 System instrument following the Ion AmpliSeq™ RNA libraries protocol (Thermo Fisher Scientific, Waltham, Massachusetts, USA). The results were mapped and aligned to the reference genome obtained from GISAID (https://www.gisaid.org/, accession ID: EPI_ISL_412973) using Geneious software, v. 9.1.5 (Biomatters, Auckland, New Zealand) (http://www.geneious.com) [6] or Torrent Suite v. 5.10.1 (Euformatics Oy, Espoo, Finland) or BWA-mem and rescued using Samtools alignment/Map (Hinxton, UK) (v 1.9).

2.2. Sequence Data Sets

The newly-characterized 59 genomes plus three previously characterized isolates by us (EPI_ISL_417445-417447) [1] were aligned with a total of 77 Italian sequences available in public databases (GISAID, https://www.gisaid.org/) on 13 May 2020 and 452 genomes sampled in different European and Asian countries (513 and 16, respectively) representing all the different viral clades described in the Nextstrain platform (https://nextstrain.org/). The final data set thus included 588 sequences. Due to the large amount of available sequences, we focused the analysis on European strains by randomly selecting sequences from each country and by excluding identical strains or strains with more than 5% of gaps. We sampled the data in order to have no temporal gaps, by grouping the sequences by country/week/clade and randomly selecting the sequences in each group. We choose 15 sequences for clade A2 and 5 sequences for other clades (therefore including A and B Pangolin lineages and different sublineages) for each European country. For countries with less than the required sequence number we kept all the sequences. The sampling dates of the entire dataset ranged from 30 December 2019 to 27 April 2020. Table S2 shows the accession IDs, sampling dates and locations of the sequences included in the dataset.

A subset of sequences assigned to the old Nextstrain A2 clade (classified as B lineage for Pangolin), was generated for dating the epidemic, including all the Italian sequences, one German (EPI_ISL_406862) and three Chinese isolates from Shanghai, ancestral to the A2 clade (EPI_ISL_416327, EPI_ISL_416334 and EPI_ISL_416386). Coalescent and birth-death phylodynamic analyses were performed on the 136 Italian A2 sequences only.

Alignment was performed using MAFFT [7] and manually cropped to a final length of 29,779 bp using BioEdit v. 7.2.6.1 (http://www.mbio.ncsu.edu/bioedit/bioedit.html).

2.3. Genetic Distance, Recombination, and Selection Pressure Analyses

The MEGA X program was used to evaluate the genetic distance between and within Italian sequences on the full length genome, with variance estimation performed using 1000 bootstrap replicates [8].

The RDP5 software was used to investigate the presence of potential recombination [9].

All of the genes were tested for selection pressure using Datamonkey (https://www.datamonkey.org/). Amino acid changes were evaluated using EPI_ISL_402123 as reference strain.

2.4. Phylogenetic and Phylodynamic Analyses

The simplest evolutionary model best fitting the sequence data was selected using the JmodelTest v.2.1.7 software [10], and proved to be the Hasegawa-Kishino-Yano model with a proportion of invariant sites (HKY+I).

The phylogenetic analysis for clade assignment was performed by RaxML [11] on the entire dataset of 588 genomes. During the period in which we were carrying out the study, the SARS-CoV-2

clade nomenclature system changed. In particular, Rambaut et al. proposed a dynamic nomenclature based on phylogenetic lineages, called Pangolin (Phylogenetic Assignment of Named Global Outbreak LINeages) [12]. For this reason, we used the old Nextstrain and the new Pangolin (freely available at https://pangolin.cog-uk.io/) systems for strain classification. The new Nextstrain classification was performed by using the available script (https://github.com/nextstrain/ncov/blob/master/docs/running.md).

The virus' phylogeny, evolutionary rates, times of the most recent common ancestor (tMRCA) and demographic growth were co-estimated in a Bayesian framework using a Markov Chain Monte Carlo (MCMC) method implemented in v.1.10.4 and v.2.62 of the BEAST package [13,14].

A root-to-tip regression analysis was made using TempEst in order to investigate the temporal signal of the dataset [15].

Different coalescent priors (constant population size and exponential growth and Bayesian skyline) and strict vs. relaxed molecular clock models were tested by means of path sampling (PS) and stepping stone (SS) sampling [16]. The evolutionary rate prior normal distribution, after informing the mean evolutionary rate, was set at mean 0.8×10^{-3} substitutions/site/year (http://virological.org/t/phylodynamic-analysis-176-genomes-6-mar-2020/356).

The MCMC analysis was run until convergence with sampling every 10,000 generations. Convergence was assessed by estimating the effective sampling size (ESS) after 10% burn-in using Tracer v.1.7 software (http://tree.bio.ed.ac.uk/software/tracer/), and accepting ESS values of 200 or more. The uncertainty of the estimates was indicated by 95% highest marginal likelihoods estimated [17] by path sampling/stepping stone methods [16].

The final trees were summarized by selecting the tree with the maximum product of posterior probabilities (pp) (maximum clade credibility or MCC) after a 10% burn-in using Tree Annotator v.1.10.4 (included in the BEAST package), and were visualized using FigTree v.1.4.2 (http://tree.bio.ed.ac.uk/software/figtree/). Posterior probabilities >0.7 were considered significant.

2.5. Birth-Death Skyline Estimates of the Effective Reproductive Number (R_e)

The birth-death skyline model implemented in Beast 2.62 was used to infer changes in the effective reproductive number (R_e), and other epidemiological parameters such as the death/recovery rate (δ), the transmission rate (λ), the origin of the epidemic, and the sampling proportion (ρ) [18]. Given that the samples were collected during a short period of time, a "birth-death contemporary" model was used.

The analyses were based on the previously selected HKY substitution model and the evolutionary rate was set to the value of 0.8×10^{-3} subs/site/year, which corresponds to the mean substitution rate estimated using a relaxed clock under the exponential coalescent model as transformed into units per year.

For the birth-death skyline analysis, from one to two R_e intervals and a log-normal prior with a mean (M) of 0.0 and a variance (S) of 1.0 were chosen, which allows the R_e values to change between <1 (0.193) to >5. A normal prior with M = 48.7 and S = 15 (corresponding to a 95% interval from 24.0 to 73.4) was used for the rate of becoming uninfectious. These values are expressed as units per year and reflect the inverse of the time of infectiousness (5.3–19 days, mean 7.5) according to the serial interval estimated by Li et al. [19]. Sampling probability (ρ) was estimated assuming a prior Beta (alpha = 1.0 and beta = 999), corresponding to a minority of the sampled cases (between 10^{-5} to 10^{-3}). The origin of the epidemic was estimated using a normal prior with M = 0.1 and S = 0.05 in units per year.

The MCMC analyses were run for 100 million generations and sampled every 10,000 steps.

Convergence was assessed on the basis of ESS values (ESS > 200). Uncertainty in the estimates was indicated by 95% highest posterior density (95%HPD) intervals.

The mean growth rate was calculated on the basis of the birth and recovery rates ($r = \lambda - \delta$), and the doubling time was estimated by the equation: doubling time = $\ln(2)/r$ [20].

3. Results

3.1. Phylogenetic Analysis of the Whole Dataset

No recombination events were observed in the entire dataset according to analyses with RDP5 software.

Phylogenetic analysis by maximum likelihood showed that the Italian sequences were included in a single SARS-CoV-2 clade (the old Nextstrain A2 clade, corresponding to new Nextstain clades 20A and 20B) with the exception of three sequences: Two from Chinese patients visiting Italy at the end of January 2020 after being infected in Wuhan and one characterized by us from an Italian subject, living in Padua, sampled in March 2020, not reporting any recent trip outside Italy or contacts with subjects affected by COVID-19 (pp = 0.99) (Figure 1, clade 19A).
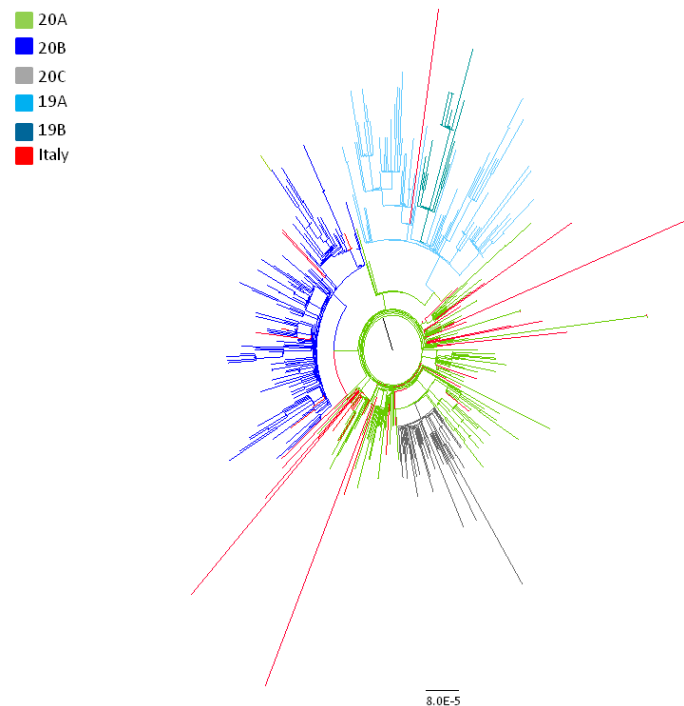
Figure 1. Maximum likelihood tree of the full dataset including 588 SARS-CoV-2 genomes. Nextstrain classification is indicated by colors as reported in the legend. Italian strains are highlighted in red.

Recently, new nomenclature systems have been proposed for the SARS-CoV-2 clades. The new lineage assignment of 62 Italian isolates is reported on Table 1 with the correspondence to other naming systems (old and new Nextstrain). All of our isolates belonged to the lineage B.1, only one isolate was classified as lineage B.

Table 1. Pangolin lineage classification of 62 Italian strains included in the study.

Lineage (Pangolin)	Total	%	From	Nextstrain New	Nextstrain Old
B	1	1.6	PD (1)	19A	nd
B.1	47	75.8	MI (15), PS(7), AN (1), MC (1) PD (8), BG (1), CR (3), SI (3), AR (3), GR (1), BS (4)	20A, nd	A2a
B.1.1	11	17.7	MI (4), PD (1), SI (4), GR (1), AR (1)	20B	A2a
B.1.34	1	1.6	MI (1)	nd	A2a
B.1.5	2	3.2	MI (1), BG (1)	20A	A2a

PD: Padua, MI: Milan, PS: Pesaro, AN: Ancona, MC: Macerata, BG: Bergamo, CR: Cremona, SI: Siena, AR: Arezzo, GR: Grosseto, BS: Brescia, nd: not determined.

3.2. Genetic Distances Analysis

The overall mean *p*-distance between all the Italian isolates was 2.3 (SE:0.3) s/10,000 nts, corresponding to a mean of 6.4 (SE: 0.8) substitutions per genome. The non-synonymous distance (dN) was 2.0 (SE: 0.4) non-syn s/10,000 non-syn nts while the overall synonymous mean distance (dS) was equal to 2.4 (SE: 0.05) syn s/10000 syn nts (dN/dS = 0.83). A higher heterogeneity was observed through months as, stratifying the genetic distances on the basis of the sampling time, we observed a higher heterogeneity among the strains isolated in February (*n* = 19) compared to those collected in March (*n* = 96) or April (*n* = 21) (Table 2).

Table 2. Mean genetic divergence within and between Italian strains according to the sampling time (substitutions per 10,000 sites).

Time	Within				Time	Between			
	p Distance (SE)	**Nucleotide (SE)**	**dS (SE)**	**dN (SE)**		**p Distance (SE)**	**Nucleotide (SE)**	**dS (SE)**	**dN (SE)**
February	3.8 (0.6)	9.6 (1.5)	3.5 (1.1)	3.8 (0.6)	February vs. March	3.1 (0.4)	8.1 (1.3)	2.9 (0.8)	2.8 (0.4)
March	1.9 (0.3)	5.4 (0.8)	2.2 (0.5)	1.5 (0.4)	March vs. April	2.3 (0.3)	6.6 (0.8)	2.1 (0.6)	2.0 (0.5)
April	2.4 (0.3)	6.8 (0.9)	1.7 (0.8)	2.1 (0.5)	February vs. April	3.7 (0.5)	10 (1.5)	2.7 (0.8)	3.5 (0.6)

SE: Standard error, dS: synonymous distance, dN: non-synonymous distance.

3.3. Differences in Amino Acids

Considering only the non-synonymous mutations and comparing the Italian genomes with the common ancestor (China, EPI_ISL_402123), there were 159 amino acid substitutions affecting different viral genes, (112 in ORF 1a/1b, 19 in S, 12 in ORF 3a, 4 in M, 3 in ORF7a, 6 in N, and one each in Orf7b, 8 and 10) of which only 15 (9.4%) were observed in 2 or more isolates, as summarized in Table 3. No amino acid changes were observed in the E gene. The previously described substitution D614G in the Spike protein was present in all the isolates belonging to the lineage B.1 and in the strain from Padua belonging to lineage B.

Table 3. SARS-CoV2 mutations identified in Italian strains.

Genome Region	Mutation	*n*/Total	Percentage (%)
ORF 1ab	S443F	2/135	1.5
	H3076Y	2/135	1.5
	L3606F	3/131	2.3
	P4715L	133/136	97.8
	E5689D	2/135	1.5
	R5919K	2/123	1.6
S	A570D	2/129	1.6
	D614G	128/130	98.5
	G1046V *	3/134	2.2
ORF 3a	G251V	3/134	2.2
M	D3G	21/133	15.8
ORF 7a	G70C	2/134	1.5
N	R203K-G204R	52/133	39.1
	V246I	3/136	2.2

* mutation under significant selective pressure.

Considering the Italian isolates, only 1 site resulted under significant selecting pressure by three different methods (MEME, FEL, FUBAR): Site 1,046 in the Spike protein that was present in three isolates from Padua. This G1046V mutation is located in the S2 subunit, between heptad repeat 1 and 2 domains. Mutations R203K-G204R in N gene were always simultaneously detected. It appears that

these mutations discontinue a serine-arginine (S-R) dipeptide by introducing a lysine in-between them, having impacts on structure and function in the mutated N protein.

Fifty-two sequences in our dataset carried these mutations, particularly 11 of the 59 whole genome newly-characterized; six of these were from Tuscany, four from Milan and one from Padua.

3.4. Time Reconstruction of the SARS-CoV-2 Italian Lineage B.1 Phylogeny

Root-to-tip regression analysis of the temporal signal from the Italian B.1 subset revealed a weak association between genetic distances and sampling days (a correlation coefficient of 0.31 and a coefficient of determination (R^2) of 9.9×10^{-2}).

Comparison by BF test of the marginal likelihoods obtained by path sampling (PS) and stepping stone sampling (SS) of the strict vs. relaxed molecular clock (uncorrelated log-normal) showed that the second performed better than the former (strict vs. relaxed molecular clock BF(PS) = −71.9 and BF(SS) = −71.4 for relaxed clock). Comparison of the different demographic models showed that the BSP and the exponential growth models best fitted the data (BSP vs. constant population size BF(PS) = 27.9 and BF(SS) = 30.2 for BSP; constant population size vs. exponential growth BF(PS) = 7.3 and BF(SS) = 8.6) (Table S3).

The mean tMRCA of the tree root (Figure 2) was estimated at 107 days before present (BP) (95%HPD: 91.2–113.1), corresponding to 11 January 2020 (from 5 January to 27 January). The tMRCA of the subclade including all the Italian sequences was estimated to be 92.4 (95%HPD: 76.6–95) days BP, corresponding to 25 January (between 23 January and 10 February).

Figure 2. SARS-CoV-2 tree of 136 Italian strains plus one German and three Chinese isolates from Shanghai, showing statistically-significant support for clades along the branches (posterior probability >0.7). Large red and purple circles indicated highest posterior probability ranging from 1 to 0.9. Calendar dates of the tree root and the Italian clade were showed in red. The light blue box highlighted the three Padua isolates carrying G1046V mutation in S protein.

The Bayesian tree of the Italian sequences showed 15 small significant subclades including two to ten isolates (Figure 2).

3.5. Phylodynamic Analysis of the Italian Dataset

The Bayesian skyline plot of the Italian isolates showed an increase in the number of infections in the period between late February and mid-March 2020, with a rapid exponential growth between 4 and 16 March when it reached a plateau continuing until the last sampling time (Figure 3).
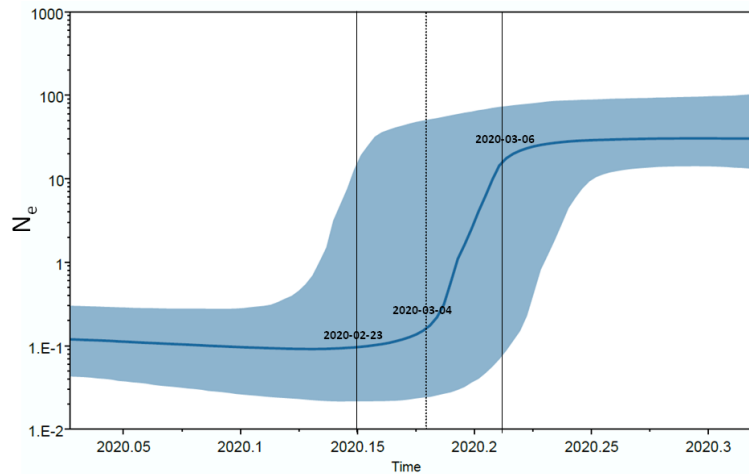
Figure 3. Bayesian Skyline plot of the SARS-CoV-2 outbreak. The Y axis indicates effective population size (Ne) and the X axis shows the time in fraction of years. The thick solid line represents the median value of the estimates, and the grey area the 95% HPD.

The Bayesian birth-death skyline plot of the R_e estimates with 95%HPD with a single R group (corresponding to R_0) estimated a mean value of 2.25 (1.5–3.1). Figure 4 (panels a and b) shows the changes of R_e since the origin of the epidemic and suggests that R_e was higher than 1 since the early days (mean initial R_e = 1.4, 95%HPD: 0.08–2.9). The curve started to grow in early February and peaked to a mean value of 2.3 (95%HPD: 1.5–3.5) in the first half of March, and has since remained at this value. The curve obtained with three R_e groups showed a slight decrease at mid-March (Figure 4, panel b).
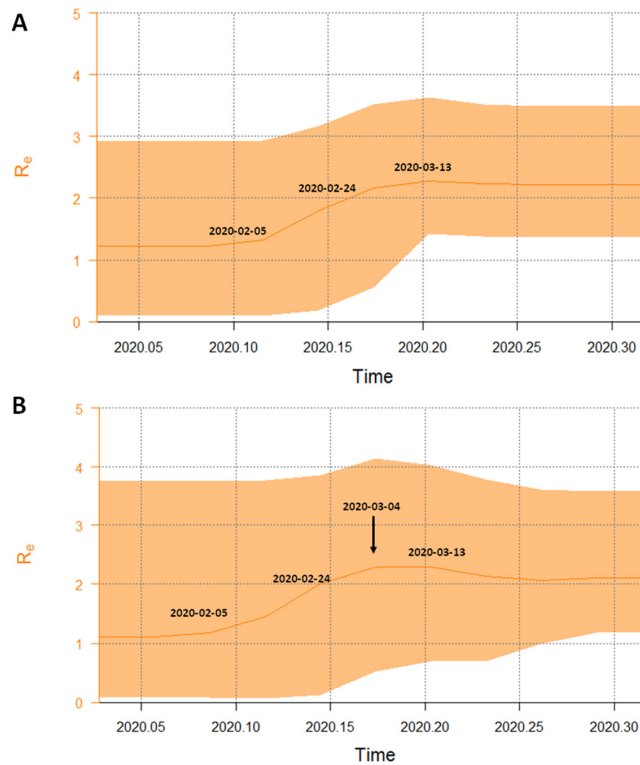
Figure 4. Part **A**: birth-death skyline plot of the SARS-CoV-2 outbreak allowing one R_e intervals. Part **B**: birth-death skyline plot of the SARS-CoV-2 outbreak allowing three R_e intervals. The curves and the orange areas show the mean R_e values and their 95% confidence intervals. The Y and X axes indicate R values and time in years, respectively.

The origin of the epidemic was estimated at a mean 80.3 days BP (credibility interval: 60–109), corresponding to 7 February (between 9 January and 27 February). The recovery rate was estimated about 7.26 days (CI 4.7–16.0 days), and the transmission rate (λ) increased from 71.7 to 115.96 in units per year (corresponding to a growth rate of 0.06 and 0.18 year^{-1}). On the basis of these data, the doubling time decreased from 5.1 days to 3.1 days in the period between early February and mid-March.

4. Discussion

Molecular tracing of SARS-CoV-2 coupled with advanced Bayesian and Maximum likelihood phylogenetic analysis provide detailed information about the epidemiology and evolution of emerging infections and helps to improve our understanding on the mechanisms of spreading of the epidemic.

In a previous study [1], we characterized the viral sequences obtained from the first three patients coming from the Codogno area who were hospitalized at the very beginning of the epidemic in Italy. The Codogno strains correlated with an isolate from an outbreak occurred in Bavaria around 20 January [4]. The present analysis shows that all but one of 62 SARS-CoV-2 sequences obtained from 22 February to the end of April in different Northern and Central Italian areas belong to a single clade, corresponding to the Pangolin lineage B.1, the old Nextstrain subclade A2a and the new Nextstrain clades 20A and 20B (https://nextstrain.org/blog/2020-06-02-SARSCoV2-clade-naming) [1,12]. About 1 out of 4 isolates were classified in different descendant lineages, always included in the main B.1 lineage (such as B.1.1 and B.1.5), most on a temporal basis, being these lineages more represented among the genomes sampled in the second half of March and April (9/14, 64%), while B.1 lineage was more represented in the genomes obtained in February and first half of March (33/47, 70.2%).

This observation was also confirmed by other Italian studies [1,3]. The same clade is now the most widespread in the world and includes most of the published genomes [5]. The genetic distances among the Italian strains were relatively short, corresponding to an average of about 6.4 mutations per viral genome, even if single isolates may have a higher number of changes. After grouping the sequences according with the sampling months, while the within group mean genetic distances were higher in February compared to subsequent months, the genetic distance between different months increased with time. This observation confirms a continuous evolution of the viral genome (with the emergence of new divergent variants) mainly driven by genetic drift. No significant difference was observed between the non-synonymous and the synonymous substitutions (dn/ds = 0.8), suggesting the absence of relevant selective forces driving the evolution of the viral genome. This observation is further confirmed by the analysis of site-specific selective pressure in the Italian strains, which only showed a single site under significant positive selection in the S protein (position 1046) observed in three strains from Padua. Including in the phylogenetic tree 3 isolates from Shanghai and one from the first patient of the Bavarian cluster, being at the root of the B.1 lineage, the dated tree obtained suggests that SARS-CoV-2 entered Italy between late January and early February 2020. This timing matches with the first autochthonous European cluster of SARS-CoV-2 transmission in Bavaria (Germany), originated on 20 January [1,4,21] by the introduction of a strain carried by the index patient coming from Shanghai, where the virus had been circulating since January. The skyline plot analysis of the Italian clade shows an exponential increase of the effective number of infections from late February to mid-March, in excellent agreement with the known epidemiological data (https://www.epicentro.iss.it/coronavirus/sars-cov-2-dashboard). In particular, a very rapid growth of the epidemic was detected between the beginning of March and the middle of the same month, when the curve reaches a plateau up to the end of sampling (27 April). The mean value of R_0 was estimated as 2.25 (1.5 to 3.1) in the entire period. A similar result was obtained by Stadler et al. on a smaller sample of 11 sequences mainly from patients with known travel history to Italy (https://virological.org/t/phylodynamic-analyses-based-on-11-genomes-from-the-italian-outbreak/426). The estimated basic reproduction number (R_0) for SARS-CoV-2 has ranged mainly from 2 to 4, according to the different methods employed for the evaluation [22]. In Italy, values between 2.4 and 3.6 have been estimated in the early phase of COVID-19 epidemic before the control

measures were taken [23–25]. Predictive mathematical models are fundamental to understand the dynamics of the epidemic, plan effective control strategies and verify the efficacy of those applied.

Using a birth-death skyline, we analyzed the changes of R_e during the epidemic in Italy over the entire period. We observed that the R_e was >1 since the first decade of February, suggesting that the infection was circulating within the population before the first notified (hospitalized) COVID-19 cases. The R_e skyline plot reached a value of 2.3 in the first days of March, together with the rapid increase observed in the number of infections by BSP, and slightly decreased thereafter, in agreement with the official data on the course of the epidemic. Between February and March the estimated doubling time of the epidemic decreased from 5.1 to 3.1 days. This value was smaller than that obtained by us for the epidemic in China [26] and might be interpreted as a consequence of a delayed application of more stringent containment measures in Italy. In fact, a slight decrease of the R_e value was observed only after mid-March, when a more rigorous social distancing was enforced across the entire country. The persistence of a R_e value higher than one until April, in partial contrast with the epidemiological data (https://covstat.it/), could be due to the fact that our estimate was influenced by the circulation of the virus in the community, which is larger than the number of the officially registered clinical cases. It is well known that only a small minority of SARS-CoV-2 infections require hospitalization and that in Italy the number of cases of infection has widely exceeded the number of official reports. In a recent study, the prevalence of anti-SARS-CoV-2 antibodies in asymptomatic blood donors living in Milan was shown to increase from February to April, when the prevalence reached its maximum (about 7%) (https://www.medrxiv.org/content/10.1101/2020.05.11.20098442v2). However, in Italy the numbers of active cases began to decrease only in the second half of April, when the present study had already been stopped. Further studies on extended data collection will be required to estimate the effects of the containment measures.

The only one genome characterized in our study not belonging to lineage B.1 was isolated in a 76-year-old man living in the province of Padua (Veneto), who survived to serious COVID-19 manifestations despite old age and the presence of several comorbidities. He denied any contact with infected subjects and did not travel abroad. This virus belongs to the same lineage (B) of the first 2 cases imported into Italy from the Hubei region, China, at the end of January 2020, before Italy suspended flights from China. The couple landed at the Milan airport and travelled to other locations in Northern and Central Italy before the onset of symptoms requiring hospitalization in Rome, but they had not travelled to Padua. Thus, the origin of such a strain remains unexplained and further investigations are underway to evaluate whether this strain may have played a role in causing an epidemic, at least locally. It would also be interesting to investigate whether the currently predominant strain was for some reasons more epidemic than the initial strain, or if the spread of the latter was limited by random factors.

In conclusion, our data show the importance of molecular and phylogenetic evolutionary reconstruction in the surveillance of emerging infections. Of note, it appears that the outbreak in Italy, which involved hundreds of thousands of people, is mainly attributable to a single introduction of the virus and its uncontrolled circulation for a period of about four weeks. These results reaffirm the strategic importance of continuous surveillance and timely tracing to define and rapidly implement effective containment measures for a possible second wave of the pandemic.

and G.Z.; project administration, G.Z., C.B., and M.G.; funding acquisition, G.Z., M.G. All authors have read and agreed to the published version of the manuscript.

Conflicts of Interest: The authors declare no conflict of interest.

References

1. Zehender, G.; Lai, A.; Bergna, A.; Meroni, L.; Riva, A.; Balotta, C.; Tarkowski, M.; Gabrieli, A.; Bernacchia, D.; Rusconi, S.; et al. Genomic characterization and phylogenetic analysis of SARS-COV-2 in Italy. *J. Med. Virol.* **2020**, *29*, 25794. [CrossRef]

2. Capobianchi, M.R.; Rueca, M.; Messina, F.; Giombini, E.; Carletti, F.; Colavita, F.; Castilletti, C.; Lalle, E.; Bordi, L.; Vairo, F.; et al. Molecular characterization of SARS-CoV-2 from the first case of COVID-19 in Italy. *Clin. Microbiol. Infect.* **2020**, *26*, 954–956. [CrossRef]

3. Stefanelli, P.; Faggioni, G.; Presti, A.L.; Fiore, S.; Marchi, A.; Benedetti, E.; Fabiani, C.; Anselmo, A.; Ciammaruconi, A.; Fortunato, A.; et al. Whole genome and phylogenetic analysis of two SARS-CoV-2 strains isolated in Italy in January and February 2020: Additional clues on multiple introductions and further circulation in Europe. *Eurosurveillance* **2020**, *25*, 2000305. [CrossRef]

4. Rothe, C.; Schunk, M.; Sothmann, P.; Bretzel, G.; Froeschl, G.; Wallrauch, C.; Zimmer, T.; Thiel, V.; Janke, C.; Guggemos, W.; et al. Transmission of 2019-nCoV Infection from an Asymptomatic Contact in Germany. *N. Engl. J. Med.* **2020**, *382*, 970–971. [CrossRef]

5. Korber, B.; Fischer, W.M.; Gnanakaran, S.; Yoon, H.; Theiler, J.; Abfalterer, W.; Hengartner, N.; Giorgi, E.E.; Bhattacharya, T.; Foley, B.; et al. Tracking Changes in SARS-CoV-2 Spike: Evidence that D614G Increases Infectivity of the COVID-19 Virus. *Cell* **2020**. [CrossRef]

6. Kearse, M.; Moir, R.; Wilson, A.; Stones-Havas, S.; Cheung, M.; Sturrock, S.; Buxton, S.; Cooper, A.; Markowitz, S.; Duran, C.; et al. Geneious Basic: An integrated and extendable desktop software platform for the organization and analysis of sequence data. *Bioinformatics* **2012**, *28*, 1647–1649. [CrossRef]

7. Katoh, K.; Standley, D.M. MAFFT Multiple Sequence Alignment Software Version 7: Improvements in Performance and Usability. *Mol. Biol. Evol.* **2013**, *30*, 772–780. [CrossRef]

8. Kumar, S.; Stecher, G.; Li, M.; Knyaz, C.; Tamura, K. MEGA X: Molecular Evolutionary Genetics Analysis across Computing Platforms. *Mol. Boil. Evol.* **2018**, *35*, 1547–1549. [CrossRef]

9. Lott, M.; Murrell, B.; Golden, M.; Khoosal, A.; Muhire, B. RDP4: Detection and analysis of recombination patterns in virus genomes. *Virus Evol.* **2015**, *1*, 1. [CrossRef]

10. Posada, D. jModelTest: Phylogenetic Model Averaging. *Mol. Boil. Evol.* **2008**, *25*, 1253–1256. [CrossRef]

11. Stamatakis, A. RAxML version 8: A tool for phylogenetic analysis and post-analysis of large phylogenies. *Bioinformatics* **2014**, *30*, 1312–1313. [CrossRef]

12. Rambaut, A.; Holmes, E.; Hill, V.; O'Toole, Á.; McCrone, J.; Ruis, C.; Du Plessis, L.; Pybus, O.G. A dynamic nomenclature proposal for SARS-CoV-2 to assist genomic epidemiology. *bioRxiv* **2020**. [CrossRef]

13. Suchard, M.A.; Lemey, P.; Baele, G.; Ayres, D.L.; Drummond, A.J.; Rambaut, A. Bayesian phylogenetic and phylodynamic data integration using BEAST 1.10. *Virus Evol.* **2018**, *4*, vey016. [CrossRef]

14. Bouckaert, R.R.; Vaughan, T.G.; Barido-Sottani, J.; Duchêne, S.; Fourment, M.; Gavryushkina, A.; Heled, J.; Jones, G.; Kühnert, D.; De Maio, N.; et al. BEAST 2.5: An advanced software platform for Bayesian evolutionary analysis. *PLoS Comput. Boil.* **2019**, *15*, e1006650. [CrossRef]

15. Rambaut, A.; Lam, T.T.; Carvalho, L.M.; Pybus, O.G. Exploring the temporal structure of heterochronous sequences using TempEst (formerly Path-O-Gen). *Virus Evol.* **2016**, *2*, vew007. [CrossRef]

16. Baele, G.; Lemey, P.; Bedford, T.; Rambaut, A.; Suchard, M.A.; Alekseyenko, A.V. Improving the Accuracy of Demographic and Molecular Clock Model Comparison While Accommodating Phylogenetic Uncertainty. *Mol. Boil. Evol.* **2012**, *29*, 2157–2167. [CrossRef]

17. Suchard, M.A.; Weiss, R.E.; Sinsheimer, J.S. Bayesian selection of continuous-time Markov chain evolutionary models. *Mol. Boil. Evol.* **2001**, *18*, 1001–1013. [CrossRef]

18. Stadler, T.; Kühnert, D.; Bonhoeffer, S.; Drummond, A.J. Birth-death skyline plot reveals temporal changes of epidemic spread in HIV and hepatitis C virus (HCV). *Proc. Natl. Acad. Sci. USA* **2012**, *110*, 228–233. [CrossRef]

19. Li, Q.; Guan, X.; Wu, P.; Wang, X.; Zhou, L.; Tong, Y.; Ren, R.; Leung, K.S.; Lau, E.H.; Wong, J.Y.; et al. Early Transmission Dynamics in Wuhan, China, of Novel Coronavirus–Infected Pneumonia. *N. Engl. J. Med.* **2020**, *382*, 1199–1207. [CrossRef]

20. Walker, P.; Pybus, O.G.; Rambaut, A.; Holmes, E. Comparative population dynamics of HIV-1 subtypes B and C: Subtype-specific differences in patterns of epidemic growth. *Infect. Genet. Evol.* **2005**, *5*, 199–208. [CrossRef]

21. Spiteri, G.; Fielding, J.; Diercke, M.; Campese, C.; Enouf, V.; Gaymard, A.; Bella, A.; Sognamiglio, P.; Moros, M.J.S.; Riutort, A.N.; et al. First cases of coronavirus disease 2019 (COVID-19) in the WHO European Region, 24 January to 21 February 2020. *Eurosurveillance* **2020**, *25*, 2000178. [CrossRef]

22. Liu, Y.; A Gayle, A.; Wilder-Smith, A.; Rocklöv, J. The reproductive number of COVID-19 is higher compared to SARS coronavirus. *J. Travel Med.* **2020**, *27*, 27. [CrossRef]

23. D'Arienzo, M.; Coniglio, A. Assessment of the SARS-CoV-2 basic reproduction number, R0, based on the early phase of COVID-19 outbreak in Italy. *Biosaf. Heal.* **2020**. [CrossRef]

24. Gatto, M.; Bertuzzo, E.; Mari, L.; Miccoli, S.; Carraro, L.; Casagrandi, R.; Rinaldo, A. Spread and dynamics of the COVID-19 epidemic in Italy: Effects of emergency containment measures. *Proc. Natl. Acad. Sci. USA* **2020**, *117*, 10484–10491. [CrossRef]

25. Yuan, J.; Li, M.; Lv, G.; Lu, Z.K. Monitoring transmissibility and mortality of COVID-19 in Europe. *Int. J. Infect. Dis.* **2020**, *95*, 311–315. [CrossRef]

26. Lai, A.; Bergna, A.; Acciarri, C.; Galli, M.; Zehender, G. Early phylogenetic estimate of the effective reproduction number of SARS-CoV-2. *J. Med. Virol.* **2020**, *92*, 675–679. [CrossRef] [PubMed]

Maraviroc as a potential HIV-1 latency-reversing agent in cell line models and *ex vivo* CD4 T cells

Ilaria Vicenti[1,*], Filippo Dragoni[1], Martina Monti[2], Claudia Maria Trombetta[3], Alessia Giannini[1], Adele Boccuto[1], Francesco Saladini[1], Barbara Rossetti[4], Andrea De Luca[1,4]†, Annalisa Ciabattini[1], Gabiria Pastore[1], Donata Medaglini[1], Giancarlo Orofino[5], Emanuele Montomoli[2,3] and Maurizio Zazzi[1]

Abstract

Recent studies have suggested that the CCR5 antagonist maraviroc (MVC) may exert an HIV-1 latency reversal effect. This study aimed at defining MVC-mediated induction of HIV-1 in three cell line latency models and in *ex vivo* CD4 T cells from six patients with suppressed viraemia. HIV-1 induction was evaluated in TZM-bl cells by measuring HIV-1 LTR-driven luciferase expression, and in ACH-2 and U1 latently infected cell lines by measuring cell-free (CFR) and cell-associated (CAR) HIV-1 RNA by qPCR. NF-κB p65 was quantified in nuclear extracts by immunodetection. In *ex vivo* CD4 T cells, CAR, CFR and cell-associated DNA (CAD) were quantified at baseline and 1–7–14 days post-induction (T1, T7, T14). At T7 and T14, the infectivity of the CD4 T cells co-cultured with MOLT-4/CCR5 target cells was evaluated in the TZM-bl assay (TZA). Results were expressed as fold activation (FA) with respect to untreated cells. No LTR activation was observed in TZM-bl cells at any MVC concentration. NF-κB activation was only modestly upregulated (1.6±0.4) in TZM-bl cells with 5 μM MVC. Significant FA of HIV-1 expression was only detected at 80 μM MVC, namely on HIV-1 CFR in U1 (3.1±0.9; *P*=0.034) and ACH-2 cells (3.9±1.4; *P*=0.037). CFR was only weakly stimulated at 20 μM in ACH-2 (1.7±1.0 FA) cells and at 5 μM in U1 cells (1.9±0.5 FA). Although no consistent pattern of MVC-mediated activation was observed in *ex vivo* experiments, substantial FA values were detected sparsely on individual samples with different parameters. Notably, in one sample, MVC stimulated all parameters at T7 (2.3±0.2 CAD, 6.8±3.7 CAR, 18.7±16.7 CFR, 7.3±0.2 TZA). In conclusion, MVC variably induces HIV-1 production in some cell line models not previously used to test its latency reversal potential. In *ex vivo* CD4 T cells, MVC may exert patient-specific HIV-1 induction; however, clinically relevant patterns, if any, remain to be defined.

INTRODUCTION

HIV-1 latency is the hallmark of persistent infection because cells, mostly long-lived CD4 memory T cells, harbouring integrated replication-competent virus, are not targeted by either antiretrovirals or immune attack, preventing HIV-1 eradication even with prolonged fully suppressive therapy [1]. Currently, several compounds, including drugs licensed for treatment of conditions different from HIV-1 infection, are being considered as agents awakening virus in latently infected cells and eventually leading to cell death as a consequence of virus production and/or immune attack [2]. Reversing HIV-1 latency coupled with potent fully suppressive antiretrovirals and possibly therapeutic vaccination is the conceptual basis for the shock and kill eradication strategy [3]. Recent data suggested that maraviroc (MVC), the first approved anti-HIV-1 agent targeting a cellular factor, may exert an HIV-1 latency reversal effect at least under some experimental conditions [4, 5], resulting in the inclusion of MVC in the list of potential latency-reversing agents (LRAs) [6].

MVC binds to the CCR5 chemokine receptor, preventing target cell recognition by CCR5-tropic, or briefly R5, virus [7]. Although the rationale for MVC use remains the

demonstration of a susceptible R5 virus population through HIV-1 genotyping or phenotyping, the binding of MVC to CCR5 triggers a series of cellular events per se, independently from the virus coreceptor tropism or even from the HIV-1-positive status, and hence MVC is being considered in the treatment of other diseases, including cancer, graft versus host and inflammatory diseases [8]. Indeed, the interaction of CCR5 with its natural ligands modulates T cell response [9, 10] and the blockade of this receptor by treatment with MVC has the potential to combine the antiviral and the immunomodulatory effect. This hypothesis was based on results from pivotal trials when MVC treatment was shown to increase CD4 T cell counts even in the context of virological failure [11] and to decrease immune activation and inflammation markers more than the efavirenz comparator arm [12]. In a small observational study, MVC seemed to be involved in a larger recovery of CD4 T cells with respect to darunavir/ritonavir, both coupled with raltegravir and etravirine [13]. Adding MVC to standard therapy at primary HIV-1 infection also resulted in a time-dependent CD4 cell increase independently of co-receptor usage [14]. In HIV-1-associated neurocognitive disease, the reduction of HIV-1-related chronic inflammation induced by MVC translates into improvement of neurocognitive test performance [15, 16]. *In vitro*, MVC interferes with CCR5 and CCR2 internalization, impairing T-cell chemotaxis [17], and modulates cell surface expression of different molecules involved in immune recognition and function, resulting in a global effect thought to be beneficial through decreased inflammation and immune activation [18]. However, MVC-induced benefits independent of its antiviral activity were later questioned due to the unfavourable effect on the CD4-to-CD8 cell ratio as a consequence of reduced decrease or even an increase in CD8 T cell counts [19–22].

A possible role for MVC in the reduction of the latent HIV-1 reservoir has been investigated in several intensification studies. While beneficial effects on immunological activation were confirmed in most [23–25] but not all [19] studies, in the majority of cases MVC intensification did not lead to a significant change in HIV-1 reservoir [24–30]. Notably, these studies differed considerably in their design, including cases where MVC was used in combination with other drugs and/or immunomodulatory factors, preventing or confounding the measurement of net MVC effects [26–29]. Two independent groups from Spain have indeed shown a modest reduction in HIV-1 reservoir following intensification of treatment with MVC alone, either in patients with recent HIV-1 infection [31] or in patients with suppressed viraemia [23].

As a follow-up of the latter work, Madrid-Elena *et al.* [5] showed that MVC increased unspliced HIV-1 RNA levels in resting CD4 T cells in association with enhanced expression of NF-κB-dependent genes. NF-κB is a key T cell transcription factor that regulates HIV-1 transcription and replication and is a preferential target of candidate latency-reversal agents (LRAs) targeting protein kinase C (PKC) pathways [32]. These findings are supported by *in vitro* data from using IL-7-treated CD4 T cells as a model for HIV-1 latency [4].

This study aimed at defining MVC-mediated HIV-1 induction in three cell line latency models and in *ex vivo* CD4 T cells collected from six patients with suppressed viraemia.

METHODS

Cell lines and drugs

Cell lines were purchased by Centre for AIDS Reagents, NIBSC. TZM-bl adherent cell lines (ARP 5011) were propagated in Dulbecco's modified Eagle's medium (DMEM; Euroclone) supplemented with 10% foetal bovine serum (FBS; Euroclone) and 1% penicillin/streptomycin (PS; Euroclone). ACH-2 (ARP 138) and U1/HIV-1 (ARP 139), two latently infected cell lines carrying one and two copies of HIV-1 provirus, respectively, were propagated in RPMI 1640 (Euroclone) supplemented with 2 mM L-glutamine (Euroclone), 1% PS and 10% FBS. All cells were grown in a humidified incubator at 37 °C with 5% CO_2.

MVC (AIDS Reagent Program, catalogue no. 11580), ionomycin (ION; Sigma, catalogue no.19657), phorbol-12-myristate-13-acetate (PMA; Sigma, catalogue no.P8139) and phytohaemagglutinin (PHA; Sigma, catalogue no. L8754) were provided as powder, resuspended in DMSO (MVC, ION, PMA) or phosphate-buffered saline (PBS; PHA) and stored at −20 °C.

Determination of coreceptor CCR5 expression by flow cytometry

TZM-bl, U1/HIV-1 and ACH-2 cells were seeded (1×10^6 cells/well) in V-bottom 96-well plates (Sarstedt) and incubated for 30 min at 4 °C with BV421-conjugated anti-CCR5 (clone 2D7/CCR5, BD Biosciences), at the proper dilution, previously titrated. Samples were fixed with BD Cytofix according to the manufacturer's instructions (BD Biosciences) and acquired on a BD LSR Fortessa X20 flow cytometer (BD Biosciences), storing ~$5–10\times10^5$ for each sample. Data analysis was performed using FlowJo v10 (TreeStar).

Cytotoxicity assay

Drug cytotoxicity was measured on ACH-2, U1/HIV-1 and TZM-bl cell lines and CD4 T cells derived from uninfected donors using the CellTiter-Glo 2.0 Luminescent Cell Viability Assay (Promega), according to the manufacturer's protocol. CD4 T cells were prepared from peripheral blood mononuclear cells (PBMCs) as described below. After 24 h incubation, the luminescent signal generated by the cells treated with the test compound was compared to that generated by the cells treated with DMSO to determine the 50% cytotoxic concentration (CC_{50}).

Cell line stimulation and measurement of HIV-1 induction

One million ACH-2 and U1/HIV-1 and 20000 pre-seeded TZM-bl were induced with fourfold serial MVC dilutions (80, 20, 5, 1.25, 0.31 µM), with PHA (10 µg ml⁻¹) or with ION (1 µg ml⁻¹) plus PMA (50 ng ml⁻¹) (ION+PMA). Experiments were

performed in quadruplicates for TZM-bl and in triplicates for ACH-2 and U1/HIV-1. Control cells (CCs) were treated with 0.16% DMSO and HIV-1 induction was evaluated after 24 h of stimulation.

TZM-bl adherent cell line induction was evaluated by measuring HIV-1 LTR-driven luciferase expression. Briefly, after medium removal, cells were lysed by Glo-Lysis Buffer (Promega) as indicated by manufacturer and transferred into a white luminescence plate, adding one volume of Bright-Glo Luciferase Reagent (Promega). Relative luminescence units (RLU) were acquired by the GloMax Discover Reader (Promega). The RLU of treated cells were compared to those of the negative control and activation of HIV-1 LTR was reported as FA with respect to the CCs.

HIV-1 expression in ACH-2 and U1 were evaluated by measuring cell-free (CFR) and cell-associated HIV-1 RNA (CAR) by quantitative real-time PCR (qPCR). After 24 h stimulation, cell pellets and supernatants were collected and DNA was extracted, treated with DNase and quantified by qPCR, as described below. CAR copies were normalized per million cells, whereas CFR copies were normalized per ml. Normalized copies were compared to those of the negative control and activation was reported as FA with respect to the CCs.

NF-ĸB measurement

NF-κB MVC-mediated induction was evaluated at 3, 6 and 24 h in TZM-bl, and at 24 h in U1, ACH-2 and donor CD4 T cells. After induction, cells were collected and NE-PER Nuclear and Cytoplasmic Extraction Reagents (Thermo Scientific) were used to obtain the nuclear extracts as described by manufacturer. During the first lysis step, the total protein amount was determined by a Bradford protein assay (Bio-Rad). NF-κB DNA-binding activity was detected in nuclear extracts by the NF-κB (p65) Transcription Factor Assay kit (Cayman Chemical). Absorbance values derived from three independent experiments were normalized to the total amount of protein detected by the Bradford assay. Normalized absorbance values were compared to those of the negative control and activation of NF-κB was reported as FA with respect to the CCs.

Patient selection and induction of CD4 T cells

Access to residual anonymized blood samples derived from clinical practice was initially obtained through informed patient consent as approved by the local Ethics Committee at the University Hospital of Siena and at the Hospital Amedeo Savoia of Turin. Patients' adherence to therapy was estimated to be optimal as measured by pharmacy refill records at both clinical units. The six HIV-1-positive blood samples chosen were derived from patients with undetectable viraemia (below 50 copies ml^{-1}) for at least 2 years. A variable volume of blood was collected at subsequent visits from each patient to allow induction experiments. The final quantity of CD4 T cells ranged from 1.3×10^7 to 3.4×10^7.

PBMCs were collected from fresh blood by density gradient centrifugation using Lympholyte-H (Cedarlane), according to the manufacturer's protocol. CD4 T cells were isolated from total PBMCs by negative immunomagnetic selection using the EasySep Human CD4 T Cell Isolation kit (StemCell Technologies). CD4 T cells were propagated at 37 °C with 5% CO$_2$ in lymphocyte medium composed of RPMI 1640 medium supplemented with 2 mM ʟ-glutamine, 10% FBS, 1% PS, 20 U ml^{-1} human Interleukin-2 and 12.5 mM HEPES.

After 36 h culturing, before induction, 1×10^6 CD4 T cells were collected from each culture to perform CAR, CFR and cell-associated HIV-1 DNA (CAD) baseline analyses (T0). Then, CD4 T cells were divided in three different T25 flasks and induced with 5 μM MVC, with ION+PMA (1 μg ml^{-1} plus 50 ng ml^{-1}) used as positive control and 0.16% DMSO used as control. After 24 h (T1), 1×10^6 CD4 T cells and 2 ml of supernatant were collected from each flask to perform CAR, CAD and CFR analyses. The remaining cultures were centrifuged, washed with PBS 1× to remove any residue of inductors and resuspended in lymphocyte medium with 5 μg ml^{-1} of hexadimethrine bromide (polybrene, Sigma). Subsequently, induced CD4 T cells were co-cultured with MOLT-4/CCR5 cells in a 10:1 ratio to permit viral outgrowth, as adapted from Buzon *et al.* and Laird *et al.* [33, 34]. After 7 and 14 days post-induction, the same procedure was repeated to perform CAR, CFR and CAD T7 and T14 analyses, respectively. At T7 and T14, the infectivity of co-cultures was determined using a modified version of the TZM-bl cell-based assay (TZA) developed by Sanyal *et al.* [35]. Briefly, 1×10^5 cells (CD4 T cells and MOLT-4/CCR5) were collected from each flask, diluted fivefold and added to pre-seeded TZM-bl in a 96-well plate. After 48 h, the luciferase activity was measured as reported above. As described by Sanyal *et al.* [35], a negative control made of CD4 T cells derived from uninfected donors co-cultivated with MOLT-4/CCR5 was induced and treated in parallel and subjected to the TZA. Data analysis was performed as suggested, and the maximum likelihood estimate was applied to determine the infectious units per million (i.u.p.m.) cells by using the online system available at http://silicianolab.johnshopkins.edu. The results were expressed as i.u.p.m. ml^{-1} with 95% upper and lower confidence intervals.

Nucleic acids extraction, reverse transcription and quantification

Total nucleic acid extraction from infected cells and from supernatant was performed using the ZR Viral RNA kit (Zymo Research) according to the manufacturer's instructions. Supernatants were enriched by centrifugation for 1 h and 30 min at 16000 *g* at 4 °C, prior to extraction. CAD was determined on cellular extracts by qPCR as described by Vicenti *et al.* [36], with minor modifications. Briefly, HIV-1 DNA and the housekeeping albumin gene were co-amplified in a duplex qPCR to normalize the total HIV-1 DNA amount as copies per million cells [37]. The reaction mixture included 5 μl of cellular nucleic acid extract, 12.5 μl Premix Ex *Taq* (probe qPCR) (Takara), 10 pmol each HIV-1 primer, 5 pmol each albumin primer, and 2.5 pmol each HIV-1 and albumin probe in a final volume of 25 μl. The reaction was run in the Light Cycler 96 system (Roche) for 45 cycles, each including

10 s at 95 °C and 30 s at 60 °C after the first denaturation step (90 s at 95 °C). Based on Probit analysis, the analytical sensitivity of the qPCR assay was 0.9 and 1.6 HIV-1 DNA copies per reaction as defined by the 50% and 95% hit rate. Data acquisition and handling were carried out using Light Cycler 96 software version 1.1.0.1320. To quantify CAR and CFR, cellular and supernatant extracts, respectively, were treated with DNase (DNase I Amplification Grade, Sigma) and cDNA was generated by random hexamer-driven reverse transcription using 20 µl of DNase-treated RNA as template, 664 µM dNTPs, 6 µl of 5× ImProm-II Reaction Buffer, 50 ng hexanucleotides, 1.5 mM $MgCl_2$, 20 U RNasin Plus RNase Inhibitor and 1U of ImProm-II Reverse Transcriptase (Promega) in a final volume of 30 µl. The reactions included an initial 5 min step at 25 °C, followed by 45 min at 37 °C and a 5 min final step at 80 °C. CAR and CFR qPCR reactions were performed as indicated for CAD, using 5 µl of cDNA; all qPCR reactions were performed in duplicate. CAR results were normalized as copies per million cells considering the input of total DNA used, as determined by albumin quantification.

Determination of co-receptor usage and subtype assignment

Co-receptor tropism of clinical isolates was measured phenotypically by a homebrew single-cycle assay as previously published [38] and genotypically by sequencing the V3 loop region. Subtype was determined by sequencing the *integrase* gene. Briefly, 500 ng of DNA obtained by whole blood extraction (High Pure Viral Nucleic Acid kit, Roche) were amplified in a two-step PCR protocol using GoTaq Hot Start Polymerase (Promega). Primer details are provided in Table S1, (available in the online version of this article). Nested PCR products were evaluated by electrophoresis on an agarose gel and bidirectional DNA sequencing was performed using the BrilliantDye Terminator kit v1.1 (Nimagen) with the same primers as used in the nested PCR. Sequencing reactions were treated with the X-Terminator Purification kit (Applied Biosystems) in a 96-well plate and resolved by capillary electrophoresis on the 3130xl Genetic Analyzer

(Applied Biosystems). Following sequence analysis and editing (DNAStar Lasergene 7.1.0 Seqman Pro module), coreceptor tropism was predicted by Geno2Pheno (http://coreceptor.geno2pheno. org/index.php), setting 10% as the false-positive rate cut-off. Subtype was assigned using the Stanford prediction algorithm (https://hivdb.stanford.edu/).

Statistical analysis

GraphPad Prism 5.0 (GraphPad, San Diego, CA, USA)was used for statistical analyses and plotting of results. Data are expressed as mean±SD unless indicated otherwise. Induction was expressed as FA with respect to untreated cells. Differences among inducers were analysed by the Kruskal–Wallis test in the cell line experiments. In *ex vivo* CD4 cell experiments, activation by MVC and by the reference ION+PMA was analysed at T1, T7 and T14 by the Wilcoxon signed rank test. *P* values of <0.05 were considered statistically significant.

RESULTS

HIV-1 induction in cell line models

MVC was not cytotoxic in the tested range (160–0.31 µM) in any of the three cell lines evaluated or in purified CD4 T cells from blood donors. CCR5 was clearly expressed on 99.9% of TZM-bl, 99.1% of U1/HIV-1 and 20.1% of ACH-2 cells (Fig. 1). The potential role of MVC as LRA was evaluated in TZM-bl by measuring the LTR-driven luciferase expression and in low (ACH-2) and high (U1/HIV-1) CCR5-expressing lymphoblastoid cell lines by measuring CAR and CFR production. NF-κB expression was evaluated in nuclei of stimulated cells by assessing the DNA-binding activity of the p65 active form. The effects of HIV-1 inducers were measured at 24 h to reduce exposure to drugs: this time is sufficient to obtain a good stimulation of HIV-1 RNA and it is also the best time–condition to observe NF-κB activity, as determined in set-up experiments performed at 3, 6 and 24 h (data not shown).

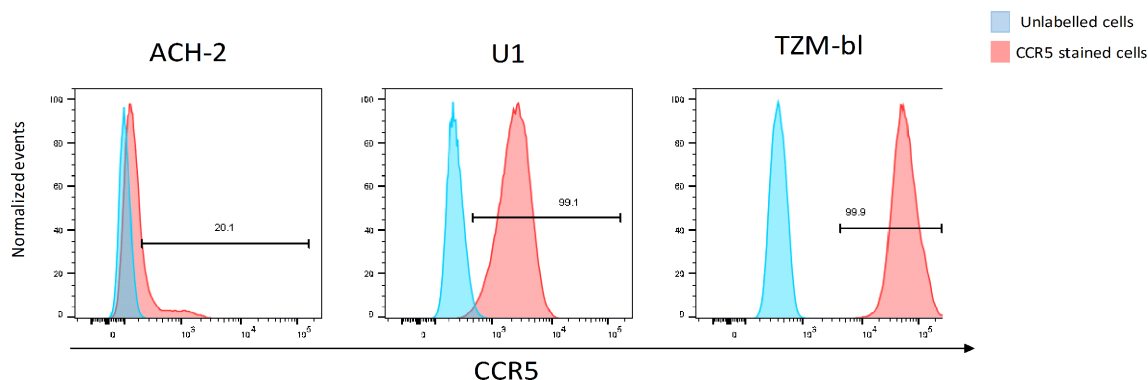No LTR activation was observed in TZM-bl cells at any MVC concentration (Fig. 2). Similar results were obtained

Fig. 1. CCR5 co-receptor expression on cell lines. ACH-2, U1/HIV-1 and TZM-bl adherent cell lines were propagated in RPMI 1640 or DMEM/FBS and stained with BV421-conjugated anti-CCR5 monoclonal antibody. Red histograms indicate CCR5-positive cells, while overlaid blue histograms indicate unstained controls. Data shown are representative from three independent experiments.
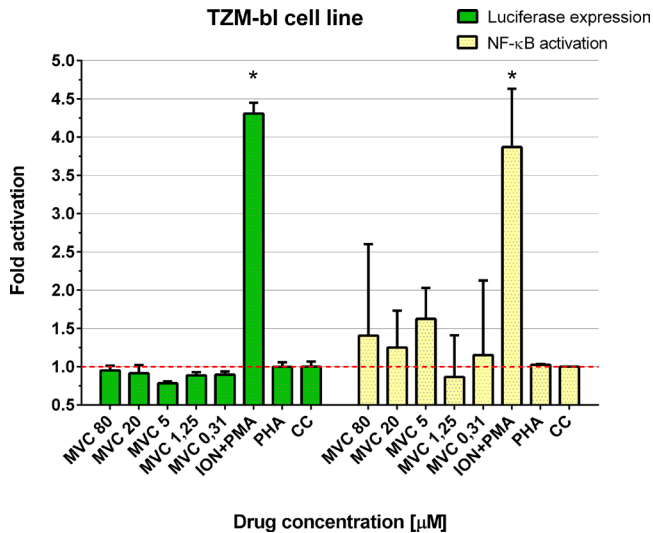
Fig. 2. HIV-1 induction in TZM-bl cell line by MVC, ION+PMA and PHA, as measured by luciferase reporter and NF-κB expression. Results are expressed as fold activation (FA) (*P <0.05) with respect to the control cells (CCs), represented graphically by a dashed red line. Experiments were performed in quadruplicate for luciferase and in triplicate for NF-κB.

with PHA (1.0±0.1 FA), while the reference LRA combination ION+PMA exerted a substantial activation (4.3±0.1 FA). NF-κB binding activity in TZM-bl cells was only modestly upregulated at 5 μM MVC (1.6±0.4 FA). The combination of ION+PMA induced NF-κB expression (3.9±0.8 FA). However, PHA (1.0±0.0 FA) was also not active, further demonstrating that PHA has no latency reversal activity in this model. (Fig. 2, Table S2).

At 80 μM, MVC induced significant HIV-1 CFR expression in U1/HIV-1 cells (3.1±0.9 FA; *P*=0.034) and ACH-2 cells

(3.9±1.4 FA; *P*=0.037), and at the same concentration minimal induction of CAR was observed in ACH-2 (1.7±0.7 FA). A weak MVC induction of CFR was only observed at 20 μM in ACH-2 (1.7±1.0 FA) and at 5 μM in U1/HIV-1 cells (1.9±0.5 FA). NF-κB expression was not upregulated at any MVC concentration in either U1/HIV-1 (0.5±0.1 FA) or ACH-2 (0.6±0.1 FA). The effects of PHA were small and comparable to those of MVC and much smaller than those of ION+PMA, which significantly increased all induction measurements in both cell lines (Fig. 3, Table S2). Although 5 μM MVC minimally activates HIV-1 expression (only in U1/HIV-1 cells as measured by CFR), this concentration was selected for *ex vivo* experiments on patient CD4 T cells because it is closer to the plasma concentrations achieved *in vivo* during therapy [39].

HIV-1 induction in *ex vivo* CD4 T cells from HIV patients

The median duration of virological suppression (plasma HIV-1 RNA <50 copies ml⁻¹) for the six patients included in the study was 8.5 years (IQR 7.00–12.25). The median baseline CD4 T cells count was 679 (IQR 654–929) cells mm⁻³. Two patients started antiretroviral treatment during acute HIV-1 infection. Four patients had a subtype B virus infection and only one harboured an X4 virus. (Table 1).

CAD, CAR and CFR levels were determined at baseline (T0, before stimulation). CAD was detectable in five patients (median 220 copies per 10⁶ CD4 T cells, IQR 179–224), CAR was detectable in all samples (median 341 copies per 10⁶ CD4 T cells, IQR 191–440) and CFR was only detectable in two patients (7 and 11 copies ml⁻¹). Notably, patient 2 had the lowest CAR value and no detectable CAD and CFR (Table 2).

Cells were stimulated with MVC or ION+PMA or not stimulated (CCs) and CAR, CAD and CFR were measured at each time point (T1, T7 and T14), while TZA was performed at
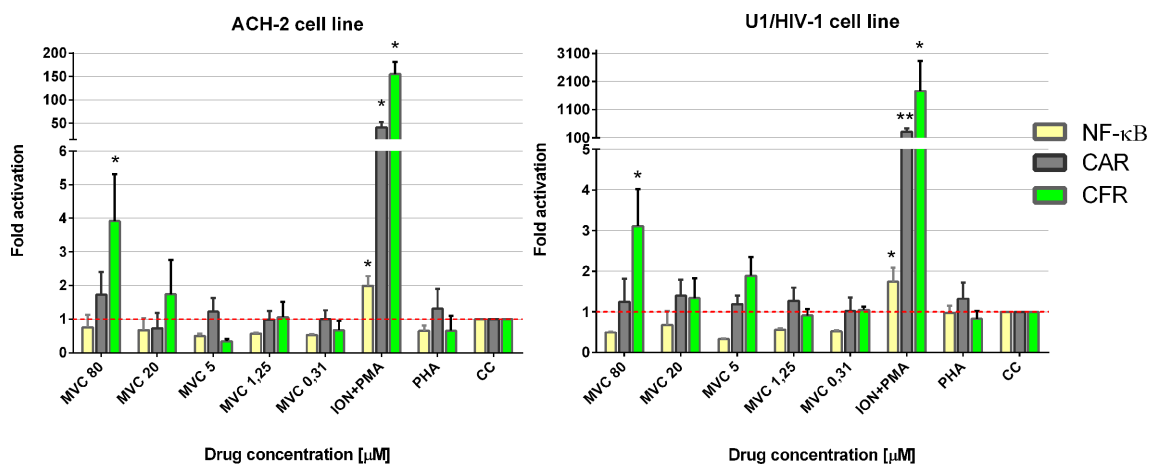

Fig. 3. HIV-1 induction in ACH-2 and U1/HIV-1 by MVC, ION+PMA and PHA, as measured by cell-associated HIV-1 RNA (CAR), cell-free HIV-1 RNA (CFR) and NF-κB expression. Results are expressed as fold activation (FA) (*P <0.05 and **P <0.01) with respect to the control cells (CCs), represented graphically by a dashed red line. Experiments were performed in triplicate.

Table 1. Clinical features of the six patients included in the *ex vivo* study

Sample ID	Age (years)	Sex	Duration of virological suppression (years)	CD4 T cells at baseline (cells mm^{-3})	Current treatment	Subtype	Tropism
1	48	Male	7	649	TAF/FTC/RPV	B	R5
2	80	Male	13	1009	ATV/c+3TC	B	X4
3	72	Male	10	670	3TC+DTG+MVC	B	R5
4	46	Male	15	1307	3TC+DTG+MVC	F	R5
5	50	Male	7	689	TAF/FTC/RPV	C	R5
6	46	Male	6	434	TAF/FTC/RPV	B	R5

3TC, lamivudine; ATV/c, atazanavir-boosted cobicistat; DTG, dolutegravir; FTC, emtricitabine; MVC, maraviroc; RPV, rilpivirine; TAF, tenofovir alafenamide.

T7 and T14, as described in the Methods section. Raw data are reported in Table S3. Comparing the values for MVC or ION+PMA with respect to CCs at each time point in whole samples, significant activation, expressed as median (IQR), was detected with ION+PMA at T1, as measured by CAR [2872 (1174–5599) vs 40 (1-94) copies ml^{-1}, *P*=0.028], at T7 by CAD [105 (41-282) vs 60 (3-151) copies per 10^6 cells, *P*=0.043], CAR [658 (371-973) vs 45 (14-95) copies per 10^6 cells, *P*=0.028] and CFR [420 (52–1108) vs 13 (2-66) copies ml^{-1}, *P*=0.043], at T14 by CAD [92 (48-111) vs 2 (0–161) copies per 10^6 cells, *P*=0.046] and CFR [85 (21–30197) vs 1 (0–3) copies ml^{-1}, *P*=0.028]. By contrast, MVC did not significantly activate HIV-1 expression at any time point as measured by any of the four parameters (Fig. S1).

When inspecting MVC induction readouts in samples from individual patients (Fig. 4), substantial FA values were detected sparsely with different parameters. In sample 1, MVC increased CAD expression 21.7-fold at T14, CFR expression 3.0-fold at T1 and virus infectivity at T7 and T14 as measured by TZA (2.9 and 3.5 FA, respectively). In sample 2, MVC stimulated all parameters at T7 (2.3-fold for CAD, 6.8-fold for CAR, 18.7-fold for CFR and 7.3-fold for TZA) and CFR at T14 (27.6-fold). The MVC-mediated stimulation observed

with sample 3 was weak as detected by CAD (only 2.2-fold at T1) and TZA (2.6-fold at T7) and more substantial at T7 and T14 with CAR (29.5-fold and 4.2-fold, respectively).

In sample 4, MVC increased CAR expression 3.7-fold at T7, CFR expression 2-fold and virus infectivity at T14 as measured by TZA (3.2-fold). Notably, this sample was an outlier in terms of ION+PMA induction, with FA values spanning 10^3 to 10^9 for all indicators, far greater than in all other cases. The same sample also had the highest CAR/CAD ratio at T0. MVC only induced CAD expression at T7 (19.2-fold) in sample 5 and at T7 and T14 in sample 6 (21.0-fold and 2.1-fold, respectively).

DISCUSSION

While some candidate HIV-1 provirus LRAs have shown measurable *in vitro* activity, none has been substantially effective *in vivo* [40]. Therefore, the search for clinically relevant LRAs remains open. Recently, MVC, an HIV-1 entry inhibitor already approved for clinical use, was included in the list of potential LRAs [6]. This activity would make MVC a unique drug, combining the ability to awaken the latent provirus and block new infections. This would open up multiple possibilities for MVC, including administration in acute HIV-1 infection to limit the virus reservoir [41], as well as use in pilot eradication studies based on the shock and kill strategy. In addition, a latency reversal effect of MVC could explain the apparently unfavourable effect on viraemia shown in MVC simplification studies, particularly when HIV-1 relapses occurred at low level and/or transiently [42, 43]. Indeed, such relapses could be attributed to release of virus from reservoir following MVC-mediated induction rather than true virological failure. This could reposition MVC as an effective agent in treatment simplification.

Table 2. HIV-1 cell-associated RNA (CAR), cell-associated DNA (CAD) and cell-free RNA (CFR) measured at 36 h of CD4 T cell culture, before induction. CAR and CAD were expressed as copies/10^6 CD4 T cells, while CFR was expressed as copies ml^{-1}. Results are shown as the mean±SD of duplicate experiments

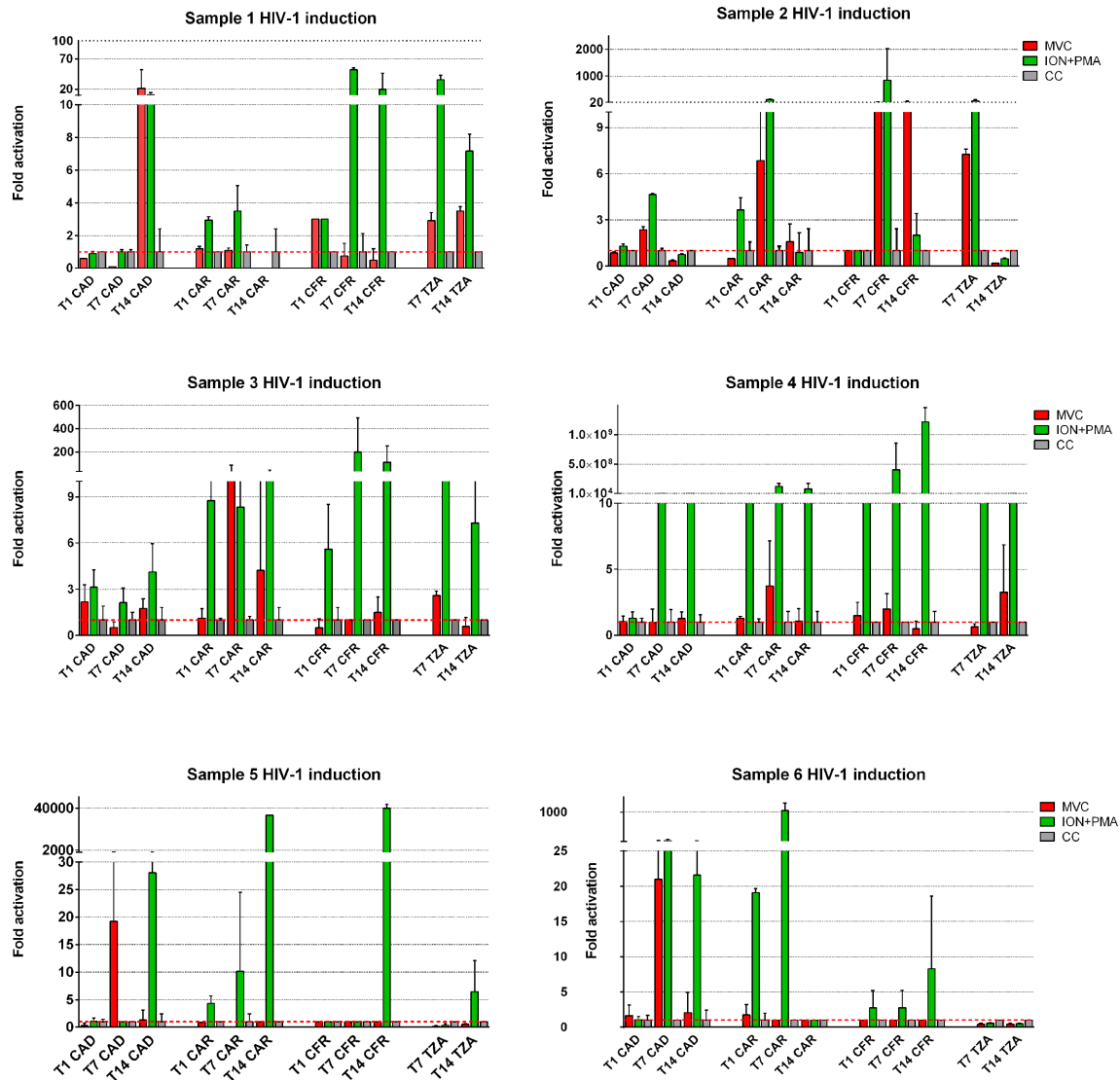| Sample ID	CAR	CAD	CFR
1	378±111	482±116	ND*
2	107±10	ND*	ND*
3	461±209	220±99	7±1
4	896±288	179±28	11±5
5	154±7	156±80	ND*
6	304±11	224±26	ND*

*ND, not detected.

However, the potential of MVC as an LRA is presently based on limited published data, derived from a single study *in vivo* [5] and supported by preliminary *in vitro* data [4]. In the work by Lopez Huertas *et al.* [4], MVC-mediated HIV-1 stimulation was evaluated with two cell models: (i) CD4 T cells transiently transfected with the pLTR-LUC construct

Fig. 4. MVC (5 µM)-mediated HIV-1 induction in *ex vivo* CD4 T cells from the six patients included in the study. ION+PMA was used as positive control for HIV-1 latency reversal. Cell-associated HIV RNA (CAR), cell-free HIV RNA (CFR) and cell-associated HIV-1 DNA (CAD) were measured by real-time PCR; infectivity was determined by TZA. Experiments were performed in duplicate for CAD, CAR and CFR and in quadruplicate for TZA. Results are expressed as fold activation (FA) with respect to the control cells (CCs), represented graphically by a dashed red line.

driving HIV-1-inducible luciferase expression and (ii) HIV-1 latency models based on CD4 T cells treated with CCL19 or IL-7. In the first model, LTR-dependent transcription was only enhanced sevenfold in CD4 T cells treated with 5 µM MVC (*P* <0.005); in the second one, the effect of MVC in the reactivation of latent HIV-1 was statistically significant at different MVC concentrations, but only in cells treated with IL-7. Madrid Elena *et al.* [5] studied the LRA effect of MVC *in vivo* in a group of 20 patients whose antiretroviral treatment was intensified for 10 days with MVC: the amount of unspliced RNA increased significantly (*P*=0.014) following intensification with respect to baseline. Unfortunately, no control group was included to rule out stochastic changes in HIV transcription independently of MVC treatment.

To further investigate the potential role of MVC as an LRA, we designed a combined study including an expanded set of *in vitro* cell line models as well as a pilot *ex vivo* analysis of CD4 T cells obtained from patients under prolonged suppressive therapy. These models had not previously been used to test MVC as an LRA.

In TZM-bl cells, MVC did not stimulate HIV-1 LTR-driven expression and a minimal increase in NF-κB expression was obtained at 5 µM MVC. Comparably higher NF-κB activation was previously reported in HeLa overexpressing CCR5 following MVC induction for 2–6 h at the same concentration [5]. The lack of MVC-mediated LTR activation in TZM-bl cells does not exclude MVC effects in the context of active

HIV-1 infection, considering that this cell line produces a reporter signal that is proportional to the amount of Tat. However, in this cell system, the combination of ION+PMA results in fourfold induction of HIV LTR transcription in a Tat-independent fashion. Similar data were obtained in the same system with TNF-alfa [44]. In the two lymphoblastoid cell lines harbouring inducible proviral HIV-1 DNA (U1/HIV-1 and ACH-2), MVC significantly increased HIV-1 expression only at the highest concentration tested (80 μM) and only minimally activated latent HIV-1 at lower concentrations in the U1/HIV-1 cell line, which expresses the CCR5 coreceptor far more than ACH-2 cells. Globally, MVC effects *in vitro* were generally modest but greater than those observed for PHA induction. The data obtained in this and previous works suggest that the effects of MVC on latent HIV-1 are cell line-specific, depending on the expression of CCR5, the nature of virus latency and the intracellular milieu. This means that insights derived from a specific cell line model are not generalizable or directly applicable to the *in vivo* setting.

In *ex vivo* CD4 T cells, MVC appeared to exert a weak stimulation but without a consistent pattern in specific indicators or at defined time points. Actually, we detected a wide range of FA for any given indicator in different samples, suggesting that MVC induction can be patient-specific, possibly associated with CCR5 surface expression. Due to the need for replicate analysis in the key experiments, we were not able to save material for measuring CCR5 expression levels in patient-derived CD4 T cells, thus it was not possible to assess the role of inter-individual variability in CCR5 expression in the response to MVC induction. In addition, the small number of patients included in this part of the study may have missed the opportunity to demonstrate minor MVC effects. On the other hand, our study comprehensively considered a wider set of indicators compared to previous works [4, 5]. In particular, we expanded the investigation on the amount and nature of the virus produced following induction by measuring CFR and assaying virus infectivity by TZA, respectively, because virus production has more relevant implications than CAR or CAD variations following exposure to LRAs. Interestingly, control CD4 T cell cultures in the absence of stimulation had negligible CFR levels at T0 through T14, although infectious particles were revealed when supernatants were passed onto the CD4/MOLT-4 CCR5 virus amplification co-culture system used in TZA. This highlights the need to control for spontaneous HIV-1 reactivation in any experiment on latency reversal, both *in vitro* [45] and *in vivo* [46].

As a more general perspective, profiling patients under prolonged suppressive therapy in terms of virus inducibility is of clinical interest. For example, *ex vivo* experiments showing ease of virus induction may advise against lowering drug pressure, such as in a switch from triple to dual therapy, a practice gaining popularity after successful clinical studies [47]. By contrast, patients showing poor *ex vivo* HIV-1 induction should be considered as ideal candidates for pilot eradication studies. Reference *in vitro* HIV-1 inducers, such as ION+PMA, can be used for this purpose without the need to restrict the choice to drugs that can be used *in vivo*. For example, ION+PMA induced HIV-1 expression in CD4 T cells from patient 4 far more than any other case in our study (FA values ranging from 10^3 to 10^9), suggesting an excellent response to shock and kill strategies. While progress with LRAs is certainly ongoing, there is still much to investigate to define the best *in vitro* model(s) predicting response to protocols aiming at disrupting HIV-1 latency *in vivo*. Cell line-based systems can be helpful for selecting the best candidate LRAs and setting up reliable assays. However, further essential steps should be made with *ex vivo* systems to fully appreciate the predictably high impact of inter-patient variability and guide the development of effective eradication strategies.

References

1. Sengupta S, Siliciano RF. Targeting the latent reservoir for HIV-1. *Immunity* 2018;48:872–895.

2. Spivak AM, Planelles V. Novel latency reversal agents for HIV-1 cure. *Annu Rev Med* 2018;69:421–436.

3. Margolis DM, Garcia JV, Hazuda DJ, Haynes BF. Latency reversal and viral clearance to cure HIV-1. *Science* 2016;353:aaf6517.

4. López-Huertas MR, Jiménez-Tormo L, Madrid-Elena N, Gutiérrez C, Rodríguez-Mora S et al. The CCR5-antagonist maraviroc reverses HIV-1 latency in vitro alone or in combination with the PKC-agonist bryostatin-1. *Sci Rep* 2017;7:2385.

5. Madrid-Elena N, García-Bermejo ML, Serrano-Villar S, Díaz-de Santiago A, Sastre B et al. Maraviroc is associated with latent HIV-1 reactivation through NF-κB activation in resting CD4+ T cells from HIV-infected individuals on suppressive antiretroviral therapy. *J Virol* 2018;92.

6. Sadowski I, Hashemi FB. Strategies to eradicate HIV from infected patients: elimination of latent provirus reservoirs. *Cell Mol Life Sci* 2019;76:3583–3600.

7. Wood A, Armour D. The discovery of the CCR5 receptor antagonist, UK-427,857, a new agent for the treatment of HIV infection and AIDS. *Prog Med Chem* 2005;43:239–271.

8. Woollard SM, Kanmogne GD. Maraviroc: a review of its use in HIV infection and beyond. *Drug Des Devel Ther* 2015;9:5447–5468.

9. Lederman MM, Penn-Nicholson A, Cho M, Mosier D. Biology of CCR5 and its role in HIV infection and treatment. *JAMA* 2006;296:815–826.

10. Corbeau P, Reynes J. CCR5 antagonism in HIV infection: ways, effects, and side effects. *AIDS* 2009;23:1931–1943.

11. Asmuth DM, Goodrich J, Cooper DA, Haubrich R, Rajicic N *et al.* CD4+ T-cell restoration after 48 weeks in the Maraviroc treatment-experienced trials MOTIVATE 1 and 2. *J Acquir Immune Defic Syndr* 2010;54:394–397.

12. Funderburg N, Kalinowska M, Eason J, Goodrich J, Heera J *et al.* Effects of maraviroc and efavirenz on markers of immune activation and inflammation and associations with CD4+ cell rises in HIV-infected patients. *PLoS One* 2010;5:e13188.

13. Cossarini F, Galli A, Galli L, Bigoloni A, Salpietro S *et al.* Immune recovery and T cell subset analysis during effective treatment with maraviroc. *J Antimicrob Chemother* 2012;67:2474–2478.

14. Ripa M, Pogliaghi M, Chiappetta S, Galli L, Pensieroso S *et al.* Dynamics of adaptive and innate immunity in patients treated during primary human immunodeficiency virus infection: results from Maraviroc in HIV Acute Infection (MAIN) randomized clinical trial. *Clin Microbiol Infect* 2015;21–876.e1–876.e4.

15. Ndhlovu LC, Umaki T, Chew GM, Chow DC, Agsalda M *et al.* Treatment intensification with maraviroc (CCR5 antagonist) leads to declines in CD16-expressing monocytes in cART-suppressed chronic HIV-infected subjects and is associated with improvements in neurocognitive test performance: implications for HIV-associated neurocognitive disease (hand). *J Neurovirol* 2014;20:571–582.

16. Gates TM, Cysique LA, Siefried KJ, Chaganti J, Moffat KJ *et al.* Maraviroc-intensified combined antiretroviral therapy improves cognition in virally suppressed HIV-associated neurocognitive disorder. *AIDS* 2016;30:591–600.

17. Yuan J, Ren HY, Shi YJ, Liu W, yun RH, jin SY. *In Vitro* immunological effects of blocking CCR5 on T cells. *Inflammation* 2015;38:902–910.

18. Arberas H, Guardo AC, Bargalló ME, Maleno MJ, Calvo M *et al. In vitro* effects of the CCR5 inhibitor maraviroc on human T cell function. *J Antimicrob Chemother* 2013;68:577–586.

19. Hunt PW, Shulman NS, Hayes TL, Dahl V, Somsouk M *et al.* The immunologic effects of maraviroc intensification in treated HIV-infected individuals with incomplete CD4+ T-cell recovery: a randomized trial. *Blood* 2013;121:4635–4646.

20. Rusconi S, Vitiello P, Adorni F, Colella E, Focà E *et al.* Maraviroc as intensification strategy in HIV-1 positive patients with deficient immunological response: an Italian randomized clinical trial. *PLoS One* 2013;8:e80157.

21. Chan ES, Landay AL, Brown TT, Ribaudo HJ, Mirmonsef P *et al.* Differential CD4+ cell count increase and CD4+:CD8+ ratio normalization with maraviroc compared with tenofovir. *AIDS* 2016;30:2091–2097.

22. Serrano-Villar S, Caruana G, Zlotnik A, Pérez-Molina JA, Moreno S. Effects of maraviroc versus efavirenz in combination with zidovudine-lamivudine on the CD4/CD8 ratio in treatment-naive HIV-infected individuals. *Antimicrob Agents Chemother* 2017;61.

23. Gutiérrez C, Díaz L, Vallejo A, Hernández-Novoa B, Abad M *et al.* Intensification of antiretroviral therapy with a CCR5 antagonist in patients with chronic HIV-1 infection: effect on T cells latently infected. *PLoS One* 2011;6.

24. Wilkin TJ, Lalama CM, McKinnon J, Gandhi RT, Lin N *et al.* A pilot trial of adding maraviroc to suppressive antiretroviral therapy for suboptimal CD4+ T-cell recovery despite sustained virologic suppression: ACTG A5256. *J Infect Dis* 2012;206:534–542.

25. Cillo AR, Hilldorfer BB, Lalama CM, McKinnon JE, Coombs RW *et al.* Virologic and immunologic effects of adding maraviroc to suppressive antiretroviral therapy in individuals with suboptimal CD4+ T-cell recovery. *AIDS* 2015;29:2121–2129.

26. Ananworanich J, Chomont N, Fletcher JL, Pinyakorn S, Schuetz A *et al.* Markers of HIV reservoir size and immune activation after treatment in acute HIV infection with and without raltegravir and maraviroc intensification. *J Virus Erad* 2015;1:116–122.

27. Katlama C, Lambert-Niclot S, Assoumou L, Papagno L, Lecardonnel F *et al.* Treatment intensification followed by interleukin-7 reactivates HIV without reducing total HIV DNA: a randomized trial. *AIDS* 2016;30:221–230.

28. Lafeuillade A, Wainberg M, Gougeon ML, de LSK, Halfon P *et al.* Highlights from the 2014 International Symposium on HIV & Emerging Infectious Diseases (ISHEID): From cART management to the end of the HIV pandemic. *AIDS Res Ther* 2014;11.

29. Ostrowski M, Benko E, Yue FY, Kim CJ, Huibner S *et al.* Intensifying antiretroviral therapy with raltegravir and maraviroc during early human immunodeficiency virus (HIV) infection does not accelerate HIV reservoir reduction. *Open Forum Infect Dis* 2015;2.

30. Markowitz M, Evering TH, Garmon D, Caskey M, La Mar M *et al.* A randomized open-label study of 3- versus 5-drug combination antiretroviral therapy in newly HIV-1-infected individuals. *J Acquir Immune Defic Syndr* 2014;66:140–147.

31. Puertas MC, Massanella M, Llibre JM, Ballestero M, Buzon MJ *et al.* Intensification of a raltegravir-based regimen with maraviroc in early HIV-1 infection. *AIDS* 2014;28:325–334.

32. Jiang G, Dandekar S. Targeting NF-κB signaling with protein kinase C agonists as an emerging strategy for combating HIV latency. *AIDS Res Hum Retroviruses* 2015;31:4–12.

33. Buzon MJ, Martin-Gayo E, Pereyra F, Ouyang Z, Sun H *et al.* Long-Term antiretroviral treatment initiated at primary HIV-1 infection affects the size, composition, and decay kinetics of the reservoir of HIV-1-infected CD4 T cells. *J Virol* 2014;88:10056–10065.

34. Laird GM, Eisele EE, Rabi SA, Lai J, Chioma S *et al.* Rapid quantification of the latent reservoir for HIV-1 using a viral outgrowth assay. *PLoS Pathog* 2013;9:e1003398.

35. Sanyal A, Mailliard RB, Rinaldo CR, Ratner D, Ding M *et al.* Novel assay reveals a large, inducible, replication-competent HIV-1 reservoir in resting CD4+ T cells. *Nat Med* 2017;23:885–889.

36. Vicenti I, Meini G, Saladini F, Giannini A, Boccuto A *et al.* Development of an internally controlled quantitative PCR to measure total cell-associated HIV-1 DNA in blood. *Clin Chem Lab Med* 2018;56:e75–e77.

37. Mazet-Wagner AA, Baclet MC, Loustaud-Ratti V, Denis F, Alain S. Real-Time PCR quantitation of hepatitis B virus total DNA and covalently closed circular DNA in peripheral blood mononuclear cells from hepatitis B virus-infected patients. *J Virol Methods* 2006;138:70–79.

38. Vicenti I, Lai A, Giannini A, Boccuto A, Dragoni F *et al.* Performance of Geno2Pheno[coreceptor] to infer coreceptor use in human immunodeficiency virus type 1 (HIV-1) subtype A. *J Clin Virol* 2019;111:12–18.

39. Abel S, Back DJ, Vourvahis M. Maraviroc: pharmacokinetics and drug interactions. *Antivir Ther* 2009;14:607–618.

40. Ait-Ammar A, Kula A, Darcis G, Verdikt R, De Wit S *et al.* Current status of latency reversing agents facing the heterogeneity of HIV-1 cellular and tissue reservoirs. *Front Microbiol* 2019;10:3060.

41. Chomont N, Okoye AA, Favre D, Trautmann L. Wake me up before you go: a strategy to reduce the latent HIV reservoir. *AIDS* 2018;32:293–298.

42. Pett SL, Amin J, Horban A, Andrade-Villanueva J, Losso M *et al.* Maraviroc, as a switch option, in HIV-1-infected individuals with stable, well-controlled HIV replication and R5-tropic virus on their first nucleoside/nucleotide reverse transcriptase inhibitor plus ritonavir-boosted protease inhibitor regimen: week 48 results of the randomized, multicenter March study. *Clin Infect Dis* 2016;63:122–132.

43. Rossetti B, Gagliardini R, Meini G, Sterrantino G, Colangeli V *et al.* Switch to maraviroc with darunavir/r, both QD, in patients with suppressed HIV-1 was well tolerated but virologically inferior to

standard antiretroviral therapy: 48-week results of a randomized trial. *PLoS One* 2017;12:e0187393.

44. **Sanghavi SK**, **Reinhart TA**. Increased expression of TLR3 in lymph nodes during simian immunodeficiency virus infection: implications for inflammation and immunodeficiency. *J Immunol* 2005;175:5314–5323.

45. **Read DF**, **Atindaana E**, **Pyaram K**, **Yang F**, **Emery S** *et al*. Stable integrant-specific differences in bimodal HIV-1 expression

patterns revealed by high-throughput analysis. *PLoS Pathog* 2019;15:e1007903.

46. **Cillo AR**, **Hong F**, **Tsai A**, **Irrinki A**, **Kaur J** *et al*. Blood biomarkers of expressed and inducible HIV-1. *AIDS* 2018;32:699–708.

47. **Badowski M**, **Pérez SE**, **Silva D**, **Lee A**. Two's a company, three's a crowd: a review of initiating or switching to a two-drug antiretroviral regimen in treatment-naïve and treatment-experienced patients living with HIV-1. *Infect Dis Ther* 2020;9:185–208.